REPORT NO. FAA-RD-77-44

DOT-FA76WA-3843
JUNE 1976

STUDY TO IMPROVE AIRFRAME TURBINE ENGINE ROTOR BLADE CONTAINMENT

C. O. GUNDERSON

JULY 1977

FINAL REPORT

Prepared for

U.S. DEPARTMENT OF TRANSPORTATION
FEDERAL AVIATION ADMINISTRATION
Systems Research & Development Service
Washington, D.C. 20590

NOTICE

This document is disseminated under the sponsorship of the Department of Transportation in the interest of information exchange. The United States Government assumes no liability for its contents or use thereof.

The United States Government does not endorse products or manufacturers. Trade or manufacturers' names appear herein solely because they are considered essential to the object of this report.

Technical Report Documentation Page

1 Report No. FAA-RD-77-44	2 Government Accession No.	3. Recipient's Catalog No
4. Title and Subtitle: STUDY TO IMPROVE AIRFRAME TURBINE ENGINE ROTOR BLADE CONTAINMENT,		5. Report Date: July 1977
		6 Performing Organization Code
7 Author(s): C. O. Gunderson		8 Performing Organization Report No. MDC-J7615
9 Performing Organization Name and Address: MCDONNELL DOUGLAS CORPORATION, Douglas Aircraft Company, 3855 Lakewood Boulevard, Long Beach, California 90846		10 Work Unit No (TRAIS)
		11 Contract or Grant No. DOT-FA76WA-3843
12 Sponsoring Agency Name and Address: FEDERAL AVIATION ADMINISTRATION, Systems Research and Development Service, Washington, D.C. 20590		13 Type of Report and Period Covered: Final Report. June '76 - Feb '77
		14 Sponsoring Agency Code: ALG-313 (NJH)

15 Supplementary Notes

16 Abstract: An evaluation was made of energies and trajectories for a range of fan, compressor, and turbine blade fragments from high bypass ratio fan engines for typical 3 and 4 engine wide body airplanes. The weight for local armor was established. The effects of fan blade fragment impacts for areas up to 30° forward of the fan plane of rotation were investigated.

Tests using simulated titanium blade fragments and various inlet and nacelle materials were used to determine energy absorption capabilities. The effects of fragment impact angles, size, and rotation and penetration characteristics with steel and aluminum honeycomb; sheet steel; multiple steel layers; and Kevlar aramid fiber material containment systems were explored. Emperical and analytical armor weight determinations were verified by test. Estimates were made for the effect of added weight for airframe installed armor on fuel burned and fuel cost.

In view of the adequacy of prevailing installation practices, further armor for the range of fragments considered would not appear to significantly enhance flight safety. While liberated fan blade fragments ahead of the engine do not affect the operation of remaining engines or jeopardize continued safety, they can produce undesirable secondary damage which should be considered in its own light with respect to local protection.

17 Key Words	18. Distribution Statement
High Bypass Engines, Blade Fragment Containment, Airframe Mounted Fragment Armor, Armored Wide Body 3 and 4 Engine Airplanes	

19. Security Classif. (of this report)	20. Security Classif. (of this page)	21. No. of Pages	22. Price
Unclassified	Unclassified	230	

Form DOT F 1701.7 8-72 Reproduction of completed page authorized

METRIC CONVERSION FACTORS

Approximate Conversions to Metric Measures

Symbol	When You Know	Multiply by	To Find	Symbol
		LENGTH		
in	inches	*2 5	centimeters	cm
ft	feet	30	centimeters	cm
yd	yards	0 9	meters	m
mi	miles	1,6	kilometers	km
		AREA		
in^2	square inches	6.5	square centimeters	cm^2
ft^2	square feet	0 09	square meters	m^2
yd^2	square yards	0.8	square meters	m^2
mi^2	square miles	2.6	square kilometers	km^2
	acres	0 4	hectares	ha
		MASS (weight)		
oz	ounces	28	grams	g
lb	pounds	0.45	kilograms	kg
	short tons (2000 lb)	0 9	tonnes	t
		VOLUME		
tsp	teaspoons	5	milliliters	ml
Tbsp	tablespoons	15	milliliters	ml
fl oz	fluid ounces	30	milliliters	ml
c	cups	0.24	liters	l
pt	pints	0 47	liters	l
qt	quarts	0.95	liters	l
gal	gallons	3 8	liters	l
ft^3	cubic feet	0,03	cubic meters	m^3
yd^3	cubic yards	0,76	cubic meters	m^3
		TEMPERATURE (exact)		
°F	Fahrenheit temperature	5/9 (after subtracting 32)	Celsius temperature	°C

*1 in = 2.54 (exactly). For other exact conversions and more detailed tables, see NBS Misc. Publ. 286, Units of Weights and Measures. Price $2.25. SD Catalog No. C13.10:286.

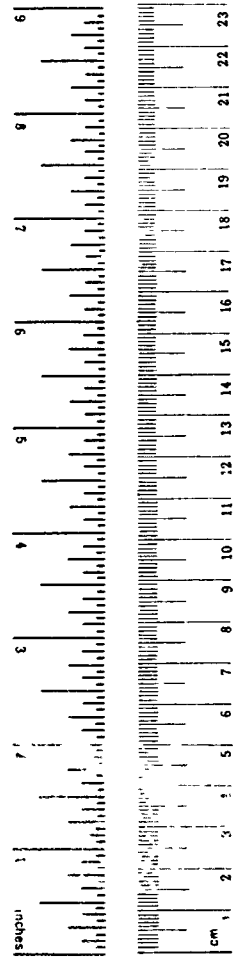

Approximate Conversions from Metric Measures

Symbol	When You Know	Multiply by	To Find	Symbol
		LENGTH		
mm	millimeters	0 04	inches	in
cm	centimeters	0 4	inches	in
m	meters	3 3	feet	ft
m	meters	1.1	yards	yd
km	kilometers	0 6	miles	mi
		AREA		
cm^2	square centimeters	0,16	square inches	in^2
m^2	square meters	1 2	square yards	yd^2
km^2	square kilometers	0 4	square miles	mi^2
ha	hectares (10,000 m^2)	2 5	acres	
		MASS (weight)		
g	grams	0 035	ounces	oz
kg	kilograms	2.2	pounds	lb
t	tonnes (1000 kg)	1.1	short tons	
		VOLUME		
ml	milliliters	0 03	fluid ounces	fl oz
l	liters	2.1	pints	pt
l	liters	1 06	quarts	qt
l	liters	0.26	gallons	gal
m^3	cubic meters	35	cubic feet	ft^3
m^3	cubic meters	1 3	cubic yards	yd^3
		TEMPERATURE (exact)		
°C	Celsius temperature	9/5 (then add 32)	Fahrenheit temperature	°F

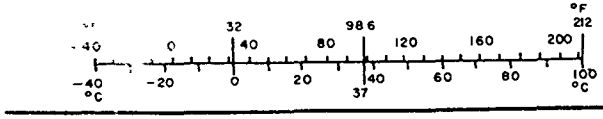

TABLE OF CONTENTS

		PAGE
1.0	SUMMARY	1
2.0	INTRODUCTION	4
3.0	STUDY DESCRIPTION	5
4.0	MULTIPLE BLADE FRAGMENT EVALUATION	7
	4.1 UNCONTAINED MULTIPLE BLADE FRAGMENT ENERGIES	7
	4.2 AIRFRAME EXPOSURE AREAS	16
	4.3 ENGINE INSTALLATION ARMOR WEIGHTS	21
	4.4 AIRCRAFT AND INDIVIDUAL COMPONENT FRAGMENT VULNERABILITY	36
5.0	BLADE TIP FRAGMENT EVALUATION	55
	5.1 INLET ARMOR FOR CF6 POWERED STUDY AIRPLANES	58
	5.1.1 INLET CONSTRUCTION FOR THE CF6 ENGINE	58
	5.1.2 WING INLET ARMOR FOR CF6-50 ENGINE	61
	5.1.3 TAIL INLET ARMOR FOR CF6-50 ENGINE	70
	5.1.4 TOTAL INLET ARMOR WEIGHT	72
	5.2 INLET ARMOR FOR THE JT9D POWERED STUDY AIRPLANE	76
	5.2.1 INLET CONSTRUCTION FOR THE JT9D ENGINE	76
	5.2.2 WING INLET ARMOR FOR JT9D ENGINE	76
	5.2.3 TAIL INLET ARMOR FOR JT9D ENGINE	85
	5.2.4 TOTAL INLET ARMOR WEIGHT	88
	5.3 ARMOR INSTALLATION REQUIREMENTS	89
6.0	BLADE FRAGMENT IMPACT TESTS	90
	6.1 TEST FACILITY	90
	6.2 INSTRUMENTATION	94
	6.3 TEST FRAGMENT SIZE	94
	6.4 ARMOR THICKNESS TESTS	98
	6.5 ENERGY ABSORPTION BY AIRFRAME STRUCTURES	100
	6.5.1 ENERGY ABSORPTION BY STAINLESS STEEL HONEYCOMB (STRESSKIN) PANELS	100
	6.5.2 EFFECT OF FRAGMENT SIZE ON STRESSKIN ENERGY ABSORPTION	113
	6.5.3 EFFECT OF IMPACT ANGLE ON STRESSKIN ENERGY ABSORPTION	129

PAGE

6.5.4 ENERGY ABSORPTION BY BONDED ALUMINUM HONEYCOMB PANELS 142

6.5.5 EFFECT OF IMPACT ANGLE ON ALUMINUM HONEYCOMB ENERGY ABSORPTION 151

6.5.6 ENERGY ABSORPTION BY SHEET STEEL 156

6.5.7 EFFECTS OF FRAGMENT SIZE ON SOLID SHEET STAINLESS STEEL ENERGY ABSORPTION 172

6.5.8 EFFECT OF MULTIPLE LAYERS 177

6.5.9 EFFECTS OF FRAGMENT ROTATION 180

6.5.10 KEVLAR ARMOR SYSTEM 186

7.0 EFFECT OF INSTALLED ARMOR WEIGHT ON AIRPLANE PERFORMANCE 209

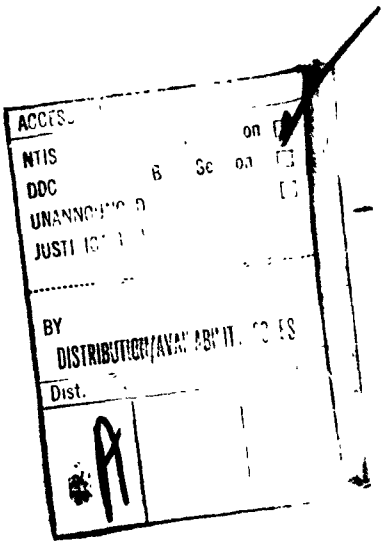

LIST OF ILLUSTRATIONS

Figure		Page
1	Typical Fragments Evaluated	7
2	JT9D-59A Engine Cutaway	8
3	CF6-50 Engine Cutaway	9
4	Energy Absorbed vs Material Thickness	14
5	Blade Failure Impingement Zones - 3 Engine Airplane	17
6	Engine Arrangement - 3 Engine Airplane	18
7	Blade Failure Impingement Zones - 4 Engine Airplane	19
8	CF6-50 Engine Instl. No. 2 H.P. Turbine, Blade Impingement Zone	22
9	CF6-50 Engine Instl. No. 4 L.P. Turbine, Blade Impingement Zone	23
10	JT9D Profile Cutaway with Armor Locations	24
11	JT9D Cross Section Showing Armor for #1 Eng.- 3 Eng. A/P	25
12	JT9D Cross Section Showing Armor for #2 Eng.- 3 Eng. A/P	26
13	JT9D Cross Section Showing Armor for #3 Eng.- 3 Eng. A/P	27
14	JT9D Cross Section Showing Armor for #1 or #2 Eng. - 4 Eng.A/P	28
15	JT9D Cross Section Showing Armor for #3 or #4 Eng. - 4 Eng.A/P	29
16	CF6-50 Profile Cutaway with Armor Locations	30
17	CF6-50 Cross Section Showing Armor for #1 Eng. - 3 Eng.A/P	31
18	CF6-50 Cross Section Showing Armor for #2 Eng. - 3 Eng.A/P	32
19	CF6-50 Cross Section Showing Armor for #3 Eng. - 3 Eng.A/P	33
20	CF6-50 Cross Section Showing Armor for #1 or #2 Eng. - 4 Eng. A/P	34
21	CF6-50 Cross Section Showing Armor for #3 or #4 Eng. - 4 Eng. A/P	35

LIST OF ILLUSTRATIONS (Cont'd)

Figure		Page
36	3-1/2 Inch Diameter Fragment Gun	95
37	Sabot/Fragment Configuration	96
38	3-1/2 Inch Diameter Fragment Gun Muzzle	97
39	Curved Panel Test Setup	103
40	Energy vs Velocity^2 3/4 Inch Thick Stresskin Tangential Impingement	104
41	3/4 Inch Stresskin Test Panel Inner Surface, 4 x 7 x .25 In. Fragment, 624 FPS Impact Velocity	105
42	3/4 Inch Stresskin Test Panel Outer Surface, 4 x 7 x .25 In. Fragment, 624 FPS Impact Velocity	105
43	3/4 Inch Stresskin Test Panel Outer Surface, 4 x 7 x .25 In. Fragment, 624 FPS Impact Velocity	106
44	Outer Surface of Test Panel & Breakwire Fence Screens after Test B-121-1	106
45	Front View Closeup of Breakwire Fence Screen after Test Shot of B-121-1	107
46	Side View Closeup of Breakwire Fence Screen after Test Shot B-121-1	107
47	3/4 Inch Stresskin Test Panel Inner Surface, 4 x 7 x .25 In. Fragment, 768 FPS Impact Velocity	108
48	3/4 Inch Stresskin Test Panel Outer Surface, 4 x 7 x .25 In. Fragment, 768 FPS Impact Velocity	108
49	3/4 Inch Stresskin Test Panel Inner Surface, 4 x 7 x .25 In. Fragment, 964 FPS Impact Velocity	109
50	3/4 Inch Stresskin Test Panel Outer Surface, 4 x 7 x .25 In. Fragment, 964 FPS Impact Velocity	109

LIST OF ILLUSTRATIONS (Cont'd)

Figure		Page
51	3/4 Inch Stresskin Test Panel Inner Surface, 4 x 7 x .25 In. Fragment, 537 FPS Impact Velocity	110
52	3/4 Inch Stresskin Test Panel Outer Surface, 4 x 7 x .25 In. Fragment, 537 FPS Impact Velocity	110
53	3/4 Inch Stresskin Test Panel Inner Surface, 4 x 7 x .25 In. Fragment, 377 FPS Impact Velocity	111
54	3/4 Inch Stresskin Test Panel Outer Surface, 4 x 7 x .25 In. Fragment, 377 FPS Impact Velocity	111
55	3/4 Inch Stresskin Test Panel Inner Surface, 4 x 5 x .25 In. Fragment, 577 FPS Impact Velocity	112
56	3/4 Inch Stresskin Test Panel Outer Surface, 4 x 5 x .25 In. Fragment, 577 FPS Impact Velocity	112
57	Energy vs. Velocity^2 - 3/4 Inch Thick Stresskin, Tangential Impingement,.55 Lb. Fragment	116
58	3/4 Inch Stresskin Test Panel Inner Surface, 3 x 5 x 0.25 In. Fragment, 566 FPS Impact Velocity	117
59	3/4 Inch Stresskin Test Panel Outer Surface, 3 x 5 x 0.25 In. Fragment, 566 FPS Impact Velocity	118
60	3/4 Inch Stresskin Test Panel Inner Surface, 3 x 5 x 0.25 In. Fragment, 767 FPS Impact Velocity	119
61	3/4 Inch Stresskin Test Panel Outer Surface, 3 x 5 x 0.25 In. Fragment, 767 FPS Impact Velocity	120
62	3/4 Inch Stresskin Test Panel Inner Surface, 3 x 5 x 0.25 In. Fragment, 952 FPS Impact Velocity	121
63	3/4 Inch Stresskin Test Panel Outer Surface, 3 x 5 x 0.25 In. Fragment, 952 FPS Impact Velocity	122
64	3/4 Inch Stresskin Test Panel Inner Surface 3 x 5 x 0.25 In. Fragment, 815 FPS Impact Velocity	123
65	3/4 Inch Stresskin Test Panel Outer Surface, 3 x 5 x 0.25 In. Fragment, 815 FPS Impact Velocity	124

LIST OF ILLUSTRATIONS (Cont'd)

Figure		Page
66	3/4 Inch Stresskin Test Panel Inner Surface, 3 x 5 x 0.25 In. Fragment, 1138 FPS Impact Velocity	125
67	3/4 Inch Stresskin Test Panel Outer Surface, 3 x 5 x 0.25 In. Fragment, 1138 FPS Impact Velocity	126
68	3/4 Inch Stresskin Test Panel Inner Surface, 3 x 5 x 0.25 In. Fragment, 1006 FPS Impact Velocity	127
69	3/4 Inch Stresskin Test Panel Outer Surface, 3 x 5 x 0.25 In. Fragment, 1006 FPS Impact Velocity	128
70	Normal Shot Test Setup	131
71	Energy vs Velocity^2, Normal Impingement, 3/4 In. Stresskin	132
72	3/4 Inch Stresskin Test Panel, Inner Surface, 3 x 5 x 0.25 In. Fragment, 562 FPS Impact Velocity	133
73	3/4 Inch Stresskin Test Panel, Outer Surface, 3 x 5 x 0.25 In. Fragment, 562 FPS Impact Velocity	134
74	3/4 Inch Stresskin Test Panel, Inner Surface, 3 x 5 x 0.25 In. Fragment, 766 FPS Impact Velocity	135
75	3/4 Inch Stresskin Test Panel, Outer Surface, 3 x 5 x 0.25 In. Fragment, 766 FPS Impact Velocity	136
76	3/4 Inch Stresskin Test Panel, Inner Surface, 3 x 5 x 0.25 In. Fragment, 965 FPS Impact Velocity	137
77	3/4 Inch Stresskin Test Panel, Outer Surface, 3 x 5 x 0.25 In. Fragment, 965 FPS Impact Velocity	138
78	3/4 Inch Stresskin Test Panel, Inner Surface, 4 x 7 x 0.25 In. Fragment, 627 FPS Impact Velocity	139
79	3/4 Inch Stresskin Test Panel, Outer Surface. 4 x 7 x 0.25 In. Fragment, 627 FPS Impact Velocity	139
80	3/4 Inch Stresskin Normal Impact Test Setup, Front View, Prior to Test Shot with 4 x 7 x 0.25 In. Fragment at 627 FPS Impact Velocity	140
81	3/4 Inch Stresskin Normal Impact Test Setup, Back View, 4 x 7 x 0.25 In. Fragment at 627 FPS Impact Velocity	140

LIST OF ILLUSTRATIONS (Cont'd)

Figure		Page
82	3/4 Inch Stresskin Test Panel, Inner Surface, 4 x 7 x 0.25 In. Fragment, 938 FPS Impact Velocity	141
83	3/4 Inch Stresskin Test Panel, Outer Surface, 4 x 7 x 0.25 In. Fragment, 938 FPS Impact Velocity	141
84	Energy vs Velocity^2 - 2 Inch Aluminum Honeycomb, Tangential Impingement, 1.1 Lb. Fragment	144
85	Energy vs Velocity2 - Tangential Impingement, 2 Inch Aluminum Honeycomb, .55 Lb. Fragment	145
86	2 Inch Aluminum Honeycomb Test Panel, Outer Surface, 4 x 7 x 0.25 In. Fragment, 615 FPS Impact Velocity	146
87	2 Inch Aluminum Honeycomb Test Panel, Outer Surface, 4 x 7 x 0.25 In. Fragment, 615 FPS Impact Velocity	146
88	2 Inch Aluminum Honeycomb Test Panel, Outer Surface, 4 x 7 x 0.25 In. Fragment, 474 FPS Impact Velocity	147
89	2 Inch Aluminum Honeycomb Test Panel, Outer Surface, 4 x 7 x 0.25 In. Fragment, 474 FPS Impact Velocity	147
90	2 Inch Aluminum Honeycomb Test Panel, Inner Surface, 4 x 7 x 0.25 In. Fragment, 745 FPS Impact Velocity	148
91	2 Inch Aluminum Honeycomb Test Panel, Outer Surface, 4 x 7 x 0.25 In. Fragment, 745 FPS Impact Velocity	148
92	2 Inch Aluminum Honeycomb Test Panel, Inner Surface, 4 x 7 x 0.25 In. Fragment, 902 FPS Impact Velocity	149
93	2 Inch Aluminum Honeycomb Test Panel, Outer Surface, 4 x 7 x 0.25 In. Fragment, 902 FPS Impact Velocity	149
94	2 Inch Aluminum Honeycomb Test Panel, Inner Surface, 4 x 7 x 0.25 In. Fragment, 569 FPS Impact Velocity	150
95	2 Inch Aluminum Honeycomb Test Panel, Outer Surface, 4 x 7 x 0.25 In. Fragment, 569 FPS Impact Velocity	150
96	3/4 Inch Aluminum Honeycomb Test Panel, Inner Surface, 4 x 7 x 0.25 In. Fragment, 427 FPS Impact Velocity	153
97	3/4 Inch Aluminum Honeycomb Test Panel, Outer Surface, 4 x 7 x 0.25 In. Fragment, 427 FPS Impact Velocity	153

LIST OF ILLUSTRATIONS (Cont'd)

Figure		Page
98	3/4 Inch Aluminum Honeycomb Test Panel, Inner Surface, 4 x 7 x 0.25 In. Fragment, 751 FPS Impact Velocity	154
99	3/4 Inch Aluminum Honeycomb Test Panel, Outer Surface, 4 x 7 x 0.25 In. Fragment, 751 FPS Impact Velocity	154
100	3/4 Inch Aluminum Honeycomb Test Panel, Inner Surface, 4 x 7 x 0.25 In. Fragment, 367 FPS Impact Velocity	155
101	3/4 Inch Aluminum Honeycomb Test Panel, Outer Surface, 4 x 7 x 0.25 In. Fragment, 367 FPS Impact Velocity	155
102	Flat Panel Test Setup	159
103	Absorbed Energy vs Thickness, 3 x 5 x 0.25 In. Fragment Impacted Upon Flat Steel Sheet	161
104	Absorbed Energy vs Thickness^2, 3 x 5 x 0.25 In. Fragment Impacted Upon Flat Steel Sheet	162
105	.033 In. Stainless Steel Sheet Test Setup, 3 x 5 x 0.25 In. Fragment at 443 FPS Impact Velocity	163
106	.033 In. Stainless Steel Sheet Test Panel, Back Surface, 3 x 5 x 0.25 In. Fragment, 443 FPS Impact Velocity	163
107	.038 In. Stainless Steel Test Panel, Front Surface, 3 x 5 x 0.25 In. Fragment, 471 FPS Impact Velocity	164
108	.038 In. Stainless Steel Test Panel, Back Surface, 3 x 5 x 0.25 In. Fragment,471 FPS Impact Velocity	164
109	.062 In. Stainless Steel Test Panel, Front Surface, 3 x 5 x 0.25 In. Fragment, 780 FPS Impact Velocity	165
110	.062 In. Stainless Steel Test Panel, Back Surface, 3 x 5 x 0.25 In. Fragment, 780 FPS Impact Velocity	165
111	.088 In. Stainless Steel Test Panel, Front Surface, 3 x 5 x 0.25 In. Fragment, 1006 FPS Impact Velocity	166
112	.088 In. Stainless Steel Test Panel, Back Surface, 3 x 5 x 0.25 In. Fragment, 1006 FPS Impact Velocity	166
113	Back Stop Fence After B-121-16 Test Shot	167

LIST OF ILLUSTRATIONS (Cont'd)

Figure		Page
114	.081 In. Shainless Steel Test Panel, Front Surface, 3 x 5 x 0.25 In. Fragment, 591 FPS Impact Velocity	168
115	.081 In. Stainless Steel Test Panel, Back Surface, 3 x 5 x 0.25 In. Fragment, 591 FPS Impact Velocity	168
116	0.127 In. Stainless Steel Test Panel, Front Surface, 3 x 5 x 0.25 In. Fragment, 990 FPS Impact Velocity	169
117	0.127 In. Stainless Steel Test Panel, Rack Surface, 3 x 5 x 0.25 In. Fragment, 990 FPS Impact Velocity	169
118	0.127 In. Stainless Steel Test Panel, Front Surface, 3 x 5 x 0.25 In. Fragment, 826 FPS Impact Velocity	170
119	0.127 In. Stainless Steel Test Panel, Back Surface, 3 x 5 x 0.25 In. Fragment, 826 FPS Impact Velocity	170
120	Typical Fan Blade Fragments from In-Service Fan Blade Failure	171
121	0.127 In. Stainless Steel Test Panel, Front Surface, 4 x 7 x 0.25 In. Fragment, 525 FPS Impact Velocity	174
122	0.127 In. Stainless Steel Test Panel, Rack Surface, 4 x 7 x 0.25 In. Fragment, 525 FPS Impact Velocity	174
123	0.127 In. Stainless Steel Test Panel, Front Surface, 4 x 7 x 0.25 In. Fragment, 614 FPS Impact Velocity	175
124	0.127 In. Stainless Steel Test Panel, Back Surface, 4 x 7 x 0.25 In. Fragment, 614 FPS Impact Velocity	175
125	0.127 In. Stainless Steel Test Panel, Front Surface, 4 x 7 x 0.25 In. Fragment, 746 FPS Impact Velocity	176
126	0.127 In. Stainless Steel Test Panel, Rack Surface, 4 x 7 x 0.25 In. Fragment, 746 FPS Impact Velocity	176
127	Laminated Stainless Steel Test Panel, .048 In. Face Sheet with .040 Backup Sheet, Front Surface, 3 x 5 x .025 In. Fragment, 749 FPS Impact Velocity	179
128	Laminated Stainless Steel Test Panel, .048 In. Face Sheet with Backup Sheet, Back Surface, 3 x 5 x 0.25 In. Fragment, 749 FPS Impact Velocity	179

LIST OF ILLUSTRATIONS (Cont'd)

Figure		Page
129	Skewed Shot Test Setup	182
130	Fragment for Skewed Shot Mounted Onto Sabot	183
131	.050 In. Stainless Steel Test Panel, Inner Surface, 3 x 5 x 0.25 In. Fragment, 755 FPS Impact Velocity	184
132	.050 In. Stainless Steel Test Panel, Outer Surface, 3 x 5 x 0.25 In. Fragment, 755 FPS Impact Velocity	184
133	.063 In. Stainless Steel Test Panel, Inner Surface, 3 x 5 x 0.25 In. Fragment, 760 FPS Impact Velocity	185
134	.063 In. Stainless Steel Test Panel, Outer Surface, 3 x 5 x 0.25 In. Fragment, 760 FPS Impact Velocity	185
135	Kevlar Shroud Test Setup	192
136	Containment with Kevlar Armor Strap Assy. Reinforcing 3/4 In. Steel Stresskin. 4 x 7 x 0.25 In. Fragment with 4 In. Width Parallel to Target Surface. Looking Upstream to Trajectory.	193
137	Containment with Kevlar Armor Strap Assy. Reinforcing 3/4 In. Steel Stresskin. 4 x 7 x 0.25 In. Fragment with 4 In. Width Parallel to Target Surface. Looking Downstream to Trajectory.	193
138	Edge View of Kevlar Armor Strap Assy. with Contained Fragment 4 x 7 x 0.25 In. Fragment with 4 In. Width Parallel to Target Surface, 903 FPS Impact Velocity	194
139	Kevlar Armor Strap Assy. with Layers Folded Back to Expose Contained Fragment. 4 x 7 x 0.25 In. Fragment with 4 In. Width Parallel to Target Surface, 903 FPS Impact Velocity	194
140	3/4 Inch Steel Stresskin Reinforced with Kevlar Armor Strap Assy., Inner Surface, 4 x 7 x 0.25 In. Fragment with 4 In. Width Parallel to Target Surface, 903 FPS Impact Velocity	195
141	Containment with Kevlar Armor Strap Reinforcing 3/4 In. Steel Stresskin. 4 x 7 x 0.25 In. Fragment with 0.25 In. Edge Parallel to Target Surface. Looking Downstream to Trajectory.	195

LIST OF ILLUSTRATIONS (Cont'd)

Figure		Page
142	Containment with Kevlar Armor Strap Assy. Reinforcing 3/4 In. Steel Stresskin. 4 x 7 x 0.25 In. Fragment with 0.25 In. Edge Parallel to Target Surface. Looking Upstream to Trajectory	196
143	Inner Surface of 3/4 In. Steel Stresskin Reinforced by Kevlar Armor Strap Assy. 4 x 7 x 0.25 In. Fragment with 0.25 In. Edge Parallel to Target Surface, 903 FPS Impact Velocity	196
144	Inner Surface of Kevlar Armor Strap Assy. After Containment of 4 x 7 x 0.25 In. Fragment with 0.25 In. Edge Parallel to Target Surface	197
145	Kevlar Armor Strap Assy. with Layers Folded Back to Expose Contained Fragment. 4 x 7 x 0.25 In. Fragment with 0.25 In. Edge Parallel to Target Surface	197
146	Containment with Kevlar Armor Strap Assy. Reinforcing 2 In. Aluminum Honeycomb. 4 x 7 x 0.25 In. Fragment with 0.25 In. Edge Parallel to Target Surface. Looking Downstream to Trajectory.	198
147	Containment with Kevlar Armor Strap Assy. Reinforcing 2 In. Aluminum Honeycomb. 4 x 7 x 0.25 In. Fragment with 0.25 In. Width Parallel to Target Surface. Looking Upstream to Trajectory.	198
148	Inner Surface of 2 In. Aluminum Honeycomb Reinforced by Kevlar Armor Strap Assy. 4 x 7 x 0.25 In. Fragment with 0.25 In. Edge Parallel to Target Surface. 898 FPS Impact Velocity	199
149	Inner Surface of Kevlar Armor Strap Assy. with 4 x 7 x 0.25 In. Fragment Shot with 0.25 In. Edge Parallel to Target Surface	199
150	Non-Containment of 4 x 7 x 0.25 In. Fragment Shot with 4 In. Width Parallel to Target Surface. 2 In. Aluminum Honeycomb Target Reinforced by Kevlar Armor Strap Assy. 895 FPS Impact Velocity.	200
151	Inner Surface, 2 In. Aluminum Honeycomb Reinforced by Kevlar Armor Strap Assy. 4 x 7 x 0.25 In. Fragment Shot with 4 In. Width Parallel to Target Surface. Failed to Contain.	200

LIST OF ILLUSTRATIONS (Cont'd)

Figure		Page
152	Outer Surface of 2 In. Aluminum Honeycomb After Removal of Reinforcing Kevlar Armor Strap Assy. 4 x 7 x 0.25 In. Fragment Shot with 4 In. Width Parallel to Target Surface. Containment Unsuccessful.	201
153	Inner Surface of Kevlar Armor Strap Assy. After Unsuccessful Containment of 4 x 7 x 0.25 In. Fragment Shot with 4 In. Width Parallel to Target Surface Made of 2 In. Aluminum Honeycomb.	201
154	Internal Layers of Kevlar Armor Strap Assy. After Unsuccessful Containment of 4 x 7 x 0.25 In. Fragment Shot with 4 In. Width Parallel to Target Surface Made of 2 In. Aluminum Honeycomb.	202
155	Containment with Kevlar Armor Strap Assy. and .050 In. Annealed Stainless Steel Reinforcing Sheet Backing Up 2 In. Aluminum Honeycomb. Looking at Outer Surface of Strap Assy. Downstream to Trajectory.	203
156	Containment with Kevlar Armor Strap Assy. and .050 In. Annealed Stainless Steel Reinforcing Sheet Backing Up 2 In. Aluminum Honeycomb. Looking Normal to Outer Surface of Strap Assy. at Point of Fragment Arrestment.	203
157	Inner Surface of 2 In. Aluminum Honeycomb Panel Reinforced by .050 In. Annealed Stainless Steel Sheet and Kevlar Armor Strap Assy. Successful Containment.	204
158	Outer Surface of 2 In. Aluminum Honeycomb Panel with Reinforcing .050 Steel Sheet and Kevlar Armor Strap Assy. Successful Containment.	204
159	Kevlar Armor Strap Assy. and .050 In. Annealed Stainless Steel Reinforcing Sheet After Disassembly.	205
160	Kevlar Armor Strap Assy. with Layers Folded Back to Expose Contained Fragment. Note, Steel Material Punched from .050 In. Steel Reinforcing Sheet Wrapped Around Edge of Fragment.	205
161	Containment with Kevlar Armor Strap Assy. and .050 In. Heat Treated Stainless Steel Reinforcing Sheet Backing Up 2 In. Aluminum Honeycomb. Looking at Outer Surface of Strap Assy. Downstream of Trajectory.	206

LIST OF ILLUSTRATIONS (Cont'd)

Figure		Page
162	Containment with Kevlar Armor Strap Assy. and .050 In. Heat Treated Stainless Steel Reinforcing Sheet Backing Up 2 In. Aluminum Honeycomb. Looking at Outer Surface of Strap Assy. at Point of Fragment Arrestment.	206
163	Kevlar Armor Strap Assy. and .050 In. Heat Treated Stainless Steel Reinforcing Sheet After Disassembly.	207
164	Inner Surface of 2 In. Aluminum Honeycomb Panel Reinforced by .050 In. Heat Treated Stainless Steel Sheet and Kevlar Armor Strap Assy.	207
165	Outer Surface of 2 In. Aluminum Honeycomb Panel with Reinforcing .050 In. Heat Treated Stainless Steel Sheet and Kevlar Armor Strap Assy. Removed.	208

LIST OF TABLES

Table		Page
1	Energy Levels for Rotor Stages of JT9D-59A	11
2	Energy Levels for Rotor Stages of CF6-50	12
3	Armor Plate Weight Installation Factors	37
4	Armor Installation Weights for Single Blade Failure	38
5	Armor Installation Weights for Two Blade Failure	39
6	Armor Installation Weights for Four Blade Failure	40
7	Total Armor Weight - JT9D Engine Installation	41
8	Total Armor Weight - CF6-50 Engine Installation	42
9	Weight Comparison for Various Installation Locations for Fire Extinguisher System Armor Protection	54
10	Steel Inlet Armor for the CF6 Wing Engine on a 3 Engine Airplane (assuming no energy absorbed by the inlet material)	65
11	Steel Armor for the CF6 Engine on a 4 Engine Airplane (assuming no energy absorbed by the inlet material)	65
12	Steel Inlet Armor for Wing Engines on a 3 Engine Airplane (accounting for fragment energy absorbed by inlet material)	68
13	Steel Inlet Armor Required for a 4 Engine Airplane (accounting for fragment energy absorbed by inlet material)	69
14	Steel Armor Required For Tail Inlet for the CF6 Powered 3 Engine Airplane (assumes no energy absorbed by the inlet material)	70
15	Steel Armor Required for the Inlet for CF6 Powered 3 Engine Airplane (allowance made for energy absorbed by the inlet material)	72
16	Total Weight for Inlet Armor for Non-Interchangeable and Interchangeable Armor Installations - 3 Engine CF6 Powered Airplane	73

LIST OF TABLES (continued)

Table		Page
17	Total Weight for Inlet Armor for Non-Interchangeable and Interchangeable Armor Installations - 4 Engine CF6 Powered Airplanes	73
18	Armor For Wing Inlet 3 Engine JT9D Powered Airplane (assumes no fragment energy absorbed by inlet material)	81
19	Armor for Inlets - 4 Engine JT9D Powered Airplane (assumes no fragment energy absorbed by inlet material)	82
20	Wing Engine Armor Thickness Required (accounting for fragment energy absorbed by inlet material)	83
21	Armor for Wing Inlets 3 Engine JT9D Powered Airplane (accounts for fragment energy absorbed by inlet material)	84
22	Armor for Inlets - 4 Engine JT9D Powered Airplane (accounts for fragment energy absorbed by inlet material)	85
23	Armor for Tail (no. 2) Inlet - 3 Engine JT9D Powered Airplane (assumes no fragment energy absorbed by inlet material)	86
24	Tail Engine Armor Thickness Required (accounting for energy absorbed by inlet material)	87
25	Armor for Tail (no. 2) Inlet - 3 Engine JT9D Powered Airplane (accounting for energy absorbed by inlet material)	88
26	Total Weight for Inlet Armor for Non-Interchangeable and Interchangeable Armor Installations - 3 Engine JT9D Powered Airplane	88
27	Total Weight for Inlet Armor for Non-Interchangeable and Interchangeable Armor Installations - 4 Engine JT9D Powered Airplane	89
28	Blade Fragment Impact Test Summary	91
29	Factor Used to Establish Armor Weight	99
30	Test Results - Target - 3/4 Inch Thick Curved Steel Stresskin Panel, Fragment- 4 x 7 x 0.25 Inch Titanium Flat Plate, Tangential Impingement	102
31	Test Results - Target - 3/4 Inch Thick Curved Panel Steel Stresskin, Fragment - 3 x 5 x 0.25 Inch Titanium Flate Plate, Tangential Impingement	115

LIST OF TABLES

Table		Page
32	Test Results - Target - 3/4 Inch Thick Curved Steel Stresskin Panel, Fragment - 3 x 5 x 0.25 Inch Titanium Flat Plate, Fragment - 4 x 7 x 0.25 Inch Titanium Flat Plate, Normal Impingement	130
33	Test Results - Target - 2 Inch Thick Curved Aluminum Honeycomb Panel, Fragment - 4 x 7 x 0.25 Inch Titanium Flat Plate, Tangential Impingement	143
34	Test Results - Target - 3/4 Inch Curved Aluminum Honeycomb Panel, Fragment - 4 x 7 x 0.25 Inch Titanium Flate Plate, Normal Impingement, Run B-119-24 Tangential Impingement	152
35	Test Results - Target - Various Thicknesses of Sheet Stainless Steel Supported in a Steel Frame, Fragment 3 x 5 x 0.25 Inch Titanium Flat Plate, Fragment Impingement 60° from Normal	160
36	Test Results - Target - 0.127 Thick Sheet Stainless Steel Supported in a Steel Frame, Fragment - 4 x 7 x 0.25 Inch Titanium Flat Plate, Fragment Impingement 60° from Normal	173
37	Test Results - Target - Two Layers of Sheet Stainless Steel 0.048 Inch Thick on Impact Side and Backed Up with an 0.040 Sheet. Both Sheets Supported by a Steel Frame. Fragment - 3 x 5 x 0.25 Inch Titanium Flat Plate. Fragment Impingement 60° from Normal	178
38	Test Results - Target - Two Shots, One at 0.050 Inch Thick Curved Sheet Stainless Steel; the Other at .063 Inch Thick Curved Sheet Stainless Steel. Fragment - 3 x 5 x 0.25 Inch Titanium Flat Plate. Fragment Impingement Tangential to Target with Fragment Skewed 30°	181
39	Test Results - Target - 3/4 Inch Thick Steel Stresskin Curved Panel Backed with 6 2-Ply Kevlar Pads (Bonded in Silicone Rubber) and a 6-Ply Kevlar Strap (each ply Coated with Silicone Rubber), Fragment - 4 x 7 x 0.25 Inch Titanium Flat Plate, Tangential Impingement	190
40	Test Results - Target - 2-Inch Thick Aluminum Honeycomb Curved Panel Backed with 6 2-Ply Kevlar Pads (Bonded in Silicone Rubber) Fragment - 4 x 7 x 0.25 Inch Titanium Flat Plate, Tangential Impingement	191

LIST OF TABLES (Continued)

Tables		Page
41	Total Armor Weight for JT9D Powered Airplanes. Protected for 1, 2 and 4 Blade Failure. Armor Installed Close to Engine. Armored Nacelle and Engine Installation Not Interchangeable	209
42	Total Armor Weights for JT9D Powered Airplanes. Protected for 1, 2 and 4 Blade Failure. Armor Installed Close to Engine. Armored Nacelle and Engine Installation Interchangeable	210
43	1980 Fuel Cost for Additional Protection (Including Inlet Armor). Projected 1980 Fleet Size of 971 Wide Body Transports and Fuel at 50¢/Gallon	211
44	1980 - Fuel Cost for Providing Inlet Protection Only (Projected 1980 Fleet Size of 971 Wide Body Transports and Fuel at 50¢/Gallon)	212

1.0 SUMMARY

A study was conducted to provide some insight into the armor required and the penalties involved if engine blade fragment protection were installed in the engine nacelle or airframe on 3 and 4 engine wide body airplanes. Actual fragment impingement tests were accomplished to determine the energy absorption characteristics of various types of nacelle and inlet materials.

An evaluation was made of the fragment energy developed by 1 blade, 2 blades and included disc serrations, and 4 blades and included disc serrations, for all compressor and turbine stages on both the General Electric CF6 and Pratt & Whitney JT9D engines. With the energy known, it was found that both engines appeared to be able to marginally contain the 1 and 2 blade fragments in all compressor and turbine stages, but probably would not have adequate containment margin on some stages with the 4 blade fragment. If each blade were considered independently, each impacting at a different point on the case, full containment would probably be realized. The fan case thickness which is more directly influenced by containment considerations, was consistent with the one blade out design criteria. Containment of the 4 blade fan fragment would require the addition of a steel plate 1.212 inches thick at a weight ranging from 110 to 195 lbs per engine, depending on engine location. The consequence of the rotating unbalance of this level are of equal concern along with the containment issue. Additionally in actual experience, this case is unrealistic in that fan failures tend to be single blades plus pieces of others and are reduced in size by the containment/penetration action.

In that a companion FAA study is also being accomplished by an engine company to determine the weight involved in providing the specified protection integral with the engine, it was decided that this study should assume that all protection is provided by airframe installed armor and no fragment energy is absorbed by the engine. The engine study will include more stringent case penetration and rupture analysis treating the fragments

as partial disc failures rather than simple blade fragments and could show the engine containment method used here to be overly optimistic. However, the weight for the independent airframe supplied protection can be compared to the product of the engine study (which will be completed at some later date) to determine the relative weights for equivalent protection.

The results of the portion of this study involving armor installation show that if armor were to be installed it is important to install the armor as close to the engine case as possible to minimize the weight penalty. Fragments from the engine emanate from a relatively small apex angle at the engine case surface. A small amount of armor close to the engine can emcompass the apex and either absorb the fragment energy or deflect the fragment away from the airplane. If the armor is installed some distance from the engine, more armor area, hence increased weight, is required to subtend the fragment trajectory because of the large divergence angle from the engine case penetration apex to the airplane structure. The local installation of armor mounted externally on the engine may have a weight advantage over integral engine armor. Airframe or engine mounted armor installed close to the engines needs to cover only the rotor arc where a fragment trajectory intersects the airframe or adjacent engine. Engine integral armor generally covers a full 360° area around the engine. Local armor, however, compromises engine position interchangeability unless coverage is installed to handle all positions. Coverage for full interchangeability may be of such an extent that the weight advantage is largely cancelled particularly when accounting for the added mounting. Further, armor installed on the engine may restrict access to the engine and components and would require removal for inspection and maintenance.

Since during actual operation fan blade fragments have damaged inlet and airplane structure, considerable effort was expended in discussing the nature of these fragments and the energy absorption capabilities of the nacelle structure forward of the fan plane of rotation. Associated weight penalties for inlet protection were determined.

Test data from previous Douglas tests and from additional tests conducted under this FAA contract were used to establish armor thicknesses. Test data were required to establish energy absorption capabilities of airplane and nacelle structure and to verify empirical curves and equations. The test data were also helpful in understanding the mechanisms involved in fragment entrapment and energy absorption in a Kevlar aramid fiber material containment system.

Consideration of redundant armor independent of intrinsic engine protection represents an untenable weight penalty. From the estimated weight required to provide such specified additional protection in the nacelle and inlet, the fuel used to carry the additional armor was determined. The results show that in 1980, when the wide body airplanes will be accumulating about 10,000,000 engine hours/year, the 2500 lbs. and 3000 lbs. for armor on 3 and 4 engine aircraft respectively will result in consumption of 230,000,000 lbs. of fuel/year. At a projected cost of 50¢/gallon, this will cost over 17 million dollars per year. Provision of extended coverage for the inlet area forward of the engine fan case flange is probably a more realistic case. For this level of protection, the amount of fuel burned would be about 12,700,000 lbs/year at a cost of 1.0 million dollars/year. Both of these estimates are for interchangeable armor installations but disregard the effects of maintenance compromises and the reduction of aircraft payload required to carry the added weight.

In view of the adequacy of prevailing installation practices, further armor for the range of fragments considered would not appear to significantly enhance flight safety. While fan blade fragments that are initially contained then deflected forward of the engine do not affect the operation of remaining engines or jeopardize continued safety, they can produce undesirable and costly secondary damage which should be considered in its own light with respect to local protection.

2.0 INTRODUCTION

This investigation was conducted for the Aircraft Design Criteria Branch, Systems Research and Development Service of the Federal Aviation Administration under contract DOT FA76WA-3843.

The purpose of this investigation was to estimate the penalties associated with providing additional protection from uncontained engine failures by addition of armament in the airframe of wide body transports. Specifically evaluated are additional protection from uncontained failures resulting in a projectile,that is: a 3 x 5 inch fan blade tip, two adjacent blades including disc serrations from any stage, and four adjacent blades including serrations from any stage. The investigation was made on high bypass ratio turbofan engines which power wide body transports.

This investigation was conducted by the Douglas Aircraft Company components of the McDonnell Douglas Corporation from June 1976 through February 1977. Mr. C. O. Gunderson was the Douglas project engineer and Commander J. J. Shea was the FAA project manager.

3.0 STUDY DESCRIPTION

This investigation was conducted under contract to the Federal Aviation Administration (FAA) in response to the Request for Proposal No. LGR-6-5245 issued on 23 January 1976. This study evaluated the armor requirements that would be needed in current wide body transports if additional protection were to be provided from uncontained engine failures. The fragments for evaluation were specified by the FAA and are:

(1) 3 x 5 x .2 inch fan blade tip
(2) Two adjacent blades and their included serrations from any stage
(3) Four adjacent blades and their included serrations from any stage

In order to determine armor material requirements for additional protection, semi-empirical correlations and direct empirical results were used. Results from Douglas sponsored tests were used and, where deemed necessary for this investigation, these data were augmented by additional experiments conducted as a part of this FAA sponsored program.

The overall study approach is outlined below:

(1) The energy capability of the three specified fragments was determined for each appropriate stage of the JT9D-59 and CF6-50 engines. The energies were based on redline RPM as the limiting value for the highest takeoff thrust possible with the engine, and the highest fragment energies possible within the operating limits of the engine.

(2) The potential fragments trajectories were determined by making detailed layouts.

(3) The surface areas and locations for armor to prevent fragments from following the trajectories were determined for armor located on the engine or in the nacelle.

(4) Available data and methods were reviewed, tests were conducted to supplement available data and armor thickness and weight estimation methods were established.

(5) The weights for additional protection were estimated which included provisions for armor support. These weights were estimated for 3 and 4 engine wide body transports.

The analyses of this investigation is reported in 2 parts. These parts are: Section 4 which covers the analyses of the 2 and 4 blade fragments, and Section 5 which covers the fan blade tip fragments. Test activities which provided data for use in the analyses are described in Section 6.

4.0 MULTIPLE BLADE FRAGMENT EVALUATION

4.1 Uncontained Multiple Blade Fragment Energies

The energies for the FAA specified fragments were estimated for the highest thrust engines now in airline operation. These are the JT9D-59 and CF6-50. These engines will be in service for many years and therefore provide a logical study base. They represent the engines from the two U.S. manufacturers that power wide body airplanes in use by U.S. airlines. It was assumed that the failure which produced blade fragments occurred when the engines were operating at their design redline RPM. This represents the highest fragment energy condition within the engine operating limits and represents the takeoff thrust growth limit for the engine models studied. A pictoral representation of typical fragments is shown in Figure 1.

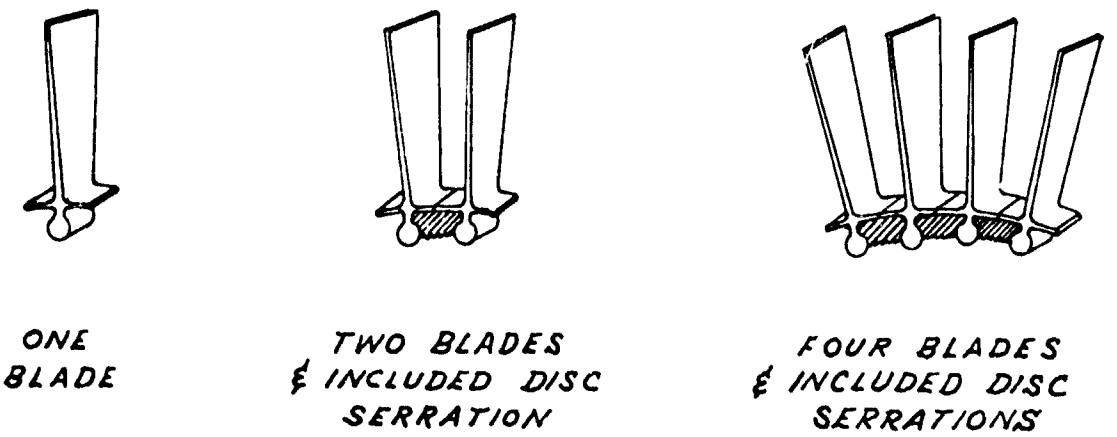

Figure 1
TYPICAL FRAGMENTS EVALUATED

Pratt & Whitney and General Electric provided scaled engine cutaway drawings showing the location of each stage and the dimensions, weights and center of gravity locations for each blade. Pratt and Whitney also provided the energy levels for the fragments with serrations. The Pratt & Whitney JT9D-59A engine cutaway is shown in Figure 2.

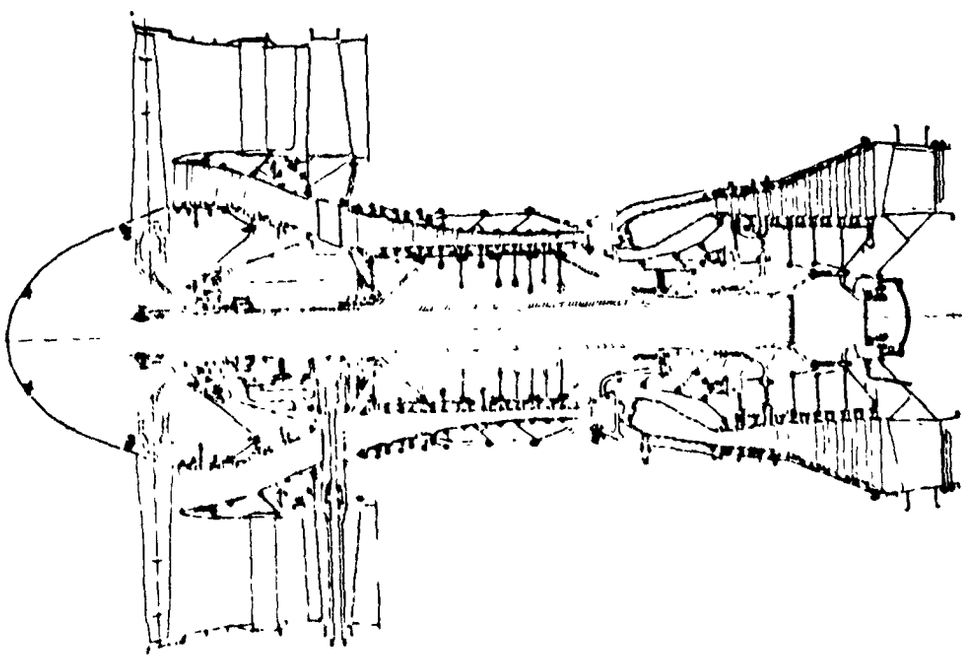

Figure 2

JT9D-59A ENGINE CUTAWAY

Figure 3 shows the General Electric CF6-50 engine cutaway.

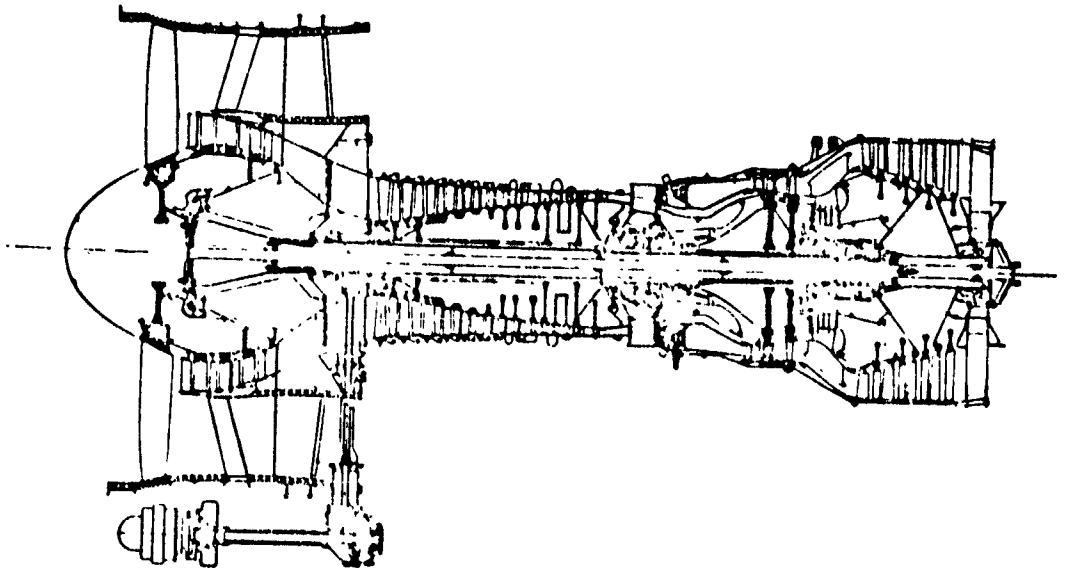

Figure 3. CF6-50 Engine Cutaway

The fragment energies at the time of failure were calculated from:

$$E = 1/2\ MV^2 = \frac{W}{2g}\ (2\pi rw)^2$$

where V = the velocity at the fragment center of gravity considering the blades and disc serrations as a single mass

M = Mass of the selected fragment and included disc serrations

g = gravitational constant

$w = \frac{RPM}{60}$ = revolutions/second at redline speed

r = radius from the center of rotation to the center of gravity of the fragment mass

W = weight of the selected fragment and disc serrations

The fragment energies for each stage of both engines from the fan, through the low compressor, high compressor, high turbine, and low turbine were determined. It was assumed that multiple blade fragments behaved as a single mass equivalent to the mass sum of all the pieces. Most of the containment literature concludes that fragments, especially the heavy fragments, will exit the engine in the plane of disc rotation and will have a rotation about the fragment center of gravity. Since the rotational energy of the fragment is low when compared to the translational energy, in this part of the study it was assumed that all the energy was in translation.

Table 1 shows the energy level of the study fragments for each rotor stage of the Pratt & Whitney JT9D-59A engine. These data were generated by Pratt & Whitney and provided to Douglas for this study.

Table 2 shows the energy levels for the CF6-50 engine. General Electric provided the data on weight and center of gravity of each blade. The additional weight for the disc serrations and the effect on the two and four blade center of gravity was assumed to be similar to the Pratt & Whitney engine. The GE data was therefore factored based on using the JT9D data to increase the weight and to reduce the center of gravity radius for determining fragment velocities.

TABLE I

ENERGY LEVELS FOR ROTOR STAGES OF JT9D-59 ENGINE

N_1 = 3780 RPM (REDLINE)
N_2 = 8011 RPM (REDLINE)

GROUP	STAGE	SINGLE ROTOR BLADE		2 BLADES & INCLUDED DISC SERRATIONS		4 BLADES & INCLUDED DISC SERRATIONS	
		WEIGHT (LB.)	ENERGY (FT-LB)	WEIGHT (LB.)	ENERGY (FT-LB)	WEIGHT (LB)	ENERGY (FT-LB)
FAN (N_1)	1	9.49	133,000	20.7	277,000	43.1	550,000
L.P. COMPRESSOR (N_1)	1.5	.217	1,840	.496	4,110	1.05	8,640
	2	.180	1,450	.398	3,150	.834	6,540
	3	.230	1,650	.498	3,470	1.03	7,160
	4	.263	1,480	.575	3,190	1.20	6,630
H.P. COMPRESSOR (N_2)	5	.253	3,610	.603	8,380	1.30	17,900
	6	.130	1,850	.290	4,060	.608	8,470
	7	.070	1,020	.155	2,220	.324	4,630
	8	.052	728	.113	1,570	.236	3,250
	9	.042	583	.091	1,250	.189	2,590
	10	.037	506	.081	1,100	.169	2,290
	11	.037	499	.082	1,090	.171	2,280
	12	.037	494	.084	1,110	.178	2,350
	13	.034	450	.083	1,080	.180	2,340
	14	.065	862	.144	1,890	.302	3,960
	15	.075	995	.170	2,230	.360	4,710
H.P. TURBINE (N_2)	1	.500	10,100	1.21	24,300	2.55	51,000
	2	.616	11,700	1.44	27,600	3.00	57,100
L.P. TURBINE (N_1)	3	.302	1,720	.637	3,570	1.31	7,260
	4	.460	2,620	.967	5,430	1.98	11,000
	5	.684	4,470	1.45	9,250	2.98	18,800
	6	.988	7,110	2.07	14,700	4.22	29,900

TABLE 2

ENERGY LEVELS FOR ROTOR STAGES OF CF6-50 ENGINE

N_1 = 3982 RPM (REDLINE)
N_2 = 10613 RPM (REDLINE)

GROUP	STAGE	SINGLE ROTOR BLADE		2 BLADES & INCLUDED DISC SERRATIONS		4 BLADES & INCLUDED DISC SERRATIONS	
		WEIGHT (LB.)	ENERGY (FT-LB)	WEIGHT (LB)	ENERGY (FT-LB)	WEIGHT (LB)	ENERGY (FT-LB)
FAN (N_1)	1	10.3	136,400	22.5	272,800	46.8	562,000
L.P. COMPRESSOR (N_1)	2	.445	3,690	.984	8,050	2.06	16,700
	3	.401	3,240	.887	7,060	1.86	14,600
	4	.363	2,640	.803	5,760	1.68	11,900
H.P. COMPRESSOR (N_2)	1	.352	5,170	.793	11,500	1.67	24,200
	2	.441	5,640	.993	12,500	2.09	26,400
	3	.209	2,603	.471	5,780	.992	12,200
	4	.137	1,820	.309	4,040	.650	8,520
	5	.110	1,580	.248	3,500	.522	7,390
	6	.073	1,070	.164	2,380	.347	5,020
	7	.064	1,020	.144	2,270	.304	4,780
	8	.053	867	.119	1,920	.252	4,060
	9	.046	810	.104	1,800	.218	3,790
	10	.070	1,210	.151	2,830	.332	5,970
	11	.052	981	.117	2,180	.247	4,590
	12	.055	1,090	.124	2,410	.261	5,080
	13	.053	1,010	.119	2,290	.252	4,740
	14	.053	1,010	.117	2,240	.247	4,730
H.P. TURBINE (N_2)	1	.566	15,100	1.35	35,900	2.82	77,300
	2	.844	21,300	2.01	50,700	4.21	109,000
L.P. TURBINE (N_1)	3	.400	3,010	.843	6,260	1.73	12,800
	4	.471	3,450	.993	7,170	2.03	14,600
	5	.520	3,550	1.10	7,380	2.24	15,000
	6	.710	4,400	1.50	9,160	3.06	18,700

The energies above are that due to engine rotation and do not account for any absorption that may occur during the failure process. One of the considerations in determining the potential fragment energies is the energy absorption due to engine case penetration.

An evaluation was therefore made to determine the degree of energy absorption to be expected from the case. The prediction of energy absorption capabilities of engine cases based on rigorous theoretical methods is complex and beyond the scope of this investigation. Experimental results were therefore used. A correlation between case thickness and energy absorption capability was established using data taken at the Watertown Arsenal under General Electric sponsorship, and data taken by Douglas. The Douglas tests and basis for the correlation are described in Section 6.4 of this report.

The correlation established is shown in Figure 4. Assuming the fragments directly impinged on the engine, the energy absorption for penetration was determined using the initial fragment energies and the engine case thicknesses. The engine cases are built such that several layers of material must be penetrated in some places, flanges may be in the fragment path, and sections are not of equal thickness. For multi-thickness, it was assumed as one thickness equivalent to the square root of the summation of the individual pieces squared. Half the flange thickness was assumed where a flange was located in a fragment path. Where the case was tapered the average thickness was used. The thickness and material in the area of each engine stage were obtained from engine cross sectional drawings.

In addition, since the correlation was based on stainless steel at room temperature, it was necessary to make corrections in areas where high case temperatures exist or where titanium or aluminum were used as the case material. It appears that the containment capability of a material is directly related to the material dynamic shear modulus. In this analysis, the containment capability of the equal thickness plate was reduced by the ratio of the dynamic shear modulus of each material to that of steel. This resulted in titanium casing developing a containment capability of 76.9% and aluminum 16.2%, compared to an equal thickness of stainless steel.

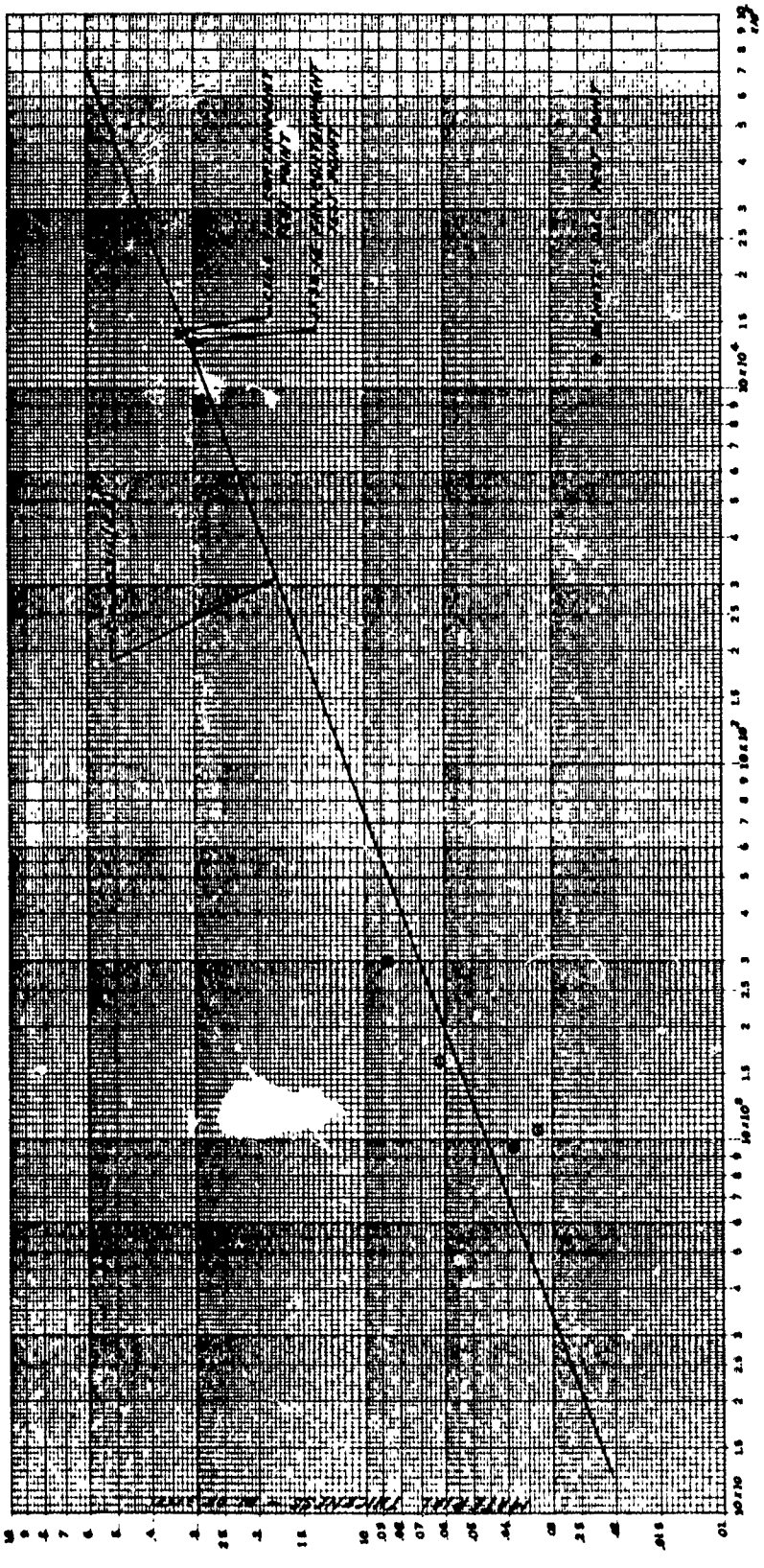

ENERGY ABSORBED ~ FT-LB

FIGURE 4 ENERGY ABSORBED VS MATERIAL THICKNESS

A correction was further made where the engine case is at elevated temperatures to account for the reduction in strength.

It was assumed for this containment evaluation that full containment was achieved even after all the engine case material in the path of the fragment had been penetrated, such as inner and outer cases, as long as the residual fragment energy was very near zero after penetrating the last layer of the engine case.

By this analysis it appeared that the engine cases of the JT9D and CF6 would be able to adequately contain the single blade fragment and could marginally contain the 2 blade compressor and turbine fragments but probably would not have adequate containment margin on some of the stages with the 4 blade fragments. If each blade were considered independently, each impacting at a different point on the case, full containment would probably be realized. The fan case was consistent with one blade out design criteria and would not contain multiple fan blades. However, the consequences of the rotating unbalance with the loss of 2 or 4 fan blades in adjacent positions are of equal concern along with the containment issue. Since it was not the intention of this study to evaluate the engine containment capability and the method used here to estimate containment could be an over simplification of a complex analysis, it was assumed that none of the energy developed by the fragments under consideration was absorbed by the engine structure and that any armor installed should be designed for the full impact energy developed by the fragments. A companion engine study sponsored by the FAA is now in progress to determine the weight involved in providing the specified protection integral with the engine. This engine study includes a more stringent case penetration and case rupture analysis which treats the fragments as partial disc failures rather than simple blade fragments. With the results of this study available, then the results of the companion engine study, being conducted by Pratt and Whitney, can be directly compared and the difference in methods of protection can be evaluated.

4.2 Airframe Exposure Areas

Layouts of a typical trijet with JT9D-59A engines installed and a quadjet with JT9D-70A engines installed are shown on Figures 5, 6 and 7. For purposes of this study, the JT9D-59A and the JT9D-70A engines and nacelles are identical. The physical difference is that there are fewer number of accessories mounted on the common gearbox of the JT9D-70A engine.

Superimposed on the airplane layouts are zones which define the trajectory paths which could be taken by any engine blade fragment directed toward the airplane structure or another engine. It was assumed that a fragment which exited beyond the limits of the aircraft structure or another engine would not impact the airframe and would only impinge the engine nacelle.

As shown on the airplane layouts, the fragment trajectories spread out from an apex starting out tangent to the engine rotor tip and covers areas of the fuselage and wing surface. Since all the engine spools rotate in the same direction, the fragments which impinge on the airplane from left wing mounted engines come from a tangent point near the top of the engine. The fragments from right wing mounted engines which are directed toward the airplane will emanate from the engine near the bottom tangent point. Any fragment directed outboard from either wing nacelle, will clear the wing by a large margin because engines are mounted well forward on pylons and the wings are swept back. On the tail engine, of the 3 engine airplane, fragments could impinge on portions of the horizontal stabilizer and rudder but the fragment trajectories are a considerable distance aft of the major portion of the horizontal and vertical spars and are even farther aft of the cabin pressure bulkhead. Directly below the tail engine is a non-pressurized, non-structural, fuselage tailcone fairing. On both the 3 and 4 engine airplanes, engine mounted on the right wing (inboard only on the 4 engine airplane) could produce fragments which may be directed under the fuselage and contact the left wing mounted engine. On the 4 engine airplane, because of the swept wings, engines mounted on the same wing do not offer a significant threat to each other. Fragments from the outboard engines could impinge on the turbine exhaust nozzle of the inboard engine but it's unlikely that any rotating parts would be hit. The wing

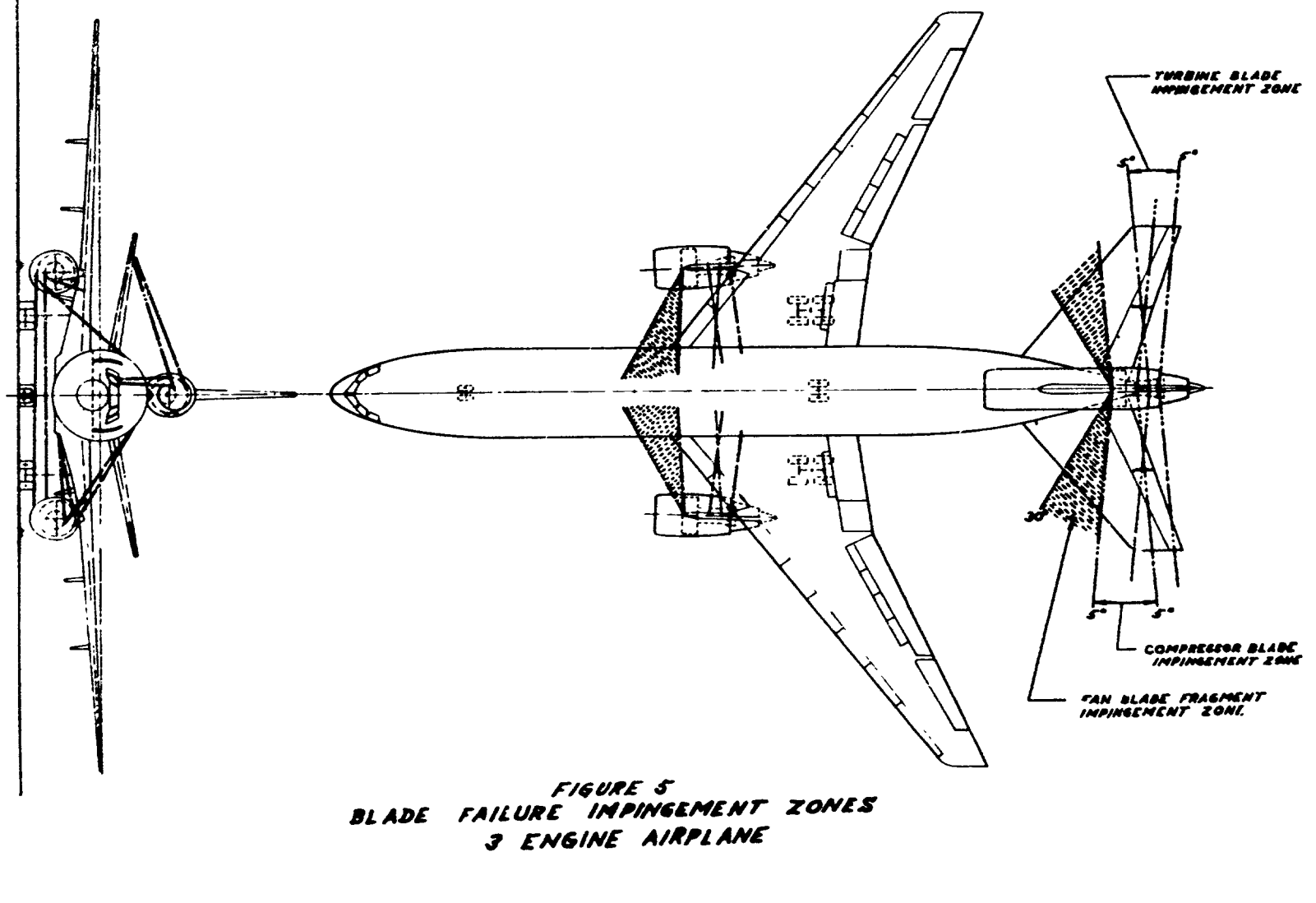

FIGURE 5
BLADE FAILURE IMPINGEMENT ZONES
3 ENGINE AIRPLANE

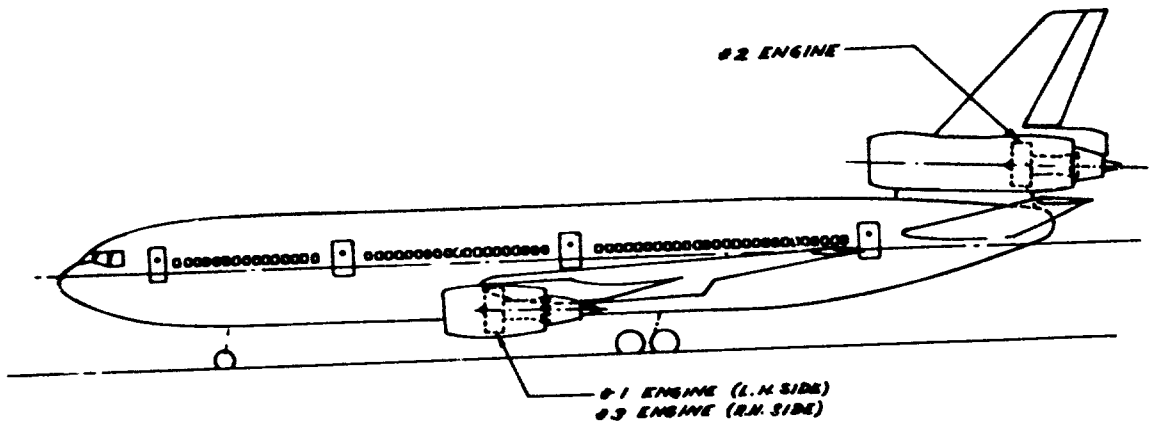

FIGURE 6
ENGINE ARRANGEMENT
3 ENGINE AIRPLANE

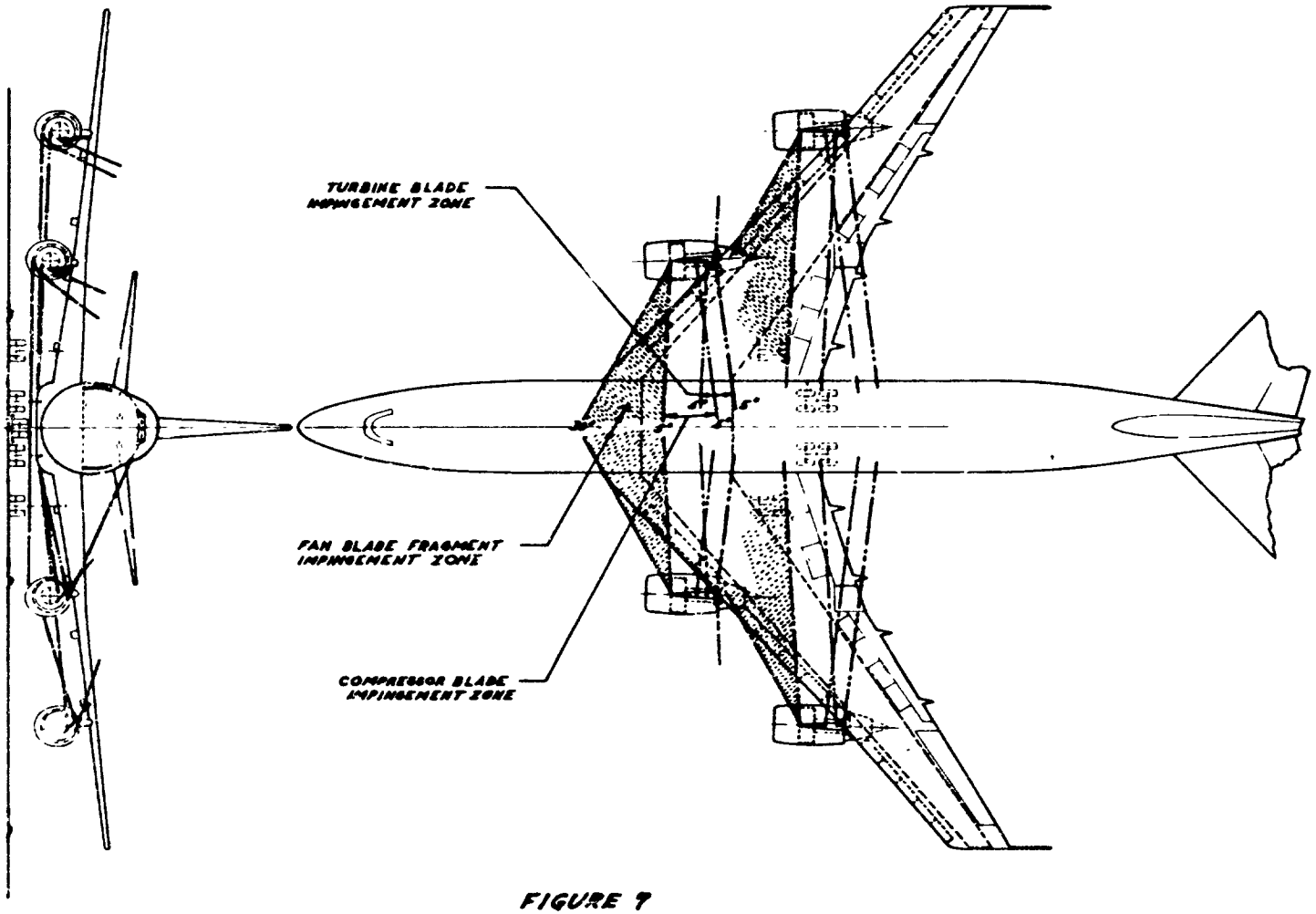

FIGURE 9
BLADE FAILURE IMPINGEMENT ZONES
4 ENGINE AIRPLANE

engines are toed in slightly (the engine centerline is not parallel to the fuselage centerline) and this effect on fragment trajectories is accounted for.

Reviewing the airplane front view shows that sections of the fuselage and wing can be exposed to fragments which emanate from a relatively small apex angle tangent to each engine.

Installing local armor (subtending the apex) on the engine or within the nacelle could effectively protect the fuselage or wing and would, in general, be expected to provide protection with maximum weight effectiveness.

The area shown on the layouts with double crosshatch covers the fragments generated by the fan. This area must be considered differently than for other rotors because of the small fragment size and the wide angle subtended (30° forward of fan plane). Inlet armor requirements to contain these fragments is described in Section 5.

In evaluating the need for additional protection, it is important to recognize design considerations in current aircraft. During the design phase of most airplanes considerable importance is given to the location of critical components. Whenever possible important components are located well out of the engine fragment trajectory path. If components must be located in this area, then every effort is made to take advantage of the protection possible by the basic airframe structure. This is done by mounting the component behind substantial spar caps, floor beams, heavy frames or behind other non-critical components. Where system runs must cross the fragment impingement areas, most often widely spaced redundant systems are employed.

A good example of protection by design of systems can be illustrated by examining Figures 8 and 9. These figures show how the critical systems are located within the CF6 engine support pylon with respect to engine fragment trajectories. Advantage is taken of the heavy spar caps on the lower pylon corner, heavy steel spar webs on the lower pylon surface and thick titanium side walls. The fragment impingement angle on the pylon side wall approaches 80° from normal and most fragments would be deflected without penetrating, this affords a high degree of protection for fuel and hydraulic lines as well as engine control cables. The fire extinguishing line and main pneumatic duct are well protected by being located within an arc subtended by the lower left hand corner spar cap. The installation of the JT9D has the same degree of protection by systems design.

4.3 Engine Installation Armor Weights

Detailed layout drawings were made to determine the armor area and weights for each engine if the additional protection were installed within the nacelle. The fragment trajectories established earlier were used to define the arc of potential fragments to determine armor areas. Armor application was considered close to the engine, in the inner fan duct wall, outer fan duct wall, fan cowl door, and in the inlet inner wall. Layouts were made for the left and right wing engine installations for the 3 and 4 engine airplanes and the tail engine installation of the 3 engine airplane. From these layouts, each armor plate segment was identified and the armor plate area determined. Armor was applied to each engine or nacelle to afford maximum airplane protection and it was applied in the optimum location depending on the position the engine was installed on the airplane. This meant that the engines and nacelles would not have position interchangeability in that an engine or nacelle armored for a left wing could not be used on the right wing without armor modification. However, the weight for interchangeable installations was also determined. The engine nacelle layouts used to determine the armor area are shown in Figure 10 through 13 for the JT9D three engine airplane and Figure 14 and 15 for the four engine airplane. Figure 16 through Figure 21 define the armor requirements for the CF6-50 engine.

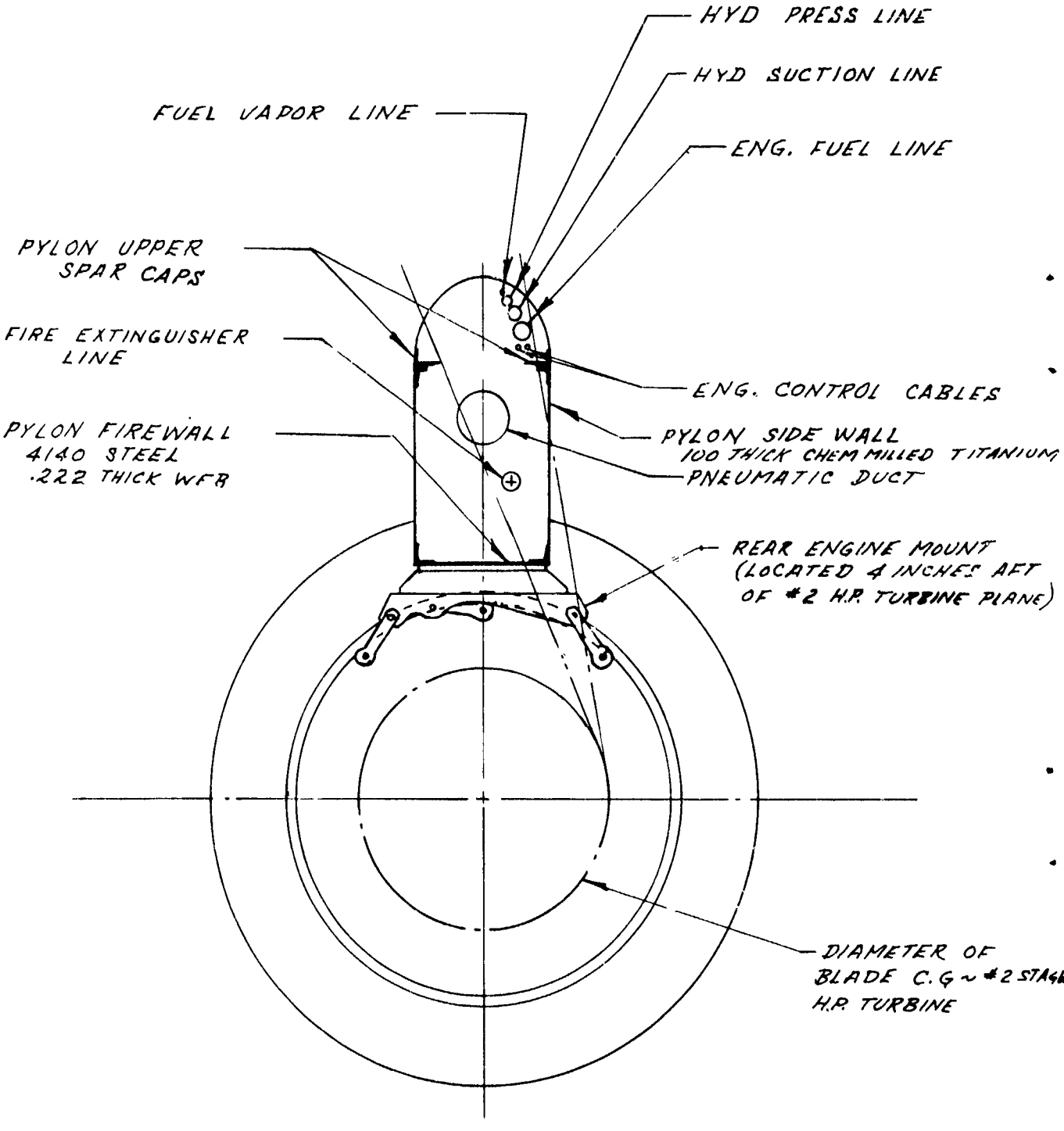

FIGURE 8

CF6-50 ENGINE INSTL.
NO. 2 H.P. TURBINE
IMPINGEMENT ZONE

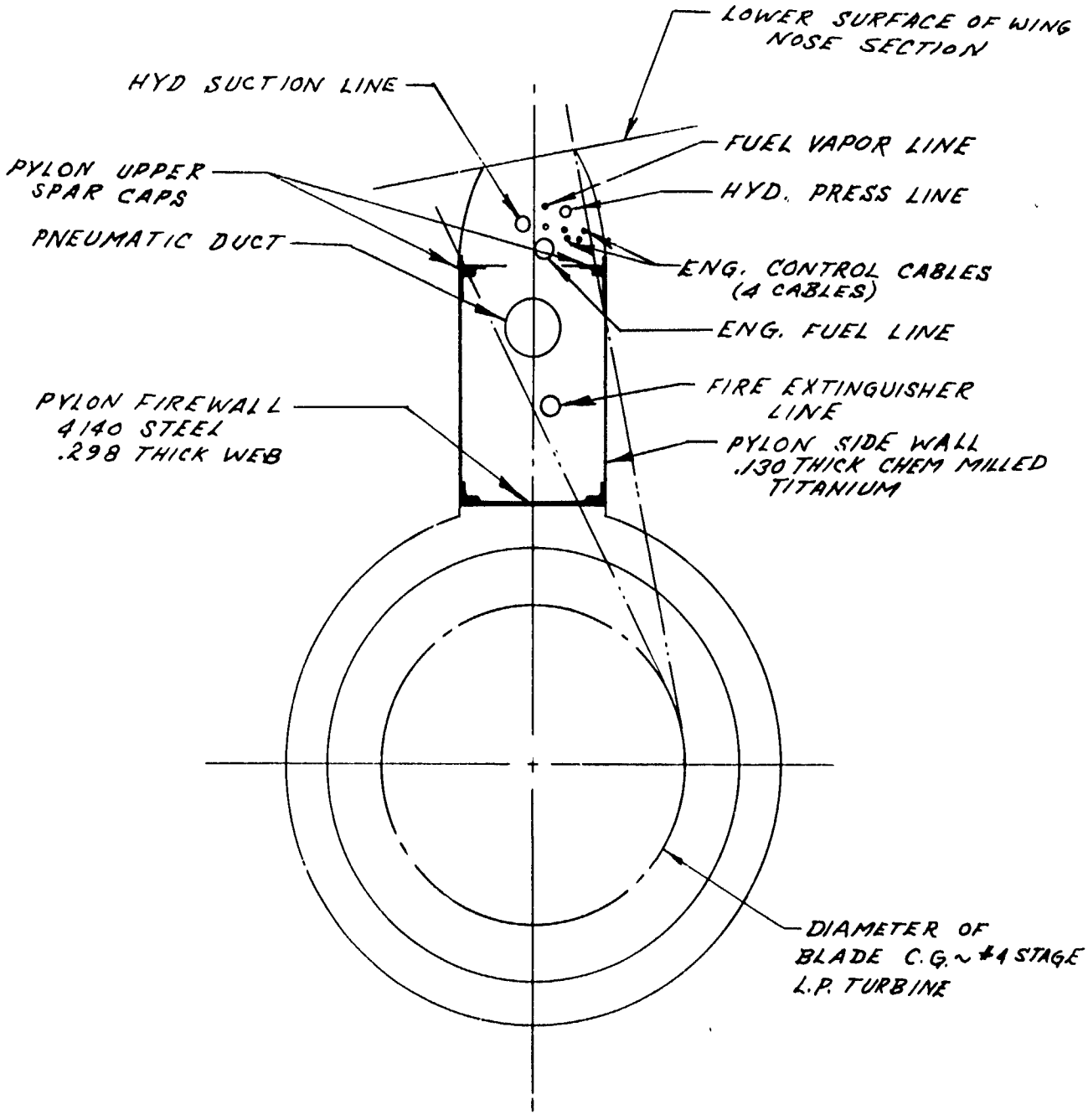

FIGURE 9
CF6-50 ENGINE INSTL.
NO. 4 L.P. TURBINE
IMPINGEMENT ZONE

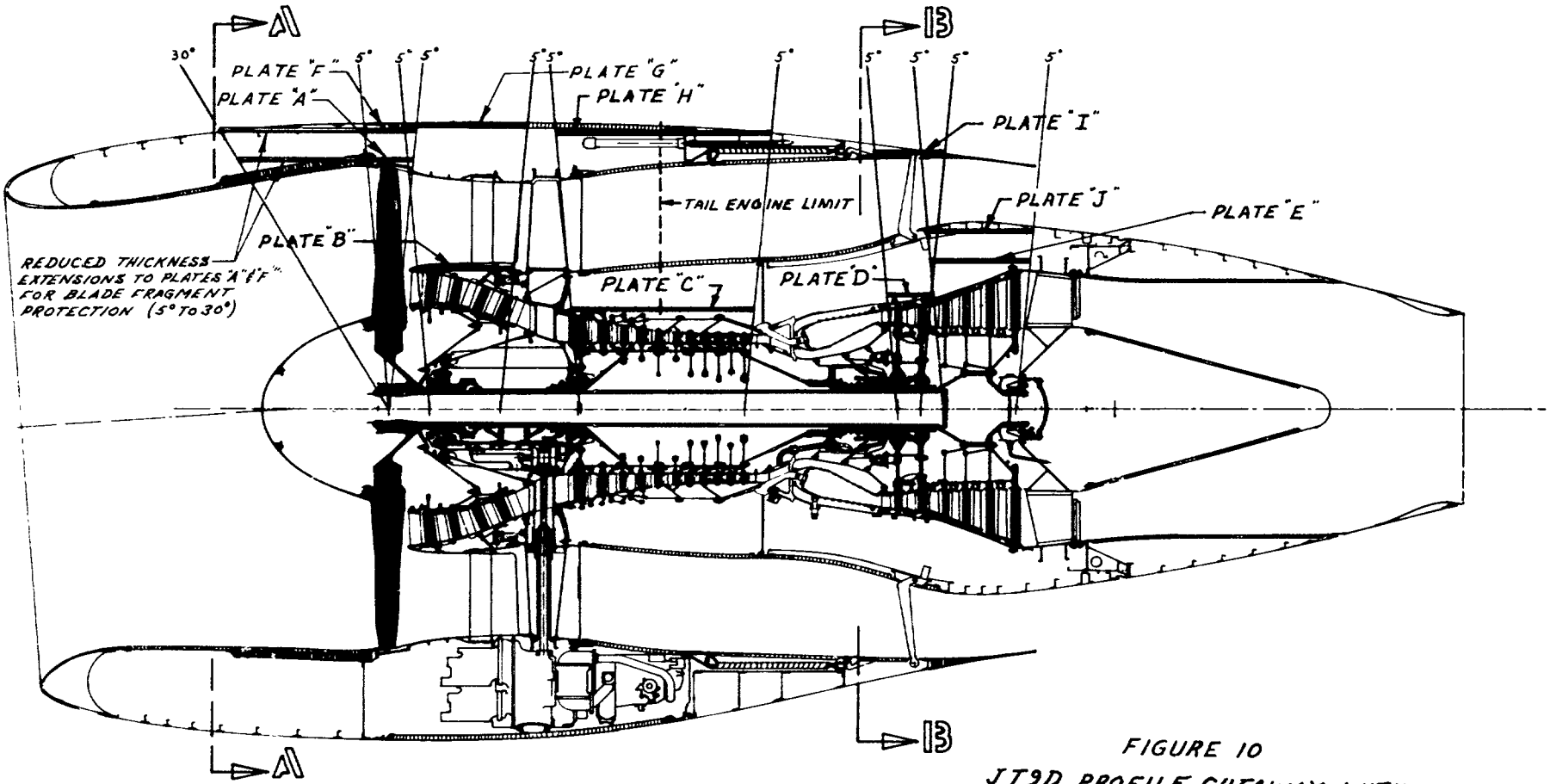

FIGURE 10
JT9D PROFILE CUTAWAY WITH ARMOR LOCATIONS

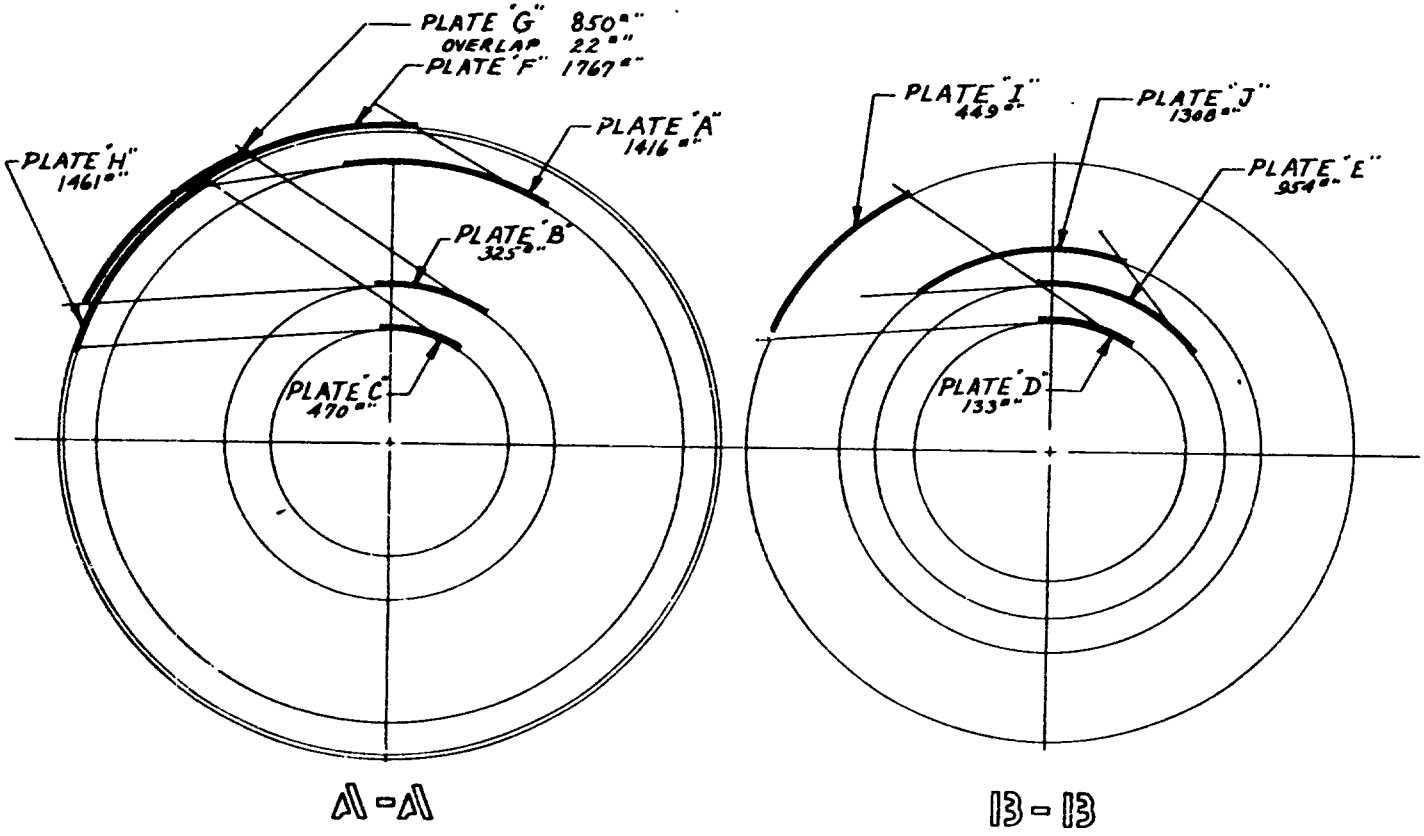

FIGURE 11
JT9D CROSS SECTION SHOWING ARMOR
FOR #1 ENGINE - 3 ENG. A/P

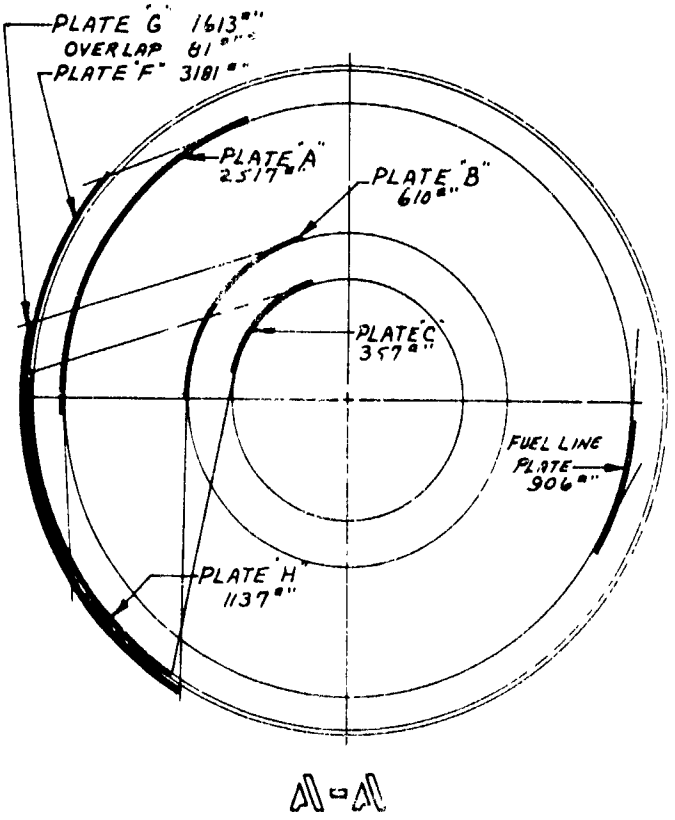

FIGURE 12
JT9D CROSS SECTION SHOWING ARMOR
FOR #2 ENGINE – 3 ENG. A/P

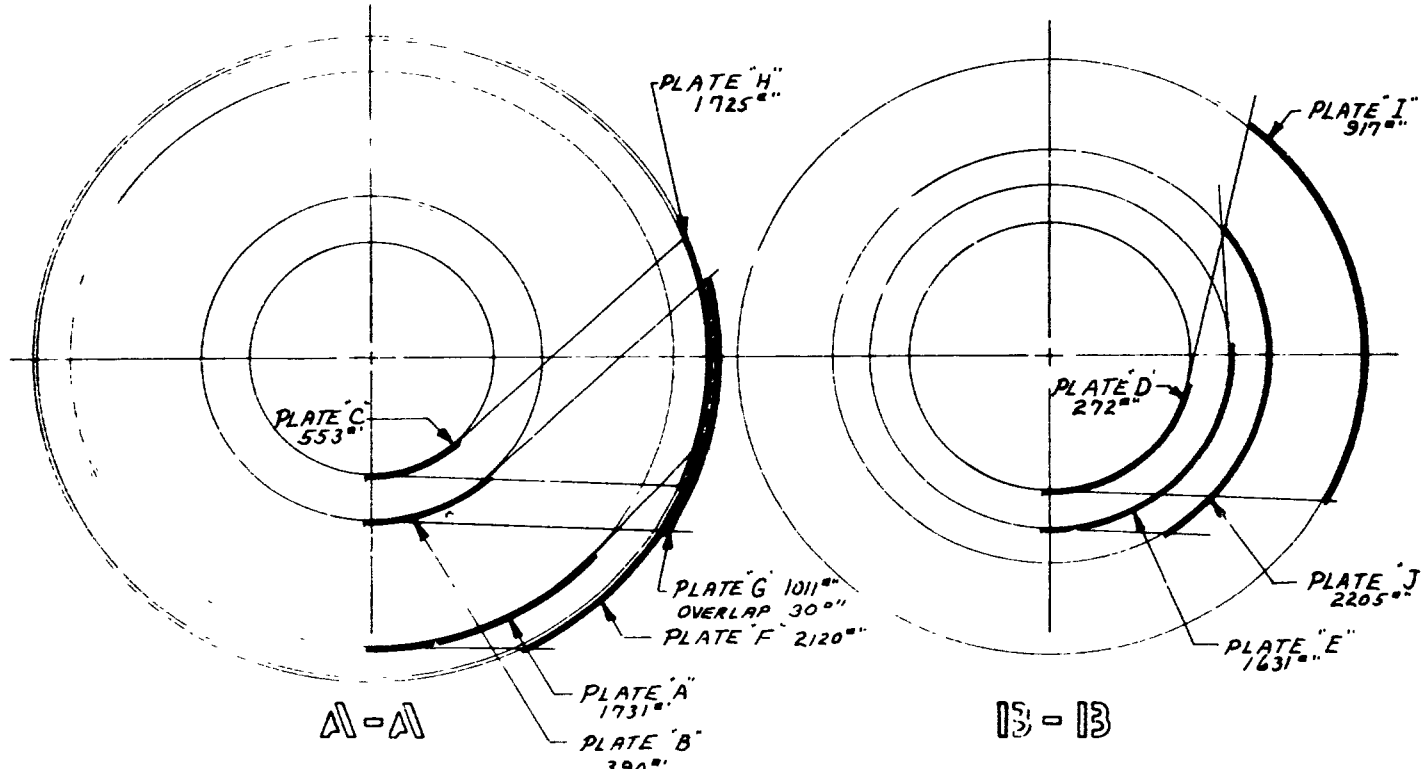

FIGURE 13
JT9D CROSS SECTION SHOWING ARMOR
FOR #3 ENGINE - 3 ENG. A/P

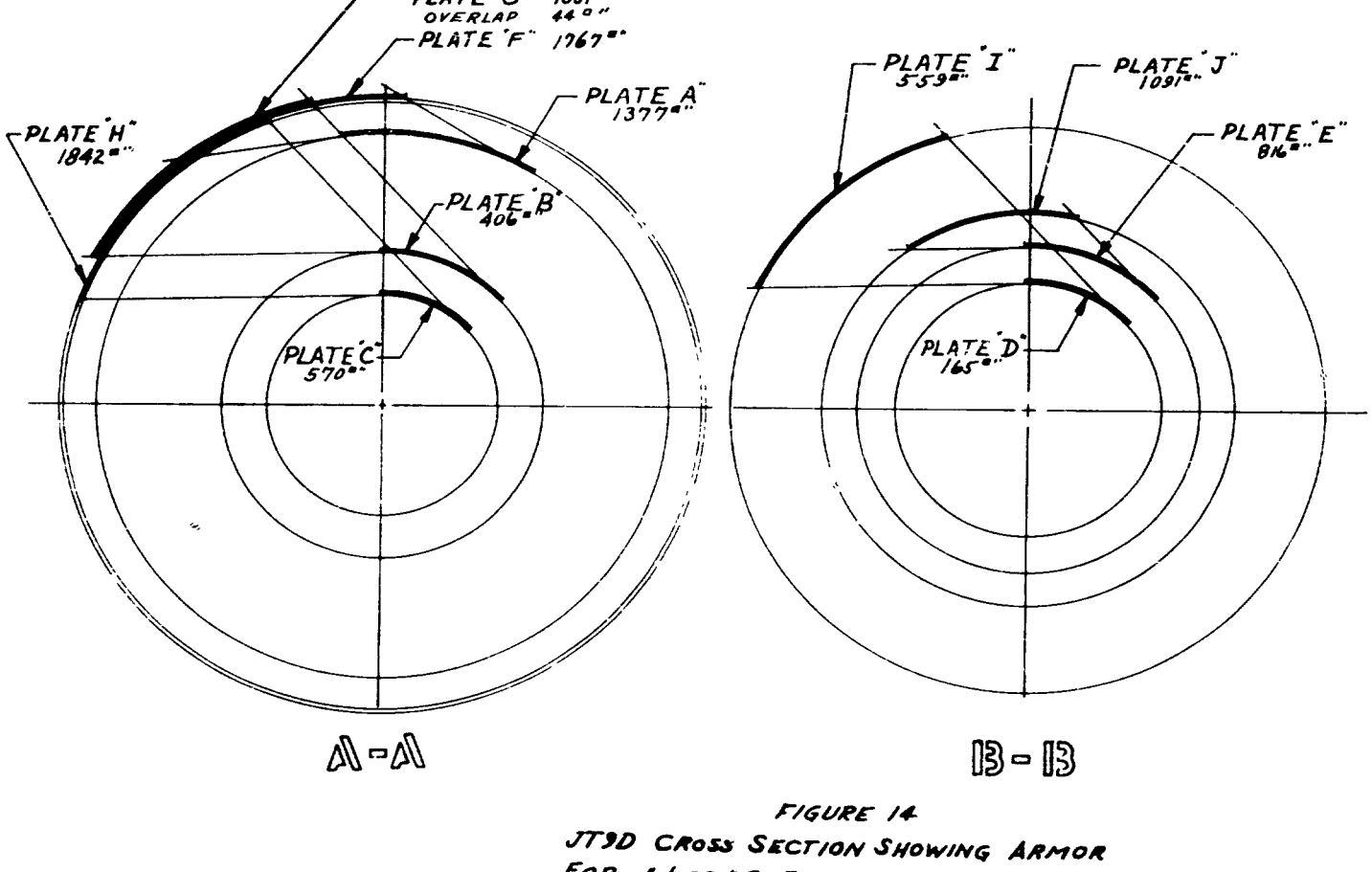

FIGURE 14
JT9D CROSS SECTION SHOWING ARMOR
FOR #1 OR #2 ENGINE - 4 ENG. A/P

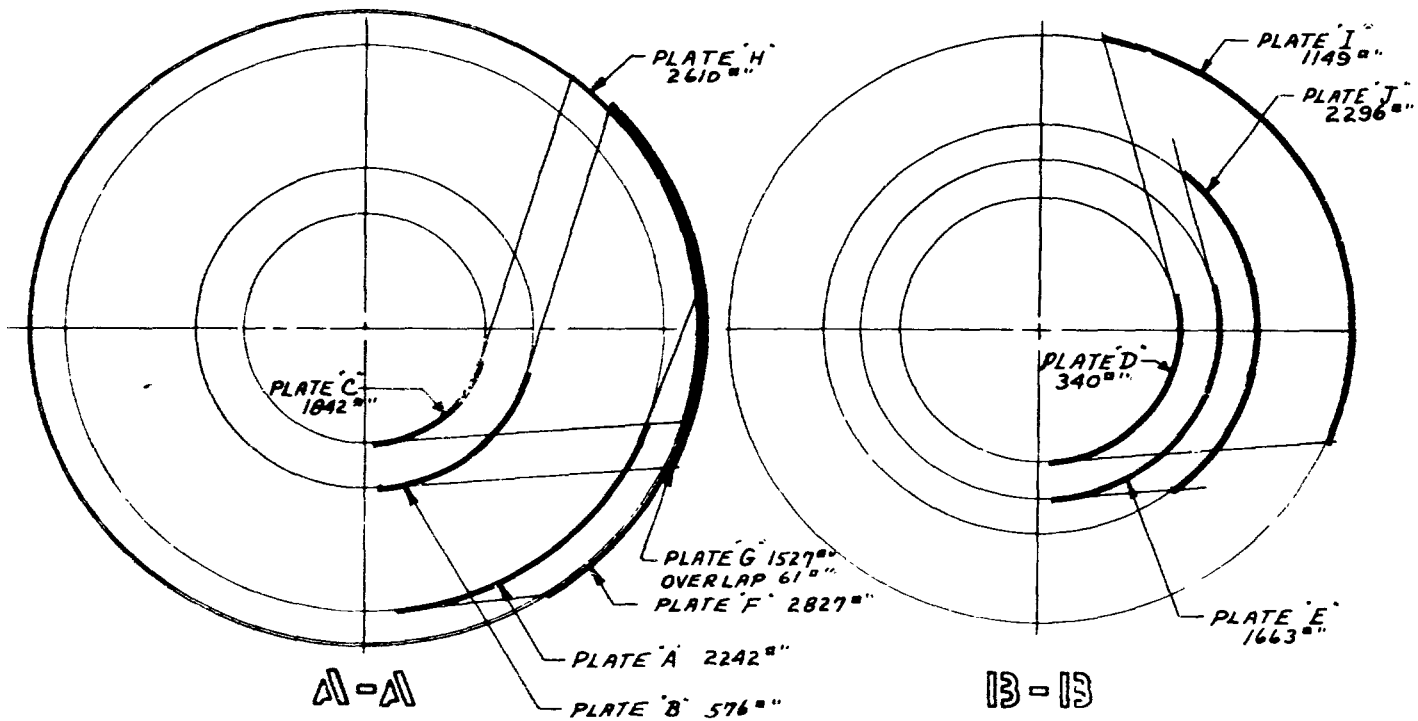

FIGURE 15
JT9D CROSS SECTION SHOWING ARMOR
FOR #3 OR #4 ENGINE - 4 ENG. A/P

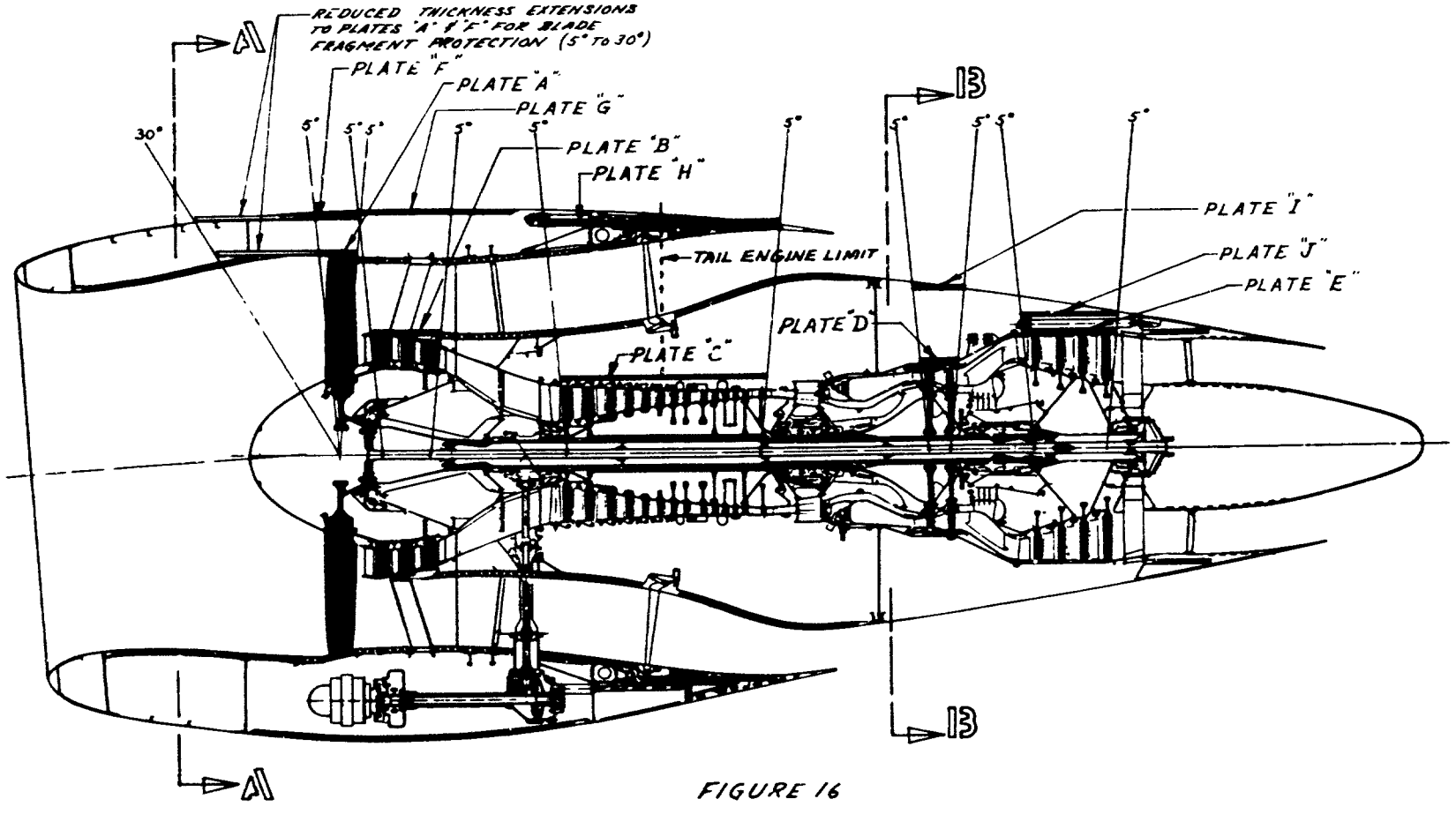

FIGURE 16
CF6-50 PROFILE CUTAWAY WITH
ARMOR LOCATIONS

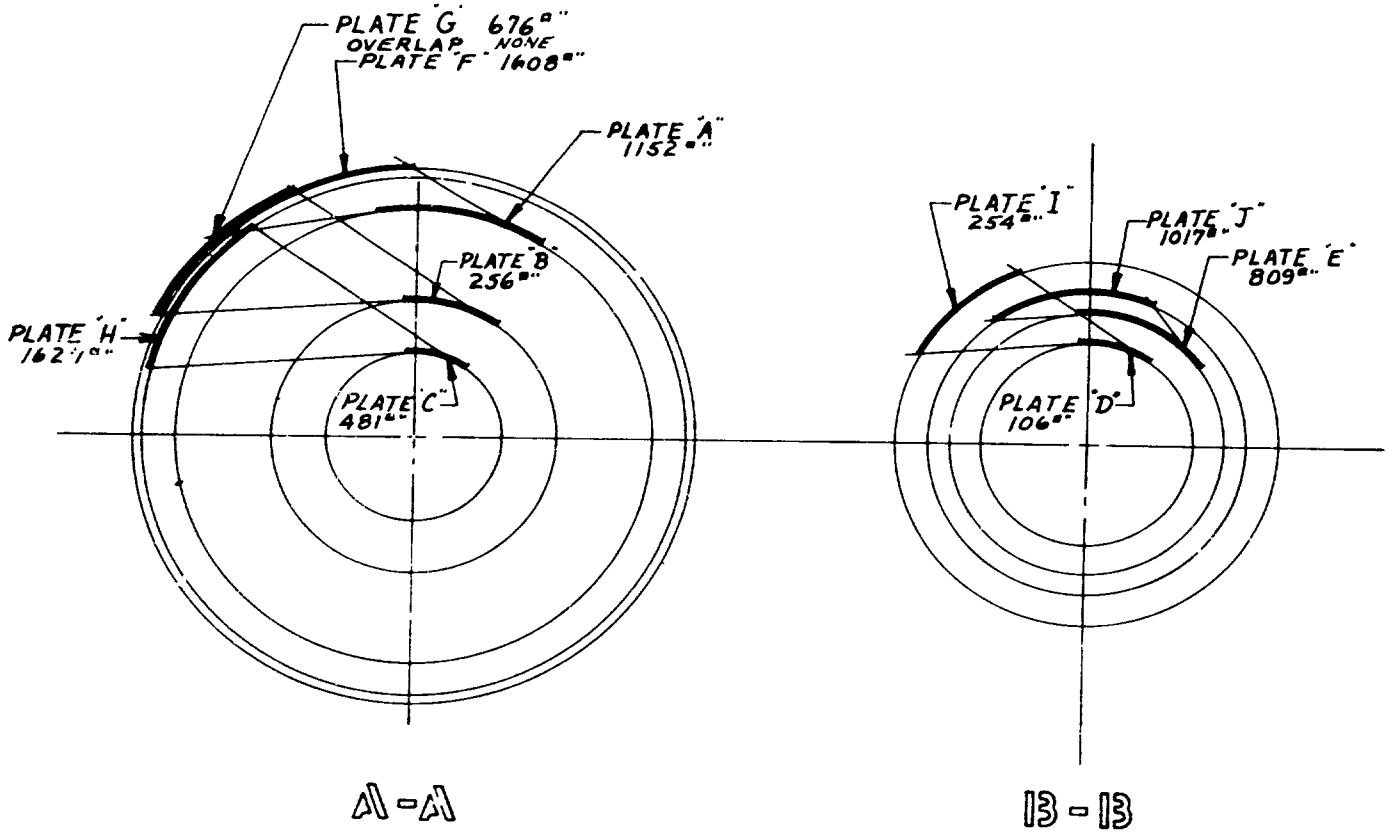

FIGURE 17

CF6-50 CROSS SECTION SHOWING ARMOR FOR #1 ENGINE - 3 ENG. A/P

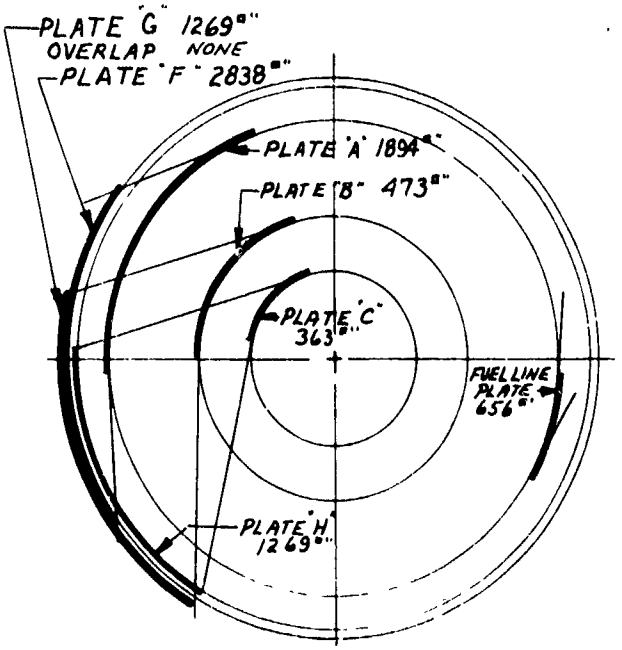

A - A

FIGURE 18
CF6-50 CROSS SECTION SHOWING ARMOR
FOR #2 ENGINE - 3 ENG A/P

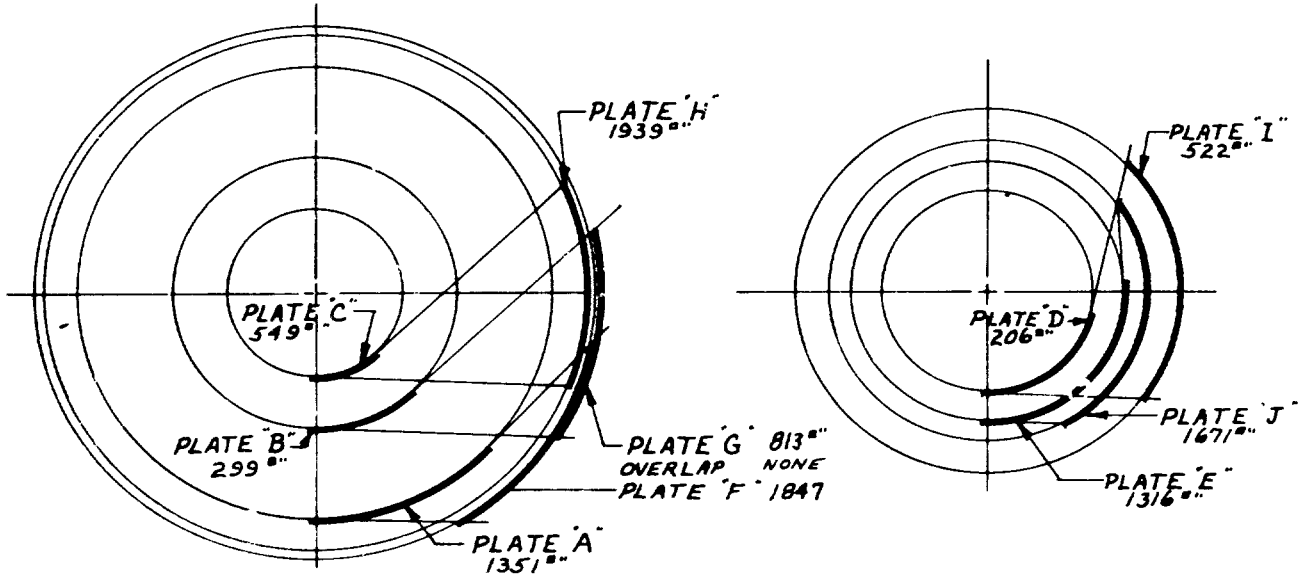

A1 - A1 B3 - B3

FIGURE 19
CF6-50 CROSS SECTION SHOWING ARMOR
FOR #3 ENGINE - 3 ENG. A/P

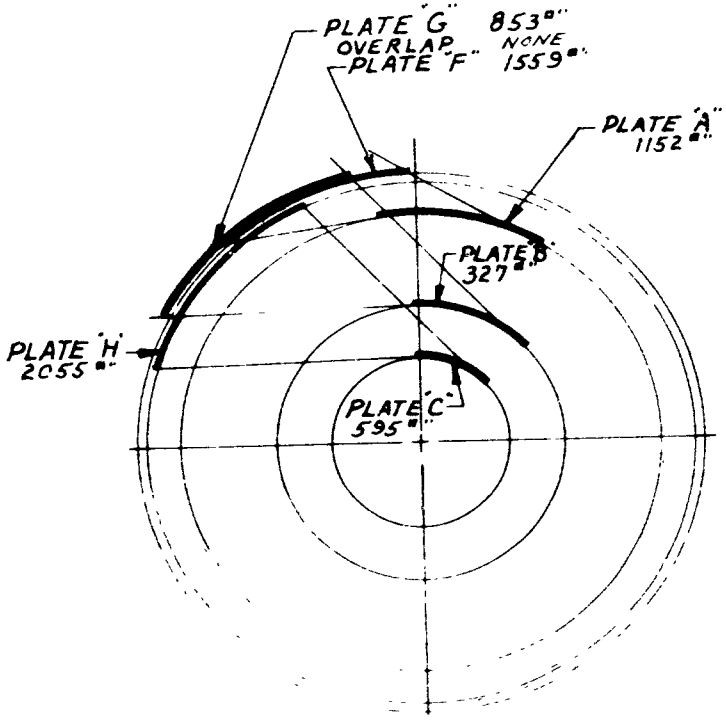

A1 - A1

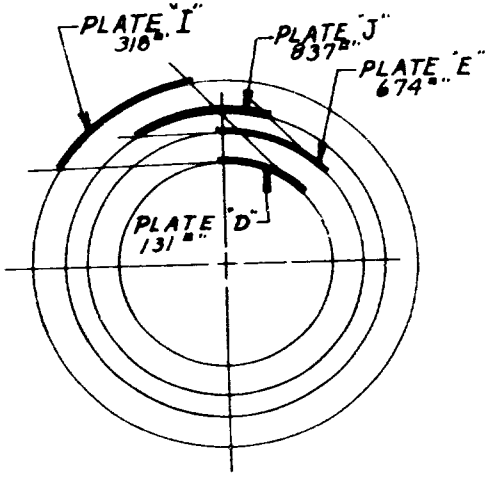

B1 - B1

FIGURE 20
CF6-50 CROSS SECTION SHOWING ARMOR
FOR #1 OR #2 ENGINE - 4 ENG. A/P

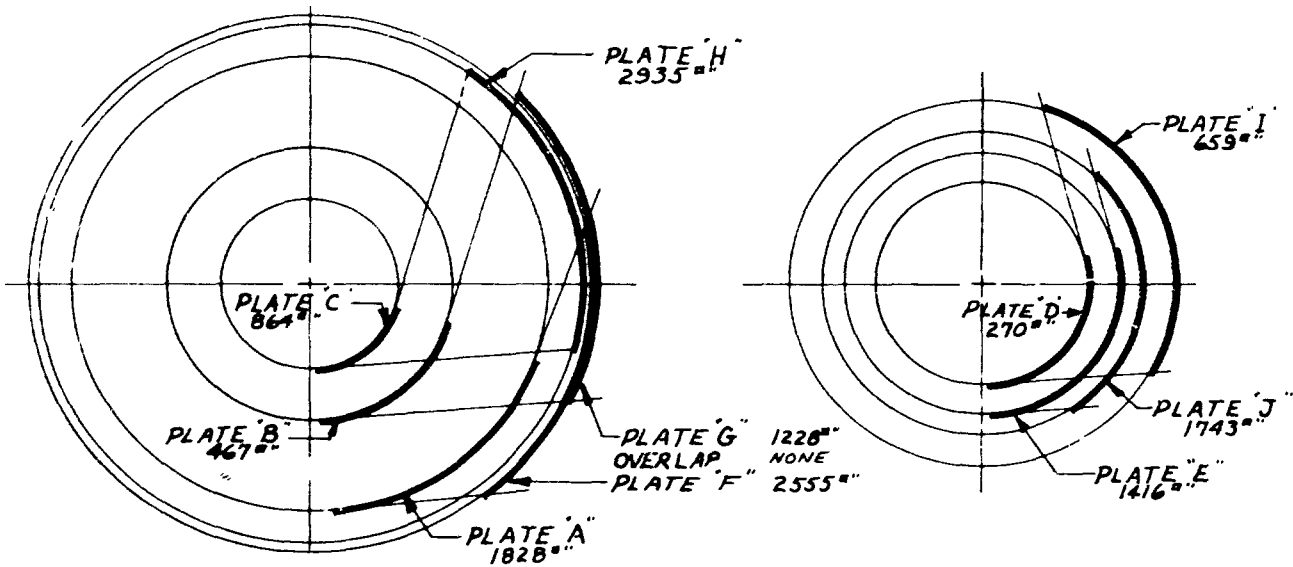

FIGURE 21

CF6-50 CROSS SECTION SHOWING ARMOR FOR #3 OR #4 ENGINE - 4 ENG. A/P

The thicknesses were determined using the correlations described in Section 6.4, the Armor Thickness Requirements Section of this report. Where there was an overlap in the fragment trajectories from two adjacent stages, the containment thickness required for the highest energy fragment was used.

The armor weights were determined for steel using the material density of 0.286 pounds per cubic inch and the areas established above for the thickness required to contain the previously established energies. In addition to the armor weights, there is support structure weights. Several armor plate installations were studied and it was determined that 2 to 25% of the total weight (armor plate and mounting) was required in the mounting and attachment. Location of the armor and how it was installed were considered in the mounting arrangement and the appropriate weight included. Table 3 shows the factors used to establish the additional weight for armor mounting and retention. Tables 4 through 6 show the armor area and weight for each cylindrical segment determined from layouts for the JT9D and CF6 engines. Tables 7 and 8 are a summary of all the armor weights.

4.4 Aircraft and Individual Component Fragment Vulnerability

As shown on Figures 5 & 7 only a small portion of the forward fuselage is exposed to fragment impingement. The remaining portion is protected by the wing lower surfaces. The fragments that can reach the fuselage must emanate from the engine fan or the first few stages of the low compressor. Because the fuselage has a circular cross-section even the most critical fragment trajectory impingement angle is quite large being approximately 33° with respect to a normal line with the surface. All other impingements are at much greater angles and as this angle increases the energy available to puncture the fuselage diminishes rapidly. As noted in the section covering inlet protection with a 3 x 5 x 0.25 inch fan fragment, sufficient energy is absorbed by the nacelle and inlet structure and that even when the fragment impinges on the fuselage at the most critical angle the fuselage and windows have ample strength to prevent penetration.

ARMOR PLATE PERIPHERIAL LOCATION IN NACELLE	ENGINE ZONE	ARMOR PLATE DESIGNATION	INSTALLATION FACTOR
INNER	FAN	PLATE A	1.08
INNER	L.P. COMPRESSOR	PLATE B	1.03
INNER	H.P. COMPRESSOR	PLATE C	1.25
INNER	H.P. TURBINE	PLATE D	1.15
INNER	L.P. TURBINE	PLATE E	1.20
OUTER	FAN	PLATE F	1.08
OUTER	L.P. COMPRESSOR	PLATE G	1.04
OUTER	H.P. COMPRESSOR	PLATE H	1.04
OUTER	H.P. TURBINE	PLATE I	1.04
OUTER	L.P. TURBINE	PLATE J	1.00

TABLE 3

ARMOR PLATE WEIGHT INSTALLATION FACTORS

TABLE 4. ARMOR INSTL. WEIGHTS FOR SINGLE BLADE FAILURE

JT 9D-59 ENGINE INSTL ARMOR LOCATED IN CLOSE TO ENGINE CASE

ENGINE LOCATION AND AIRPLANE TYPE	PLATE A (FAN)			PLATE B (I.P COMP)			PLATE C (H.P COMP)			PLATE D (H.P TURB)			PLATE E (L.P TURB)			TOTAL NACELLE ARMOR	
	AREA	AVE THICKNESS	WEIGHT	AREA	AVE THICKNESS	WEIGHT	AREA	AVE THICKNESS	WEIGHT	AREA	AVE THICKNESS	WEIGHT	AREA	AVE THICKNESS	WEIGHT	AREA	WEIGHT
#1 ENG 3 ENG AIRPL	293	310	281	325	.053	5.3	470	.046	77	123	.156	6.8	251	.077	5.5	1412	53
#2 ENG 3 ENG AIRPL	621		59.9	410		9.9	357		5.9	ZERO		ZERO	ZERO		ZERO	1488	66
#3 ENG 3 ENG AIRPL	958		92.3	390		6.3	563		9.1	272		14.0	429		9.5	2002	73
#1 & 2 ENG 4 ENG AIRPL	285		27.3	41		6.6	570		94	165		8.5	215		4.7	1641	56
#3 OR 4 ENG 4 ENG AIRPL	464		44.4	96		9.3	784		12.9	340		17.4	437		9.6	2603	94
#1,2,3 OR 4 ENG 4 ENG AIRPL	749		71.7	82		16.9	1356		22.3	505		25.9	652		14.4	4244	150
#1,2 OR 3 ENG 3 ENG AIRPL	1178	.310	112.3	1325	.055	24.5	1380	.046	22.7	405	.156	29.8	680	077	15.0	4962	195

9D-59 ENGINE INSTL. ARMOR LOCATED AT OUTER PERIPHERY OF NACELLE

ENGINE LOCATION AND AIRPLANE TYPE	PLATE F (FAN)			PLATE G (I.P COMP)			PLATE H (H.P COMP)			PLATE I (H.P TURB)			PLATE J (L.P TURB)			TOTAL NACELLE ARMOR	
	AREA	AVE THICKNESS	WEIGHT	AREA	AVE THICKNESS	WEIGHT	AREA	AVE THICKNESS	WEIGHT	AREA	AVE THICKNESS	WEIGHT	AREA	AVE THICKNESS	WEIGHT	AREA	WEIGHT
#1 ENG 3 ENG AIRPL	366	310	350	828*	.056	13.8	1461	062	22.6	449	.141	18.8	344	079	7.8	3448	98
#2 ENG 3 ENG AIRPL	668		64.0	1538*		26.5	1137		17.6	ZERO		ZERO	ZERO		ZERO	3327	106
#3 ENG 3 ENG AIRPL	439		42.0	981*		16.3	1735		26.7	917		38.5	580		13.1	4652	137
#1 OR 2 ENG 4 ENG AIRPL	366		35.0	1037*		17.3	1842		28.5	559		23.4	287		6.5	4091	111
#3 OR 4 ENG 4 ENG AIRPL	585		56.0	1466*		24.4	2610		40.4	1169		49.2	604		13.6	6414	183
#1,2 OR 3 OR 4 ENG 4 ENG AIRPL	951		91.0	2503*		41.7	4452		68.9	1708		71.6	891		20.1	10505	293
#1,2 OR 3 ENG 3 ENG AIRPL	1463	310	140.0	3341*	056	55.7	4423	052	66.9	1366	141	57.3	924	079	20.9	11517	341

CF6-50 ENGINE INSTL. ARMOR LOCATED IN CLOSE TO ENGINE CASE

ENGINE LOCATION AND AIRPLANE TYPE	PLATE A (FAN)			PLATE B (I.P COMP)			PLATE C (H.P COMP)			PLATE D (H.P TURB)			PLATE E (L.P TURB)			TOTAL NACELLE ARMOR	
	AREA	AVE THICKNESS	WEIGHT	AREA	AVE THICKNESS	WEIGHT	AREA	AVE THICKNESS	WEIGHT	AREA	AVE THICKNESS	WEIGHT	AREA	AVE THICKNESS	WEIGHT	AREA	WEIGHT
#1 ENG 3 ENG AIRPL	238	313	23.1	256	072	5.4	401	057	9.0	106	.189	6.6	489	076	12.8	1570	58
#2 ENG 3 ENG AIRPL	330		31.9	472		10.0	363		7.6	ZERO		ZERO	ZERO		ZERO	1166	42
#3 ENG 3 ENG AIRPL	280		27.0	299		6.3	549		11.2	206		13.8	796		20.8	2130	78
#1 OR 2 ENG 4 ENG AIRPL	238		23.1	327		6.9	596		12.1	131		8.1	407		10.6	1698	61
#3 OR 4 ENG 4 ENG AIRPL	378		36.6	466		9.5	864		17.6	270		16.8	856		22.3	2814	103
#1,2 OR 3 OR 4 ENG 4 ENG AIRPL	617		59.6	772		16.4	1459		29.7	401		24.9	1263		32.9	4513	164
#1,2 OR 3 ENG 3 ENG AIRPL	848	.313	82.0	1028	072	21.8	1393	057	28.4	312	189	19.4	1205	076	33.5	4866	185

CF6-50 ENGINE INSTL. ARMOR LOCATED AT OUTER PERIPHERY OF NACELLE

ENGINE LOCATION AND AIRPLANE TYPE	PLATE F (FAN)			PLATE G (I.P COMP)			PLATE H (H.P COMP)			PLATE I (H.P TURB)			PLATE J (L.P TURB)			TOTAL NACELLE ARMOR	
	AREA	AVE THICKNESS	WEIGHT	AREA	AVE THICKNESS	WEIGHT	AREA	AVE THICKNESS	WEIGHT	AREA	AVE THICKNESS	WEIGHT	AREA	AVE THICKNESS	WEIGHT	AREA	WEIGHT
#1 ENG. 3 ENG AIRPL.	323	313	32.2	676*	.073	14.7	1627	.062	30.0	254	.174	13.2	599	.076	12.9	3483	103
#2 ENG 3 ENG AIRPL	387		56.8	1269*		27.6	1269		23.4	ZERO		ZERO	ZERO		ZERO	3125	108
#3 ENG. 3 ENG AIRPL.	382		37.0	813*		17.7	1939		35.8	522		37.0	974		21.2	4630	139
#1 OR #3 ENG 4 ENG AIRPL	323		31.2	853*		18.5	2055		37.9	318		16.5	488		10.6	4037	115
#3 OR #4 ENG. 4 ENG AIRPL.	529		51.1	1228*		26.7	2935		54.12	659		34.1	1015		22.1	6366	188
#1,2,3 OR 4 ENG 4 ENG AIRPL	852		82.9	2091*		45.2	4990		92.0	977		50.6	1503		32.7	10403	303
#1,2 OR 3 ENG. 3 ENG AIRPL.	1302	313	125.9	2750*	073	59.9	4835	062	89.2	776	.174	40.2	1566	.076	34.0	11237	349

* AREA REDUCED DUE TO OVERLAP WITH FAN STAGE ARMOR

TABLE 5. ARMOR INSTL. WEIGHTS FOR TWO BLADE FAILURE

JT9D-59 ENGINE INSTL ARMOR LOCATED IN CLOSE TO ENGINE CASE

ENGINE LOCATION AND AIRPLANE TYPE	PLATE A (FAN) AREA	AVE THICKNESS	WEIGHT	PLATE B (I.P COMP) AREA	AVE THICKNESS	WEIGHT	PLATE C (H.P COMP) AREA	AVE THICKNESS	WEIGHT	PLATE D (H.P. TURB) AREA	AVE THICKNESS	WEIGHT	PLATE E (I.P. TURB) AREA	AVE THICKNESS	WEIGHT	TOTAL NACELLE ARMOR AREA	WEIGHT
#1 ENG. 3 ENG AIRPL	293	.532	482	926	.097	9.3	470	.081	13.6	137	.344	15.1	851	.135	11.6	1472	98
#2 ENG. 3 ENG AIRPL	521		85.6	610		17.7	357		10.3	ZERO		ZERO	ZERO		ZERO	1488	114
#3 ENG. 3 ENG AIRPL	348		57.2	390		11.2	553		16.0	272		30.8	439		18.9	2002	137
#1 OR 2 ENG 4 ENG AIRPL	285		46.8	406		11.7	570		16.5	165		10.7	215		10.0	1641	104
#3 OR 4 ENG. 4 ENG AIRPL	464		76.2	576		16.7	786		53.3	340		28.5	437		20.2	2603	205
#1,2,3 OR 4 ENG. 4 ENG AIRPL	749		123.1	982		28.5	1356		69.8	505		57.1	652		30.2	4244	303
#1,2 OR 3 ENG. 3 ENG AIRPL	1172	.532	192.7	1325	.097	38.4	1380	.081	90.0	405	.344	45.8	680	.135	31.5	4962	348

JT9D-59 ENGINE INSTL. ARMOR LOCATED AT OUTER PERIPHERY OF NACELLE

ENGINE LOCATION AND AIRPLANE TYPE	PLATE F (FAN) AREA	AVE THICKNESS	WEIGHT	PLATE G (I.P COMP) AREA	AVE THICKNESS	WEIGHT	PLATE H (H.P COMP) AREA	AVE THICKNESS	WEIGHT	PLATE I (H.P TURB) AREA	AVE THICKNESS	WEIGHT	PLATE J (I.P TURB) AREA	AVE THICKNESS	WEIGHT	TOTAL NACELLE ARMOR AREA	WEIGHT
#1 ENG. 3 ENG AIRPL	366	.532	60.1	820 *	.099	24.4	1461	.092	40.0	449	.297	39.7	344	.136	13.4	3440	178
#2 ENG. 3 ENG AIRPL	658		108.2	1532 *		45.1	1139		31.1	ZERO		ZERO	ZERO		ZERO	3387	184
#3 ENG. 3 ENG AIRPL	439		72.1	981 *		28.9	1725		47.2	917		81.0	690		22.6	4642	252
#1 OR 2 ENG 4 ENG AIRPL	366		60.1	1937 *		30.5	1842		50.4	559		49.4	287		11.2	4091	242
#3 OR 4 ENG 4 ENG AIRPL	585		96.1	1466 *		43.2	2610		71.4	1149		101.5	604		23.5	6414	336
#1,2,3 OR 4 ENG. 4 ENG AIRPL	951		156.3	2503 *		73.7	4452		121.9	1708		150.9	891		34.7	10505	637
#1,2 OR 3 ENG. 3 ENG AIRPL	1463	.532	240.4	3341 *	.099	98.4	4423	.092	118.3	1366	.297	180.7	924	.136	35.9	11517	614

CF6-50 ENGINE INSTL. ARMOR LOCATED IN CLOSE TO ENGINE CASE

ENGINE LOCATION AND AIRPLANE TYPE	PLATE A (FAN) AREA	AVE THICKNESS	WEIGHT	PLATE B (I.P COMP) AREA	AVE THICKNESS	WEIGHT	PLATE C (H.P COMP) AREA	AVE THICKNESS	WEIGHT	PLATE D (H.P TURB) AREA	AVE THICKNESS	WEIGHT	PLATE E (I.P TURB) AREA	AVE THICKNESS	WEIGHT	TOTAL NACELLE ARMOR AREA	WEIGHT
#1 ENG. 3 ENG AIRPL	238	.537	39.6	256	.127	9.6	481	.102	17.5	106	.417	14.5	409	.130	21.8	1570	103
#2 ENG. 3 ENG AIRPL	330		54.7	473		17.7	363		13.2	ZERO		ZERO	ZERO		ZERO	1166	86
#3 ENG. 3 ENG AIRPL	280		46.4	299		11.2	549		20.0	206		28.2	956		35.5	2130	141
#1 OR 2 ENG 4 ENG AIRPL	238		39.6	357		13.2	595		21.7	131		18.0	407		18.2	1638	110
#3 OR 4 ENG 4 ENG AIRPL	378		62.8	446		16.7	864		31.5	270		37.0	856		28.2	2814	186
#1,2,3 OR 4 ENG. 4 ENG AIRPL	617		102.3	773		28.9	1459		53.2	401		55.0	1265		56.4	4513	296
#1,2 OR 3 ENG. 3 ENG AIRPL	848	.537	140.7	1028	.127	38.5	1393	.102	50.8	312	417	42.8	1286	.130	57.3	4866	330

CF6-50 ENGINE INSTL. ARMOR LOCATED AT OUTER PERIPHERY OF NACELLE

ENGINE LOCATION AND AIRPLANE TYPE	PLATE F (FAN) AREA	AVE THICKNESS	WEIGHT	PLATE G (I.P COMP) AREA	AVE THICKNESS	WEIGHT	PLATE H (H.P COMP) AREA	AVE THICKNESS	WEIGHT	PLATE I (H.P TURB) AREA	AVE THICKNESS	WEIGHT	PLATE J (I.P. TURB) AREA	AVE THICKNESS	WEIGHT	TOTAL NACELLE ARMOR AREA	WEIGHT
#1 ENG. 3 ENG AIRPL	393	.537	55.2	676 *	.129	25.9	1627	.110	63.2	254	.349	26.4	593	.131	22.2	3483	183
#2 ENG 3 ENG AIRPL	587		97.4	1262 *		48.7	1269		41.5	ZERO		ZERO	ZERO		ZERO	3125	188
#3 ENG 3 ENG AIRPL	382		63.4	813 *		31.2	1939		63.4	522		54.2	974		36.5	4630	249
#1 OR 2 ENG 4 ENG AIRPL	383		63.5	863 *		32.1	2055		67.2	318		33.0	488		18.3	4057	205
#3 OR 4 ENG. 4 ENG AIRPL	529		87.7	1220 *		47.1	2935		96.0	659		68.4	1015		38.0	6366	337
#1,2,3 OR 4 ENG. 4 ENG AIRPL	852		141.3	2001 *		79.9	4990		163.2	977		101.4	1503		56.3	10443	592
#1,2 OR 3 ENG 3 ENG AIRPL	1302	537	216.0	2758 *	129	105.8	4835	.110	158.2	776	349	80.6	1566	.131	58.7	11237	619

* AREA REDUCED DUE TO OVERLAP WITH FAN STAGE ARMOR

TABLE 6 ARMOR INSTL WEIGHTS FOR FOUR BLADE FAILURE

JT9D-59 ENGINE INSTL. ARMOR LOCATED IN CLOSE TO ENGINE CASE

ENGINE LOCATION AND AIRPLANE TYPE	PLATE A (FAN)			PLATE B (L.P. Comp.)			PLATE C (H.P. Comp.)			PLATE D (H.P. Turb.)			PLATE E (L.P. Turb.)			TOTAL NACELLE ARMOR	
	AREA	AVE. THICKNESS	WEIGHT	AREA	AVE. THICKNESS	WEIGHT	AREA	AVE. THICKNESS	WEIGHT	AREA	AVE. THICKNESS	WEIGHT	AREA	AVE. THICKNESS	WEIGHT	AREA	WEIGHT
#1 ENG. 3 ENG. ARPL.	293	1.212	110	325	.224	81.4	470	.188	91.4	133	.676	226	261	.206	26.4	1482	319
#2 ENG. 3 ENG. ARPL.	521		195	610		40.3	967		94.0	ZERO		ZERO	ZERO		ZERO	1480	269
#3 ENG. 3 ENG. ARPL.	358		134	390		25.7	553		37.2	278		60.5	489		45.1	2002	303
#1 OR 2 ENG. 4 ENG. ARPL.	285		107	406		26.8	570		39.3	165		30.7	215		22.6	1691	231
#3 OR 4 ENG. 4 ENG. ARPL.	464		174	576		34.0	786		183.8	340		75.6	487		45.9	2603	457
#1, 2, 3 OR 4 ENG. 4 ENG. ARPL.	749		280	982		64.8	1356		166.2	505		112.3	652		68.5	4244	688
#1, 2 OR 3 ENG. 3 ENG. ARPL.	1172	1.212	439	1335	.224	87.4	1890	.188	928	405	.676	901	680	.206	71.4	4962	781

JT9D-59 ENGINE INSTL. ARMOR LOCATED AT OUTER PERIPHERY OF NACELLE

ENGINE LOCATION AND AIRPLANE TYPE	PLATE F (FAN)			PLATE G (L.P. Comp.)			PLATE N (H.P. Comp.)			PLATE I (H.P. Turb.)			PLATE J (L.P. Turb.)			TOTAL NACELLE ARMOR	
	AREA	AVE. THICKNESS	WEIGHT	AREA	AVE. THICKNESS	WEIGHT	AREA	AVE. THICKNESS	WEIGHT	AREA	AVE. THICKNESS	WEIGHT	AREA	AVE. THICKNESS	WEIGHT	AREA	WEIGHT
#1 ENG. 3 ENG. ARPL.	346	1.212	137	828 #	.228	56.2	1441	.214	93.0	449	.571	76.3	845	.310	30.5	3448	393
#2 ENG. 3 ENG. ARPL.	658		246	1578 #		103.9	1137		73.8	ZERO		ZERO	ZERO		ZERO	3387	422
#3 ENG. 3 ENG. ARPL.	499		164	981 #		66.5	1326		103.8	917		156.7	580		61.4	4642	647
#1 OR 2 ENG. 4 ENG. ARPL.	366		137	1037 #		70.3	1042		113.2	563		94.9	387		85.4	4091	445
#3 OR 4 ENG. 4 ENG. ARPL.	585		219	1466 #		99.4	2610		166.1	1149		195.1	604		53.6	6414	733
#1, 2, 3 OR 4 ENG. 4 ENG. ARPL.	951		361	2403 #		169.7	4452		284.4	1708		290.0	891		79.0	10505	1178
#1, 2 OR 3 ENG. 3 ENG. ARPL.	1443	1.212	546	3241 #	.228	226.6	4423	.214	275.2	1366	.571	232.8	924	.310	81.9	11517	1364

CF6-50 ENGINE INSTL. ARMOR LOCATED IN CLOSE TO ENGINE CASE

ENGINE LOCATION AND AIRPLANE TYPE	PLATE A (FAN)			PLATE B (L.P. Comp.)			PLATE C (H.P. Comp.)			PLATE D (H.P. Turb.)			PLATE E (L.P. Turb.)			TOTAL NACELLE ARMOR	
	AREA	AVE. THICKNESS	WEIGHT	AREA	AVE. THICKNESS	WEIGHT	AREA	AVE. THICKNESS	WEIGHT	AREA	AVE. THICKNESS	WEIGHT	AREA	AVE. THICKNESS	WEIGHT	AREA	WEIGHT
#1 ENG. 3 ENG. ARPL.	238	1.223	901	856	.892	220	991	.836	40.6	106	.831	29.0	402	.298	50.0	1870	232
#2 ENG. 3 ENG. ARPL.	330		125	473		40.7	763		98.6	ZERO		ZERO	ZERO		ZERO	1186	196
#3 ENG. 3 ENG. ARPL.	280		106	399		25.7	592		86.3	206		56.3	796		81.4	2130	316
#1 OR 2 ENG. 4 ENG. ARPL.	238		901	327		201	596		58.2	131		35.8	467		41.6	1698	246
#3 OR 4 ENG. 4 ENG. ARPL.	370		153	446		304	844		74.9	270		73.8	856		87.5	2814	416
#1, 2, 3 OR 4 ENG. 4 ENG. ARPL.	617		432	773		665	1479		183.1	401		109.6	1243		189.	4513	661
#1, 2 OR 3 ENG. 3 ENG. ARPL.	868	1.223	320	1028	.292	88.8	1993	.836	117.5	372	.831	85.3	1285	.298	131.	4966	702 #

CF6-50 ENGINE INSTL. ARMOR LOCATED AT OUTER PERIPHERY OF NACELLE

ENGINE LOCATION AND AIRPLANE TYPE	PLATE F (FAN)			PLATE G (L.P. Comp.)			PLATE N (H.P. Comp.)			PLATE I (H.P. Turb.)			PLATE J (L.P. Turb.)			TOTAL NACELLE ARMOR	
	AREA	AVE. THICKNESS	WEIGHT	AREA	AVE. THICKNESS	WEIGHT	AREA	AVE. THICKNESS	WEIGHT	AREA	AVE. THICKNESS	WEIGHT	AREA	AVE. THICKNESS	WEIGHT	AREA	WEIGHT
#1 ENG. 3 ENG. ARPL.	333	1.223	126	676 #	.292	58.7	1627	.256	183.9	264	.678	51.8	523	.299	69.7	3483	418
#2 ENG. 3 ENG. ARPL.	587		222	1269 #		116.	1749		94.6	ZERO		ZERO	ZERO		ZERO	3125	431
#3 ENG. 3 ENG. ARPL.	302		169	813 #		76.8	1889		142.6	528		105.3	974		88.3	4650	552
#1 OR 2 ENG. 4 ENG. ARPL.	333		126	1269 #		76.4	2055		156.5	318		64.1	480		41.7	4087	460
#3 OR 4 ENG. 4 ENG. ARPL.	517		200	1220 #		108.	3826		283.5	659		132.9	1015		89.8	6246	761
#1, 2, 3 OR 4 ENG. 4 ENG. ARPL.	872		322	2081 #		184.	4980		380.0	977		197.0	1503		129.	10402	1212
#1, 2 OR 3 ENG. 3 ENG. ARPL.	1302	1.223	498	3756 #	.292	264	4835	.256	340.2	996	.678	156.5	1446	.299	156.	11337	1385

AREA REDUCED DUE TO OVERLAP WITH FAN STAGE ARMOR

Fragment Size	3 Engine Airplane Total Armor Weight (lb)				4 Engine Airplane Total Armor Weight (lb)			
	(1) Non-Interchangeable Armor Installation		(2) Interchangeable Armor Installation		Non-Interchangeable Armor Installation		Interchangeable Armor Installation	
	(3) Inner	(4) Outer	Inner	Outer	Inner	Outer	Inner	Outer
1-Blade	192	341	585	1020	300	588	600	1170
2-Blade and Included Disc Serrations	349	614	1040	1840	618	1080	1240	2150
4-Blade and Included Disc Serrations	781	1360	2340	4090	1380	2360	2750	4710

(1) Non-Interchangeable Armor – Armor designed for optimum containment depending on engine location.
(2) Interchangeable Armor – Armor designed so engine or nacelle can be installed in any location.
(3) Inner – Armor installed as close to the engine as possible
(4) Outer – Armor installed in the outer portion of the nacelle.

TABLE 7 – TOTAL ARMOR WEIGHT – JT9D ENGINE INSTALLATION

FRAGMENT SIZE	3 ENGINE AIRPLANE TOTAL ARMOR WEIGHT (LB)				4 ENGINE AIRPLANE TOTAL ARMOR WEIGHT (LB)			
	(1) NON-INTERCHANGEABLE ARMOR INSTALLATION		(2) INTERCHANGEABLE ARMOR INSTALLATION		NON-INTERCHANGEABLE ARMOR INSTALLATION		INTERCHANGEABLE ARMOR INSTALLATION	
	(3) INNER	(4) OUTER	INNER	OUTER	INNER	OUTER	INNER	OUTER
1-BLADE	185	350	555	1050	328	606	656	1210
2-BLADE AND INCLUDED DISC SERRATIONS	330	620	990	1860	592	1080	1180	2170
4-BLADE AND INCLUDED DISC SERRATIONS	744	1400	2230	4190	1320	2420	2640	4850

(1) NON-INTERCHANGEABLE ARMOR - ARMOR DESIGNED FOR OPTIMUM CONTAINMENT DEPENDING ON ENGINE LOCATION.
(2) INTERCHANGEABLE ARMOR - ARMOR DESIGNED SO ENGINE OR NACELLE CAN BE INSTALLED IN ANY LOCATION.
(3) INNER - ARMOR INSTALLED AS CLOSE TO THE ENGINE AS POSSIBLE.
(4) OUTER - ARMOR INSTALLED IN THE OUTER PORTION OF THE NACELLE.

TABLE 8 - TOTAL ARMOR WEIGHT - CF6-50 ENGINE INSTALLATION

Fragments from the compressors and turbines of left inboard wing mounted engines emanate from the top of the engine and can impinge on the lower wing surface, the wing leading edge slats and the front wing spar caps and spar web. The angle of impingement on the tapered lower wing skin and spar cap is almost tangential and the aluminum wing skin in this area has a thickness of .416 inch over most of the area tapering to .120 inch in the area of the forward inboard corner. Because of the near tangential impingement angle and the thick skin, almost any reasonable size fragment striking in this area probably would not penetrate but would be deflected away from the airplane.

The smallest fragment impingement angle normal to the lower wing skin surface would result in an energy absorption capability for the wing skin as follows assuming the fragment has a perimeter of 8.5 inches. The equation used below has been used in the past to determine the energy absorption capability of homogenous metallic material. It will be shown later in Section 6.56 that the equation agrees well with experimental data obtained by test.

$$E_A = \frac{LTt^2}{12\cos^2\theta}$$

$$= \frac{(8.5)(30450)(.416)^2}{(12)(.007569)}$$

$$= 493{,}143 \text{ ft-lbs}$$

θ = 85° = Impingement Angle

$\cos\theta$ = .087 for 85°

$\cos^2\theta$ = .007569

T = 30450 psi = Dynamic Shear Modulus

L = 8.5 Inch Perimeter of Impact Face of Fragment

t = .416 inch = Armor Thickness

The 493,143 ft-lbs represents the wing skin absorption capability in the thickest skin area.

Evaluation of the thinner wing skin area by the same process provides the following:

$$t = .120$$

$$E_A = \frac{(8.5)(30450)(.120)^2}{(12)(.007569)}$$

$$E_A = 41{,}034 \text{ ft-lbs}$$

The above shows that a high level of energy absorption capability results because of the close to tangential impingement angle and even when the impact was made by a relatively small frontal area high energy fragment. From the equation it can be seen that if the fragment perimeter becomes larger the absorption capability increases directly.

Fragments from right wing mounted engines are directed from lower portions of the engine and impinge on the lower wing skin at an angle more towards normal and a fragment of sufficient size and energy could penetrate the lower wing skin at least where the skin thickness is reduced to .120 inch.

The most critical impingement angle on fragments from the right wing inboard engine would probably be about 30°, thus the absorption capability in the area of the .120 inch wing skin would be:

$$E_A = \frac{LTt^2}{12\cos^2\theta}$$

$$E_A = \frac{(8.5)\ (30450)\ (.12)^2}{(12)\ (.25)}$$

$$E_A = 1242 \text{ ft-lbs}$$

$\cos\theta = .500$ for 30°

$\cos^2\theta = .250$

$T = 30{,}450$ psi

$L = 8.5$

$t = .120$

The energy absorbed is equal to only 1242 ft-lbs and this shows the effect of the more normal impingement where with the same thickness wing skin and near tangential impingement on the left wing the absorption capability was 41034 ft-lbs or more than a 33 times the capability to resist penetration.

The fragment impingement characteristics on the lower wing surface from the inboard engines of the four engine airplane are nearly identical to those of the wing mounted engines of the three engine airplane previously discussed. However, because of the relationship of the fragment trajectory and wing surface angle, fragments from the outboard engines develop less energy in the wing puncturing direction. The left wing mounted outboard engine fragment trajectories would be even more tangential to the wing surface than they were for inboard mounted left engines. The right wing mounted outboard engine fragments would, in the most critical condition,

impinge on the wing surface at an angle of about 45° with respect to a line normal to the wing surface where on the right inboard engine this angle was about 30°. Also, the lower wing skin thickness in the area of outboard engine fragment impingement is thicker than the thinnest portion of the inboard section in that it tapers from .200 inch at the outboard limit of fragment impingement to .416 inch thick at the inboard limit. The effect of the increased angle and thicker skin on energy absorption is as follows:

$$E_A = \frac{LTt^2}{12 \cos^2\theta}$$

$$E_A = \frac{(8.5)(30450)(.200)^2}{(12)\ (.707)^2}$$

$$E_A = 1726 \text{ ft-lbs}$$

$\cos\theta = .707$ for 45°

$\cos^2\theta = .4998$

$T = 30450$ psi

$L = 8.5$ inches

$t = .200$

The right wing skin energy absorption capability of 1726 ft-lbs on the outboard section can be compared to the 1242 ft-lbs previously determined for the inboard section. The 39% improvement in absorption capability of the outboard section has resulted because the impingement angle was increased from 30° to 45° and the skin thickness was increased from.120 inch to .200 inch.

On the three engine and four engine airplanes the wing lower skin surface is also the lower wall of the fuel tank. Fragments from either inboard or outboard right wing mounted engines with sufficient energy level could penetrate the wing surface. But even though punctured, any fuel leaking out would be directed into the airstream and would not be considered a safety hazard. The wing fuel tanks are compartmentized so only the fuel in the inboard tank would be lost. Because of the type of wing construction, ample load distribution would be provided around a puncture hole through the remaining wing skin and stringers and no rip tendency would occur.

The airplane of course would be completely controllable with the asymmetric weight caused by the fuel loss along with the loss of engine thrust on an engine presumed to have failed when the puncturing fragment was generated.

The remaining vulnerable area to be considered is the area forward of the wing spar and the spar web itself. As shown on Figure 22, all of the engine controls, hydraulic suction and pressure piping, pneumatic ducting, slat extend and retract hydraulic piping, the engine fire extinguishing piping, fire extinguishing agent storage bottles and the electrical wire bundles for engine instrumentation and fuel quantity are routed forward of and along the wing spar web.

The airplane is provided with independent redundant systems powered by individual engines, and in the case of the three engine airplane a fourth electrically powered hydraulic system is available. The loss of any of the following systems does not result in hazardous airplane operation: (Assume failure occurred on number one engine on a three engine airplane).

System Failed by Fragment	Consequence
No. 1 Hydraulic System	Loss of one system and oil. No. 2, 3 and 4 systems still operable. Airplane can be flown on one system.
No. 1 Pneumatic System	Loss of system. No. 2 or 3 system is adequate to provide air conditioning and pressurization.
Slat Extend Piping	Loss of slat operation. Landing can be made without slats extended.
Slat Retract Piping	Will remain in last position. Landing can be made either extended or retracted.
Fuel Quantity Electrical System - Left Wing Only	Fuel remaining at time of incident and right tank indications are sufficient to compute fuel required to land.
Generator Power Feeder Lines	Loss of use of one generator. No. 2, 3 or APU generator can be used.

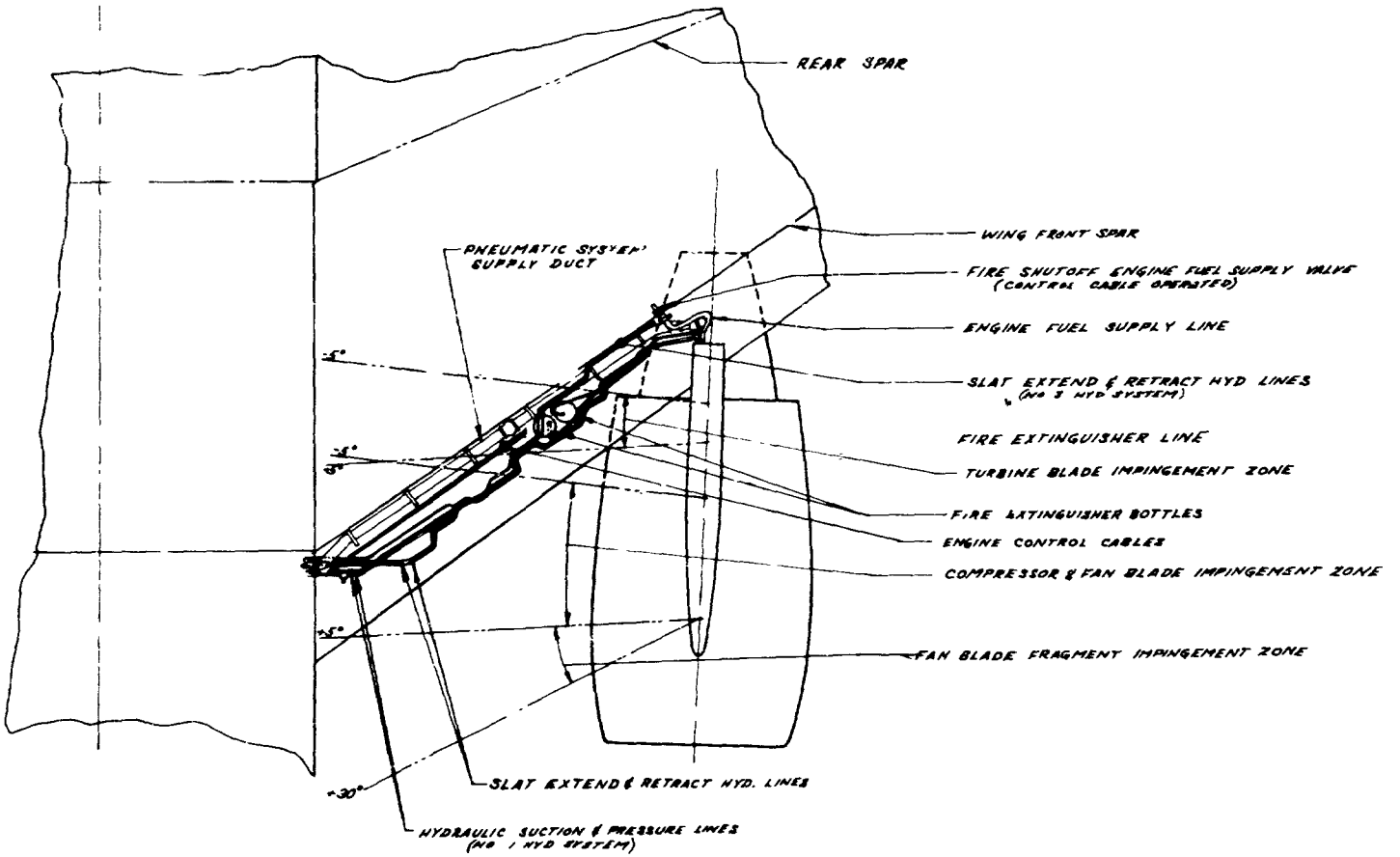

FIGURE 22
AIRPLANE SYSTEMS LOCATED IN WING LEADING EDGE

Since the loss of any or all of the above systems can be handled by other redundant systems or the airplane can be operated without the system, it would be assumed that no armor would be necessary.

The remaining systems which are in the fragment trajectory area of the forward wing spar which should be considered are the engine control cables, firex system, and the electrical system.

The engine controls include steel control cables for engine power setting, separate steel control cables to the shutoff valve on the engine mounted fuel control and additional steel control cables to a fuel shutoff valve mounted out of the fragment impingement area on the forward side of the wing spar. Severing steel control cables by fragment impingement is extremely remote in that the cables themselves present a very small target and can deflect away from the major thrust of the fragment without shearing or failing in tension. If either fuel shutoff function is disabled the other will still operate. If the power setting cables were severed the engine power would probably remain fixed but the fuel shutoff would still function, and the engine could be shut down. If the fragment were of sufficient size to disable all three systems it is likely that the engine would cease to operate but in any case the fuel to the engine could be stopped by shutting down the fuel boost pumps and transferring or dumping fuel from the tank which was feeding that engine.

The conclusion here would be that cable armor would not be warranted because of the remote possibility of a fragment impact disabling all three cable systems and the lack of serious hazard if they were disabled.

The next system to consider is the electrical system. Engine operational instrumentation relating to engine condition and power level are provided through several electrical bundles running through the fragment impingement areas. If these wires were separated by a fragment impact the engine condition and power level intelligence would be lost. This probably is of little consequence since in all probability as the result of the loss of

blade, sufficient noise or vibration would be heard or felt in the cockpit and the pilot would shut down the engine.

If the fragment generated by the engine had created a nacelle fire, which is rarely the case, and this same fragment had severed both sets of the fire detecting wires no fire warning would be provided. Also, if the fragment cut both sets of the fire extinguisher control wires then neither fire agent bottle could be discharged. Having all these things happening concurrently is again extremely remote but even under these conditions only minimal hazard exists since the engine nacelle is designed to contain a fire for fifteen minutes and it would undoubtedly by visually detected and the engine shut down within that length of time. Generally, shutting down an engine (cutting off the source of fuel for the fire) causes nacelle fires to self extinguish.

The remaining wing spar mounted system exposed to engine fragments is the fire extinguisher agent storage bottles themselves and the plumbing which conducts the fire extinguisher agent to the pylon and into the nacelle for discharge. If the single steel line is fractured the fragment would have to come from the low pressure turbine. There are no fuel lines in the low pressure turbine compartment of the nacelle, so generally no fire results. Also, punctures in the engine case in the low turbine area generally produces detectable noise, thrust losses and vibration and in all probability the engine would be shut down. Oil lines on the engine could be severed by the fragment but even if an oil fire starts in the nacelle the oil quantity is relatively small and is soon expended. Also severed oil pressure or scavenge lines would only flow measurable quantities while the engine is running and once the engine is shut down would be reduced to a small level because of the low output of the oil pumps under windmilling conditions.

o Example Showing Weight Penalty for Providing Component Armor

Although no known fragment penetrations have occurred in the area of the fire extinguishing system, additional protection for this was evaluated for establishing relative weight for armor located near this system compared to armor located near the engine.

An examination of the piping runs from the fire extinguisher agent storage bottles shows that it is exposed to trajectories emanating from both the high and low pressure turbines of the engine. If the piping and storage bottles were to be shielded from the four blade fragment and included disc serrations, one approach could be to install armor on the engine as close as possible to the engine case surface. Using the JT9D engine installation for study, this would be similar to the arrangement described earlier in this study when armor plates D and E of Figures 10, 11, and 13 were installed. The new plates would cover the same section of the engine as plates D and E in a fore and aft direction and be identical in thickness but would not need to subtend as large a portion of engine circumference since plates D and E were sized to protect the entire airframe.

By layout it was determined that the circumferential lengths of the new plates would only be 18% of the total length of plate D for the high pressure turbine section, and 19% of the plate E length for the low pressure turbine section; see Figures 23 & 24. The weights for these plates can be ratioed from the plate D and plate E weights by applying the above factors. Thus, to determine the weight required to protect the fire extinguisher systems on both wings of the candidate three engine airplane by armor applied adjacent to the engine case we use the above factors with the plate D and E weight values from Table 6.

.18 (sum of plate D weights for engines 1 and 3) +
.19 (sum of plate E weights for engines 1 and 3) =
.18 (29.6 + 60.5) + .19 (26.4 + 45.1)
= 16.2 + 13.6 = 29.8

The above 29.8 lbs. would provide sufficient steel armor to protect both wing fire extinguisher systems for the three engine airplane.

If the armor could not be installed close to the engine case, an alternative location would be to install armor in the outer portion of the nacelle similar to plates "I" and "J" on Figures 10, 11 and 13. The weight factors developed above for plates "D" and "E" would also apply in this case, i.e., weight of high pressure turbine armor would be 18% of the plate "I" weight

and the low pressure turbine armor weight would be 19% of the plate "J" weight. Again using the applicable weight values from Table 6:

.18 (sum of plate "I" weight for No. 1 and No. 3 engine) +
.19 (sum of plate "J" weight for No. 1 and No. 3 engine) =
.18 (76.3 + 155.7) + .19 (30.5 + 51.4) =
41.8 + 15.6 = 57.4 lbs

The above 57.4 lbs would provide sufficient steel armor in the outer periphery of the engine nacelles to protect both wing fire extinguisher systems for the three engine airplane. This type of installation, however, is 27.6 pounds heavier than an installation wherein the armor is located immediately adjacent to the engine case.

The next method of protection would be one in which steel armor is applied on the inner surface of the wing leading edge in the engine fragment path. As shown on Figures 23 and 24 this would involve .502 thick armor plate installations with surface areas of approximately 178 sq. inches in the L.H. wing and 315 sq. inches in the R.H. wing for high pressure turbine fragment protection and .389 thick armor plate installations with surface areas of approximately 424 sq. inches in the LH wing and 486 sq. inches in the R.H. wing for low pressure turbine fragment protection.

Since the wing leading edge structure is not designed to carry the weight for armor plate or to withstand the impact loads which could be generated, it was estimated that an additional weight equal to 25% of the armor weight would be needed for wing leading edge structural beef-up. The armor plates would be oriented to deflect the fragments under the wing and to take advantage of the largest fragment impingement angles possible. Using a material density of .286 lb/sq. in. the total installed weight of the above installation amounts to 215 pounds.

From an examination of the weight summary in Table 9 it is concluded that armor located as close as possible to the engine case is, in general, always the lightest weight approach to providing additional protection. This is due to the divergence in exposure areas for projectiles that emanate

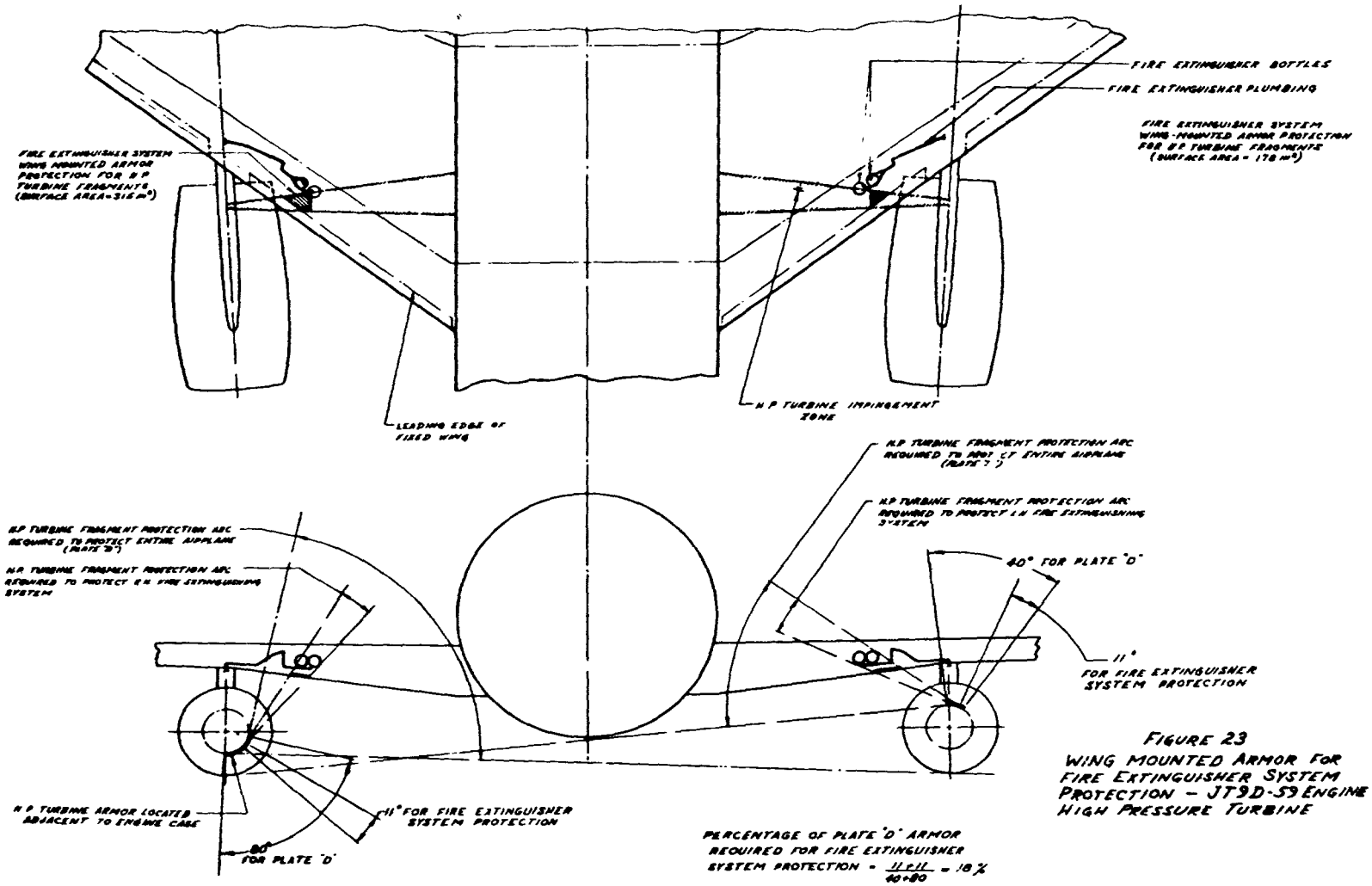

FIGURE 23
WING MOUNTED ARMOR FOR FIRE EXTINGUISHER SYSTEM PROTECTION – JT9D-59 ENGINE HIGH PRESSURE TURBINE

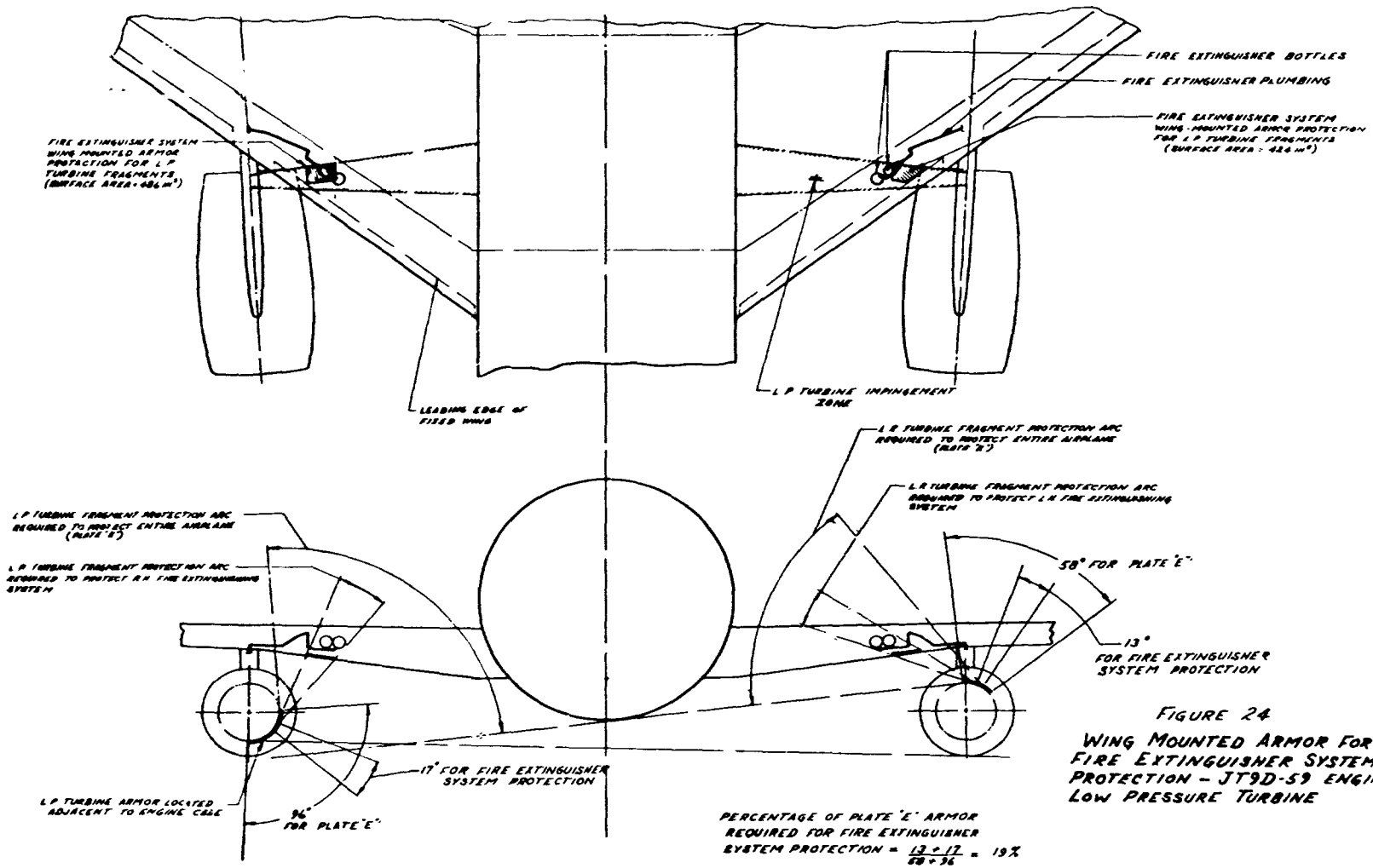

FIGURE 24

WING MOUNTED ARMOR FOR FIRE EXTINGUISHER SYSTEM PROTECTION – JT9D-59 ENGINE LOW PRESSURE TURBINE

from the engine.

TYPE OF FRAGMENT PROTECTION	INSTALLATION WEIGHT FOR INBOARD WING ENGINES POUNDS PER AIRPLANE
Steel Armor Mounted on Engine Surface	29.8
Steel Armor Mounted in Nacelle (Outer Periphery)	57.4
Steel Armor Mounted in Wing Leading Edge	215.0

Table 9. Weight Comparison for Various Installation Locations for Fire Extinguisher System Armor Protection

5.0 BLADE TIP FRAGMENT EVALUATION

After reviewing actual secondary inlet damage caused by fan blade tip fragments, it was possible to develop some theories on the mechanism involved with a blade failure, the trajectory taken by the fragment after being liberated from the main portion of the blade, and the energy developed in the inlet wall penetrating direction. The results of test conducted during this study were also helpful when actual inlet damage was compared to damage created under controlled conditions.

First, as the fragment breaks away from the main portion of the fan blade it comes in contact with the surface of the engine containment ring opposite the blade tips. It is probably driven around the containment ring some distance by the adjacent blade. Considerable tip load is developed due to the centripetal force reacted on the fragment to make it follow the containment case radius and the friction developed between the fragment and the case. (If no fan case were present, the fragment would leave the plane of rotation tangential to the blade tips). The high tip load and the driving force caused by adjacent blades creates a bending load in the fragment and even a full blade (failed at the inner dovetail) tends to fail at the point of maximum bending and this results in a whole blade breaking into smaller fragments.

Secondly, while the fragment is in contact with the sloped surface of the containment ring (which may only be a small portion of a revolution) a force is developed tending to cause the blade fragment to move forward. This could be analogous to a weight on an inclined plane. The forward force developed would be directly proportional to mass of the fragment, and the coefficient of friction at the rubbing surface. Also, since the blade tip has an angle of attack, the tip tends to auger forward following a spiral path along the containment case similar to following a screw thread.

The distance the blade fragment travels forward while following a spiraling path around the containment ring or inlet depends on the initial energy imparted to the fragment which includes the mass and the velocity at the time of failure and the friction coefficient developed at the surface. If we assumed that the entire inlet was cylindrical in shape and was capable

of containing the fragment, the fragments would spiral forward and because of the surface friction would come to rest at some point. Blade tip aerodynamics would have some effect on the forward movement due to blade lift but this effect would be small.

The fact that some fragments do lose energy without penetrating the inlet introduces another mechanism which causes secondary damage. Smaller fragments will lose translational energy due to friction and only move a short distance forward of the plane of fan rotation. When this happens, they intrude back into the rotating fan plane due to the airflow in the inlet and are batted either forward or aft depending on the point of fragment contact with the rotating blade and the relationship to the fragment center of gravity. The intruding fragment can create additional fragments by damaging additional blades or the fragment could be batted forward or broken into smaller fragments by the impact.

Figure 25 shows the predicted velocity along the fragment trajectory for spiraled fragments and for batted or ricocheted fragments. The spiraled fragments develop inlet surface penetrating forces tangential to the surface and for batted fragment the velocity normal to the surface governs the penetrating force. Figure 25 also shows the maximum normal velocity for batted fragments. The normal velocity curve was taken from previous Douglas work which accounted for the point at which the fragment impacted the rotating blade and since this occurrence is random, only the maximum trajectory velocity and normal velocity are shown. Fragment impacts near the fan tip result in a relatively high trajectory velocity but the fragment direction is near parallel to the inlet surface thus very low forces are developed normal to the surface and the likelihood of penetration is remote. Impacts close to the fan hub result in a trajectory more normal to the inlet surface but the velocity is low and again the penetration energy is low. The maximum normal force developed at the inlet surface results from fragment impacts at radii within 40 to 60% of the fan blade span length. As the fragment to inlet surface impact point moves forward the normal velocity is reduced since for the fragment to reach the more forward points the impingement angle from normal must be increased resulting in less normal force. The fragment strikes the inlet surface in a more glancing direction.

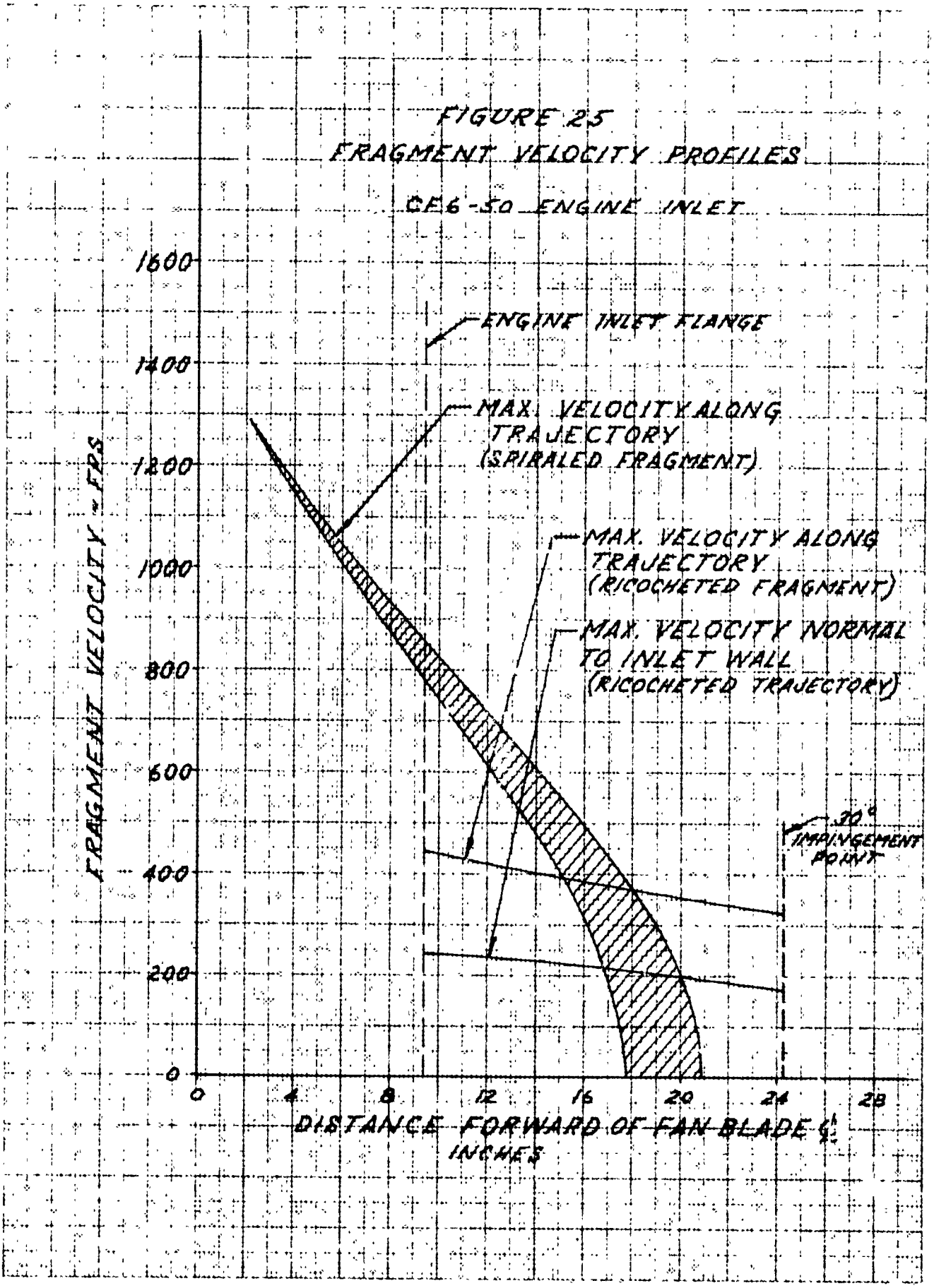
FIGURE 25
FRAGMENT VELOCITY PROFILES
CF6-50 ENGINE INLET
ENGINE INLET FLANGE
MAX. VELOCITY ALONG TRAJECTORY (SPIRALED FRAGMENT)
MAX. VELOCITY ALONG TRAJECTORY (RICOCHETED FRAGMENT)
MAX. VELOCITY NORMAL TO INLET WALL (RICOCHETED TRAJECTORY)
30° IMPINGEMENT POINT
FRAGMENT VELOCITY - FPS
1600
1400
1200
1000
800
600
400
200
0
0
4
8
12
16
20
24
28
DISTANCE FORWARD OF FAN BLADE ℄
INCHES

With the spiraling fragment, it is difficult to predict exactly what the velocity would be along the trajectory in that the fragment skids over different materials along its path and each material has a different coefficient of friction. The fragment would first contact the fan tip rub strip then acoustic material within the containment ring or inlet. Because of the friction coefficient difference the spiraled trajectory curve covers a band of velocities and for this study the upper line was used.

There are some effects of fragment size and mass but for this part of the study only the 3 x 5 x 0.25 inch 0.55 lb fragment was considered. The test portion of the report, however, also includes a fragment of 4 x 7 x 0.25 inches at 1.1 lbs.

5.1 Inlet Armor for CF6 Powered Study Airplanes

5.1.1 Inlet Construction for the CF6 Engine - The wing inlets on the CF6 study airplanes have a single layer 3/4 inch thick bonded aluminum honeycomb in the inner barrel. The honeycomb is bonded with 0.025 inch thick 2014-T6 aluminum sheet perforated with 0.050 inch diameter holes on the fragment impact side and 0.020 inch thick 2014-T6 solid sheet on the exit side. The core is a 0.003 inch thick ribbon of 5052 aluminum bonded in a 3/8 inch diamond pattern. The sketch on Figure 26 shows the inlet installed on the engine and the relationship of the attach flange to the fragment trajectory.

The tail inlet on the 3 engine airplane is composed of a steel stresskin bellmouth bolted to the engine inlet flange and a stresskin transition ring which seals between the bellmouth and fixed inlet; See Figure 27. Stresskin is an all stainless steel honeycomb which is fabricated by spot welding the core, which has flanges, to the inner and outer face sheets making a panel 3/4 inches thick. The bellmouth portion has the inner sheet perforated with 0.094 inch diameter holes for noise absorption. The inner sheet of both the bellmouth and transition ring is 0.016 inches thick and the outer sheet is 0.012 inch thick; both are 316L stainless steel. The core is 0.0035 inches thick spotwelded to the face sheets in a 3/8 inch diamond pattern.

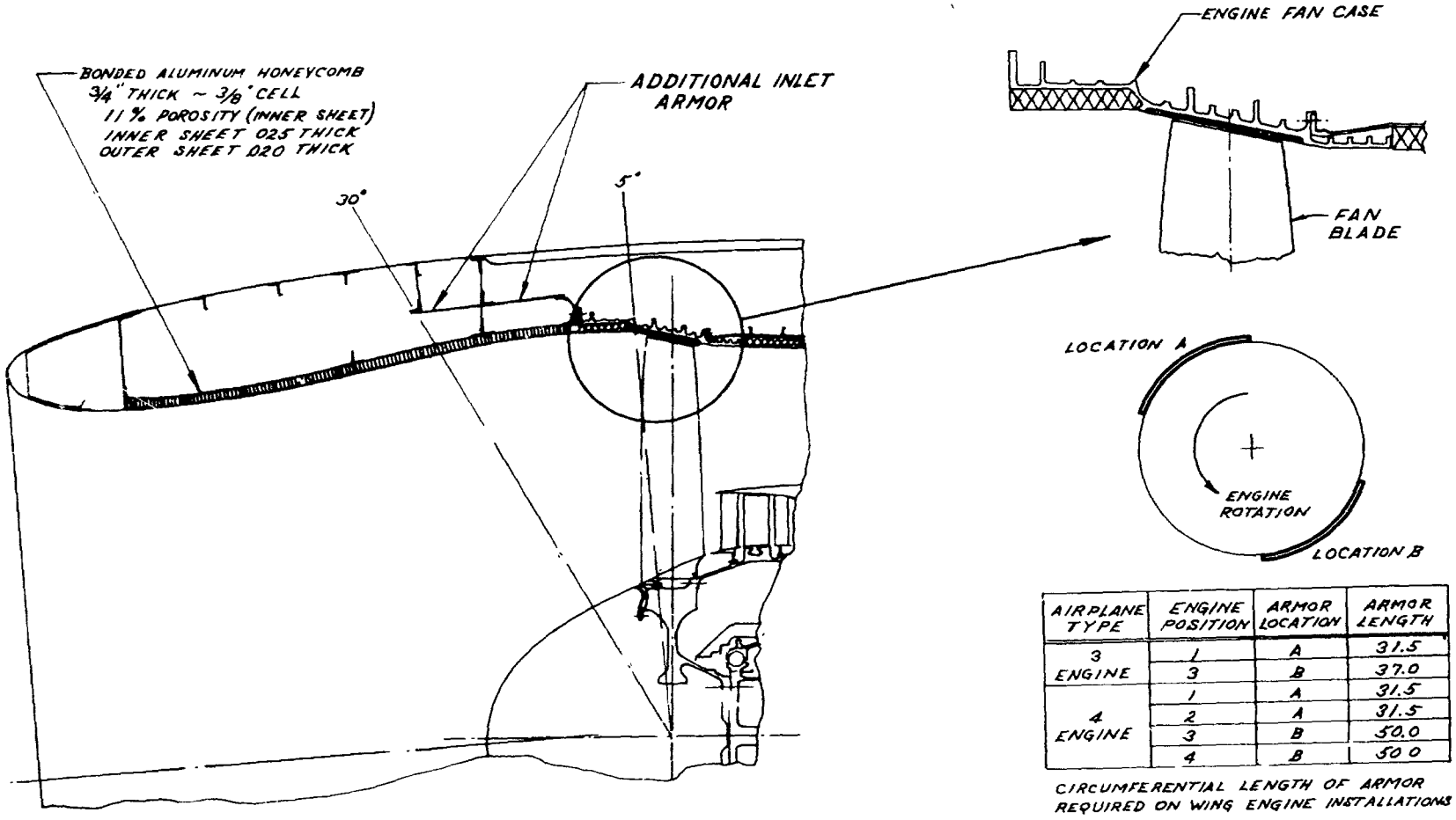

AIRPLANE TYPE	ENGINE POSITION	ARMOR LOCATION	ARMOR LENGTH
3 ENGINE	1	A	31.5
	3	B	37.0
4 ENGINE	1	A	31.5
	2	A	31.5
	3	B	50.0
	4	B	50.0

CIRCUMFERENTIAL LENGTH OF ARMOR REQUIRED ON WING ENGINE INSTALLATIONS

FIGURE 26. CF6-50C ENGINE INLET FOR WING INSTL

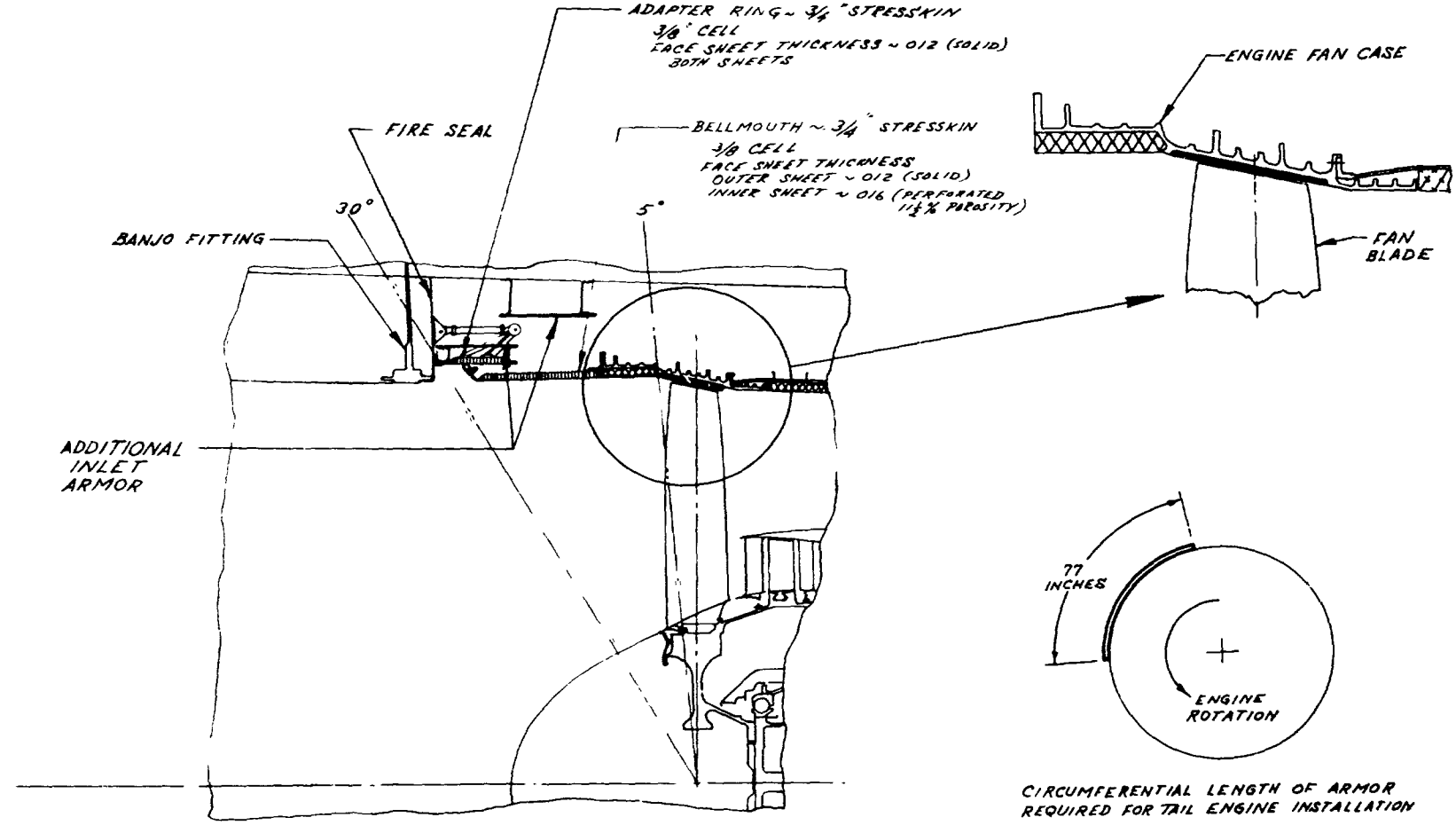

FIGURE 27. CF6-50C ENGINE INLET FOR TAIL INSTL.

5.1.2 Wing Inlet Armor for CF6-50 Engine - By reviewing Figure 26, it can be observed that the inlet can be exposed to fragments spiraled or batted forward. The spiraled fragments enter the inlet material in a tangential manner while batted or ricocheted fragments involve a fragment entrance velocity more normal to the surface. The CF6 engine has an inlet extension which is part of the containment system and this extension is adequate to contain either type of fragment, spiraled or recocheted, since here we are only concerned with the 3 x 5 x 0.25 inch fragment and the engine containment system is designed for an entire blade.

In the area just forward of the attach ring see (Figure 26) the inlet is exposed to a spiraling fragment with a velocity of about 850 ft/sec assuming the coefficient of friction used is correct. The energy developed by a 3 x 5 x 0.25 inch fragment at .55 lbs would be equal to:

$$E = \frac{W}{2g}(V)^2 = \frac{.55}{64.4}(850)^2 = 6170 \text{ ft-lbs}$$

W = .55 lbs
g = gravitational constant = 32 2 ft/sec^2
V = Velocity = 850 ft/sec

Assuming the fragment entered the armor in a near tangential manner, to be conservative, say 70° from normal, the steel thickness to contain would be:

$$t^2 = \frac{E\,(12\cos^2\theta)}{LT}$$

$$t^2 = \frac{(6170)(12)(.342)^2}{(6.5)(188500)} = .00706$$

$$t = \sqrt{.00706} = .084 \text{ inches}$$

E = energy ft-lbs
L = 6.5 fragment perimeter(inches)
T = 188500 psi dynamic shear modulus for steel
θ = 70°

$\cos\theta = .342$

t = steel thickness to contain, (inches)

Considering the batted fragment at the same station the fragment would enter the inlet at a normal impact angle at a velocity of 250 ft/sec; see Figure 25 . The energy would be as follows:

$$E = \frac{.55}{64.4}(250)^2 = 534 \text{ ft-lbs}$$

The steel thickness required to contain would be:

$$t^2 = \frac{E\,(12\cos^2\theta)}{LT} = \frac{(534)\,(12)}{(6.5)(188500)}$$

$$t = \sqrt{.0052} = .072 \text{ inches}$$

$\theta = 90°$

$\cos\theta = 1$

Since the previous calculation for the spiraled fragment at this station indicated .084 inch thick steel material was required to contain and was thicker than required for the batted normal impingement the thicker material would have to be installed.

At 12 inches forward, the spiraled fragment would be slowed to about 715 ft/sec and would develop the following energy:

$$E = \frac{W}{2g}(V)^2 = \frac{.55}{64.4}(715)^2 = 4366 \text{ ft-lbs}$$

which would require steel armor thickness equivalent to:

$$t^2 = \frac{E\,(12\cos^2\theta)}{LT} = \frac{(4366)\,(12)\,(.342)^2}{(6.5)(188500)}$$

$$t = \sqrt{.0050} = .070 \text{ inches}$$

At this same plane for the normal impingement batted fragment the velocity would be about 240 ft/sec and the energy would be as follows:

$$E = \frac{W}{2g}(V)^2 = \frac{.55}{64.4}(240)^2 = 492 \text{ ft-lbs}$$

The steel thickness required to contain would be:

$$t^2 = \frac{E\,(12\cos^2\theta)}{LT} = \frac{(492)\,(12)}{(6.5)\,(188500)} = 00482$$

$$t = \sqrt{.00482} = .069 \text{ inches}$$

As shown the steel thickness required for spiraled fragment containment at the 12 inch point was .070 thick and for the batted fragment was .069. Therefore, the steel thickness forward of the 12 inch point would be controlled by normal impingement fragments and the thickness determined would be more than adequate to contain the spiraled fragment.

At 18 inches forward only the normal impingement is considered; the fragment velocity would be about 210 ft/sec and the energy would be:

$$E = \frac{W}{2g}(V)^2 = \frac{.55}{64.4}(210)^2 = 376 \text{ ft-lbs}$$

The steel thickness to contain would be:

$$t^2 = \frac{E(12\cos^2\theta)}{LT} = \frac{(376)\,(12)}{(6.5)\,(188500)} = .00368$$

$$t = \sqrt{.00368} = .060 \text{ inches}$$

At 24 inches forward again only the normal impingement need be considered at a velocity of 180 ft/sec and the energy would be:

$$E = \frac{W}{2g}V^2 = \frac{.55}{64.4}(180)^2 = 277 \text{ ft-lbs}$$

The steel thickness required to contain would be:

$$t^2 = \frac{E\,(12\cos^2\theta)}{LT} = \frac{(277)\,(12)}{(6.5)\,(188500)} = .0027$$

$$t = \sqrt{.0027} = .052 \text{ inches}$$

The armor would be tapered as shown in Figure 28.

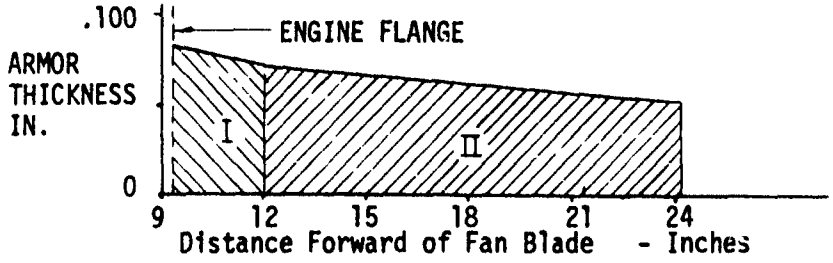

Figure 28. Armor Thickness for the CF6 Engine Inlet

The average thickness of Section I would be:

$$t_{ave} = \frac{.084 + .070}{2} = \frac{154}{2} = .077 \text{ inches}$$

The average thickness of Section II would be:

$$t_{ave} = \frac{.070 + .052}{2} = \frac{122}{2} = .061 \text{ inches}$$

Utilizing these thicknesses the total armor weight is then calculated.

From Figure 26 the length of armor to subtend the arc of protection is shown for 3 and 4 engine airplanes. For example, for the #1 engine this length would be 31.5 inches. From Figure 26, the fore and aft requirement of armor width is determined to be 2.6 inches for Section I and 12.2 for Section II.

Using #1 engine as an example and assuming there is no energy absorbed by the inlet structure, and sheet steel is used at .286 lb/in^3, the armor weight would be:

$W = L \times W \times t_{ave} \times .286 \times 1.25$

L = Length from Figure

w = Width from Figure

t_{ave} = Average thickness from previous calculation for I and II

.286 lb/in^3 = steel density

1.25 = installation factor established by layout

Section I = W = 31.5 x 2.6 x .077 x .286 x 1.25 = 2.2 lbs

Section II = W = 31.5 x 12.2 x .061 x .286 x 1.25 = 8.4

Total Weight = 10.6 lbs

Tables 10 and 11 provide the dimensions and total weight for 3 and 4 engine airplane inlet armor.

Engine Position	Section	Armor Dimensions			Armor Density lb/in^3	Instal. Factor	Armor Weight lbs
		Length (inches)	Width (inches)	Average Thickness (inches)			
1	I	31.5	2.6	.077	.286	1.25	2.2
	II	31.5	12.2	.061	.286	1.25	8.4
	Total Armor Weight for #1 Engine Inlet						10.6
3	I	37.0	2.6	.077	.286	1.25	2.7
	II	37.0	12.2	.061	.286	1.25	9.8
	Total Armor Weight for #3 Engine Inlet						12.5
Total Weight Wing Engine Armor							23.1 lbs

Table 10. Steel Inlet Armor for the CF6 Wing Engine on a 3 Engine Airplane (assuming no energy absorbed by the inlet material)

Engine Position	Section	Armor Dimensions			Armor Density lb/in^3	Instal. Factor	Armor Weight lbs
		Length (inches)	Width (inches)	Average Thickness (inches)			
1	I	31.5	2.6	.077	.286	1.25	2.2
	II	31.5	12.2	.061	.286	1.25	8.4
	Total Armor Weight for #1 Engine Inlet						10.6
2	I	31.5	2.6	.077	.286	1.25	2.2
	II	31.5	12.2	.061	.286	1.25	8.4
	Total Armor Weight for #2 Engine Inlet						10.6
3	I	50	2.6	.077	.286	1.25	3.6
	II	50	12.2	.061	.286	1.25	13.3
	Total Armor Weight for #3 Engine Inlet						16.9
4	I	50	2.6	.077	.286	1.25	3.6
	II	50	12.2	.061	.286	1.25	13.3
	Total Armor Weight for #4 Engine Inlet						16.9
TOTAL WEIGHT FOR AIRPLANE							55 lbs.

Table 11. Steel Armor for the CF6 Engine on a 4 Engine Airplane (assuming no energy absorbed by the inlet material)

By utilizing the data developed during the test portion of this study and taking advantage of the energy absorption capabilities of the inlet material the inlet armor weight could be reduced. Referring to Figure 25, the fragment velocity at the inlet flange was 850 ft/sec and the energy previously calculated was 6170 ft-lbs. From test it was determined if the 3/4 inch honeycomb inlet were impacted tangentially could absorb 2395 ft-lbs. Thus the energy remaining from the fragment near the inlet flange after penetration would be as follows:

$$E_R = 6170 - 2395 = 3775 \text{ ft-lbs}$$

Thus, the steel armor would only need to absorb the 3775 ft-lbs at a velocity of:

$$V^2 = \frac{(E)\ (64.4)}{.55} = \frac{(3775)\ (64.4)}{.55} = 442018$$

$$V = 665 \text{ ft/sec}$$

and an armor thickness of:

$$t^2 = \frac{E\ (12\ \cos^2\theta)}{LT} = \frac{(3775)\ (12)\ (.342)^2}{(6.5)\ (188500)} = .00432$$

t = .066 inch at the inlet flange where without accounting for the inlet material the steel thickness required was determined at a value of .084 inches.

At this same plane it was also determined previously that the batted fragment required steel at .072 inches. However, during testing it was found that 3/4 inch aluminum honeycomb would absorb 113 ft-lbs of energy when the fragment impacted normal to the surface. Thus after penetrating the honeycomb the fragment energy remaining would be:

$$E_R = 534 - 113 = 421 \text{ ft-lbs}$$

Thus the steel armor thickness required would be:

$$t^2 = \frac{E\ (12\ \cos^2\theta)}{LT} = \frac{(421)\ (12)}{(6.5)\ (188500)} = .00412$$

t = .064 inches

Therefore the .066 inch thick armor determined for the spiral fragment would also contain the batted fragment.

At 12 inches forward only normal impingements need be considered, since the inlet material could absorb sufficient energy from the spiraled fragment. At this plane, 492 ft-lbs of energy is developed in the normal direction and the remaining energy after penetration would be:

$$E_R = 492 - 113 = 379 \text{ ft-lbs}$$

The steel thickness required would be:

$$t^2 = \frac{E\ (12 \cos^2\theta)}{LT} = \frac{(379)\ (12)}{(6.5)\ (188500)} = .0037$$

Accounting for energy absorption the thickness required was .061 inches.

At 18 inches forward the fragment energy normal to the surface was determined to be 376 ft-lbs and taking advantage of the honeycomb absorption, the remaining energy would be:

$$E_R = 376 - 113 = 263 \text{ ft-lbs}$$

The thickness of armor required would be:

$$t^2 = \frac{E\ (12 \cos^2\theta)}{LT} = \frac{(263)\ (12)}{(6.5)\ (188500)} = .00257$$

$t = \sqrt{.00257} = .051$ inches where without considering absorption, .060 inch thick armor was required.

Finally, at the 24 inch point, 277 ft-lbs of energy was developed and accounting for absorption by penetration of the honeycomb the energy remaining would be:

$$E_R = 277 - 113 = 164 \text{ ft-lbs}$$

The steel thickness required to contain would be:

$$t^2 = \frac{E\ (12 \cos^2\theta)}{LT} = \frac{(164)\ (12)}{(6.5)\ (188500)} = .0016$$

$t = \sqrt{.0016} = .040$ inches compared to .052 previously determined with

no absorption by the honeycomb.

The armor could then be tapered as shown in Figure 29:

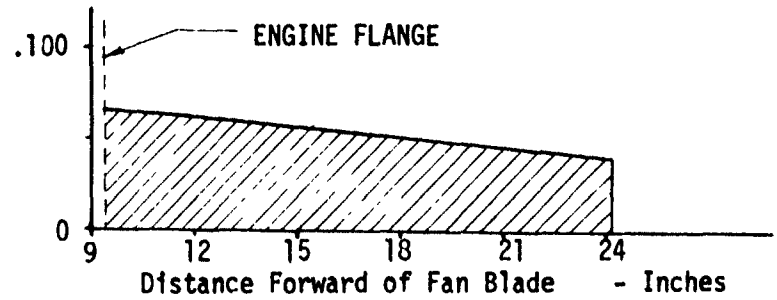

Figure 29. Inlet Armor Thickness Required (assumes some energy absorbed by inlet material)

The average thickness would be:

$$t_{ave} = \frac{.066 + .061 + .051 + .040}{4} = .054 \text{ inches}$$

The total armor weight considering the absorption capability of the aluminum honeycomb would be as follows on Table 12:

Engine Position	Armor Dimensions			Armor Density lb/in^3	Installation Factor	Armor Weight lbs.
	Length (inches)	Width (inches)	Average Thickness (inches)			
1	31.5	14.8	.054	.286	1.25	9.0
3	37.0	14.8	.054	.286	1.25	10.6
Total Weight Wing Engine Armor						19.6

Table 12. Steel Inlet Armor for Wing Engines on a 3 Engine Airplane (accounting for fragment energy absorbed by inlet material)

Accounting for the energy absorbed by the inlet material saves about 3.5 pounds for wing inlet armor on the 3 engine airplane for the total weight. See Section 5.1.3 for the tail inlet.

For the four engine airplane considering the absorption capability of aluminum honeycomb the armor weight would be as follows on Table 13:

Engine Position	Armor Dimensions			Armor Density lb/in^3	Installation Factor	Armor Weight lbs
	Length (inches)	Width (inches)	Average Thickness (inches)			
1	31.5	14.8	.054	.286	1.25	9.0
2	31.5	14.8	.054	.286	1.25	9.0
3	50	14.8	.054	.286	1.25	14.3
4	50	14.8	.054	.286	1.25	14.3
Total Weight for Airplane						46.6 lbs

Table 13.Steel Inlet Armor Required for a 4 Engine Airplane (accounting for fragment energy absorbed by inlet material)

Accounting for the energy absorption of the inlet material saves about 8.6 lbs total on the four engine airplane.

5.1.3 Tail Inlet Armor for CF6-50 Engine - The same procedure used to establish the fragment velocity and energy levels for the wing inlet were used for the tail inlet for the 3 engine airplane. In Section 5.1.2, the armor thickness was determined for the wing engines and it was first assumed that no energy was absorbed by the inlet material. For the tail engine these same thicknesses would apply but because of the way the bellmouth is mounted on the engine, without having an outer structure like the wing inlet, armor mounting would be more difficult and would require more weight to be assigned for mounting. A preliminary layout indicated that the armor mounting factor should be 1.50 when compared to the 1.25 factor used for the wing inlet armor. For the tail inlet evaluation the armor would need to cover an arc equivalent to a length of 77 inches as shown on Figure 27.

The weight using the previous thicknesses shown on Figure 28 would be as shown on Table 14.

Engine Position	Section	Armor Dimensions			Armor Density (lb/in^3)	Installation Factor	Armor Weight (lbs)
		Length (inches)	Width (inches)	Average Thickness (inches)			
Tail (no. 2)	I	77	2.6	.077	.286	1.50	6.6
	II	77	12.2	.061	.286	1.50	24.6
Total Armor Weight Tail Engine							31.2

Table 14.Steel Armor Required for Tail Inlet for the CF6 Powered 3 Engine Airplane (assumes no energy absorbed by the inlet material)

Following the same method used on the wing inlet but taking into account the absorption capability of the stresskin inlet material, determined by test, the total weight for armor can be reduced considerably. The tests indicated that this particular stresskin configuration can absorb 3349 ft-lbs of energy when impacted tangentially by a 3 x 5 x 0.25 inch 0.55 lb fragment and 1240 ft-lbs when impacted in a normal direction.

Just forward of the attach flange it was previously determined that spiraled fragments could develop an energy equal to:

$$E = 6170 \text{ ft-lbs}$$

Thus, after penetrating the stresskin the fragment energy remaining would be:

$$E_R = 6170 - 3349 = 2821 \text{ ft-lbs}$$

To contain this level of energy would require a steel thickness of:

$$t^2 = \frac{E\ 12\ \cos^2\theta}{L_T} = \frac{(2821)\ (12)\ (.342)^2}{(6.5)\ (188500)} = .0032$$

$$t = \sqrt{.0032} = .057 \text{ inches}$$

where it had been previously determined that without accounting for inlet material energy absorption .084 thick armor would be required. In considering the batted or ricocheted fragment it was previously determined that the maximum energy developed by the fragment in the normal direction was:

$$E = 534 \text{ ft-lbs}$$

However, the test data indicated that the stresskin can absorb 1240 ft-lbs in the normal direction. Thus the inlet has excess containment margin for impacts from batted fragments of the size and energy considered. The containment margin would be as follows:

$$E_M = 1240 - 534 = 706 \text{ ft-lb}$$

Since excess containment margin exists, the batted fragment impingements can be ignored.

As the spiraled fragment moves forward the velocity and energy is reduced and at the point the material energy capability and the tangential fragment energy are equal no further armor is required. This velocity can be calculated as follows using the material absorption energy level:

$$E = \frac{W}{2g} V^2$$

$$V^2 = \frac{(E)\ (2g)}{W} = \frac{(3349)\ (64.4)}{.55} = 392137$$

$$V = \sqrt{392137} = 626 \text{ ft/sec}$$

From the curve Figure 25 showing the spiraled fragment trajectory velocity at various distances forward of the inlet flange and at 626 ft/sec it will be found that the equilibrium point would occur at a distance of 13.6 inches. Therefore, the armor would need to extend from the inlet flange at 9.4 inches forward of the fan blade centerline to 13.6 inches or a total length of 4.2 inches. Theoretically, the armor could taper from a zero thickness on the forward edge to .057 inches at the aft edge. This would be impractical to rivet in place so it was assumed that the minimum thickness at the forward edge would be .020 inches thick.

The average thickness then would be:

$$t_{ave} = \frac{.057 + .020}{2} = .039 \text{ inches}$$

The only required armor would then be a Section 4.2 inches wide forward of the inlet flange at an average thickness of .039 inches. Table 15 shows the total weight required.

Engine Position	Armor Dimensions			Armor Density (lb/in^3)	Instal. Factor	Armor Weight (lbs)
	Length (inches)	Width (inches)	Average Thickness (inches)			
Tail (no. 2)	77	4.2	.039	.286	1.50	5.4
Total Armor Weight Tail Engine						5.4

Table 15. Steel Armor Required for the Inlet for CF6 Powered 3 Engine Airplane (allowance made for energy absorbed by the inlet material)

By comparing Table 14 and 15 it will be apparent that by accounting for the energy absorption capability of the inlet material, in this case stresskin, the armor weight was reduced from 31.2 lbs to 5.4 lbs. This amounts to a weight savings of 25.8 lbs.

5.1.4 Total Inlet Armor Weight - The preceding analysis assumed that the armor installation was tailored to each engine and the amount of armor required was based on the engine position. For actual installation, the inlet armor for wing engines would need to be position interchangeable.

Thus, the total weight for inlet position interchangeability would be as shown in Table 16 and 17.

Engine Position	Armor Weight Non-Interchangeable (lbs)	Armor Weight Interchangeable (lbs)
1	10.6	23.1
2	31.2	31.2
3	12.5	23.1
TOTAL	54.3	77.4

Table 16. Total Weight for Inlet Armor for Non-Interchangeable and Interchangeable Armor Installations - 3 Engine CF6 Powered Airplane

Engine Position	Armor Weight Non-Interchangeable (lbs)	Armor Weight Interchangeable (lbs)
1	10.6	27.5
2	10.6	27.5
3	16.9	27.5
4	16.9	27.5
TOTAL	55	110

Table 17. Total Weight for Inlet Armor for Non-Interchangeable and Interchangeable Armor Installations - 4 Engine CF6 Powered Airplanes

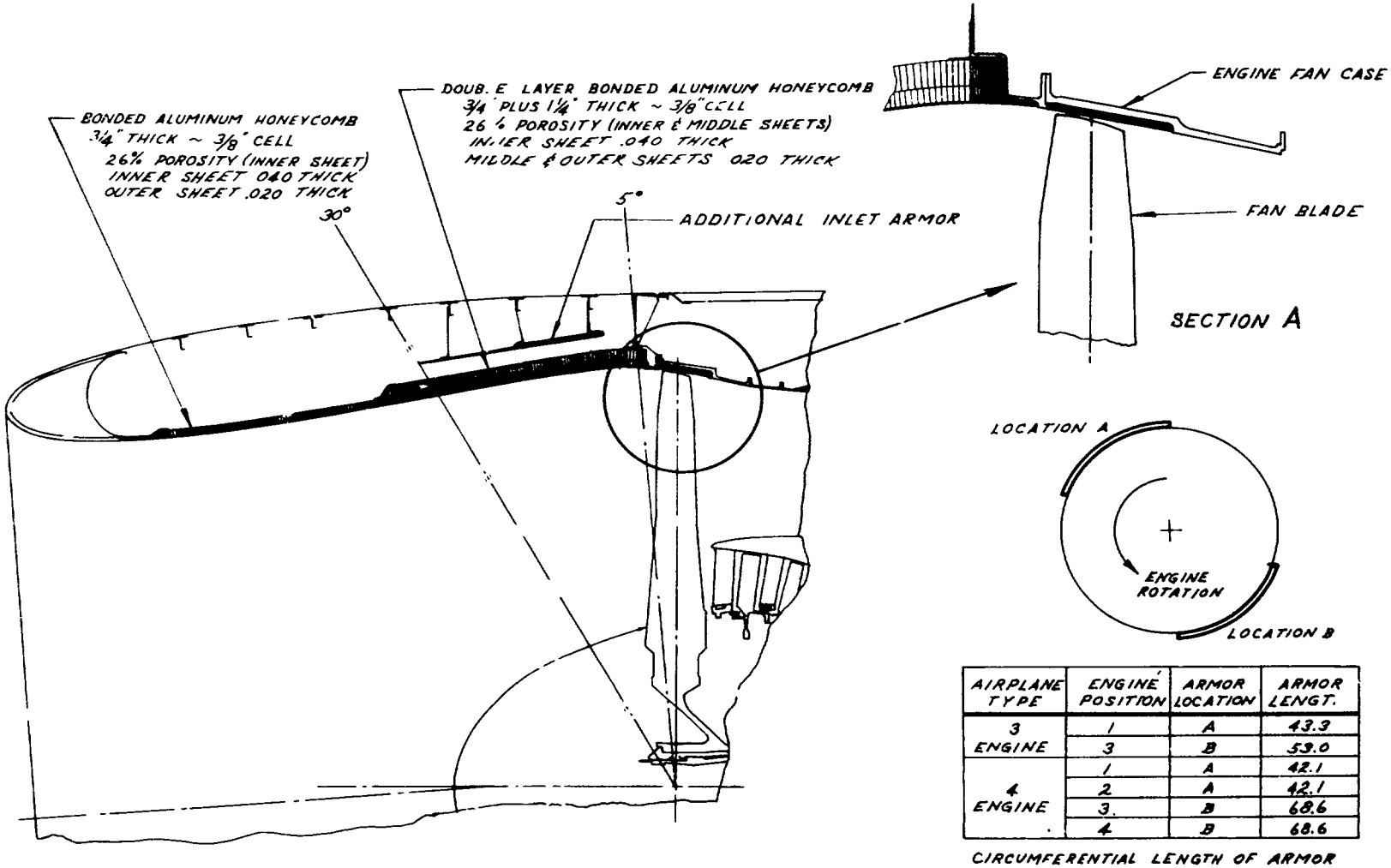

AIRPLANE TYPE	ENGINE POSITION	ARMOR LOCATION	ARMOR LENGT.
3 ENGINE	1	A	43.3
	3	B	53.0
4 ENGINE	1	A	42.1
	2	A	42.1
	3	B	68.6
	4	B	68.6

CIRCUMFERENTIAL LENGTH OF ARMOR REQUIRED ON WING ENGINE INSTALLATIONS

FIGURE 30. JT9D-59 ENGINE INLET FOR WING INSTL.

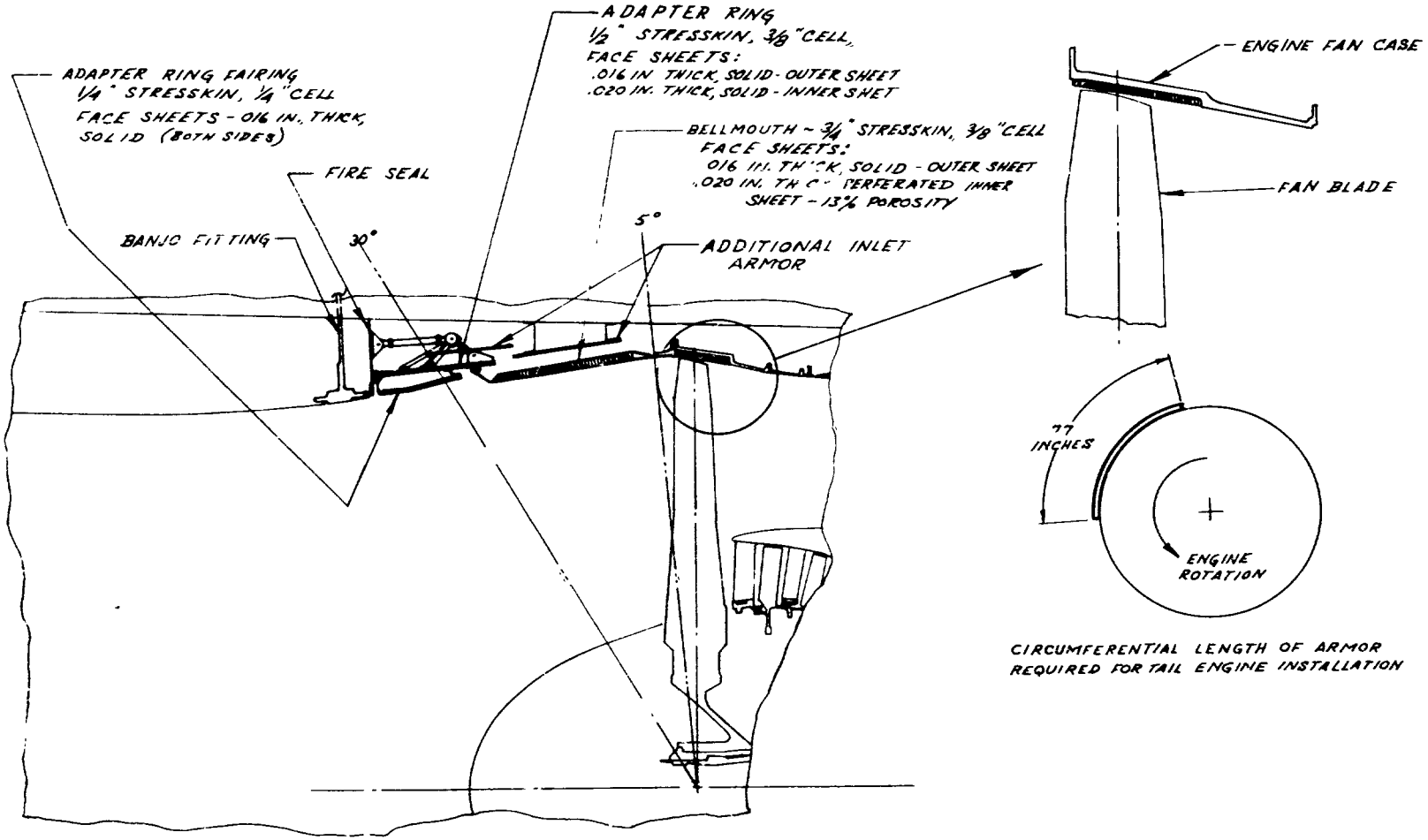

FIGURE 31. JT9D-59 ENGINE INLET FOR TAIL INSTL

5.2 Inlet Armor for the JT9D Powered Study Airplanes

5.2.1 Inlet Construction for the JT9D Engine - The wing inlets for the JT9D study airplanes have an inner barrel just forward of the fan composed of an inner layer of 3/4 inch aluminum honeycomb and bonded to the outer surface is an additional layer of 1-1/4 inch deep honeycomb making a total of depth of 2 inches of honeycomb. The aluminum sheet on the inner wall and the septum sheet between honeycomb layers are perforated with small holes and the bonded assembly provides an acoustic noise absorber to reduce fan generated noise. See Figure 30.

The inlet on the tail installation of the JT9D powered three-engine airplane is composed of a steel stresskin bellmouth bolted to the engine inlet flange and a stresskin transition ring which seals between the bellmouth and fixed inlet. See Figure 31. Stresskin is an all stainless steel honeycomb which is fabricated by spotwelding the core, which has flanges, to the face sheets. The inner face sheet of the bellmouth in this application is also perforated for noise absorption.

5.2.2 Wing Inlet Armor for JT9D Engine - As with the CF6 engine the JT9D is exposed to fan blade fragments either spiraled forward or batted forward by rotating fan blades. The predicted velocity along the fragment path for spiraled and batted fragment is shown on Figure 32. Also shown is the velocity predicted for the normal impingement of batted or ricocheted fragments. The spiraled fragments tend to enter the inlet material in a tangential trajectory. The wing inlet attach flange on the JT9D is somewhat different than for the CF6 in that a firewall bulkhead is installed just forward of the attach flange. This makes the area 7 to 8 inches forward of the flange very stiff plus in this area the steel attach flange extends forward and heavy doublers are used to conduct the inlet loads back to the attach flange. See Section A on Figure 30. Because of the inlet construction it would be capable of withstanding the impact of the 3 x 5 x 0.25 inch fragment at least to a point 8 inches forward of the fan blade center line. Therefore for this study it was assumed that no armor aft of the 8 inch point would be needed.

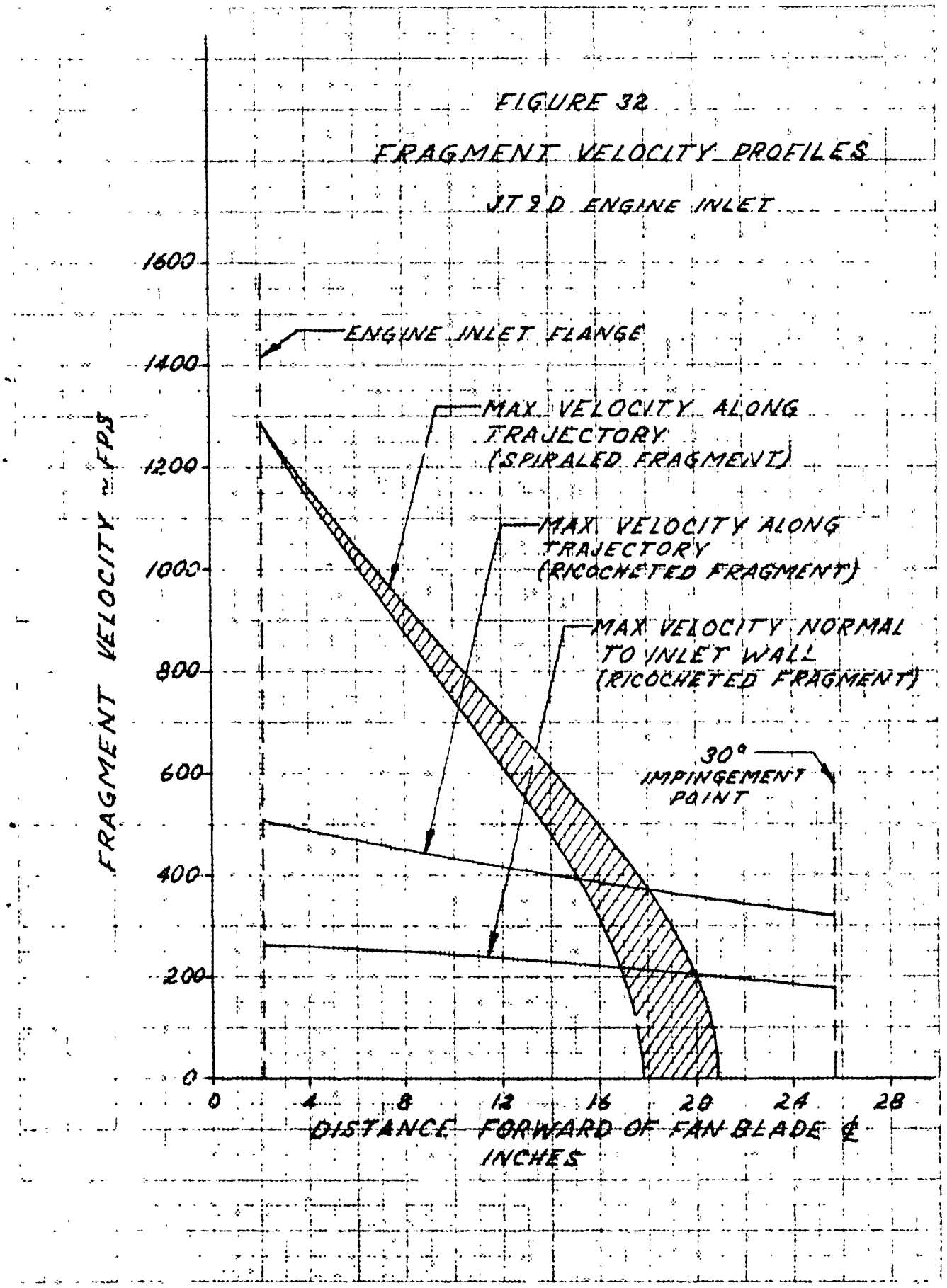
FIGURE 32
FRAGMENT VELOCITY PROFILES
JT 2D ENGINE INLET
ENGINE INLET FLANGE
MAX VELOCITY ALONG TRAJECTORY (SPIRALED FRAGMENT)
MAX VELOCITY ALONG TRAJECTORY (RICOCHETED FRAGMENT)
MAX VELOCITY NORMAL TO INLET WALL (RICOCHETED FRAGMENT)
30° IMPINGEMENT POINT
FRAGMENT VELOCITY ~ FPS
1600
1400
1200
1000
800
600
400
200
0
0
4
8
12
16
20
24
28
DISTANCE FORWARD OF FAN BLADE ℄
INCHES

As was described in Section 5.1.2 considering that no energy is absorbed by the inlet material (in this case in the area forward of the 8 inch point discussed above) the armor weight was determined.

First calculating the energy developed by the 3 x 5 x 0.25 inch spiraled fragment at the 8 inch fwd point using a velocity of 920 ft/sec from the curve on Figure 32 as follows:

$$E = \frac{W}{2g}(V)^2 = \frac{.55}{64.4}(920)^2 = 7229 \text{ ft-lbs}$$

The armor thickness required to contain this amount of energy assuming the angle of impingement on the armor plate would be close to tangential, but to be conservative it was assumed to be 70° from normal, the thickness is:

$$E = \frac{LT(t)^2}{12\cos^2\theta}$$

$$t = \frac{E(12\cos^2\theta)}{LT}$$

$$t^2 = \frac{(7229)(12)(.342)^2}{(6.5)(188500)}$$

$$t = \sqrt{.00828} = .091 \text{ inches}$$

L = impact perimeter equal to 6.5 inches for the 3 x 5 x 0.25 inch fragment

T = 188500 psi dynamic shear modulus for steel

θ = 70° assumed near tangential

$\cos\theta = .342$

At a point 12 inches forward the velocity would be 710 ft/sec from Figure 32 or an energy level of:

$$E = \frac{.55}{64.4}(710)^2 = 4305 \text{ ft-lbs}$$

The armor thickness required to contain would be:

$$t^2 = \frac{(4305)(12)(.342)^2}{(6.5)(188500)}$$

$$t = \sqrt{.0049} = .070 \text{ inches}$$

At 16 inches forward the velocity from Figure 32 would be 500 ft/sec the energy:

$$E = \frac{.55}{64.4}(500)^2 = 2135 \text{ ft-lbs}$$

The armor thickness required to contain would be:

$$t^2 = \frac{(2135)(12)(.342)^2}{(6.5)(188500)}$$

$$t = \sqrt{.0024} = .049 \text{ inches}$$

Considering the normal impingement energy at 8" forward the velocity from the curve is 250 ft/sec. The energy would be:

$$E = \frac{.55}{64.4}(250)^2 = 534 \text{ ft-lbs}$$

The thickness would be:

$$t^2 = \frac{(534)(12)}{(6.5)(188500)} = .0052$$

$$t = \sqrt{.0052} = .072 \text{ inches}$$

The thickness of .072 inches for normal impingement is less than the .091 inches determined for tangential impingement at the 8 inch station thus the .091 inch thickness would be used. At 12 inches the normal velocity would be 240 ft/sec and the energy:

$$E = \frac{.55}{64.4}(240)^2 = 492 \text{ ft-lbs}$$

The armor thickness required would be:

$$t^2 = \frac{(492)(12)}{(6.5)(188500)} = .0048$$

$$t = \sqrt{.0048} = .069 \text{ inches}$$

The thickness is basically equal to the thickness required to contain the spiraled fragment .070 inches compared to .069 inches at this same station thus forward of 12 inches the normal impingement would develop greater energy.

Taking the normal impingement at 16 inches the normal velocity is 220 ft/sec and the armor thickness is:

$$E = \frac{.55}{64.4} (220)^2 = 413 \text{ ft-lbs}$$

$$t^2 = \frac{(413)(12)}{(6.5)(188500)} = .0040$$

$$t = \sqrt{.0040} = .063 \text{ inches}$$

where at this same station the thickness required for armor to protect against the spiraled fragment was .049 inches. At 20 inches the normal impingement velocity is 205 ft/sec and the energy is:

$$E = \frac{.55}{64.4} (205)^2 = 359 \text{ ft-lbs}$$

The armor thickness is:

$$t^2 = \frac{(359)(12)}{(6.5)(188500)} = .0035$$

$$t = \sqrt{.0035} = .059 \text{ inches}$$

At 25 inches near the 30° angular study requirement, the normal impingement velocity is 179 ft/sec and the energy is:

$$E = \frac{.55}{64.4} (179)^2 = 274 \text{ ft-lbs}$$

The armor thickness is:

$$t^2 = \frac{(274)(12)}{(6.5)(188500)} = .00268$$

$$t = \sqrt{.0024} = .052 \text{ inches}$$

The armor thickness forward of the fan blade centerline would taper from .052 inches on the forward edge at a constant taper ratio to the 12 inch station at a thickness of .070 inches. Then from 12 inches to 8 inches would taper from .070 to .091 inches thick to contain the spiraled fragment.

Figure 33 shows the armor thickness pictorally.

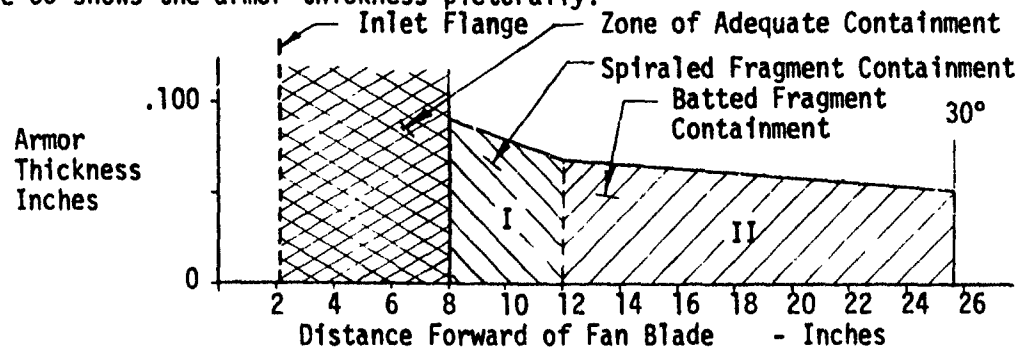

Figure 33. Inlet Armor Thickness Required (assumes no energy absorbed by inlet material)

Average Thickness I = $\frac{.091 + .070}{2}$ = .080 inches length 4 inches

Average Thickness II = $\frac{.070 + .063 + .059 + .052}{4} = \frac{.244}{4}$ = .061 inches

Length = 25.7 - 12 = 13.7 inches

The total weight for an armor system for the wing inlets for the 3 and 4 engine airplanes are shown in Tables 18 and 19. These weights are for a system which does not take credit for the energy absorbed by the inlet material.

Engine Position	Armor Section	Armor Dimensions			Armor Density lb/in^3	Installation Factor	Total Weight (lbs)
		Length (inches)	Width (inches)	Average Thickness (inches)			
1	I	43.3	4.0	.080	.286	1.25	5.0
	II		13.7	.061			12.9
							17.9
3	I	53.0	4.0	.080	.286	1.25	6.1
	II		13.7	.061			15.8
							21.9
Total Wing Engine Armor Weight							39.8

Table 18. Armor for Wing Inlet 3 Engine JT9D Powered Airplane (assumes no fragment energy absorbed by inlet material)

Engine Position	Armor Section	Armor Dimensions			Armor Density lb/in^3	Installation Factor	Total Weight (lbs)
		Length (inches)	Width (inches)	Average Thickness (inches)			
1	I	42.1	4.0	.080	.286	1.25	4.8
	II		13.7	.061			12.6
							17.4
2	I	42.1	4.0	.080	.286	1.25	4.8
	II		13.7	.061			12.6
							17.4
3	I	68.6	4.0	.080	.286	1.25	7.8
	II		13.7	.061			20.5
							28.3
4	I	68.6	4.0	.080	.286	1.25	7.8
	II		13.7	.061			20.5
							28.3
Total Armor Weight							91.4

Table 19. Armor for Inlets-4 Engine JT9D Powered Airplane (assumes no fragment energy absorbed by inlet material)

Through testing and other analysis it was found that the 2 inch thick bonded aluminum honeycomb used for inlet construction had an energy absorption capability of approximately 2958 ft-lbs of energy when impacted tangentially by the spiraled fragments. Also the same material could absorb 226 ft-lbs of energy when impacted normal to the surface. From the previous calculations the energy developed is shown in Table 20. Also the remaining energy after penetration and the armor thickness required is shown.

Type of Impact	Distance Forward of Fan Blade Center Line (inches)	Initial Energy (ft-lbs)	Inlet Energy Absorption Capability (ft-lbs)	Final Energy (ft-lbs)	Steel Armor Thickness to Contain (inches)
Spiraled Tangential	8	7229	2958	4271	.070
	12	4305	2958	1347	.039
	16	2135	2958	0	0
Batted Fragments	8	534	226	308	.055
	12	492	226	266	.051
	16	413	226	187	.043
	20	359	226	133	.036
	25	274	226	48	.022

Table 20. Wing Engine Armor Thickness Required (accounting for fragment energy absorbed by inlet material)

The armor thickness is shown pictorally in Figure 34

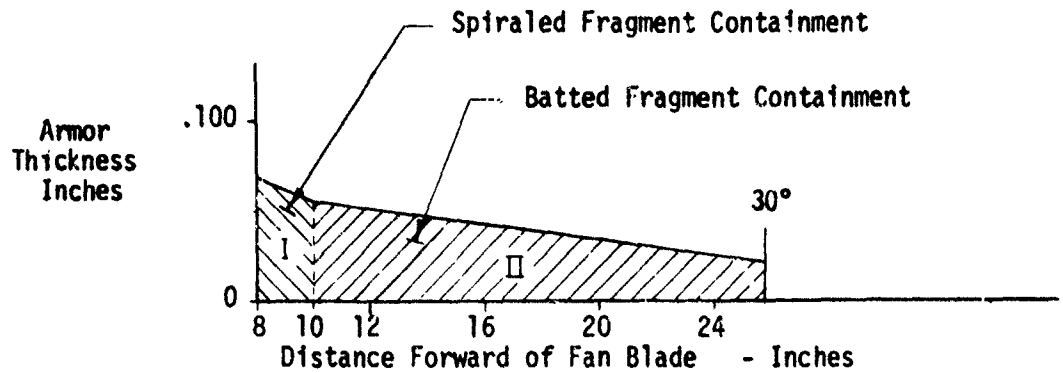

Figure 34. Inlet Armor Thickness Required (assumes some energy absorbed by inlet material)

Average Thickness I = $\frac{.070 + .053}{2}$ = .062 inches

At a Length of 2 inches

Average Thickness II = $\frac{.053 + .043 + .036 + .022}{5} = \frac{0.155}{4}$ = .041 inches

At a Length of 25.7 - 10 = 15.7 inches

It should be noted that when accounting for the inlet material absorption only 2 inches of armor at an average thickness of .062 inches is required to stop the spiraled fragments. Where previously without energy absorption accounted for 4 inches of steel at an average thickness of .080 inches was required.

The armor weight required when accounting for energy absorption by the inlet material is shown on Tables 21 and 22 for the 3 and 4 engine airplanes, respectively.

Engine Position	Armor Section	Armor Dimensions			Armor Density lb/in^3	Instal. Factor	Total Weight (lbs)
		Length (inches)	Width (inches)	Average Thickness (inches)			
1	I	43.3	2	.062	.286	1.25	1.9
	II		15.7	.041			10.0
							11.9
3	I	53	2	.062	.286	1.25	2.3
	II		15.7	.041			12.2
							14.5
Total Wing Engine Armor Weight							26.4

Table 21. Armor for Wing Inlets 3 Engine JT9D Powered Airplane (accounts for fragment energy absorbed by inlet material)

Engine Position	Armor Section	Armor Dimensions Length (inches)	Width (inches)	Average Thickness (inches)	Armor Density lbs/in^3	Installation Factor	Total Weight (lbs)
1	I	42.1	2	.062	.286	1.25	1.9
	II		15.7	.041			9.7
							11.6
2	I	42.1	2	.062	.286	1.25	1.9
	II		15.7	.041			9.7
							11.6
3	I	68.6	2	.062	.286	1.25	3.0
	II		15.7	.041			15.8
							18.8
4	I	68.6	2	.062	.286	1.25	3.0
	II		15.7	.041			15.8
							18.8
Total Armor Weight							60.8

Table 22.Armor for Inlets-4 Engine JT9D Powered Airplane (accounts for fragment energy absorbed by inlet material)

The results when accounting for the fragment energy absorbed by the inlet can be seen by comparing Table 18 and 21. For the 3 engine airplane, reducing the armor thickness when accounting for the energy absorption of the inlet material saves approximately 13 pounds. Comparing Table 19 and 22 shows that about 31 lbs would be saved on the 4 engine airplane.

5.2.3 Tail Inlet Armor for the JT9D Engine - In determining the armor required for the tail inlet, with the JT9D engine, the same levels of fragment energy calculated for the wing engines were used. Again, first the armor weight required was determined as if no energy was absorbed by the inlet material. Then the absorption capability of the inlet stresskin material was accounted for and the armor weights compared.

The stresskin bellmouth is constructed with heavy steel doublers in the engine attach flange area; thus, the inlet would be capable of withstanding the impact of either the spiraled or batted fragments up to a point 8 inches forward of the fan blade center line, which was also the same for the wing engines. So for this case, no energy absorption by inlet material, the armor thickness for the wing and tail would be the same but as may be seen on Figure 31 more coverage would be required. The sketch shows that the required armor length required would be 77 inches. The total weight and armor dimensions are shown on Table 23. As noted on the CF6 tail installation an installation factor of 1.50 was needed to install armor as no outer inlet structure is available to support the armor.

Engine Position	Armor Section	Armor Dimensions			Armor Density lb/in^3	Instal. Factor	Total Weight (lbs)
		Length (inches)	Width (inches)	Average Thickness (inches)			
Tail (no. 2)	I	77	4	.080	.286	1.50	10.6
	II		13.7	.061			27.6
Total Armor Weight for Tail Inlet							38.2

Table 23. Armor for Tail (no. 2) Inlet 3 Engine JT9D Powered Airplane (assumes no fragment energy absorbed by inlet material)

Next, accounting for the energy absorption capability, tests conducted showed that the stresskin had an energy absorption capability of approximately 3349 ft-lbs when impacted tangentially by the spiraled fragment and 1240 ft-lbs when impacted in the normal to the surface by the batted fragment.

From the previous calculations the energy developed is shown in Table 24. Also, the remaining energy after penetration and the armor thickness required is shown.

Type of Impact	Distance Forward of Fan Blade Center Line (inches)	Initial Energy (ft-lbs)	Inlet Energy Absorption Capability (ft-lbs)	Final Energy (ft-lbs)	Steel Armor Thickness to Contain (inches)
Spiraled Tangential	8	7229	3349	3880	.062
	12	4305	3349	956	.033
	16	2134	3349	0	
Batted Fragment	8	435	1240	0	0
	12	492	1240	0	0
	16	413	1240	0	0
	20	359	1240	0	0
	25	274	1240	0	0

Table 24. Tail Engine Armor Thickness Required (accounting for energy absorbed by inlet material)

From Table 24it can be observed that the stresskin can absorb all the energy developed by the batted fragment which develops normal to the surface impacts.

The spiraled fragment develops energy equal to the energy absorption capability of the stresskin at a point 13.6 inches forward of the fan blade center line thus armor would only be required between 8 and 13.6 inches or a width of 5.6 inches. The weight for this amount of armor would be as follows. See Table 25.

$$\text{Average Thickness} = \frac{.062 + .033}{2} = .048$$

Engine Position	Armor Dimensions			Armor Density lb/in^3	Installation Factor	Total Weight (lbs)
	Length (inches)	Width (inches)	Average Thickness (inches)			
Tail (no. 2)	77	5.6	.048	.286	1.50	8.9
Total Armor Weight for Tail Inlet						8.9

Table 25. Armor for Tail (no. 2) Inlet- 3 Engine JT9D Powered Airplane (accounting for energy absorbed by inlet material)

By comparing Table 23 and 25 it can be observed that a weight saving of approximately 29 lbs is realized by accounting for the energy absorbed by the inlet material.

5.2.4 Total Inlet Armor Weight - The preceding analysis assumed that the armor installation was tailored to each engine and the amount of armor required was based on the engine position. For actual installations, the inlet armor for wing engines would need to be position interchangeable. Thus, the total weight for inlet position interchangeability would be as shown on Table 26 and 27.

Engine Position	Armor Weight Non-Interchangeable (lbs)	Armor Weight Interchangeable (lbs)
1	17.9	39.8
2	38.2	38.2
3	21.9	39.8
TOTAL	78	117.8

Table 26. Total Weight for Inlet Armor for Non-Interchangeable and Interchangeable Armor Installations. 3 Engine JT9D Powered Airplane

Engine Position	Armor Weight Non-Interchangeable (lbs)	Armor Weight Interchangeable (lbs)
1	17.4	45.7
2	17.4	45.7
3	28.3	45.7
4	28.3	45.7
TOTAL	91.4	182.8

Table 27. Total Weight for Inlet Armor for Non-Interchangeable and Interchangeable Armor Installations.4 Engine JT9D Powered Airplane

5.3 Armor Installation Requirements

In the previous portion of the study an indepth armor mounting design was not carried out since it was more important to determine the weight trends using a generalized installation method. However, if armor were actually installed certain design requirements should be considered. The armor should be spaced out from the inlet material so that the armor and inlet can absorb energy independently. The armor should not be rigidly supported so that some flexibility is provided and armor deflections and even distortion can occur. If deflections and bending of the mounting system can be tolerated more energy can be absorbed when compared to a completely rigid system. Spacing the armor away from the inlet surface tends to keep the fragment within the inlet honeycomb material causing more honeycomb to be destroyed but in the process more energy is absorbed. The space between the armor and the inlet material can also serve as a fragment trap so that fragments cannot drift back into the rotating fan and create additional secondary damage. A more comprehensive design study with a test program involving armor mounting for specific designs could possibly reduce the total weight even further.

6.0 BLADE FRAGMENT IMPACT TESTS

The objective of this part of the program was to obtain data necessary to supplement available data in order to: (1) determine the energy absorption in airframe structures due to penetration from uncontained blade fragments; and (2) determine armor weight requirements to contain blade fragment projectiles. The results reported herein include tests conducted under this FAA sponsored program and other tests supported by Douglas. The tests summaries identify those sponsored by the FAA. Table 28.

6.1 Test Facility

The Douglas Blade Fragment Containment Test Facility used in the FAA sponsored tests is housed in a test cell at the Douglas Aerophysics Laboratory at El Segundo, California. The facility has two soundproof gun emplacements which provide a broad range of capability in terms of blade fragment acceleration and exit velocity, fragment size and containment target mounting. A blockhouse which is also soundproof includes a large area for instrumentation installation, data recording, and controls for remote operation of the guns.

The large gun used for the FAA tests and some of the Douglas tests is shown in Figure 35. The fragments, made of titanium plate, ground with sharp edges and corners to a rectangular shape are mounted in and supported by polyurethane sabots which serve as pistons and fragment guides when loaded into the breach of the gun. The barrel consists of a 40 foot long tube with a 5-inch-diameter bore and a 6-inch-diameter 40 foot long upstream plenum chamber. The source of pressure is a nitrogen storage tank. The pressure is released by dumping pressure between two diaphragms located several inches apart which in turn are located between the 6-inch diameter plenum and the 5-inch diameter gun barrel. The pressure between the two diaphragms is 1/2 the upstream plenum pressure so when the pressure between diaphragms is released the differential pressure causes both diaphragms to burst propelling a 5-inch diameter sabot holding the simulated blade fragment down the barrel. The sabot is retained at the gun muzzle exit by a sabot stopper/stripper and the simulated blade fragment continues to the target through a blade guide.

BLADE FRAGMENT IMPACT TEST SUMMARY

Date 1976	Run No.	Test Sponsor		Fragment Size		Fragment Orientation		Target Material
		FAA	DAC	4x7x0.25	3x5x0.25	Tangent	Normal	
9-15	B-121-1	X		X		X		3/4 In.Curved Steel Stresskin Panel
9-16	B-121-2	X		X		X		"
9-17	B-121-3	X		X		X		"
9-30	B-121-10	X		X		X		"
10- 1	B-121-11	X		X		X		"
10- 4	B-121-12	X		4x5.25x.25		X		"
3- 4	B-118-6		X		X	X		"
3- 5	B-118-7		X		X	X		"
3- 5	B-118-8		X		X	X		"
3-18	B-118-14		X		X	X		"
9-27	B-121-8	X			X	X		"
9-28	B-121-9	X			X	X		"
3- 9	B-118-11		X		X		X	"
3- 9	B-118-12		X		X		X	"
3-18	B-118-15		X		X		X	"
3-19	B-118-16		X		X		45° to normal	"
8-21	B-121-4	X		X			X	"
8-22	B-121-5	X		X			X	"
7-15	B-119-9		X	X		X		2 In. Thick Curved Aluminum Honeycomb Panel
7-19	B-119-10		X	X		X		"
7-20	B-119-11		X	X		X		"
8-28	B-119-20		X	X		X		"
8-24	B-119-21		X	X		X		"
9-23	B-121-6	X		X			X	3/4 In. Thick Curved Aluminum Honeycomb Panel
9-24	B-121-7	X		X			X	"
9- 8	B-119-24		X	X		X		Same with Kevlar Backing
10- 8	B-121-13	X			X		60° to normal	.033 In. Steel Sheet

TABLE 28 (cont.)

BLADE FRAGMENT IMPACT TEST SUMMARY

Date 1976	Run No.	Test Sponsor		Fragment Size		Fragment Orientation		Target Material
		FAA	DAC	4x7x0.25	3x5x0.25	Tangent	Normal	
10-11	B-121-14	X			X		60° to normal	.038 Inch Steel Sheet
10-12	B121-15	X			X		60° to normal	.062 Inch Steel Sheet
10-14	B-121-16	X			X		60° to normal	.088 Inch Steel Sheet
10-20	B-121-17	X			X		60° to normal	,087 Inch Steel Sheet
10-11	B-121-21	X			X		60° to normal	.127 Inch Steel Sheet
10-12	B-121-22	X			X		60° to normal	"
11-15	B-121-23	X		X			60° to normal	"
11-16	B-121-24	X		X			60° to normal	"
11-17	B-121-25	X		X			60° to normal	"
11-10	B-121-20	X			X		60° to normal	Double Layer .048/ .040 Inch Steel Sheet
11- 2	B-121-18	X			X	X 30°Skew		.050 Inch Steel Sheet
11- 9	B-121-19	X			X	X 30°Skew		.063 Inch Steel Sheet
7-23	B-119-12		X	X		X		3/4 Inch Stresskin Kevlar Pad & Strap
8-19	B-119-18		X	X		X Frag. Horiz.		"
8-13	B-119-17		X	X		X Frag. Horiz.		2 Inch Al Honeycomb Kevlar Pad & Strap "
8-19	B-119-19		X	X		X		Same with 050
8-25	B-119-22		X	X		X		Annealzed Steel
8-31	B-119-23		X	X		X		Same with heat treated 17-7 Steel

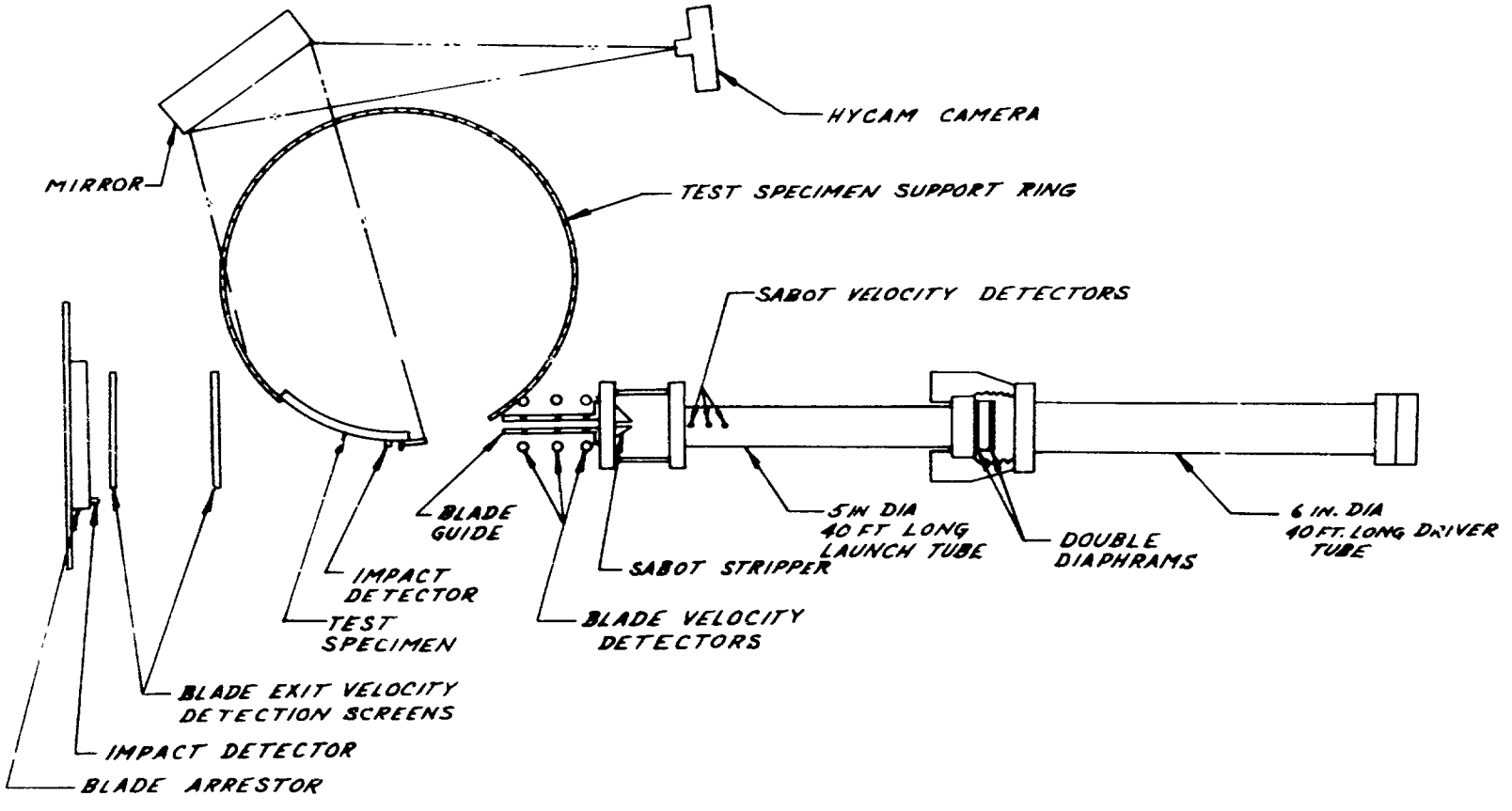

FIGURE 35
5IN DIAMETER FRAGMENT GUN

A second gun used for earlier Douglas tests was smaller in length consisting of a 246-inch long tube with a 3-1/2 inch diameater bore. This gun is shown in Figure 36. Nitrogen at approximately 150 psi is used to propel a 3-1/2 inch diameter sabot and simulated blade fragment. In this gun the pressure is released into the barrel by puncturing a mylar diaphragm. A 30 caliber rifle is used to activate a diaphragm cutter to release the nitrogen into the barrel. The rifle can be seen in the foreground of Figure 36. The sabot and test fragment configuration is shown in Figure 37. Figure 38 is a close-up of the muzzle flange and the target/backstop arrangement.

6.2 Instrumentation

The instrumentation of the smaller 3-1/2 inch gun consisted of three shorting probes at the exit end of the gun muzzle used to establish the fragment velocity just prior to hitting target specimen and breakwire fence screen for the fragment exit velocity after specimen penetration.

Instrumentation for the larger 5-inch gun is more precise in order to achieve better velocity measurement accuracy. The gun was used for higher velocity tests and since energy is proportional to velocity squared, improved precision is required to measure energy changes or absorption when a projectile passes through a panel. With the 5-inch gun, fragment velocity is measured at the exit end of the gun muzzle with three shorting probes. Fragment entrance velocity just prior to hitting the target speciment is measured with three photo diodes located in the blade guide. Fragment exit velocity after penetrating the specimen is measured with two breakwire fence screens and also with impact transducers located on the specimen and an impact plate downstream of the breakwire fence screens.

Data signals from the instrumentation on both guns was conditioned, recorded, and presented on oscilloscopes which were automatically photographed.

6.3 Test Fragment Size

The 3 x 5 x 0.2 fragment size selected for consideration by the FAA is approximately the size used in previous tests conducted by Douglas and does in fact simulate fan blade fragments found in actual damage incidents.

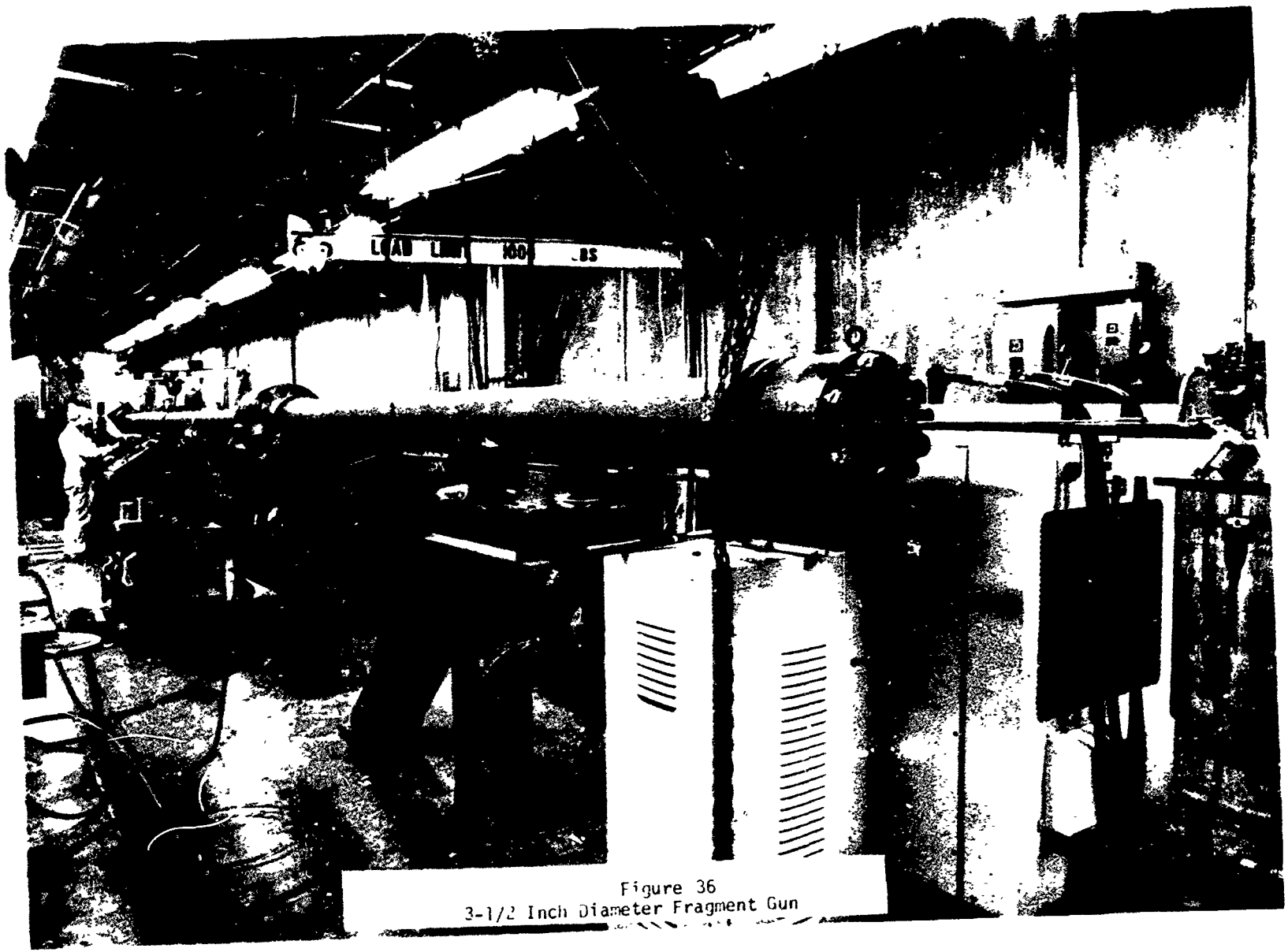

Figure 36
3-1/2 Inch Diameter Fragment Gun

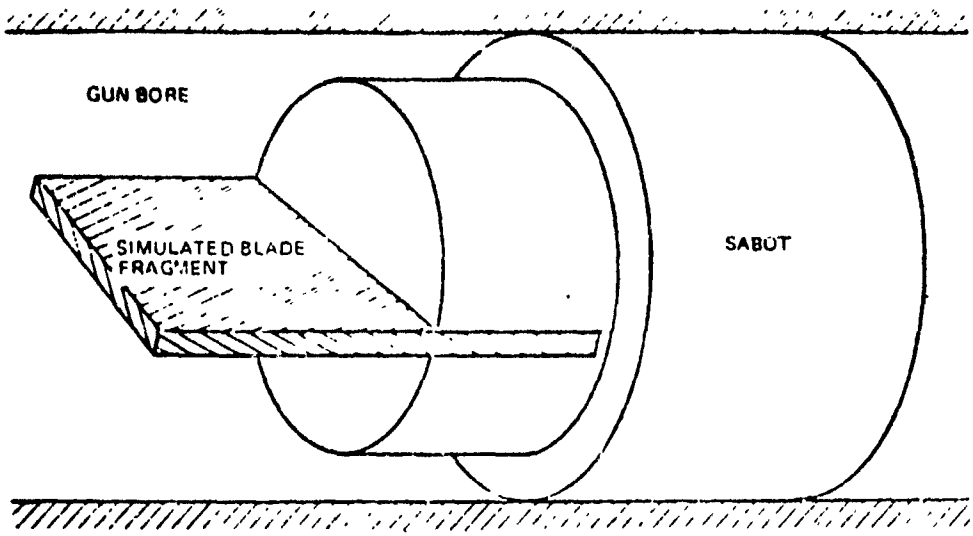

FIGURE 37. SABOT/FRAGMENT CONFIGURATION

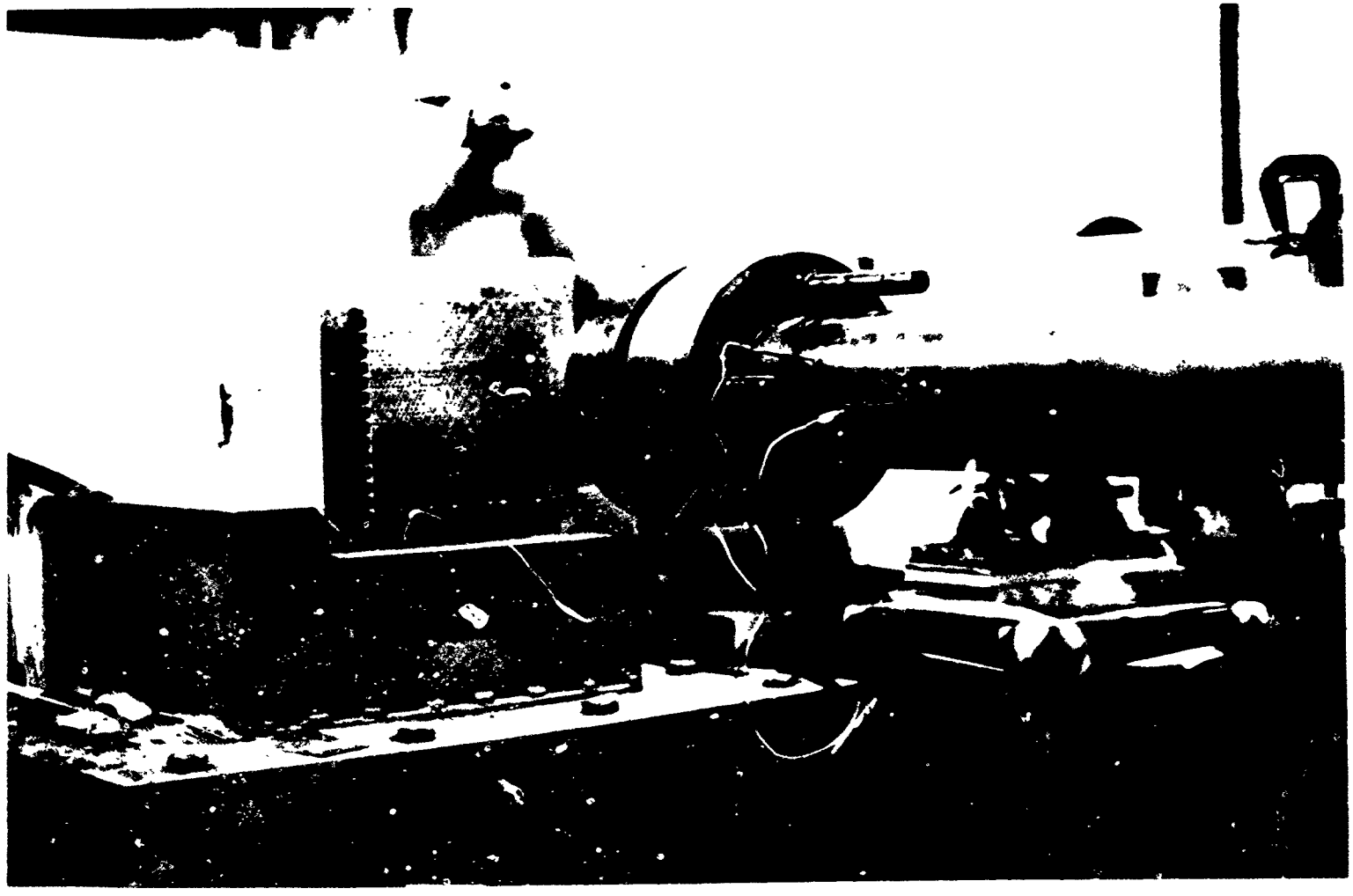

Figure 38
3-1/2 Inch Diameter Fragment Gun Muzzle

The test data obtained by Douglas was from 3 x 5 x 0.25 inch fragments. This means that the plate thickness was 0.25 inch when compared to the 0.20 inch fragment specified by the FAA for study and amounts to about a 0.10 lb weight difference. Since there were Douglas data points already available, it was deemed most cost effective to continue with the 0.25 inch thick fragment to keep the data consistent.

In previous Douglas tests, a 4 x 7 x 0.25 inch fragment at approximately 1.1 lb. was used to demonstrate the effects of increased fragments impact periphery and mass changes on certain target materials. Tests under FAA sponsorship were continued with both fragment sizes and the combined test data presented. The fragments were ground to the exact rectangular shape which meant that they had sharp edges and corners and hence added more conservatism to the test in that fragments recovered from actual fan blade failures generally have the corners knocked off and cutting edges dulled.

6.4 Armor Thickness Tests

Tests were conducted in order to establish armor thickness requirements for the blade fragment projectiles. Data was available from previous Douglas tests and literature. These were supplemented where necessary to accomplish the study reported herein.

The armor thickness required as a function of fragment energy was established based on correlating experimental data. A correlation developed by the Watertown Arsenal under General Electric sponsorship was used to establish the correlating parameters.

Tests at the Douglas Blade Fragment Test Facility were used to determine the validity of the Watertown Arsenal curve which related case thickness required for containment of fragment energy. Tests with titanium fragments shot into various thicknesses of steel plate indicated that the curve slope needed adjustment and the thickness predicted would be about 50% too thin for containment in the lower energy area but was probably valid in the high energy area. For example, when the curve indicated .030 thick armor, .045 was required or with .040 thickness indicated, .060 was needed for

containment. Further, the basic correlation did not account for temperature effects. Armor placed close to the engine, especially near the high turbine would have a considerable strength degradation due to temperature.

Pratt & Whitney compared the case thickness required for containment using stainless steel cases determined by their own analytical method to the Watertown Arsenal prediction of thickness and found that for the one blade fragment a factor of 1.5 times the thickness agreed fairly well for all but the high turbine stages and this was undoubtedly due to temperature effects. The 1.5 factor also agreed well with the Douglas test data. For the 2 and 4 blade fragments the Pratt & Whitney analysis indicated a large factor was required because of the size of the fragments. Further testing in the Douglas Facility on stainless steel confirmed that fragment size is an important factor in determining containment capability.

By changing the slope of the Watertown Arsenal curve to agree with the test data and developing factors to account for the temperature and fragment size, the armor thickness can be determined. Table 29 shows the correction factors used to correct the thickness determined from the curve on Figure 4.

ENGINE STAGE	NUMBER OF BLADES CONTAINED FACTOR X FRAGMENT ENERGY/ARMOR THICKNESS CORRELATION (CURVE FIGURE 4)					
	1		2		4	
FAN	1.0		1.30		2.25	
COMPRESSOR	1.0		1.30		2.25	
HIGH PRESSURE TURBINE	Inner	Outer	Inner	Outer	Inner	Outer
	1.33	1.20	2.1	1.8	3.1	2.6
LOW PRESSURE TURBINE	1.0		1.30		2.25	

TABLE 29. FACTOR USED TO ESTABLISH ARMOR WEIGHT

As can be seen, for single blade fragments the steel armor thickness required for containment can be determined directly from the curve except for the area near the high turbine. In the high turbine area it is necessary to increase the thickness determined from the curve by 1.33 when the armor is near the engine and 1.20 when further away. For the two blade fragment, the armor thickness determined from the curve must be increased 1.3 times to account for the fragment size and weight increase and in the high turbine area 2.1 and 1.8 to allow for the temperature effect. For the four blade fragment, the factors are 2.25 for all stages except for the high turbine where 3.1 and 2.6 are used for the inner and outer armor respectively.

These correlations can, in turn, be used to determine the energy absorption of a projectile passing through airframe structure with equivalent thickness. The equivalent thickness is the effective thickness for other than single skin construction with corrections for differences in materials based on ratioing the dynamic shear modulus.

6.5 Energy Absorption by Airframe Structures

A series of tests were conducted to determine the energy absorption of airframe structures, particularly the inlet section where fan tip fragments may impinge.

6.5.1 Energy Absorption by Stainless Steel Honeycomb (Stresskin) Panels -

The data given on Table 30 were obtained by firing a 4 x 7 x 0.25 inch titanium fragment into curved stresskin panels rigidly mounted to a barrel-like support structure as shown schematically in Figure 39. The purpose of these tests was to determine the energy absorption capability of this specific type honeycomb material and to observe the material characteristics when impacted or penetrated by a high velocity fragment.

For all of these tests, the large 40 foot long 5-inch diameter bore gun was used. The fragment was fired tangent to the target specimen surface. The fragment was oriented with the 4-inch side parallel to the target surface with the 7-inch length aligned with the trajectory. Five shots were made covering a range of impact velocities from 377 ft/sec (at which

the fragment was fully contained) to a high of 964 ft/sec. One additional shot was made to determine the effect of an intermediate mass for a fragment with the same frontal periphery and area as the previous tests.

The data plotted on Figure 40 show the initial and final energy after penetration for this size fragment at various velocities. The velocity squared term was used for convenience to allow a straight line relationship. This data plot also shows that over the range tested, regardless of impact energy level an average of about 2800 ft-lbs of energy was absorbed for a fragment of this geometry. There is some data scatter in the test results which is attributed to unavoidable introduction of some rotation to the fragment and the non-homogeneity of the target material. In some of the shots the fragment clearly hit at an angle to the surface and the thin perforated inner sheet sheared due to a corner dig. In some cases the impact may have occurred at a honeycomb nodal point and distributed the impact load over a greater area and into the inner and outer sheets at the same time. Figures 41 through 56 show the character of the damage to the stresskin panels. The data scatter is very reasonable for this type of testing and allows confidence in the accuracy of the averaged results.

TABLE 30- TEST RESULTS
TARGET - 3/4 INCH THICK CURVED STEEL STRESSKIN PANEL
FRAGMENT - 4 x 7 x 0.25 INCH TITANIUM FLAT PLATE
TANGENTIAL IMPINGEMENT

DATE 1976	RUN NO.	TEST SPONSOR		FRAGMENT WEIGHT		VELOCITY FT/SEC		ENERGY FT-LBS		ENERGY ABSORBED FT-LBS	PERCENT ENERGY ABSORBED	REMARKS
		FAA	DOUGLAS	GRAMS	POUNDS	INITIAL	FINAL	INITIAL	FINAL			
9-15	B-121-1	X		494.7	1.091	624	512	6596	4441	2155	32.6	Penetrated
9-16	B-121-2	X		496.0	1.093	768	606	10011	6233	3778	37.7	Penetrated
9-17	B-121-3	X		497.5	1.097	964	827	15830	11650	4180	26.4	Penetrated
9-30	B-121-10	X		498.8	1.100	537	440	4926	3307	1619	32.8	Penetrated
10-1	B-121-11	X		497.8	1.097	377	0	2421	0	2421	100%	Fragment Contained
* 10-4	B-121-12	X		390.8	.862	577	434	4456	2521	1935	43.4	Penetrated

* Fragment 4 x 5.25 x 0.25 same frontal area as others but shorter in length and less mass.

Target Material: Impingement Side - .016 inch thick 316L stainless steel perforated with .094 inch dia. holes 13% open area 60° hole pattern curved on 48" radius

Exit Side - 0.012 inch thick 316L stainless steel solid sheet

Core - .0035 inch thick ribbon .720 inch height 316L stainless steel 3/8 inch diamond pattern

Overall Panel Thickness - 0.748 inch

Panel Density - 1.80 lb/ft^2

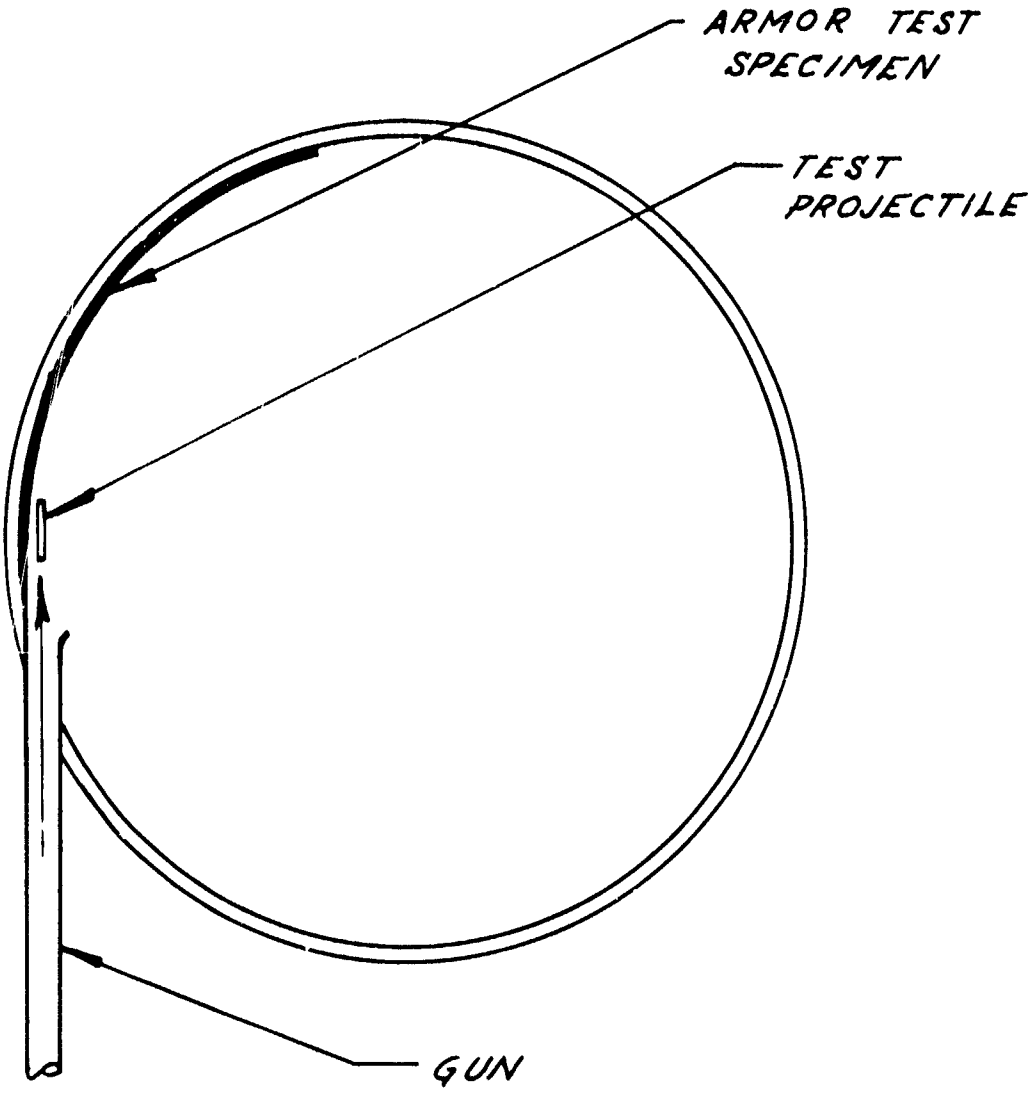

FIGURE 39
CURVED PANEL
TEST SETUP

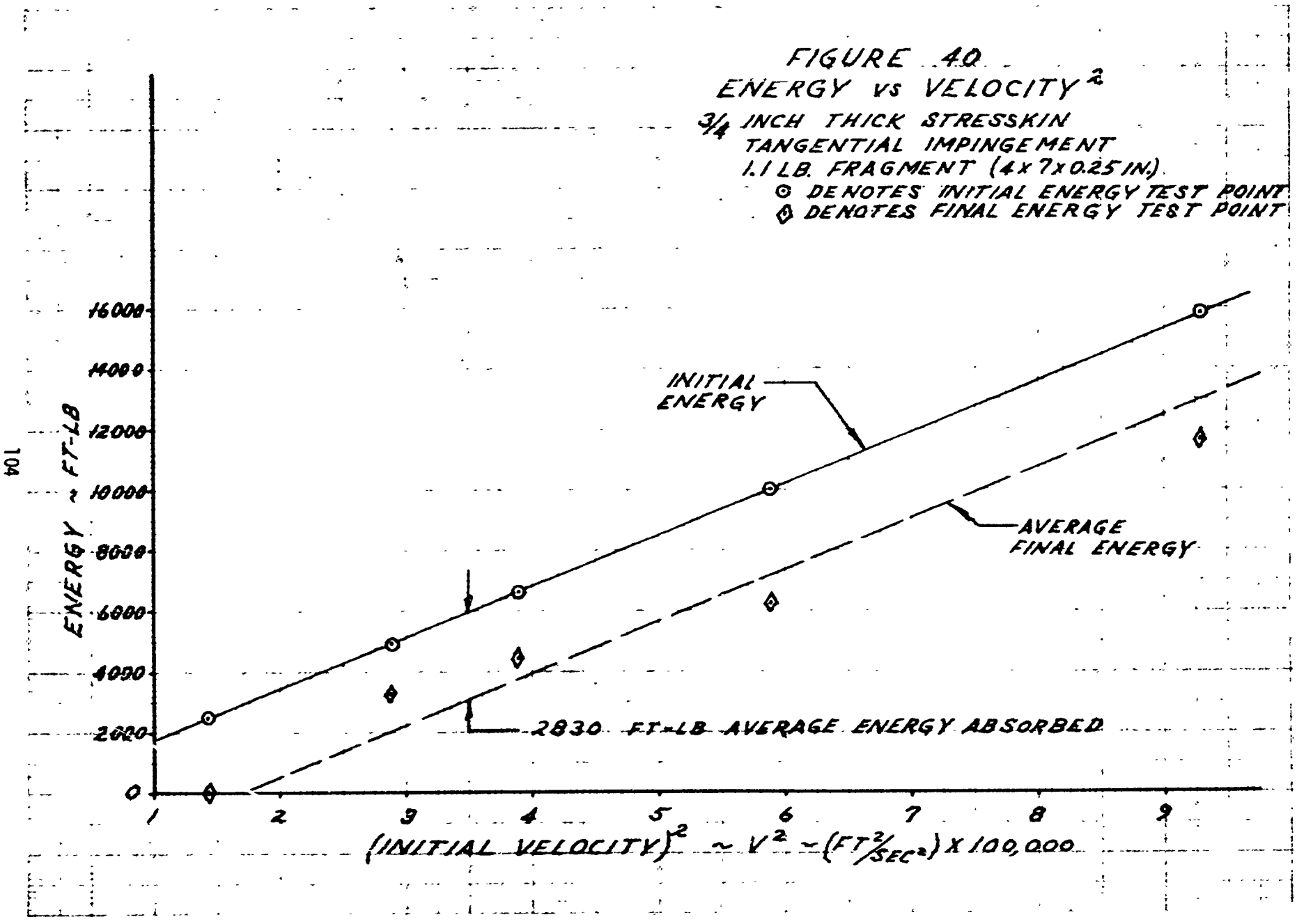
FIGURE 40
ENERGY VS VELOCITY²
3/4 INCH THICK STRESSKIN
TANGENTIAL IMPINGEMENT
1.1 LB. FRAGMENT (4 x 7 x 0.25 IN.)
⊙ DENOTES INITIAL ENERGY TEST POINT
◊ DENOTES FINAL ENERGY TEST POINT
ENERGY ~ FT-LB
16000
14000
12000
10000
8000
6000
4000
2000
0
INITIAL ENERGY
AVERAGE FINAL ENERGY
2830 FT-LB AVERAGE ENERGY ABSORBED
1
2
3
4
5
6
7
8
9
(INITIAL VELOCITY)² ~ V² ~ (FT²/SEC²) X 100,000

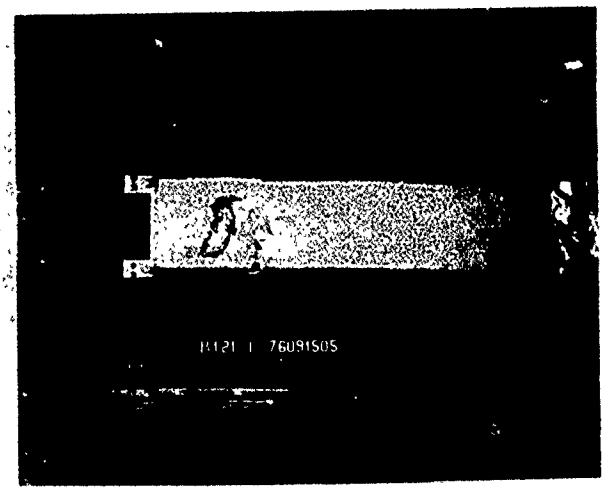

Figure 41.

3/4 Inch Stresskin Test Panel Inner Surface ,
4 x 7 x .25 In. Fragment, 624 FPS Impact Velocity

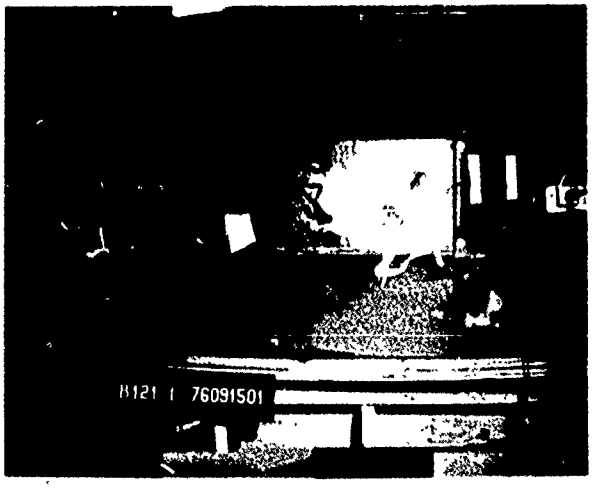

Figure 42

3/4 Inch Stresskin Test Panel Outer Surface,
4 x 7 x .25 In. Fragment, 624 FPS Impact Velocity

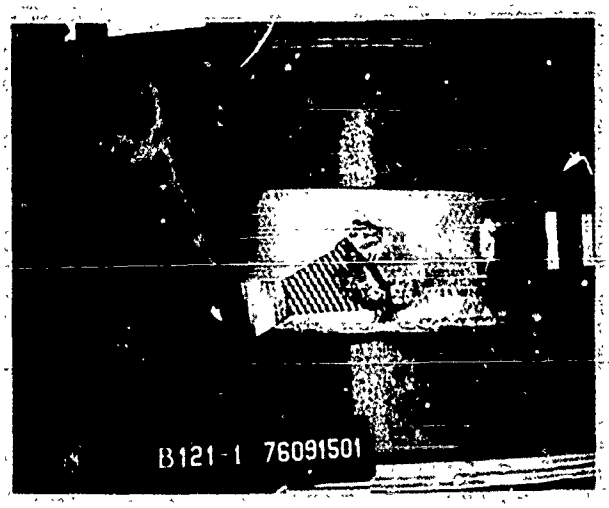

Figure 43

3/4 Inch Stresskin Test Panel Outer Surface,
4 x 7 x .25 In. Fragment, 624 FPS Impact Velocity

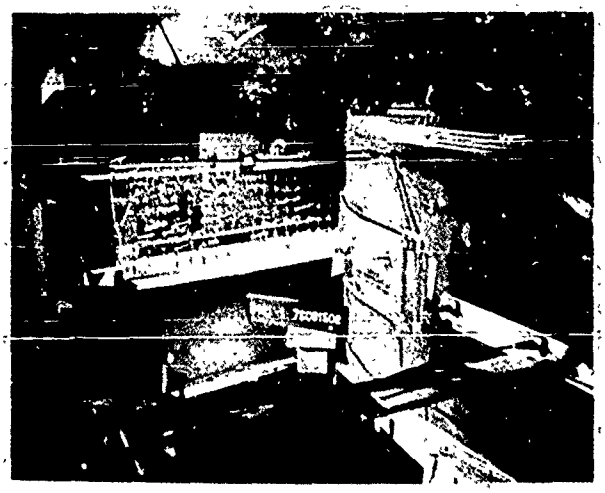

Figure 44

Outer Surface of Test Panel & Breakwire Fence Screens
after Test B-121-1

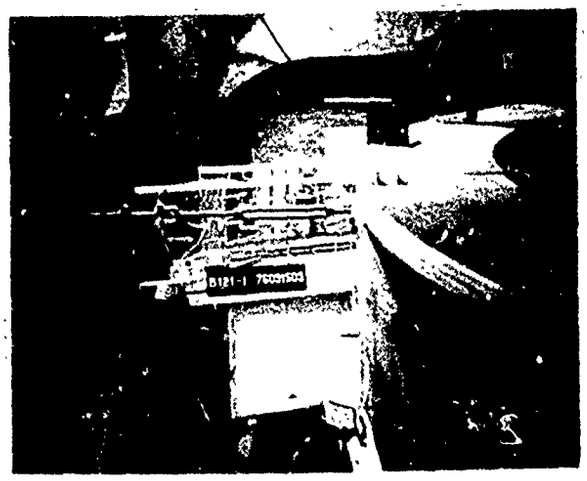

Figure 45

Front View Closeup of Breakwire Fence Screen after Test Shot of B-121-1

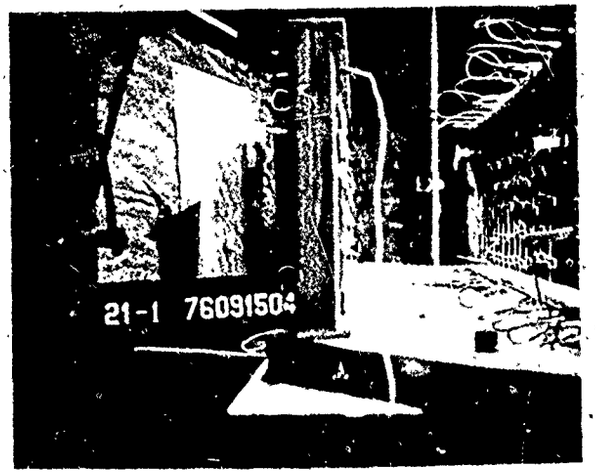

Figure 46

Side View Closeup of Breakwire Fence Screen after Test Shot B-121-1

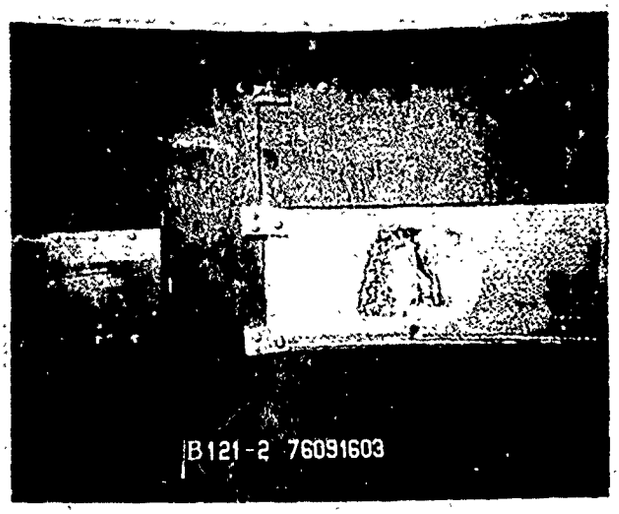

Figure 47

3/4 Inch Stresskin Test Panel Inner Surface.
4 x 7 x .25 In. Fragment, 768 FPS Impact Velocity

Figure 48

3/4 Inch Stresskin Test Panel Outer Surface,
4 x 7 x .25 In. Fragment, 768 FPS Impact Velocity

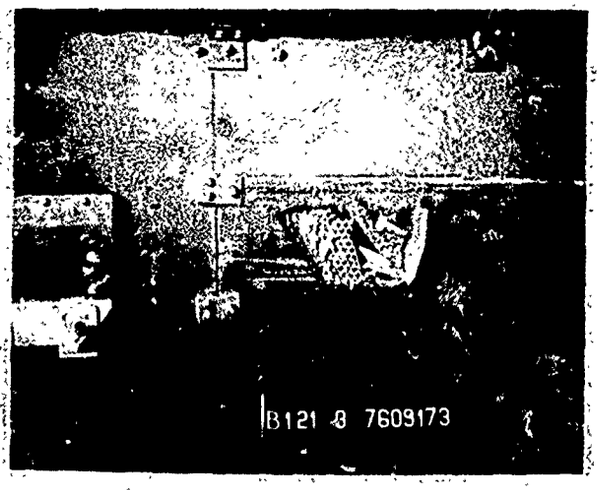

Figure 49

3/4 Inch Stresskin Test Panel Inner Surface,
4 x 7 x .25 In. Fragment, 964 FPS Impact Velocity

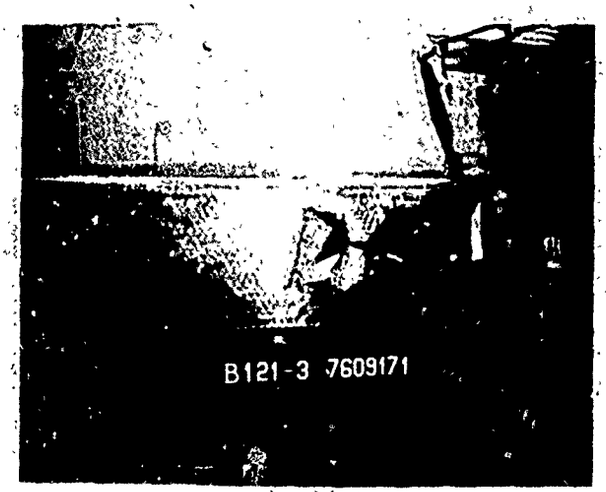

Figure 50

3/4 Inch Stresskin Test Panel Outer Surface,
4 x 7 x .25 In. Fragment, 964 FPS Impact Velocity

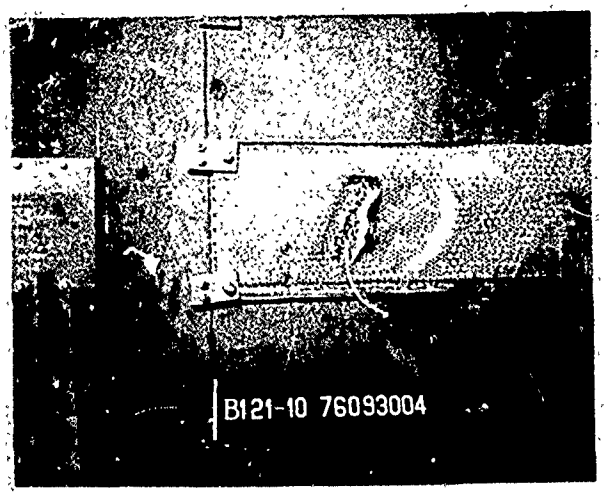

Figure 51

3/4 Inch Stresskin Test Panel Inner Surface,
4 x 7 x .25 In. Fragment, 537 FPS Impact Velocity

Figure 52

3/4 Inch Stresskin Test Panel Outer Surface,
4 x 7 x .25 In. Fragment, 537 FPS Impact Velocity

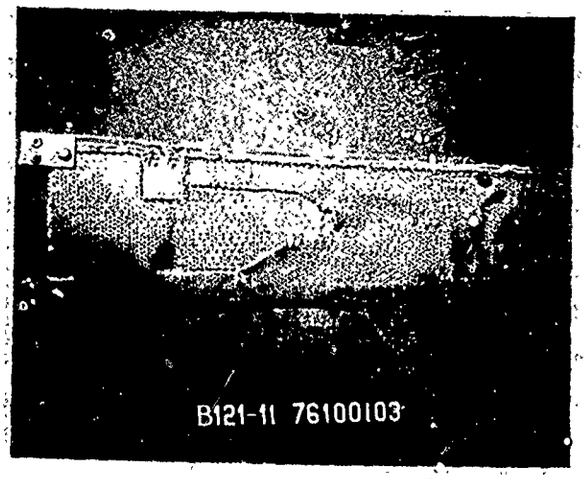

Figure 53

3/4 Inch Stresskin Test Panel Inner Surface,
4 x 7 x .25 In. Fragment, 377 FPS Impact Velocity

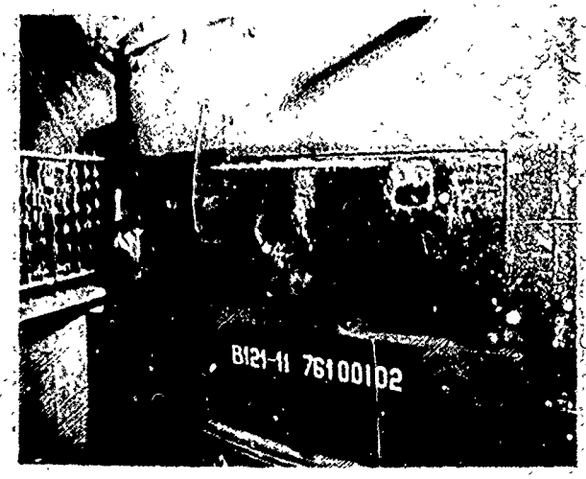

Figure 54

3/4 Inch Stresskin Test Panel Outer Surface,
4 x 7 x .25 In. Fragment, 377 FPS Impact Velocity

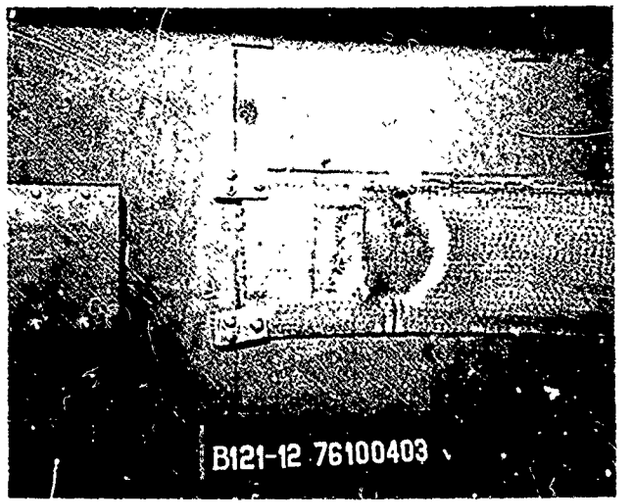

Figure 55

3/4 Inch Stresskin Test Panel Inner Surface,
4 x 5 x .25 In. Fragment, 577 FPS Impact Velocity

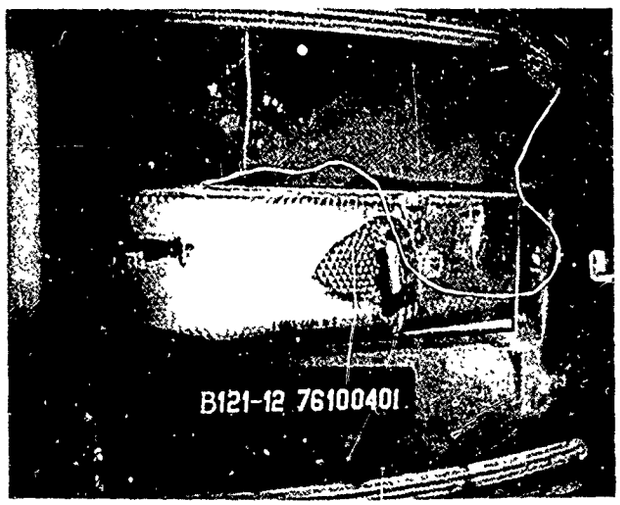

Figure 56

3/4 Inch Stresskin Test Panel Outer Surface,
4 x 5 x .25 In. Fragment, 577 FPS Impact Velocity

6.5.2 Effect of Fragment Size on Stresskin Energy Absorption - The data given on Table 31 was obtained by firing 3 x 5 x 0.25 inch titanium fragments into curved stresskin panels. The purpose of these tests was to determine the energy absorption capability of this type of honeycomb material with the smaller fragment and to compare the results with the previous tests conducted with the large fragment.

The panels were mounted and supported on the same barrel support structure used in the previous tests with the 4 x 7 x 0.25 fragment. In all the shots the fragments were fired tangential to the target surface and were oriented with the 3-inch side parallel to the surface. The first four shots were accomplished during earlier Douglas sponsored tests using the small 246 inch long 3-1/2 inch diameter bore gun. The impact velocities covered a range from a low of 566 ft/sec with the fragment being fully contained to a high of 952 ft/sec.

The last two shots were done under this contract on the large 40 foot long 5-inch diameter bore gun. These shots were at impact velocities of 1006 ft/sec and 1138 ft/sec.

Figure 57 shows the initial and final energy levels at various initial velocities. The results of these tests indicate that on an average approximately 3300 ft-lbs of energy was absorbed. However, at velocities above 1000 ft/sec the absorption dropped to a level of approximately 2400 ft-lbs. Examination of Figures 58 through 69, which are photographs of the target damage, indicated that up to and including an impact velocity of 952 ft/sec (Run B-118-8) the damage was the result of a punching action with relatively small panel destruction on the exit side. But for velocities above 1000 ft/sec, the panel destruction on both the entrance and exit side was considerably larger. Under these high velocity conditions the character of the penetration mechanism appears to change and resulted in a large rounded hole through both surfaces. Even though much more panel destruction took place at the high velocity impacts, a smaller percentage of the initial energy was absorbed. It was conjectured that because of the high impact shock wave radiating into the target material, more massive material failure occurred resulting in a large hole and therefore less friction acting to reduce the

fragment velocity as it slid through the opening. This destruction pattern alone could be the subject of further research, however the 950 ft/sec range appears to be of more interest at least for current engines when tip velocities are degraded to account for breakup and other losses associated with the penetration sequence. For most purposes in analyzing impact damage the average energy absorption of 3300 ft-lbs is probably a reasonable number.

Since B-118-6 was contained, it has been excluded from calculation of the average.

If there is a change in penetration characteristics at the higher velocities, then possibly it would be more appropriate to average the three shots below 1000 ft/sec separately from those at velocities above 1000 ft/sec.

TABLE 31 TEST RESULTS
TARGET - 3/4 INCH THICK CURVED PANEL STEEL STRESSKIN
FRAGMENT - 3 x 5 x 0.25 INCH TITANIUM FLAT PLATE
TANGENTIAL IMPINGEMENT

DATE 1976	RUN NO.	TEST SPONSOR		FRAGMENT WEIGHT		VELOCITY FT/SEC		ENERGY FT-LBS		ENERGY ABSORBED FT-LBS	PERCENT ENERGY ABSORBED	REMARKS
		FAA	DOUGLAS	GRAMS	POUNDS	INITAL	FINAL	INITIAL	FINAL			
3-4	B-118-6		X	253.48	.559	566	0	2780	0	2780	100%	Fragment Contained
3-5	B-118-7		X	260.38	.574	767	413	5243	1520	3723	71%	Penetrated
3-5	B-118-8		X	252.08	.556	952	549	7825	2602	5223	66.7	Penetrated
3-18	B-118-14		X	242.92	.536	815	497	5528	2057	3474	62.8	Penetrated
9-27	B-121-8	X		255.7	.564	1138	1013	11342	8987	2355	20.8	Penetrated
9-28	B-121-9	X		251	.553	1006	846	8690	6146	2544	29.2	Penetrated

Target Material: Impingement Side - 0.016 inch thick 316L Stainless Steel perforated with 0.094 inch diameter holes 13% open area 60° hole pattern

Exit Side - 0.012 inch thick 316L Stainless Steel solid sheet

Core - 0.0035 inch thick ribbon 0.720 inch height 316L Stainless Steel 3/8 inch diamond pattern

Overall Panel Thickness - 0.748 inch

Panel Density - 1.80 lb/ft^2

FIGURE 57

ENERGY vs. VELOCITY^2

3/4 INCH THICK STRESSKIN
TANGENTIAL IMPINGEMENT
.55 LB. FRAGMENT (3 x 5 x 0.25 IN.)

⊙ DENOTES INITIAL ENERGY TEST VALUE
◈ DENOTES FINAL ENERGY TEST VALUE

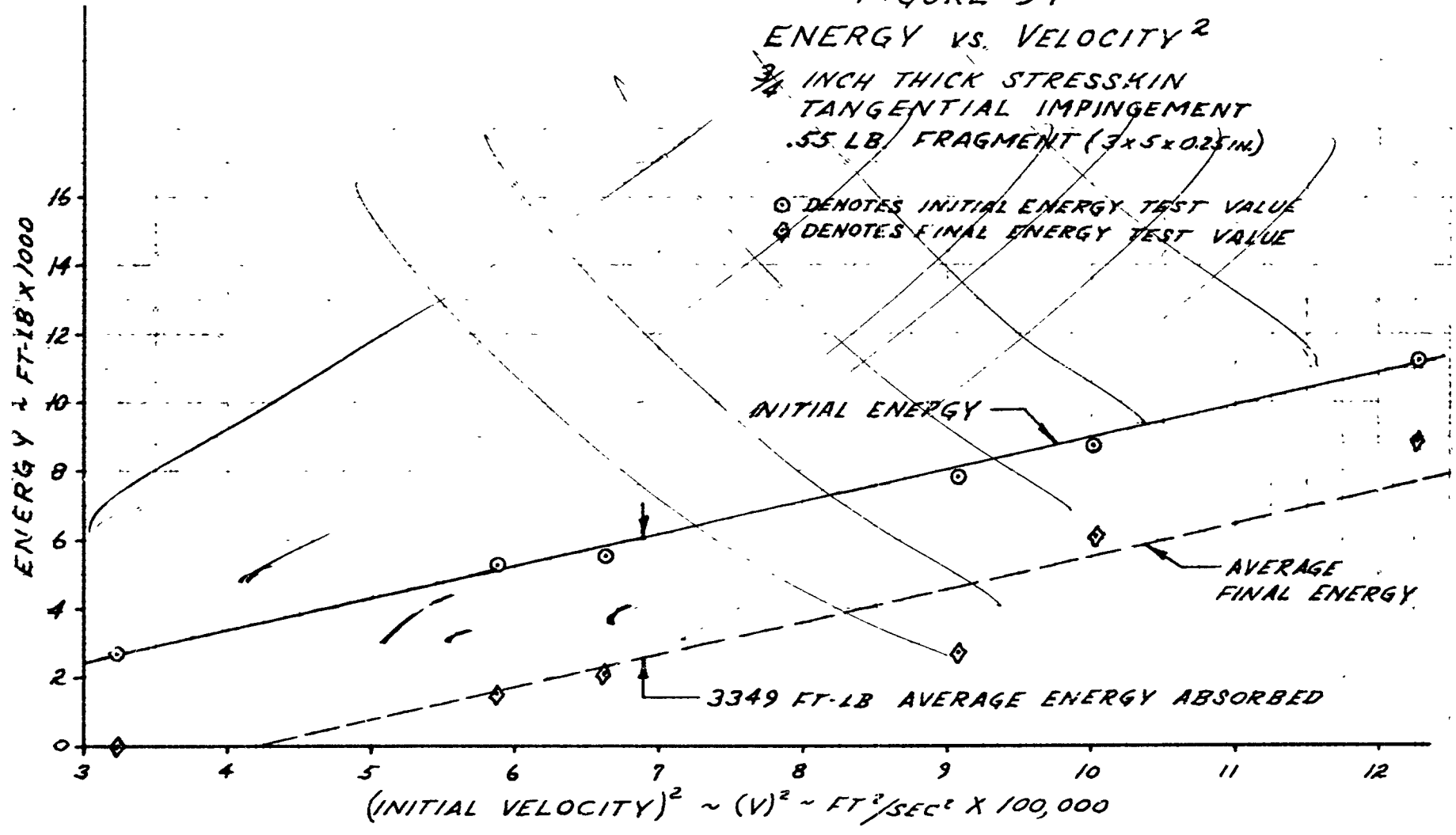

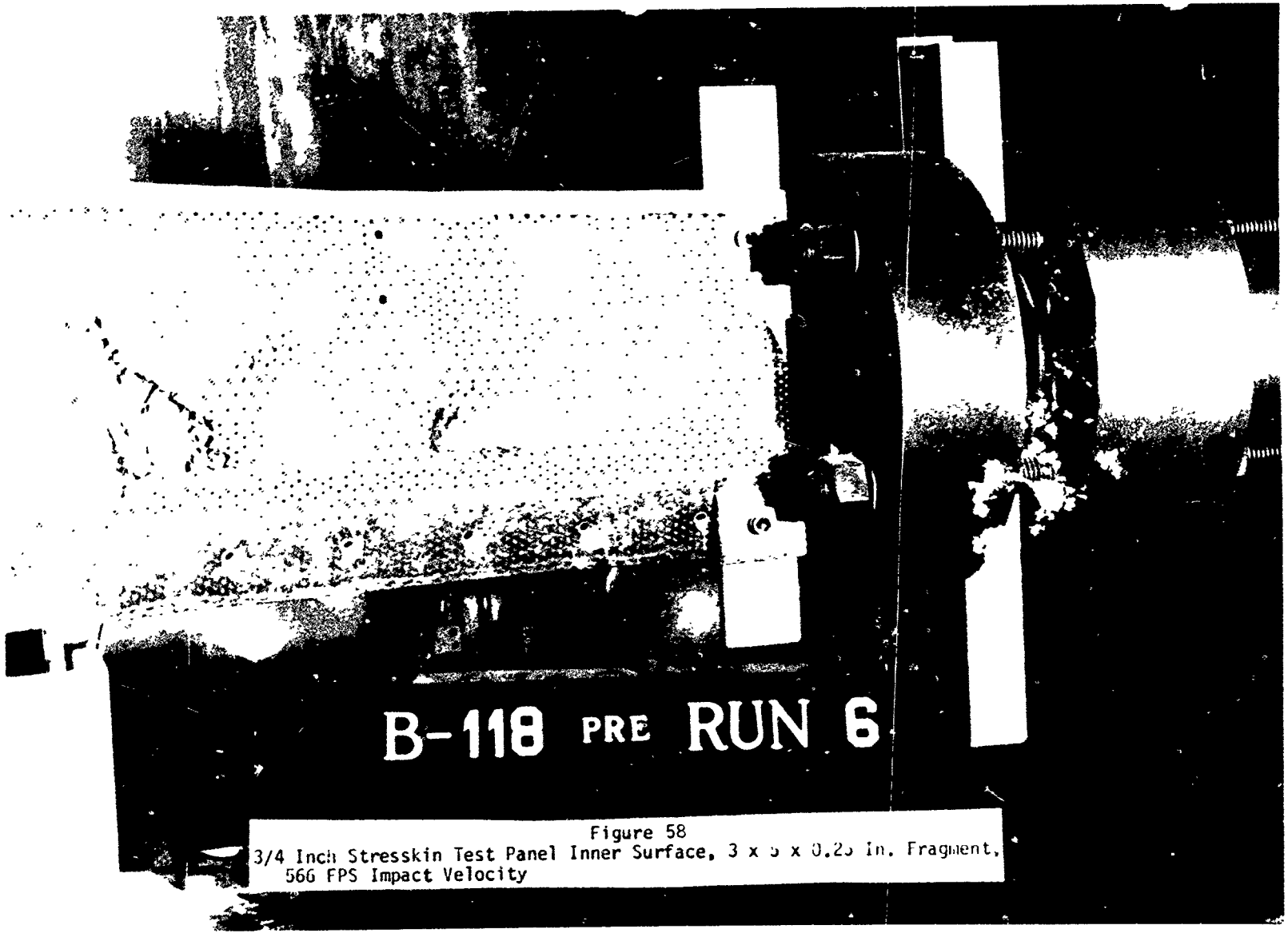

Figure 58
3/4 Inch Stresskin Test Panel Inner Surface, 3 x 3 x 0.25 In. Fragment, 566 FPS Impact Velocity

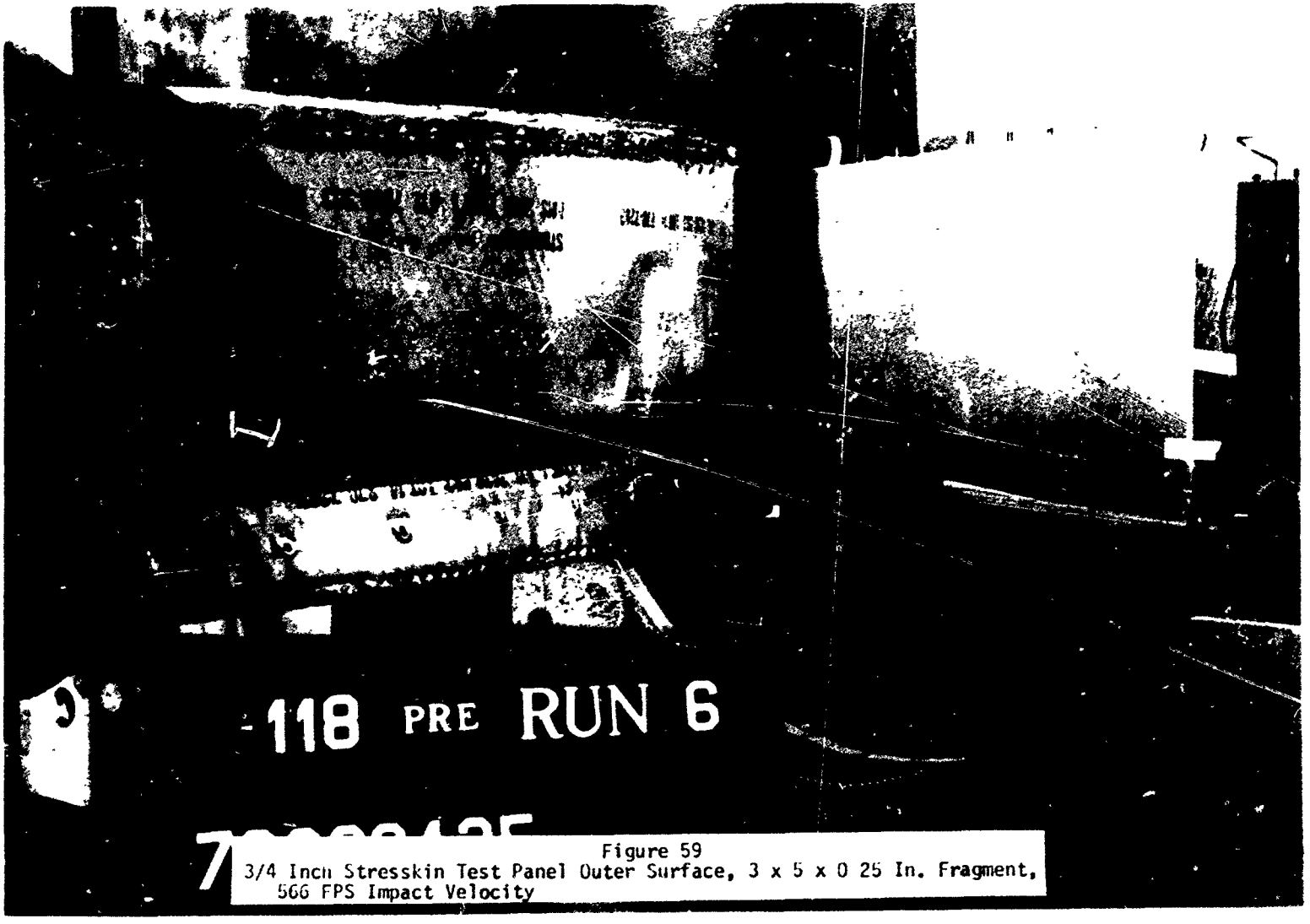

Figure 59
3/4 Inch Stresskin Test Panel Outer Surface, 3 x 5 x 0 25 In. Fragment, 566 FPS Impact Velocity

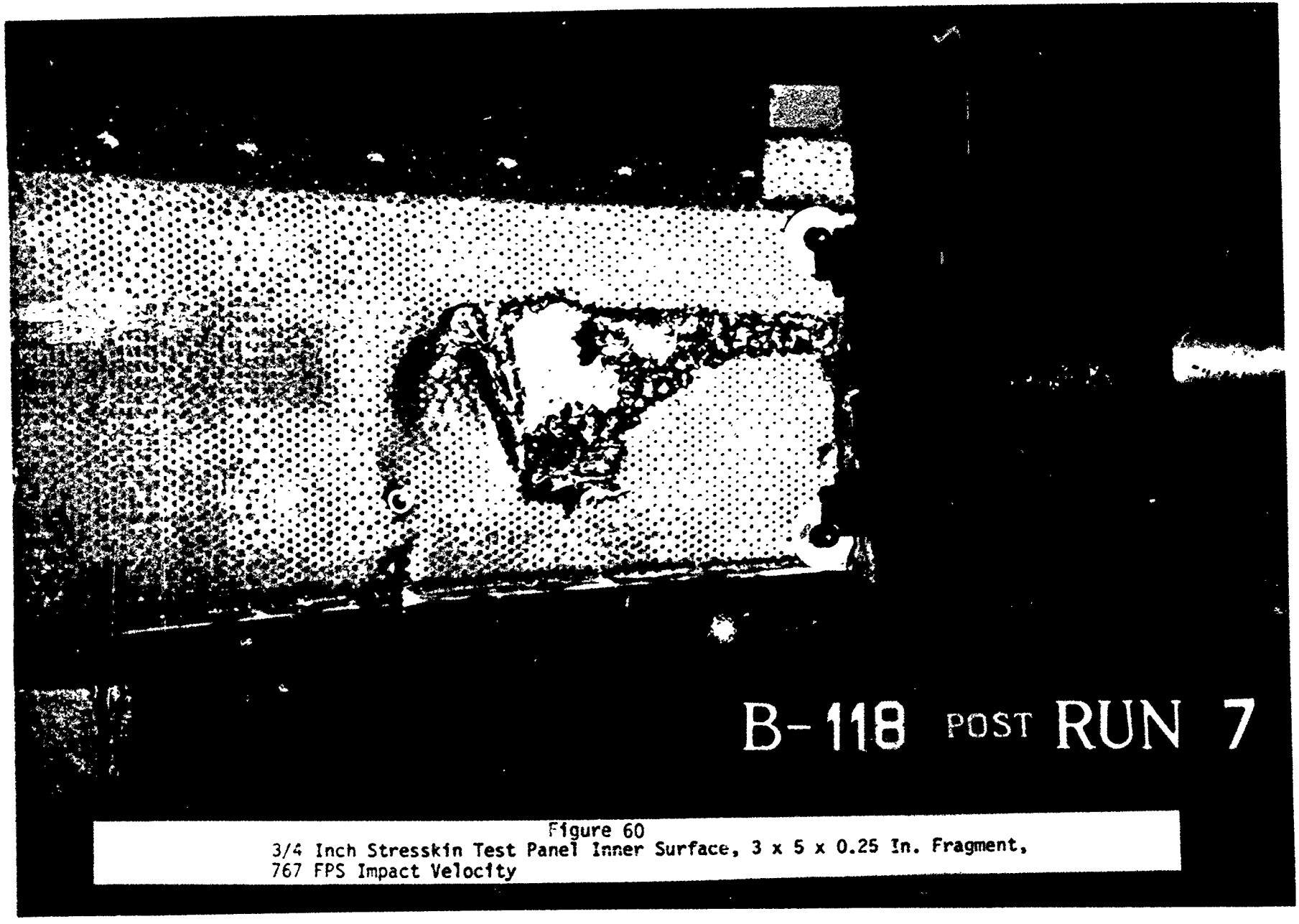

Figure 60
3/4 Inch Stresskin Test Panel Inner Surface, 3 x 5 x 0.25 In. Fragment,
767 FPS Impact Velocity

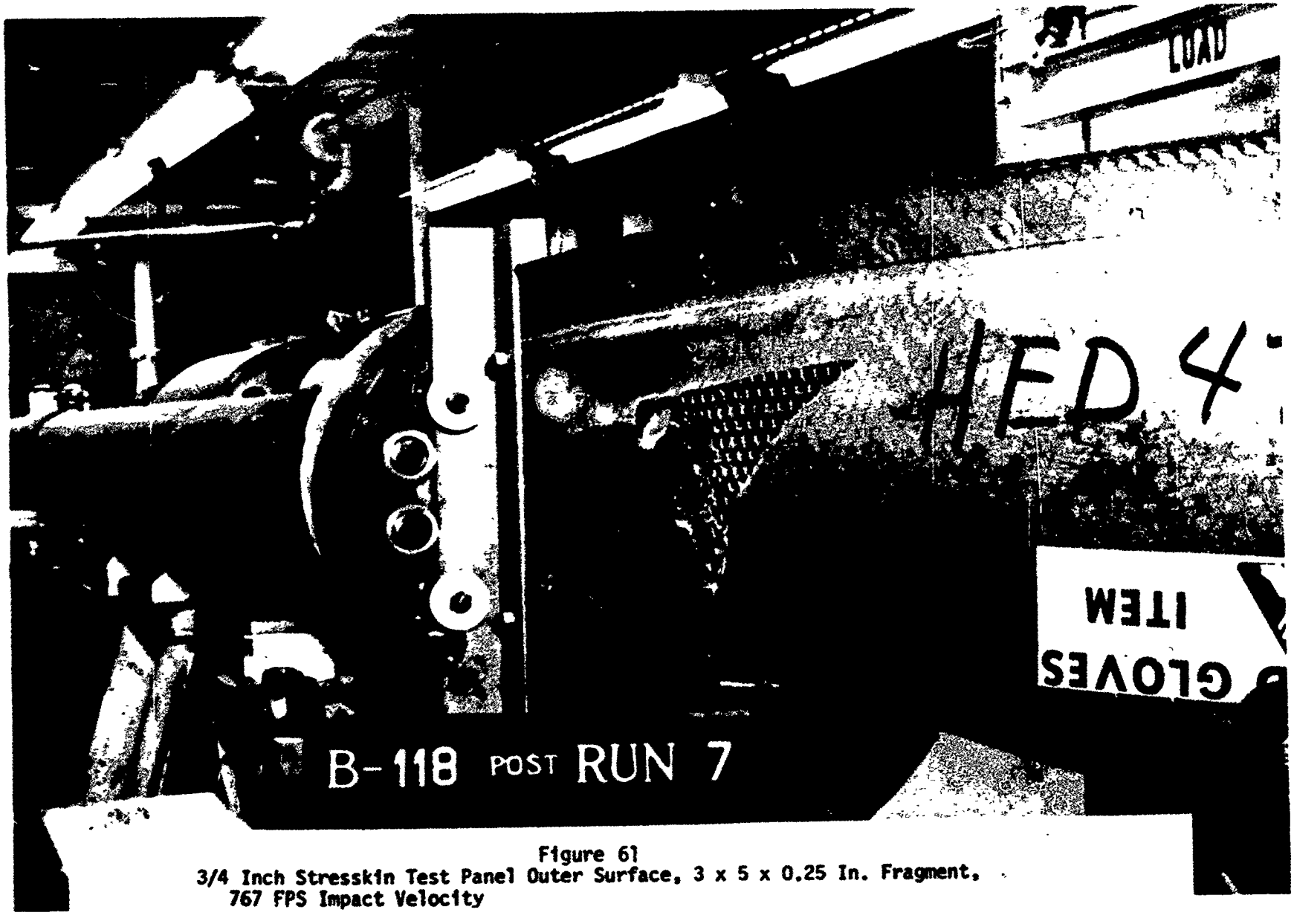

Figure 61
3/4 Inch Stresskin Test Panel Outer Surface, 3 x 5 x 0.25 In. Fragment,
767 FPS Impact Velocity

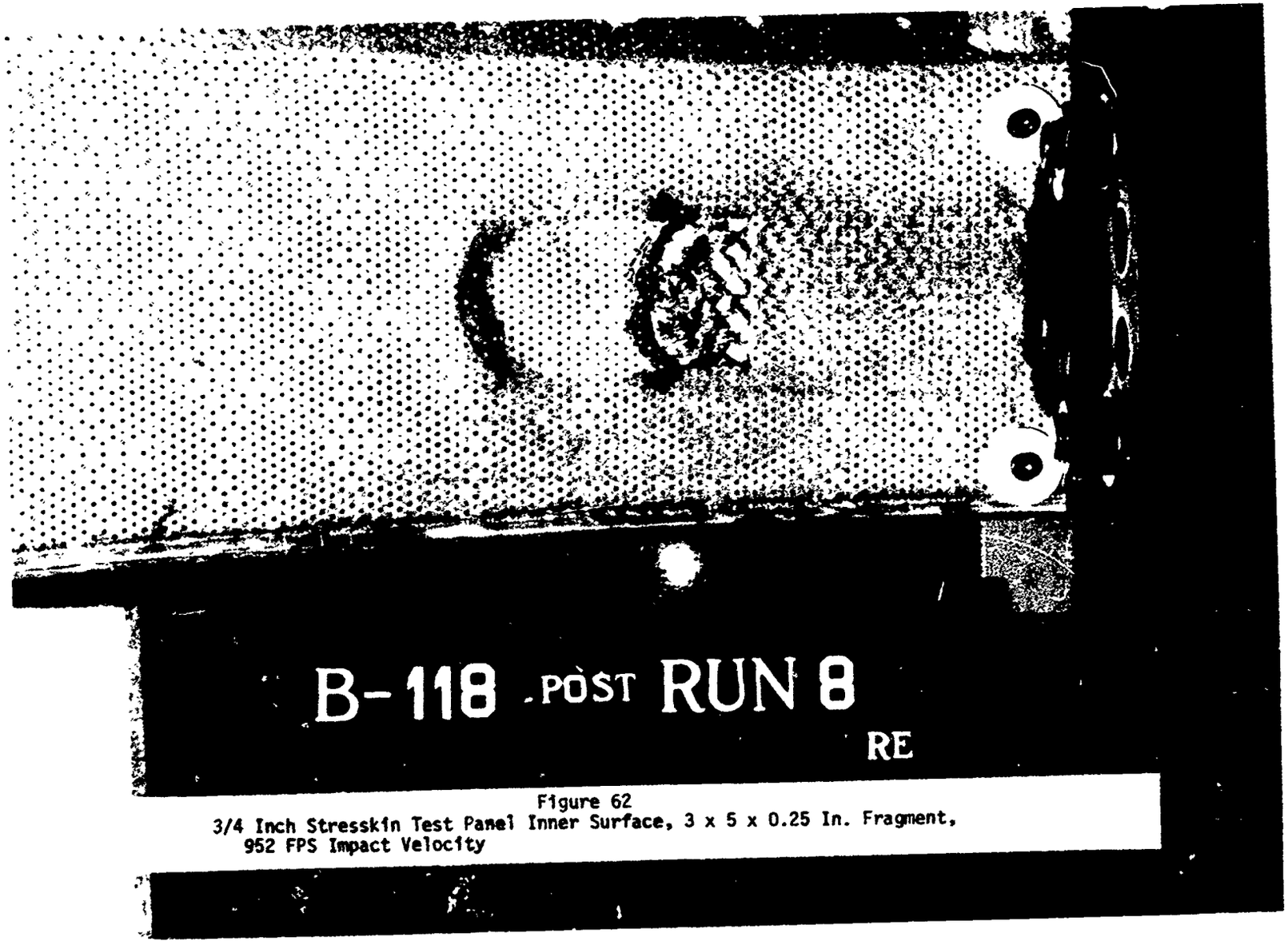

Figure 62
3/4 Inch Stresskin Test Panel Inner Surface, 3 x 5 x 0.25 In. Fragment,
952 FPS Impact Velocity

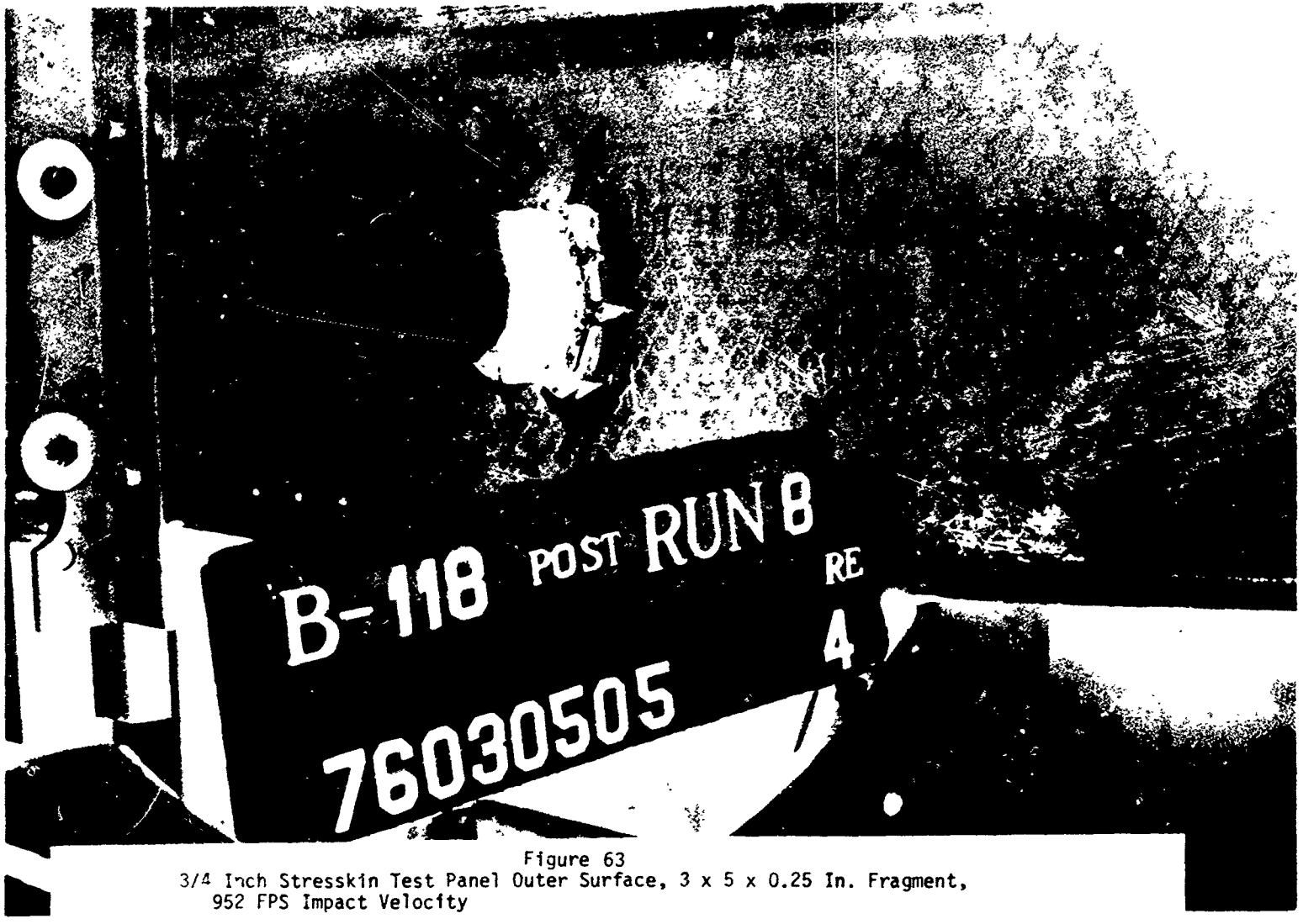

Figure 63
3/4 Inch Stresskin Test Panel Outer Surface, 3 x 5 x 0.25 In. Fragment,
952 FPS Impact Velocity

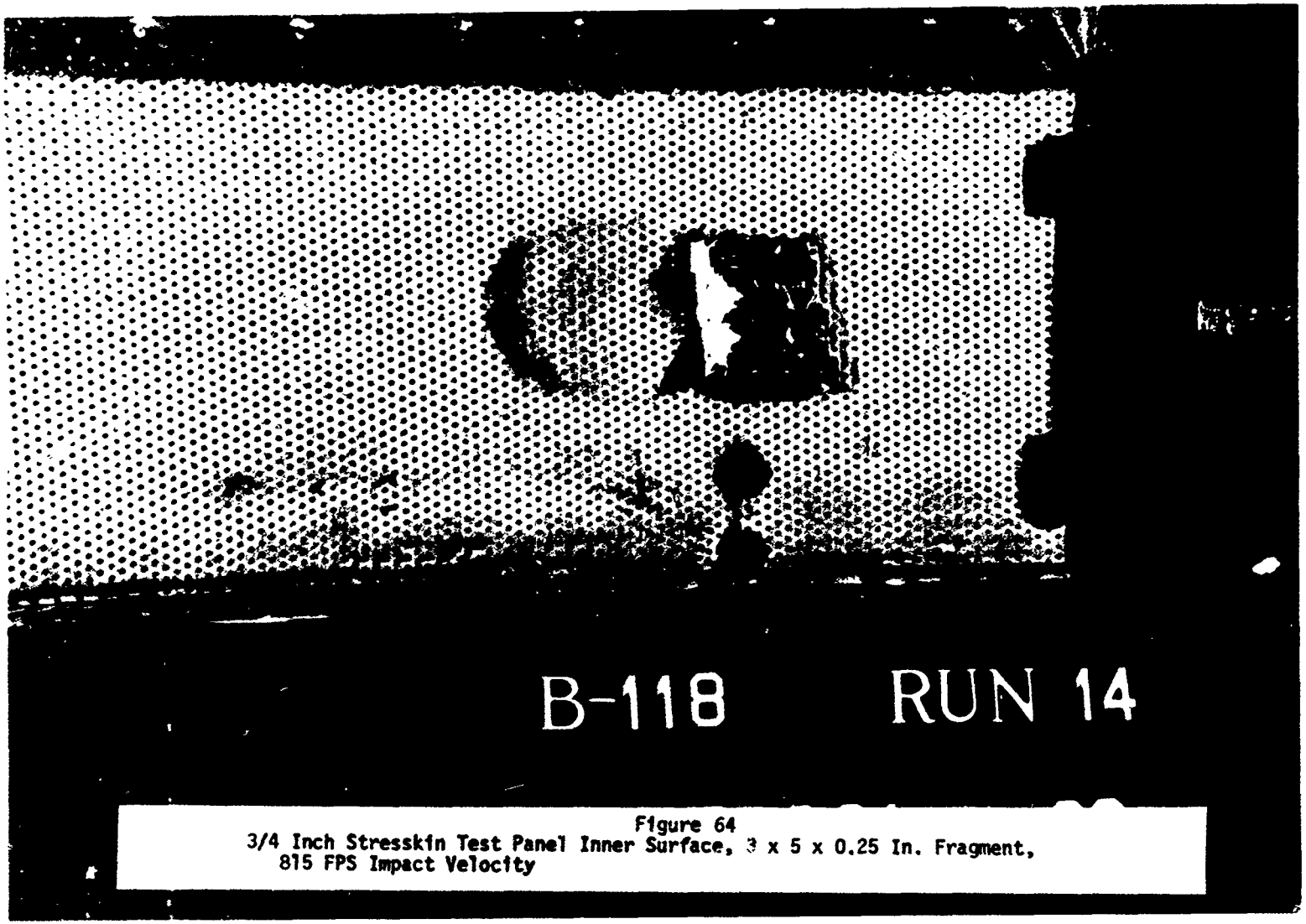

Figure 64
3/4 Inch Stresskin Test Panel Inner Surface, 3 x 5 x 0.25 In. Fragment,
815 FPS Impact Velocity

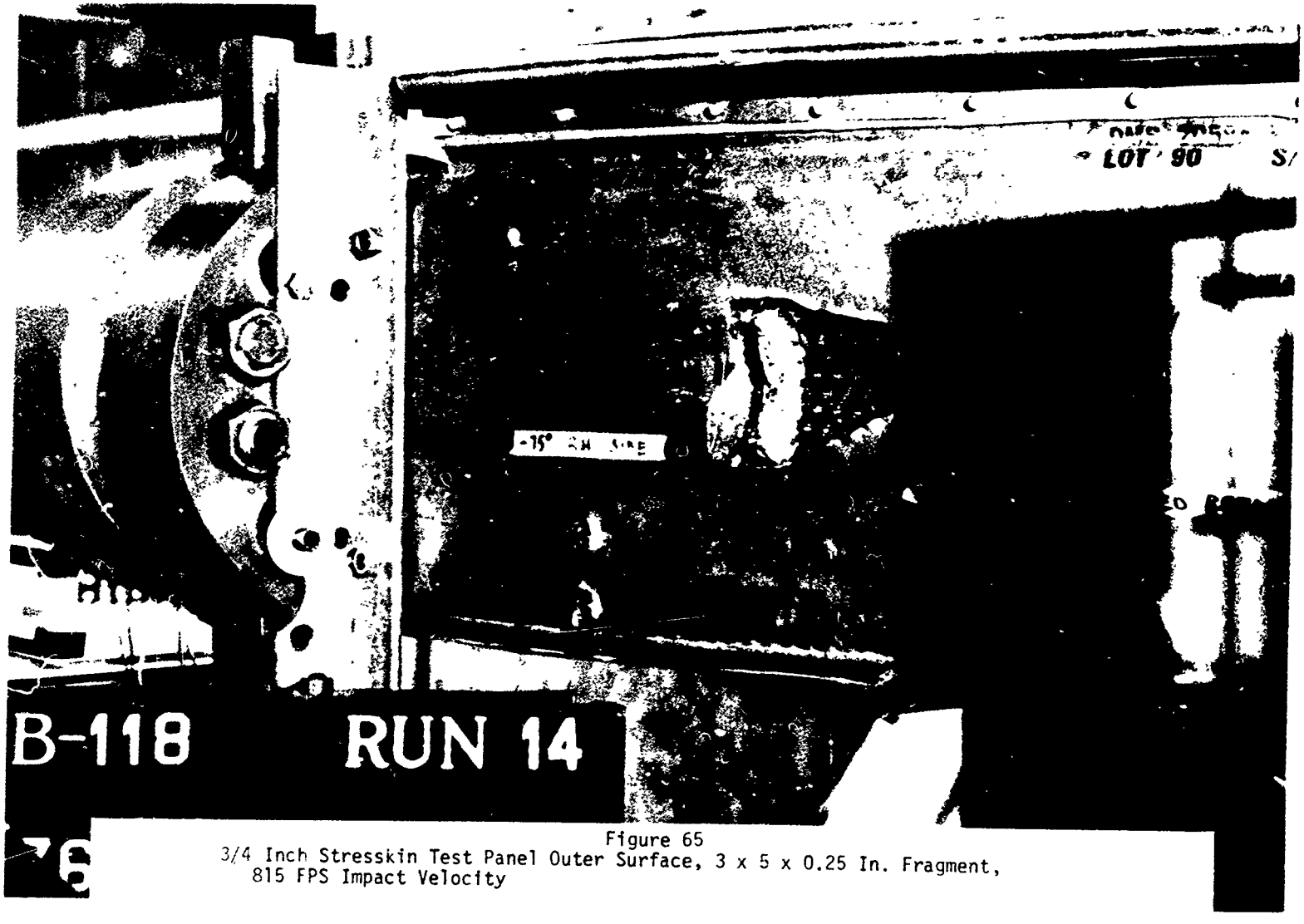

Figure 65
3/4 Inch Stresskin Test Panel Outer Surface, 3 x 5 x 0.25 In. Fragment,
815 FPS Impact Velocity

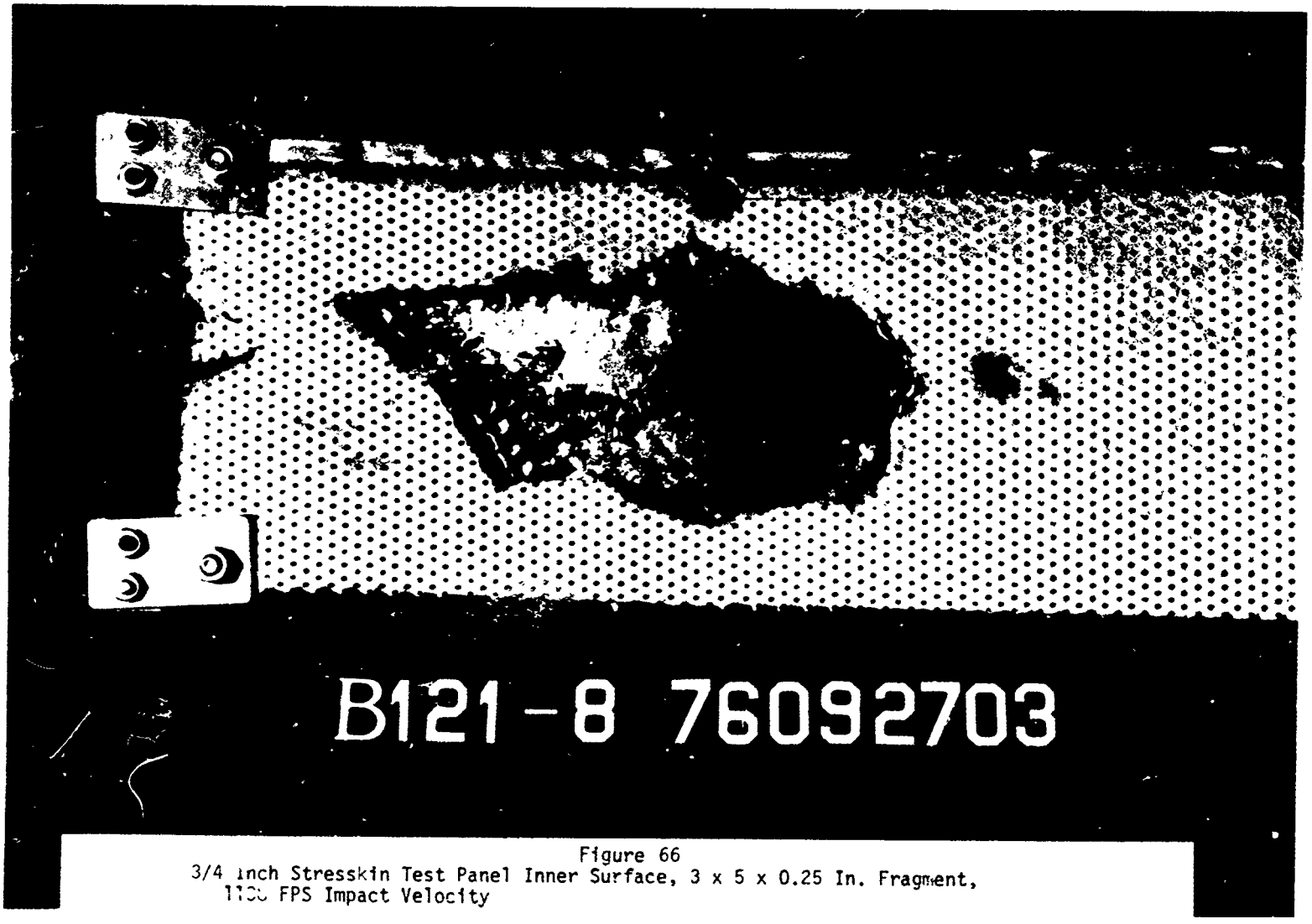

Figure 66
3/4 inch Stresskin Test Panel Inner Surface, 3 x 5 x 0.25 In. Fragment,
1150 FPS Impact Velocity

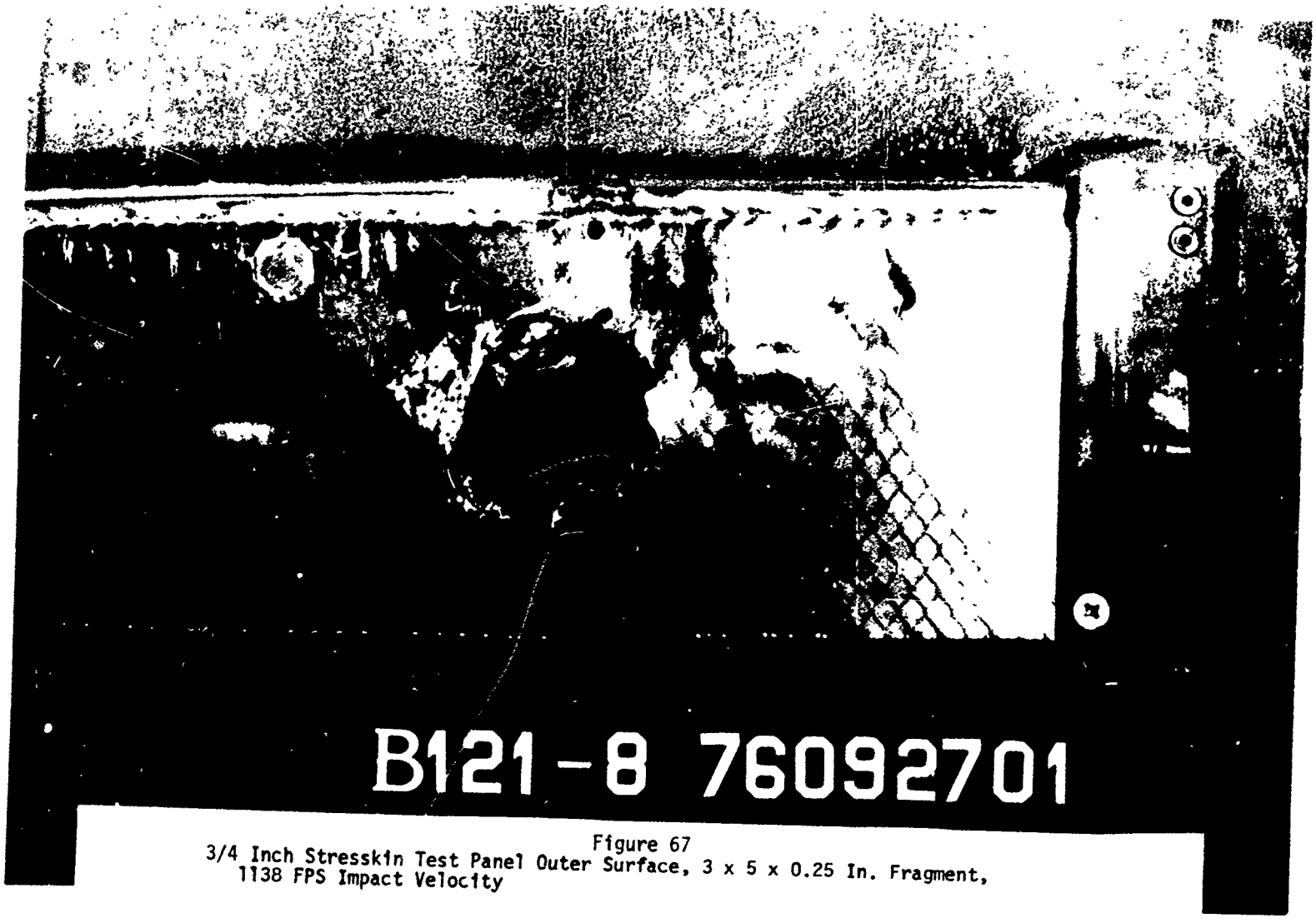

Figure 67
3/4 Inch Stresskin Test Panel Outer Surface, 3 x 5 x 0.25 In. Fragment, 1138 FPS Impact Velocity

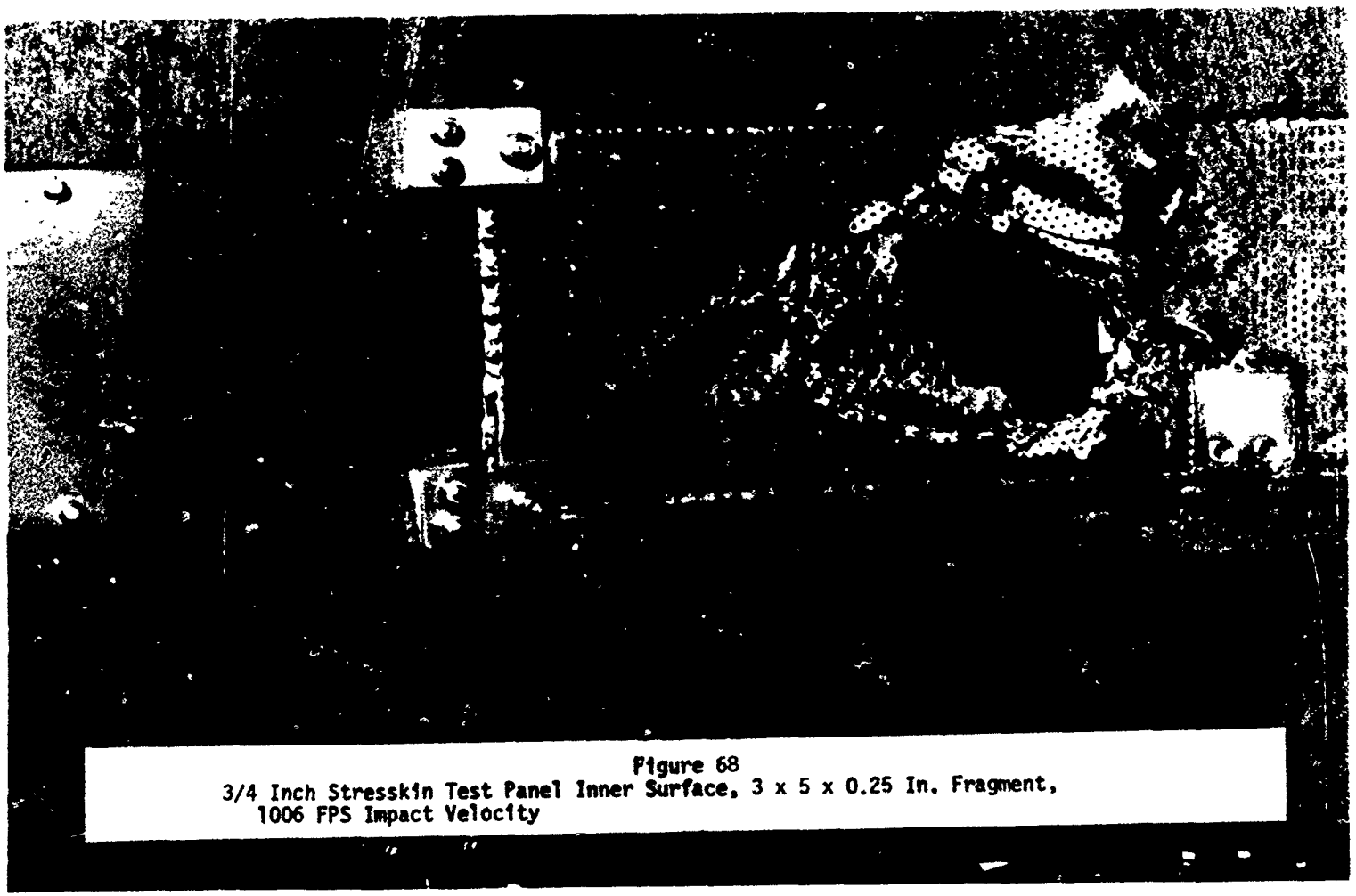

Figure 68
3/4 Inch Stresskin Test Panel Inner Surface, 3 x 5 x 0.25 In. Fragment,
1006 FPS Impact Velocity

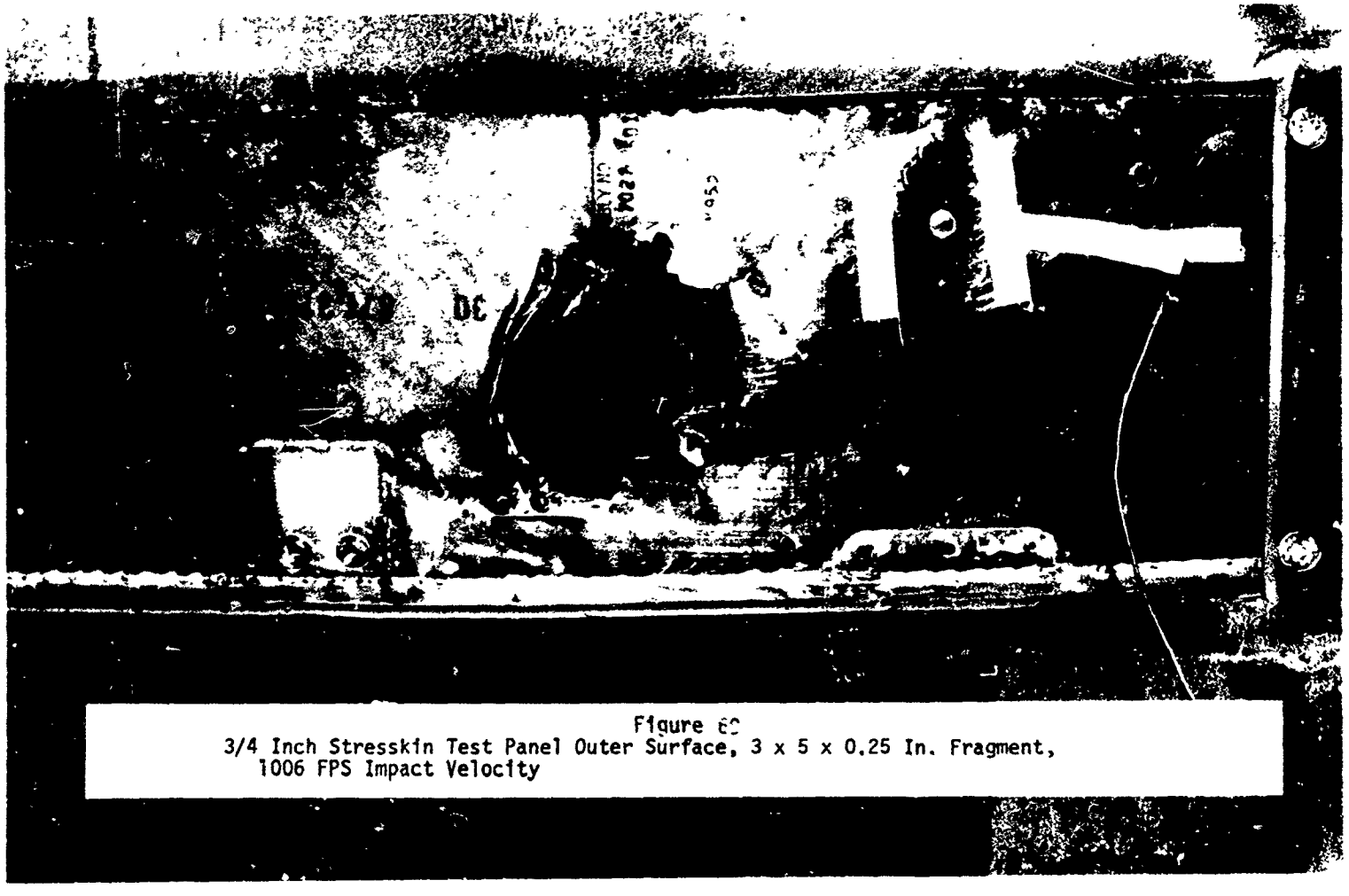

Figure 60
3/4 Inch Stresskin Test Panel Outer Surface, 3 x 5 x 0.25 In. Fragment,
1006 FPS Impact Velocity

6.5.3. Effect of Impact Angle on Stresskin Energy Absorption - The data given on Table 32 were obtained by firing titanium fragments into curved stresskin panels. The purpose of these tests was to establish the effect of trajectory impact angularity on the absorption characteristics of the 3/4-inch thick stresskin material.

The panels were clamped to a solid frame. The fragment trajectory was normal to the panel surface. The panel radius of curvature was large so the panel was almost flat. The test setup is shown on Figure 70.

The first three shots were accomplished during earlier Douglas sponsored tests using the small 3-1/2 inch diameter bore gun previously described. The impact velocities covered a range from a low of 562 ft/sec to a high of 965 ft/sec with a 3 x 5 x 0.25 inch titanium fragment.

The last two shots were accomplished under this contract using the large 5-inch bore gun. These shots were at impact velocities of 627 ft/sec and 938 ft/sec with a 4 x 7 x 0.25 inch titanium fragment.

Figure 71 shows the initial and final energy levels at various initial velocities for the 3/4-inch thick steel stresskin for normal fragment impingement. The results indicate that on an average 1240 ft-lbs of energy is absorbed when a 3 x 5 x 0.25 inch fragment penetrates and an average of 1187 ft-lbs when a 4 x 7 x 0.25 inch fragment penetrates the stresskin. The effect of fragment impingement angularity for the 3 x 5 x 0.25 inch fragment when compared to Figure 57 for tangential impingement indicates that the average absorbed energy varies from 3349 ft-lbs for tangential impingement to 1240 ft-lbs for normal (90° to target surface) impingement. The same comparison with Figure 40 for the 4 x 7 x 0.25 inch fragment shows that the absorbed energy varies from 2830 ft-lbs for tangential impingement to 1187 ft-lbs for normal (°0° to target surface) impingement.

The damage to the target specimens is shown in Figures 72 through 83.

TABLE 32 -TEST RESULTS
TARGET - 3/4 INCH THICK CURVED STEEL STRESSKIN PANEL
FRAGMENT - 3 x 5 x 0.25 INCH TITANIUM FLAT PLATE
*FRAGMENT - 4 x 7 x 0.25 INCH TITANIUM FLAT PLATE
NORMAL IMPINGEMENT

	DATE 1976	RUN NO.	TEST SPONSOR		FRAGMENT WEIGHT		VELOCITY FT/SEC		ENERGY FT-LBS		ENERGY ABSORBED FT-LBS	PERCENT ENERGY ABSORBED	REMARKS
			FAA	DOUGLAS	GRAMS	POUNDS	INITIAL	FINAL	INITIAL	FINAL			
	3-9	B-118-1		X	253.88	.560	562	533	2746	2470	276	10	Penetrated
	3-9	B-118-12		X	254.02	.560	766	645	5102	3618	1484	29	Penetrated
	3-18	B-118-15			258.02	.569	965	842	8228	6264	1964	24	Penetrated
*	8-21	B-121-4	X		517.6	1.141	627	594	6965	6251	714	10.2	Penetrated
*	8-22	B-121-5	X		492.6	1.086	938	884	14837	13178	1659	11.2	Penetrated
(1)	3-19	B-118-16		X	259.98	.573	774	637	5330	3610	1720	32.3	Penetrated

Target Material: Impingement Side - 0.016 inch thick 316L stainless steel perforated with 0.094 inch diameter holes 13% open area 60° hole pattern

Exit Side - 0.012 inch thick 316L stainless steel solid sheet

Core - 0.035 inch thick ribbon 0.720 inch height 316L stainless steel 3/4 inch diamond pattern

Panel Density - 1.80 #/ft^2 Overal Panel Thickness - 0.748 inch

(1) 45° Impingement
3 x 5 x 0.25 Fragment

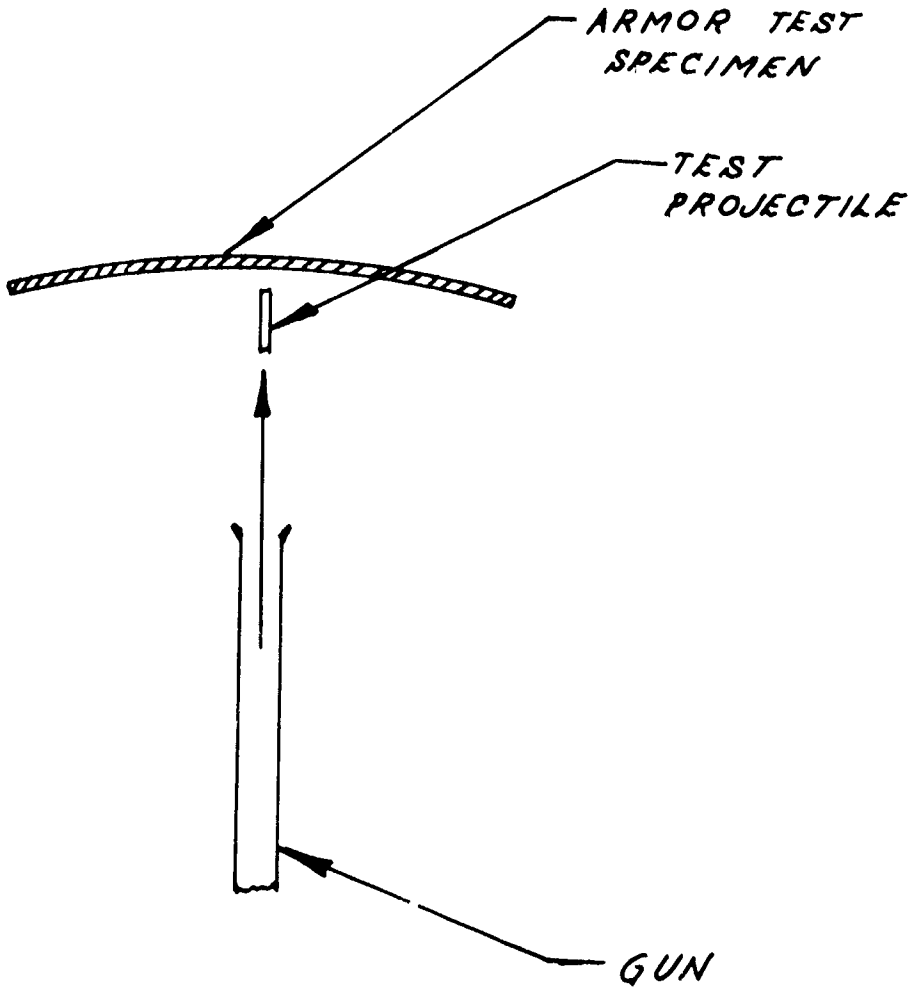

FIGURE 70
NORMAL SHOT
TEST SETUP

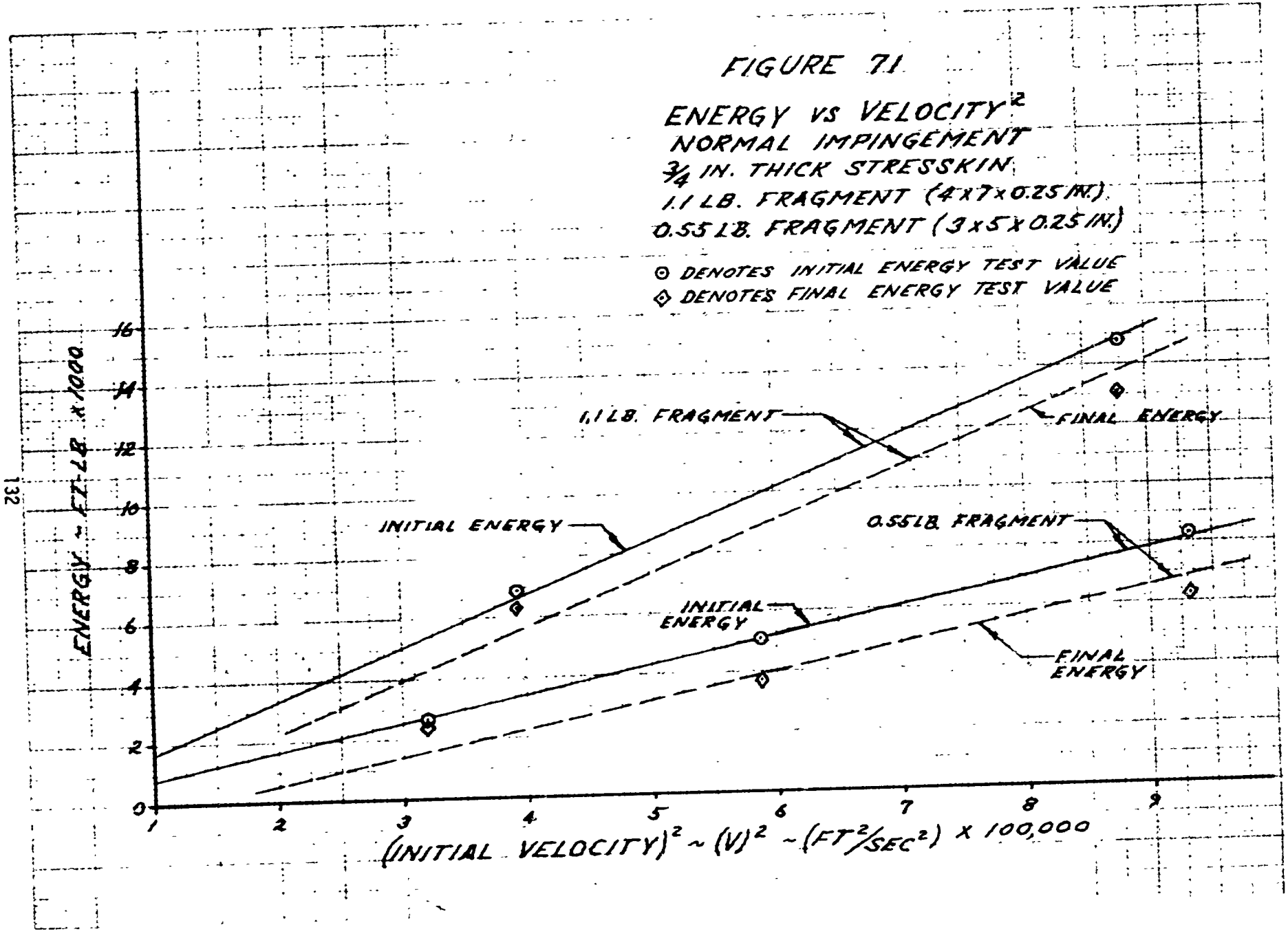
FIGURE 71
ENERGY VS VELOCITY²
NORMAL IMPINGEMENT
3/4 IN. THICK STRESSKIN
1.1 LB. FRAGMENT (4 X 7 X 0.25 IN.)
0.55 LB. FRAGMENT (3 X 5 X 0.25 IN.)
⊙ DENOTES INITIAL ENERGY TEST VALUE
◇ DENOTES FINAL ENERGY TEST VALUE
ENERGY ~ FT-LB X 1000
0
2
4
6
8
10
12
14
16
1
2
3
4
5
6
7
8
9
(INITIAL VELOCITY)² ~ (V)² ~ (FT²/SEC²) X 100,000
1.1 LB. FRAGMENT
FINAL ENERGY
INITIAL ENERGY
0.55 LB. FRAGMENT
INITIAL ENERGY
FINAL ENERGY

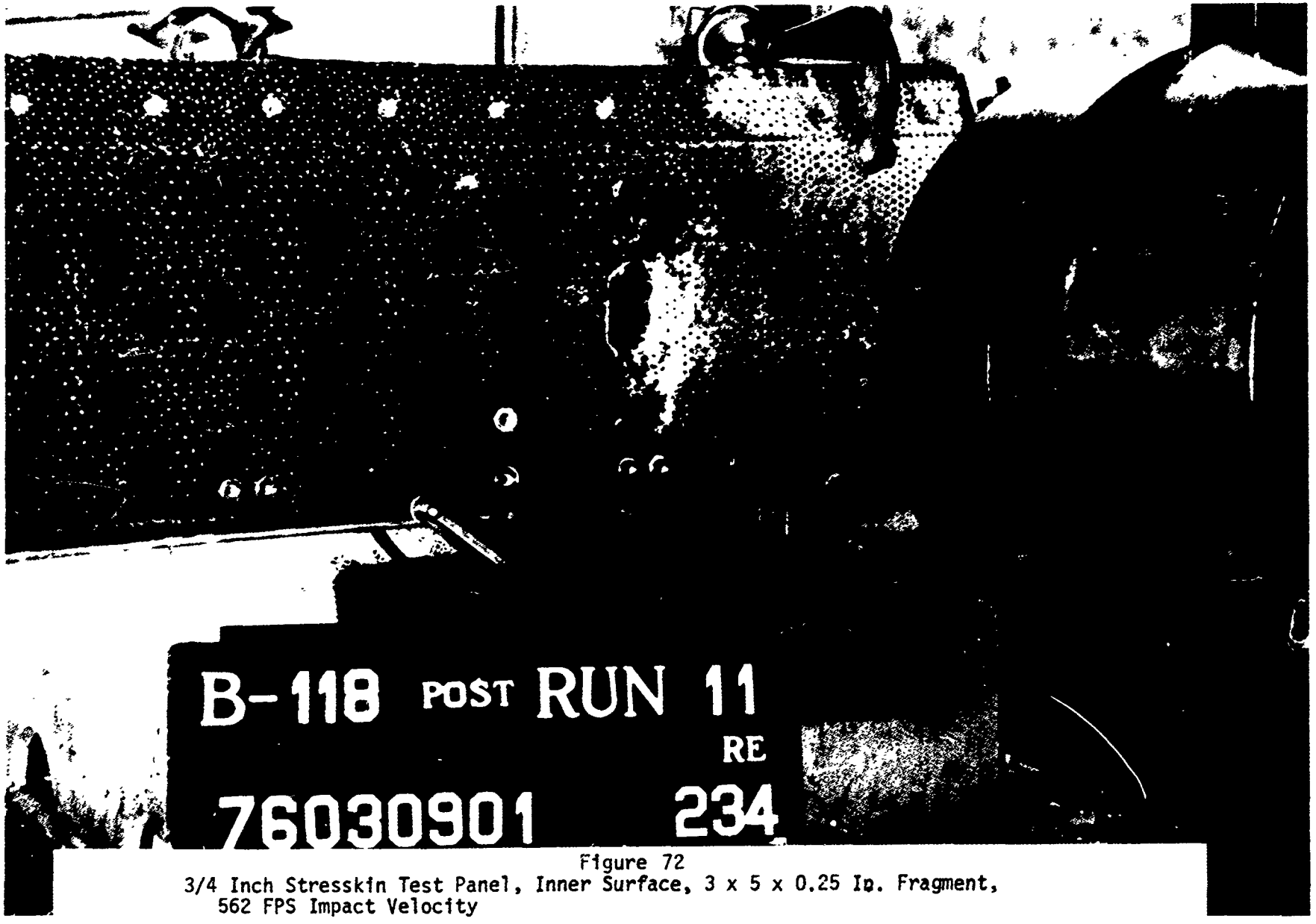

Figure 72
3/4 Inch Stresskin Test Panel, Inner Surface, 3 x 5 x 0.25 In. Fragment,
562 FPS Impact Velocity

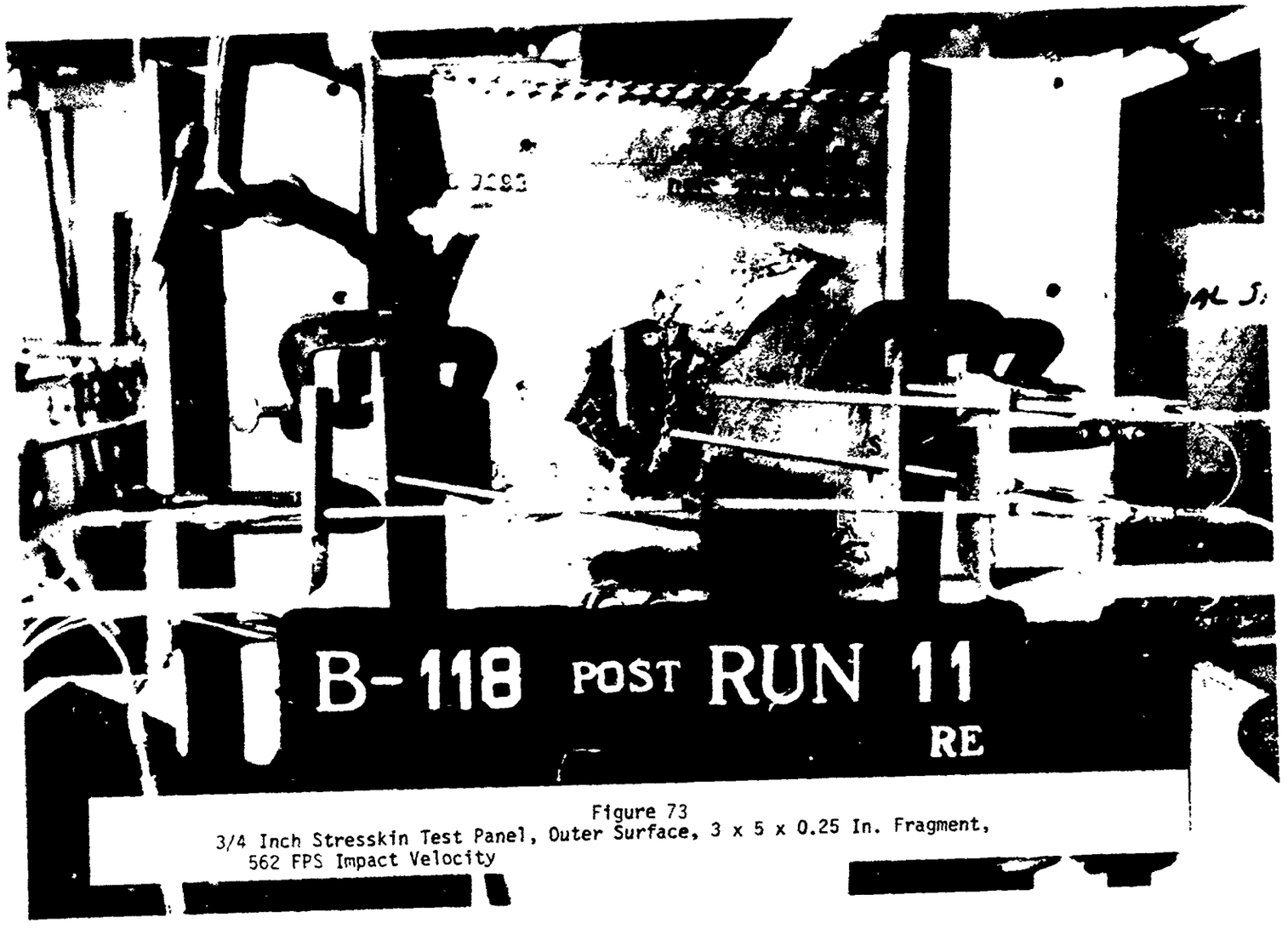

Figure 73
3/4 Inch Stresskin Test Panel, Outer Surface, 3 x 5 x 0.25 In. Fragment,
562 FPS Impact Velocity

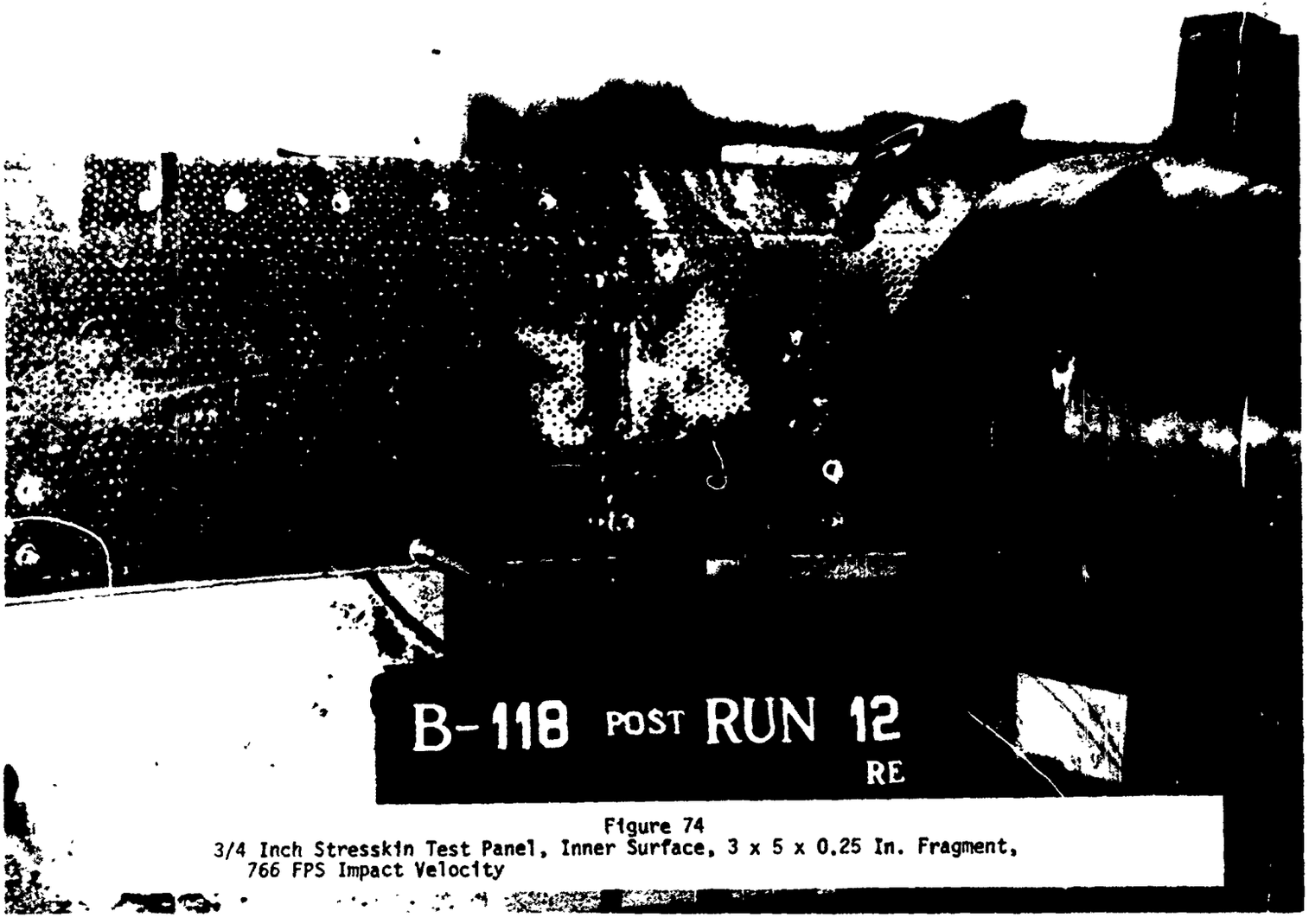

Figure 74
3/4 Inch Stresskin Test Panel, Inner Surface, 3 x 5 x 0.25 In. Fragment,
766 FPS Impact Velocity

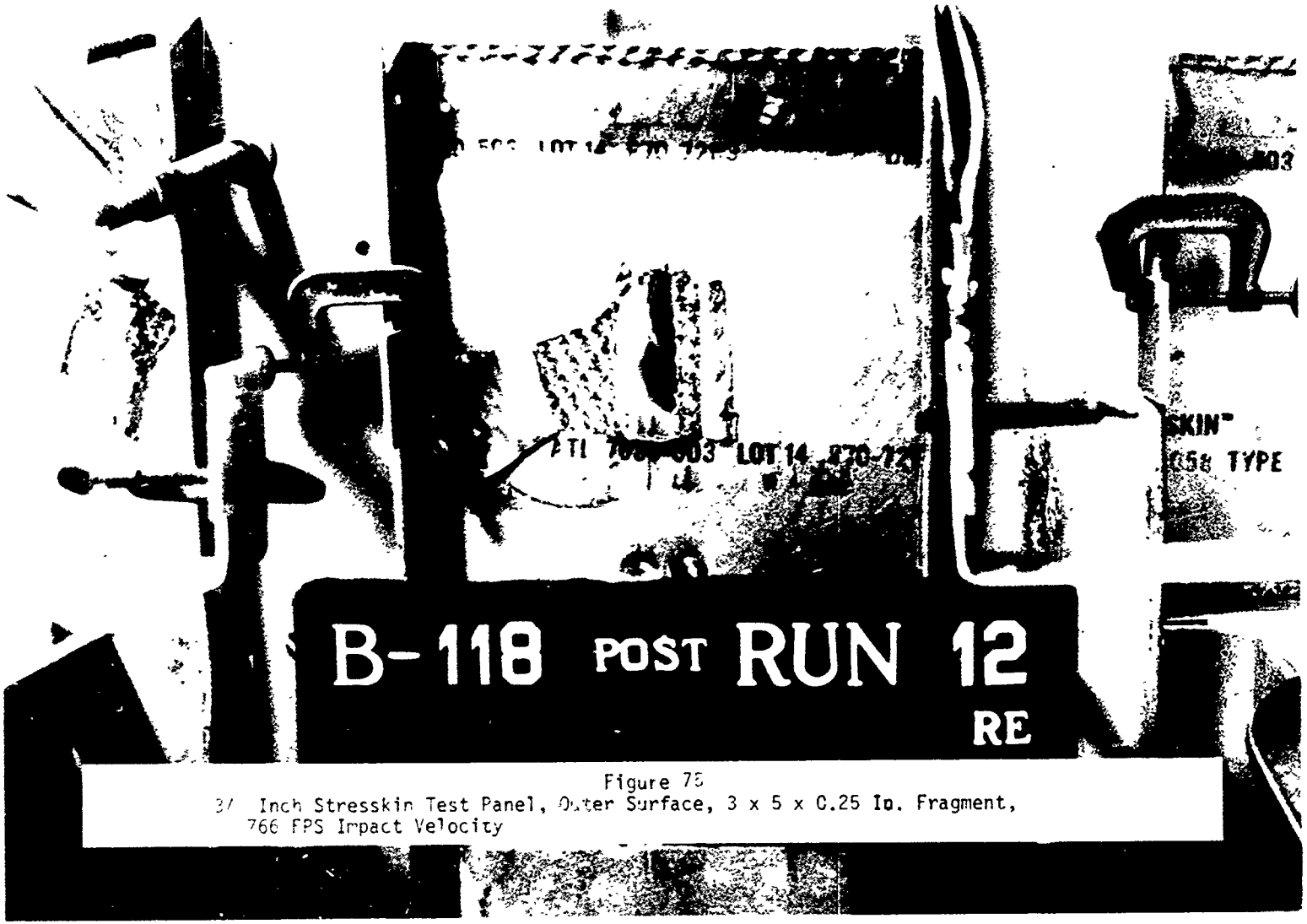

Figure 75
3/ Inch Stresskin Test Panel, Outer Surface, 3 x 5 x 0.25 In. Fragment,
766 FPS Impact Velocity

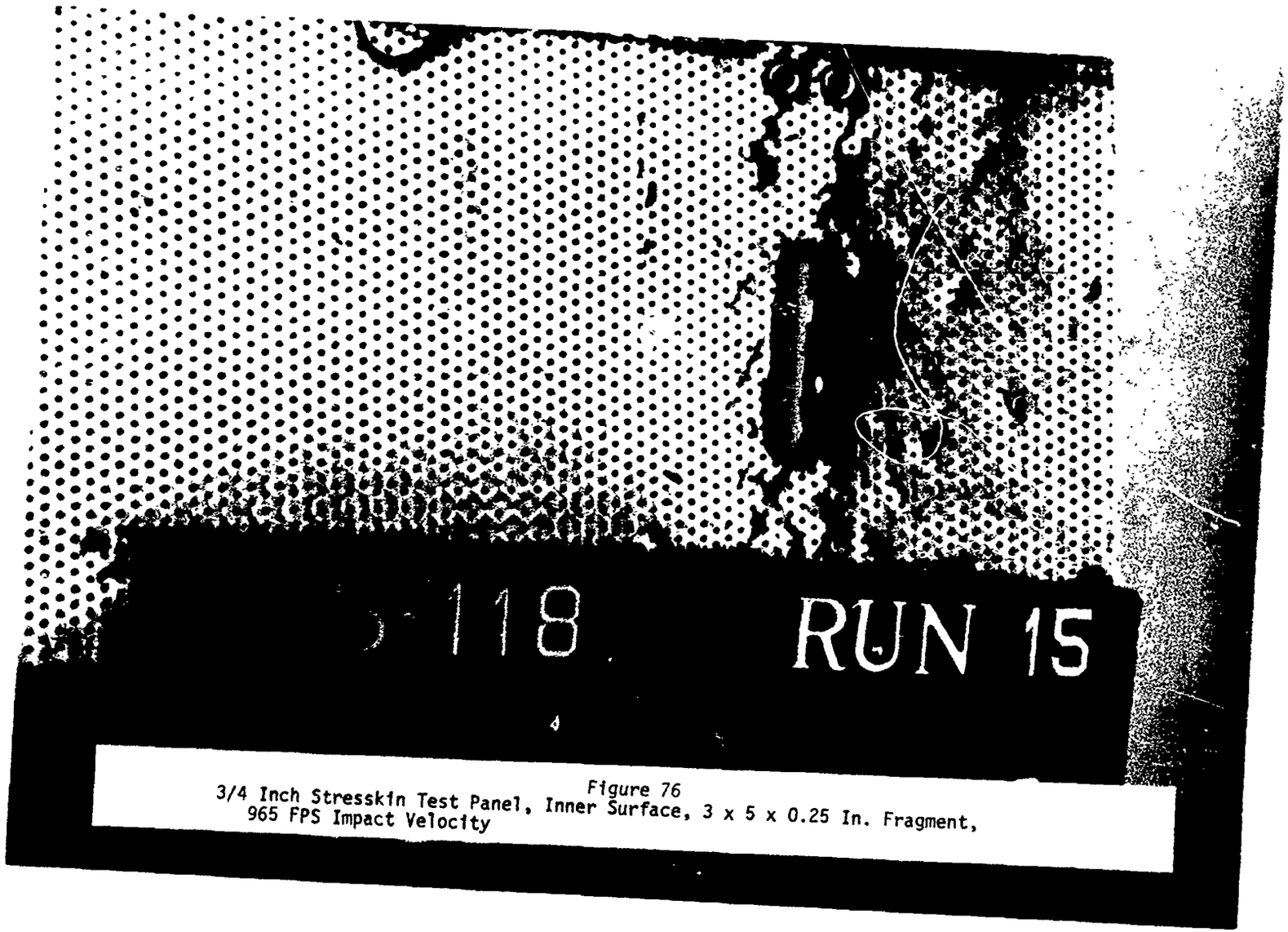

Figure 76
3/4 Inch Stresskin Test Panel, Inner Surface, 3 x 5 x 0.25 In. Fragment, 965 FPS Impact Velocity

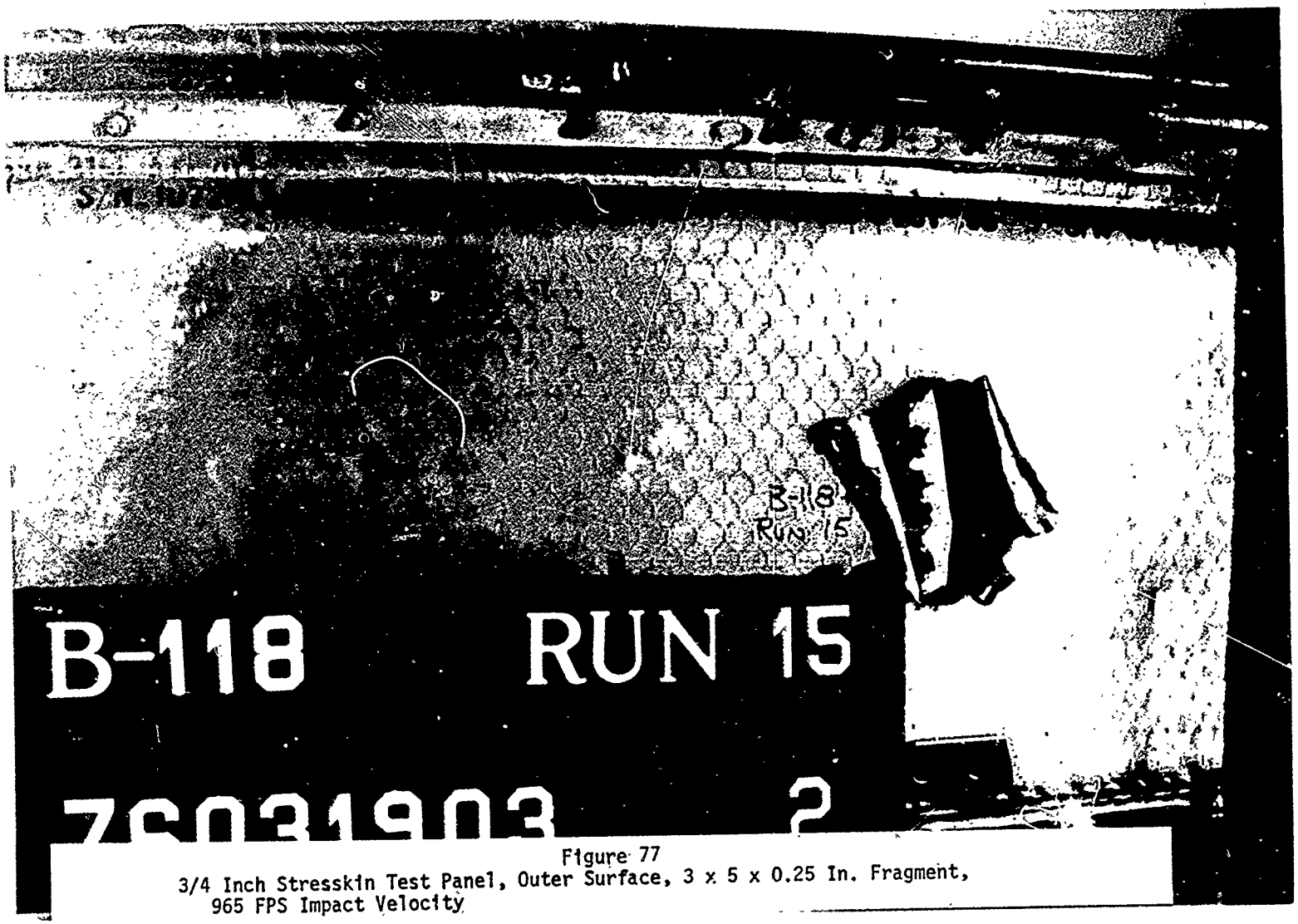

Figure 77
3/4 Inch Stresskin Test Panel, Outer Surface, 3 x 5 x 0.25 In. Fragment,
965 FPS Impact Velocity

Figure 78

3/4 Inch Stresskin Test Panel, Inner Surface,
4 x 7 x 0.25 In. Fragment, 627 FPS Impact Velocity

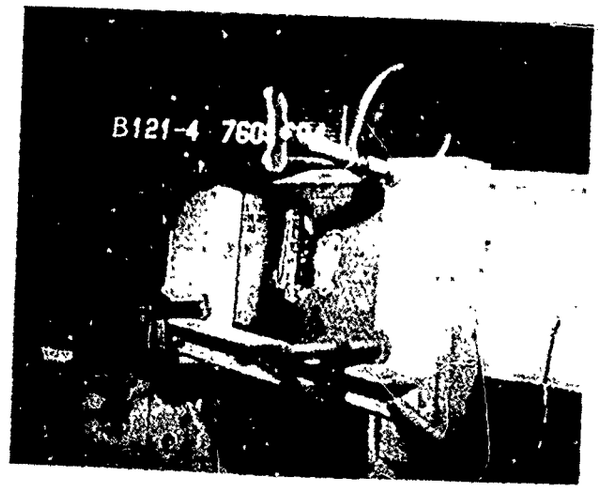

Figure 79

3/4 Inch Stresskin Test Panel, Outer Surface,
4 x 7 x 0.25 In. Fragment, 627 FPS Impact Velocity

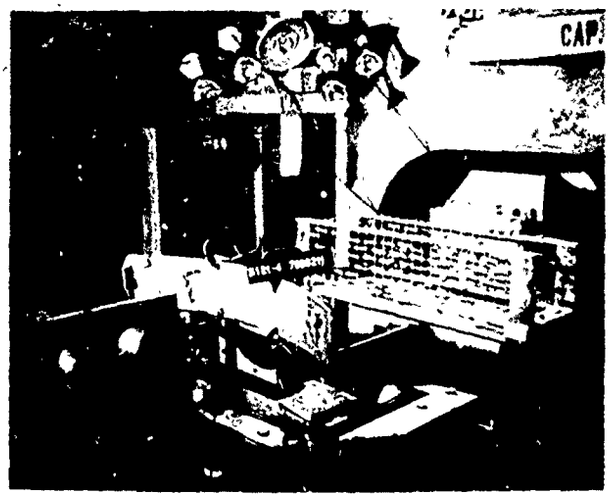

Figure 80

3/4 Inch Stresskin Normal Impact Test Setup, Front View, Prior to Test Shot With 4 x 7 x 0.25 In. Fragment at 627 FPS Impact Velocity

Figure 81

3/4 Inch Stresskin Normal Impact Test Setup, Back View, 4 x 7 x 0.25 In. Fragment at 627 FPS Impact Velocity

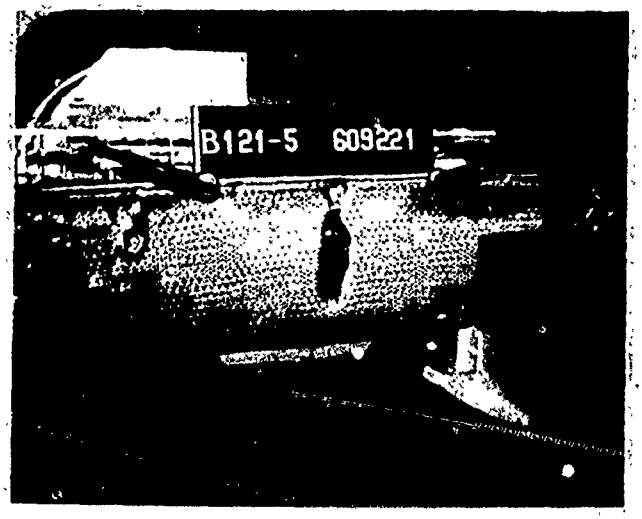

Figure 82

3/4 Inch Stresskin Test Panel, Inner Surface,
4 x 7 x 0.25 In. Fragment, 938 FPS Impact Velocity

Figure 83

3/4 Inch Stresskin Test Panel, Outer Surface,
4 x 7 x 0.25 In. Fragment, 938 FPS Impact Velocity

6.5.4 Energy Absorption by Bonded Aluminum Honeycomb Panels - The data given on Table 33 were obtained by firing 4 x 7 x 0.25 inch titanium fragments into 2-inch thick curved panels of double layer bonded aluminum honeycomb. The purpose of these tests was to determine the absorption capability of bonded aluminum structure when impacted by a high velocity fragment and to compare to equivalent test with steel stresskin.

The panels were mounted and supported on the same barrel support structure used for the tests with stresskin panels. The 40 foot long 5-inch diameter bore gun was used for all tests. The fragments were fired tangentially to the target surface and were oriented with the 4-inch side parallel to the target surface and the 7-inch length aligned with the trajectory.

These data points were obtained from previous Douglas sponsored tests and covered a range of impact velocities from a low of 474 ft/sec to a high of 902 ft/sec. In all, five data points were obtained.

Figure 84 shows the initial and final energy levels at various initial velocities for the 2-inch curved double layer bonded aluminum honeycomb material. The results indicate that on an average 2500 ft-lbs of energy will be absorbed for this particular material, impact velocity range and fragment size. It is interesting to note that on similar tests with this same fragment size fired into 3/4-inch thick curved steel stresskin panels a similar average level of energy was absorbed (2830 ft-lbs as compared to 2500 ft-lbs on this test).

Figure 85 shows that with the 3 x 5 x 0.25 inch fragment impacting 2-inch thick aluminum honeycomb an average of 2958 ft-lbs of energy should be absorbed.

Figures 86 through 95 show the extent of test panel damage incurred during this test phase.

TABLE 33 -TEST RESULTS
TARGET - 2 INCH THICK CURVED ALUMINUM HONEYCOMB PANEL
FRAGMENT - 4 x 7 x 0.25 INCH TITANIUM FLAT PLATE
TANGENTIAL IMPINGEMENT

DATE 1976	RUN NO.	TEST SPONSOR		FRAGMENT WEIGHT		VELOCITY FT/SEC		ENERGY FT-LBS		ENERGY ABSORBED FT-LBS	PERCENT ENERGY ABSORBED	REMARKS
		FAA	DOUGLAS	GRAMS	POUNDS	INITIAL	FINAL	INITIAL	FINAL			
7-15	B-119-9		X	518.56	1.143	615	553	6713	5428	1285	19	Penetrated
7-19	B-119-10		X	518.15	1.142	474	314	3984	1748	2236	56	Penetrated
7-20	B-119-11		X	518.2?	1.142	745	585	9842	6069	3773	38.3	Penetrated
8-23	B-119-20		X	519.0	1.144	902	801	14453	11397	3056	21.1	Penetrated
8-24	B-119-21		X	519.1	1.144	569	450	5751	3597	2154	37.5	Penetrated

Target Material - Impingement Side - 0.040 inch thick 2014-T6 aluminum perforated with 0.080 inch diameter holes 0.149 on centerline 26% open area 60° hole pattern

Septum Sheet - 0.020 inch thick 2014-T6 aluminum same perforations and pattern as above

Exit Side - 0.020 inch thick 2014-T6 aluminum solid sheet

Core - 0.003 inch thick ribbon 5052 aluminum 3/8 inch diamond pattern

Panel Construction - First layer 3/4 inch height second layer 1-1/4 inch height

Panel Density - 2.08 lb/ft^2

FIGURE 84

ENERGY VS. VELOCITY^2

2 IN. THICK ALUMINUM HONEYCOMB

TANGENTIAL IMPINGEMENT

1.1 LB. FRAGMENT (4X7X0.25 IN)

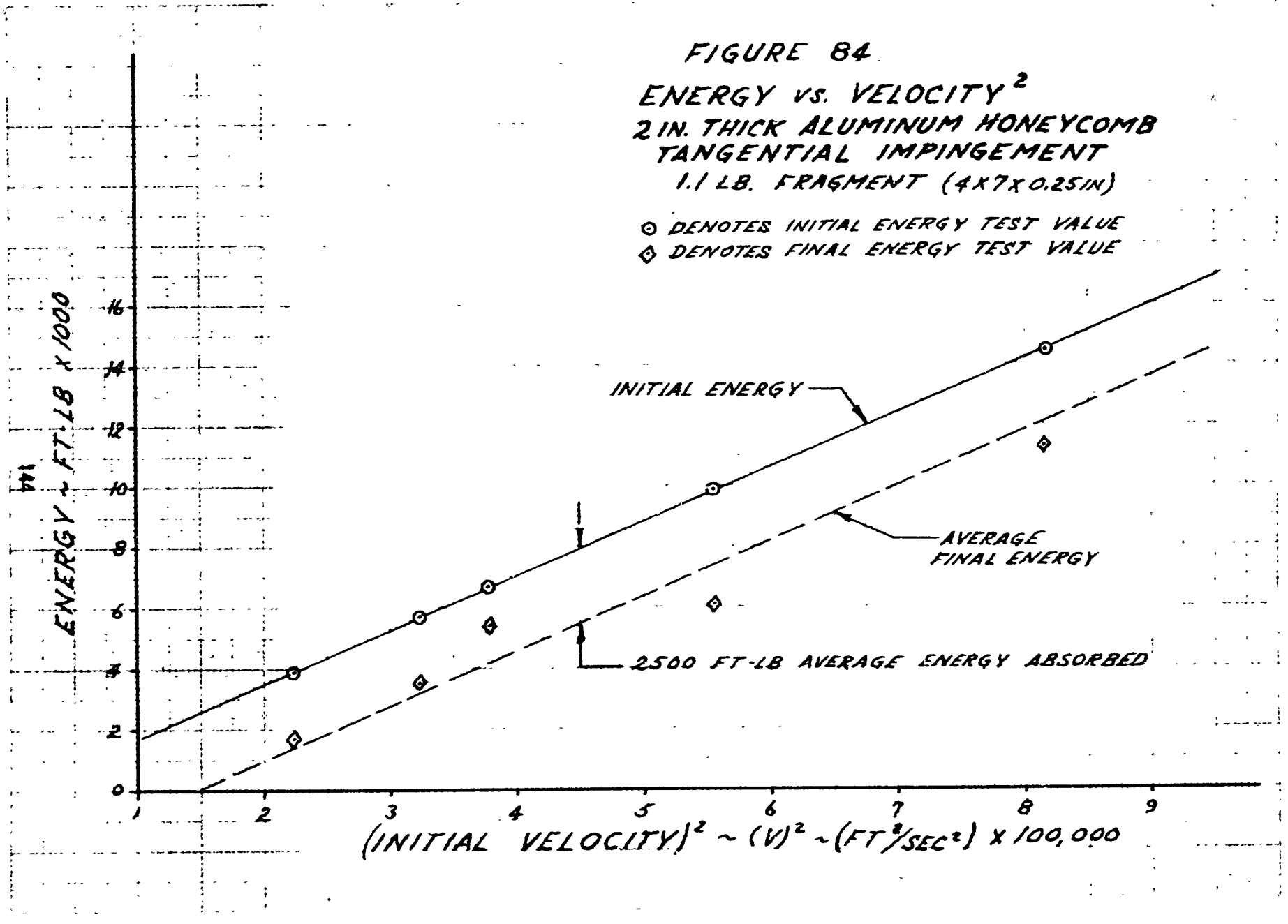

FIGURE 85

ENERGY VS. VELOCITY^2
TANGENTIAL IMPINGEMENT
2 IN. THICK ALUMINUM HONEYCOMB
.55 LB. FRAGMENT (3 x 5 x 0.25 IN.)
(ESTIMATED ENERGY ABSORBED)

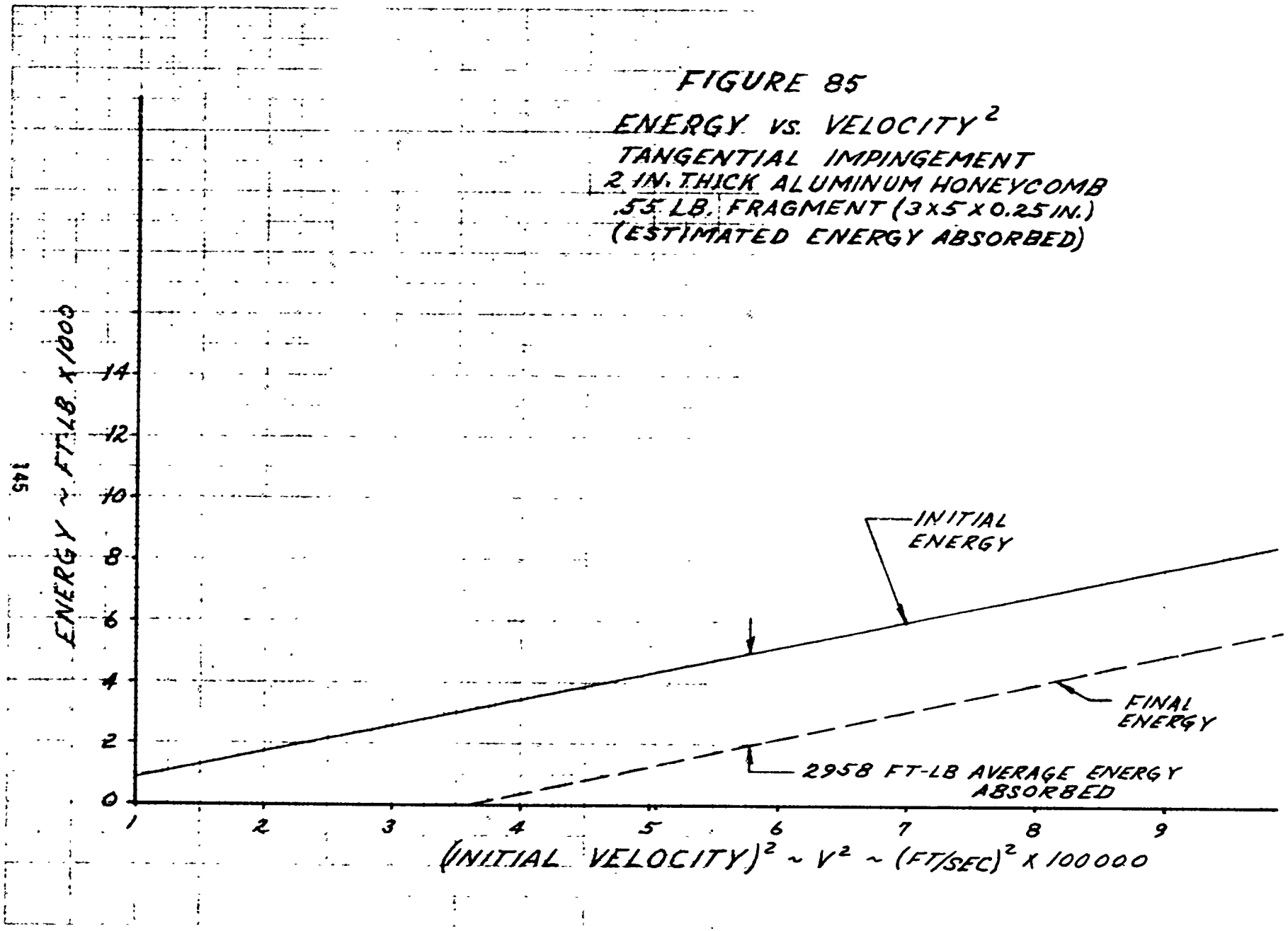

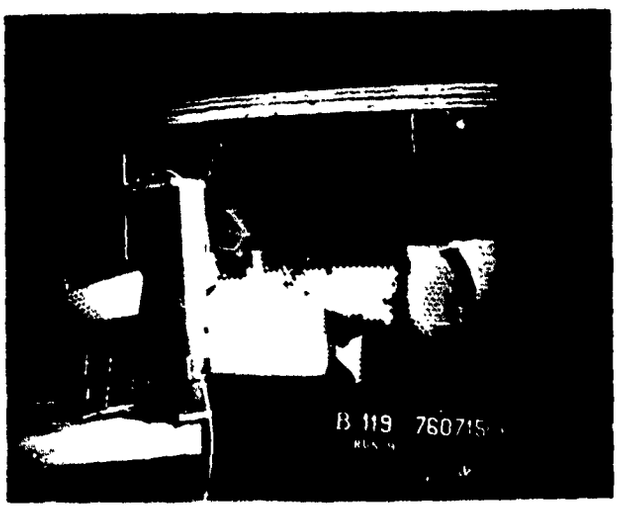

Figure 86

2 Inch Aluminum Honeycomb Test Panel, Outer Surface,
4 x 7 x 0.25 In. Fragment, 615 FPS Impact Velocity

Figure 87

2 Inch Aluminum Honeycomb Test Panel, Outer Surface,
4 x 7 x 0.25 In. Fragment, 615 FPS Impact Velocity

Figure 88

2 Inch Aluminum Honeycomb Test Panel, Outer Surface,
4 x 7 x 0.25 In. Fragment, 474 FPS Impact Velocity

Figure 89

2 Inch Aluminum Honeycomb Test Panel, Outer Surface,
4 x 7 x 0.25 In. Fragment, 474 FPS Impact Velocity

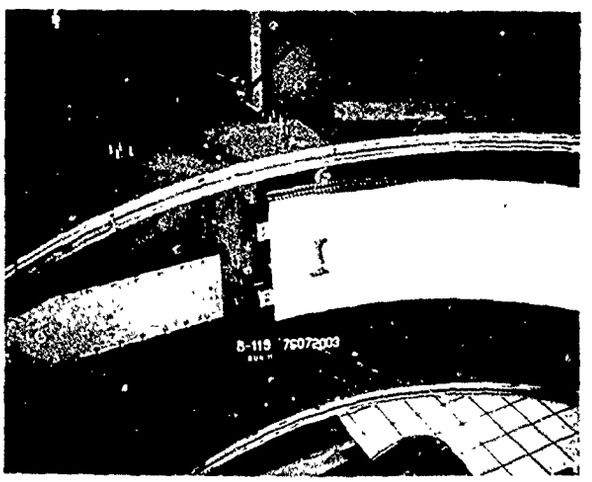

Figure 90

2 Inch Aluminum Honeycomb Test Panel, Inner Surface,
4 x 7 x 0.25 In. Fragment, 745 FPS Impact Velocity

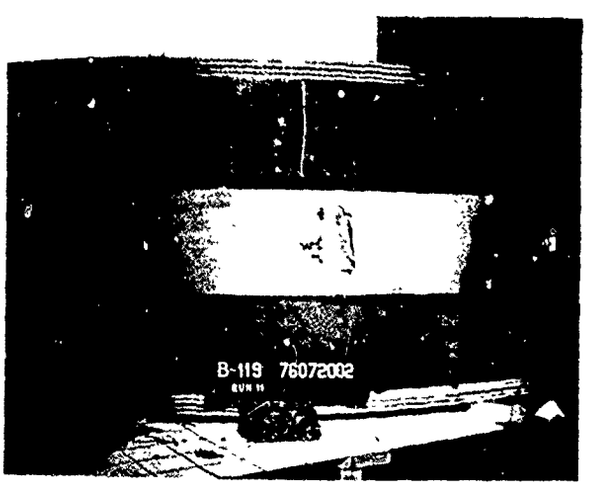

Figure 91

2 Inch Aluminum Honeycomb Test Panel, Outer Surface,
4 x 7 x 0.25 In. Fragment, 745 FPS Impact Velocity

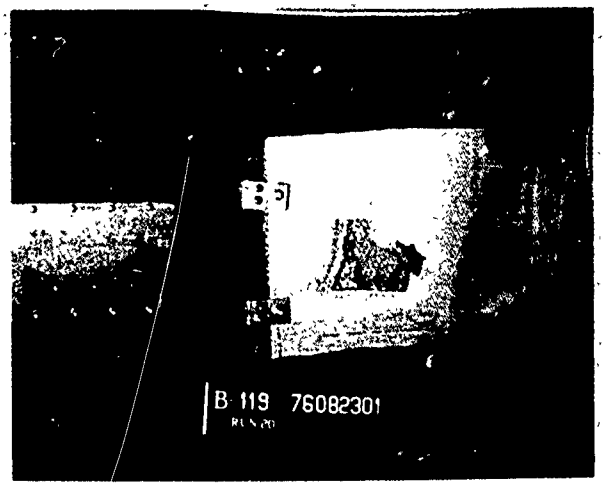

Figure 92

2 Inch Aluminum Honeycomb Test Panel, Inner Surface,
4 x 7 x 0.25 In. Fragment, 902 FPS Impact Velocity

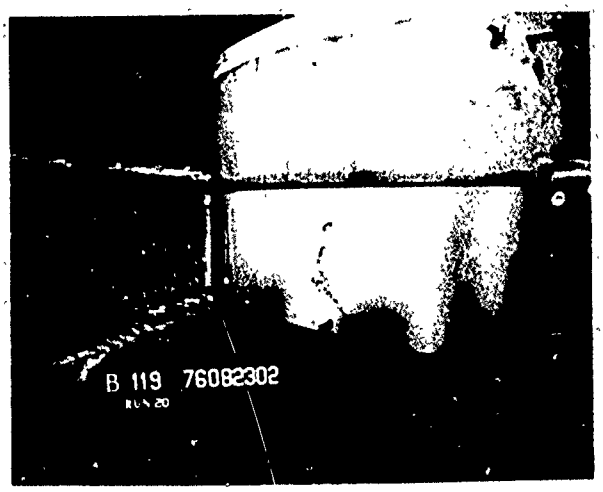

Figure 93

2 Inch Aluminum Honeycomb Test Panel, Outer Surface,
4 x 7 x 0.25 In. Fragment, 902 FPS Impact Velocity

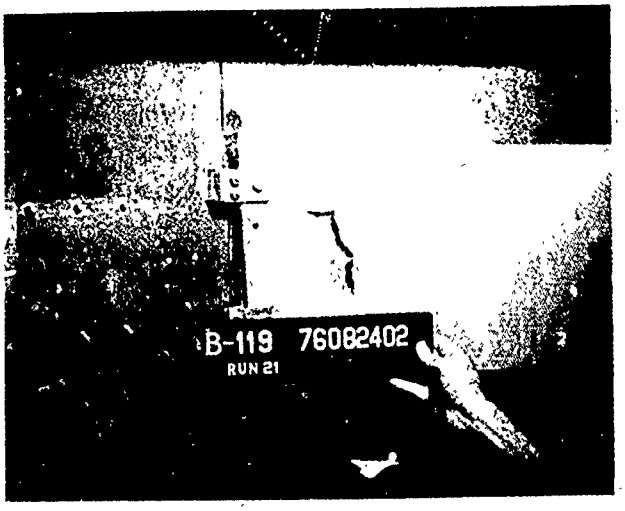

Figure 94

2 Inch Aluminum Honeycomb Test Panel, Inner Surface,
4 x 7 x 0.25 In. Fragment, 569 FPS Impact Velocity

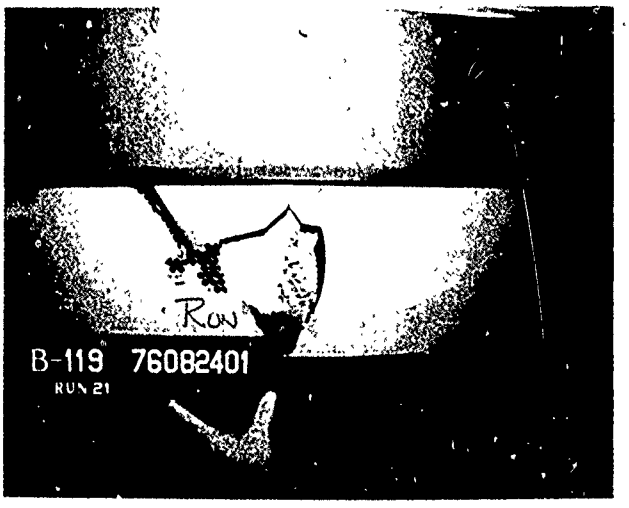

Figure 95

2 Inch Aluminum Honeycomb Test Panel, Outer Surface,
4 x 7 x 0.25 In. Fragment, 569 FPS Impact Velocity

6.5.5 Effect of Impact Angle on Aluminum Honeycomb Energy Absorption - The data given in Table 34 were obtained by firing 4 x 7 x 0.25 inch fragments into curved single layer, 3/4-inch thick bonded aluminum panels. The purpose of these tests was to establish the effect of fragment trajectory impact angularity on the absorption characteristics of the 3/4-inch thick aluminum honeycomb material.

The panels were clamped to a solid frame and the fragment trajectory was normal to the panel surface. The large 5-inch diameter bore gun was used with fragment velocities of 427 ft/sec and 751 ft/sec. The energy absorption for this test was very low averaging only slightly over 100 ft-lbs. It had been intended to repeat the test with the 3 x 5 x 0.25 fragments but since the absorption level was so low with the larger fragment any data obtained would have been within the data scatter. As can be seen on Table 34 there was only a velocity change of 8 ft/sec on one shot and a 4 ft/sec change on the other shot; a velocity measuring error of 1 ft/sec has a large effect. The normal shots on stresskin showed that with the smaller fragment approximately 53 more ft-lbs were absorbed than with the large fragment. This amounts to about 4.5% increase in energy absorption. If the average absorption for the 4 x 7 x 0.25 inch fragment is 108 ft-lbs on the 3/4-inch aluminum honeycomb, the average for the 3 x 5 x 0.25 inch fragment would be about 113 ft-lbs. This appeared to be reasonable and no tests were conducted.

Test data was obtained for one shot with the same fragment size and 3/4-inch aluminum honeycomb material but with a tangential fragment trajectory. This showed an absorption level of 2395 ft-lbs compared to about 100 ft-lbs for the normal trajectory.

The damage to the target specimens is shown on Figures 96 through 101.

TABLE 34 -TEST RESULTS
TARGET - 3/4 INCH CURVED ALUMINUM HONEYCOMB PANEL
FRAGMENT - 4 x 7 x 0.25 INCH TITANIUM FLAT PLATE
NORMAL IMPINGEMENT
* RUN B-119-24 TANGENTIAL IMPINGEMENT

	DATE 1976	RUN NO.	TEST SPONSOR		FRAGMENT WEIGHT		VELOCITY FT/SEC		ENERGY FT-LBS		ENERGY ABSORBED FT-LBS	PERCENT ENERGY ABSORBED	RESULTS
			FAA	DOUGLAS	GRAMS	POUNDS	INITIAL	FINAL	INITIAL	FINAL			
	9-23	B-121-6	X		492.6	1.086	427	419	3075	2461	114	4%	Penetrated
	9-24	B-121-7	X		498.0	1.098	751	747	9616	9514	102	1%	Penetrated
*	9-8	B-119-24		X	519.2	1.145	367	0	2395	0	2395	100%	Contained

Target Material: Impingement Side - 0.025 inch thick 2014-T6 aluminum perforated with 0.050 inch diameter holes 0.139 on centerline 12% open area 60° hole pattern

Exit Side - 0.020 inch thick 2014-T6 aluminum solid sheet

Core - 0.003 inch thick ribbon 5052 aluminum 3/8 inch diamond pattern

Panel construction - Single layer 3/4 inch height

Panel Density - 1.21 lb/ft^2

* On this test Kevlar pads and straps were installed on test specimen but fragment remained within honeycomb material

Figure 96

3/4 Inch Aluminum Honeycomb Test Panel, Inner Surface,
4 x 7 x 0.25 In. Fragment, 427 FPS Impact Velocity

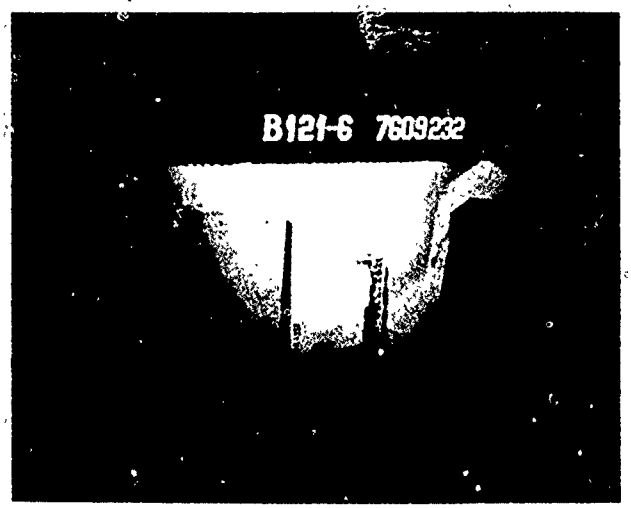

Figure 97

3/4 Inch Aluminum Honeycomb Test Panel, Outer Surface,
4 x 7 x 0.25 In. Fragment, 427 FPS Impact Velocity

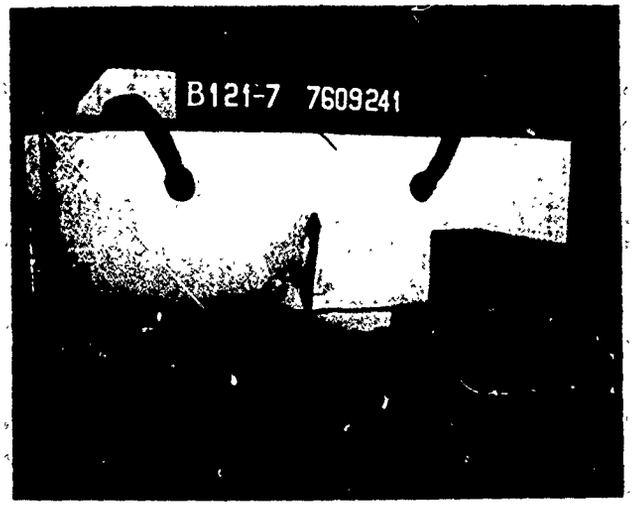

Figure 98

3/4 Inch Aluminum Honeycomb Test Panel, Inner Surface,
4 x 7 x 0.25 In. Fragment, 751 FPS Impact Velocity

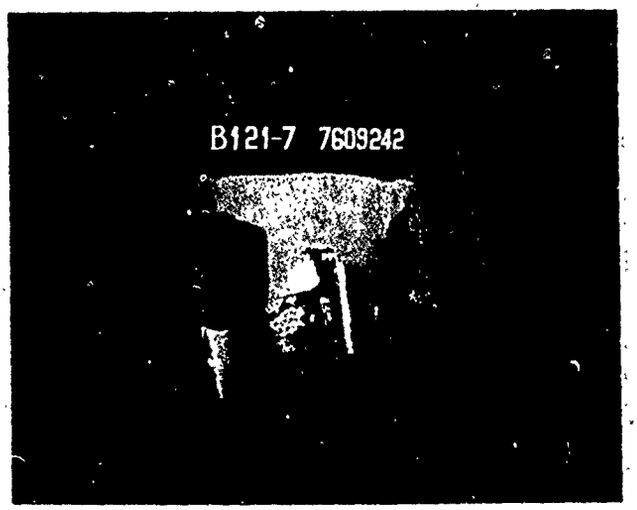

Figure 99

3/4 Inch Aluminum Honeycomb Test Panel, Outer Surface,
4 x 7 x 0.25 In. Fragment, 751 FPS Impact Velocity

Figure 100

3/4 Inch Aluminum Honeycomb Test Panel, Inner Surface,
4 x 7 x 0.25 In. Fragment, 367 FPS Impact Velocity

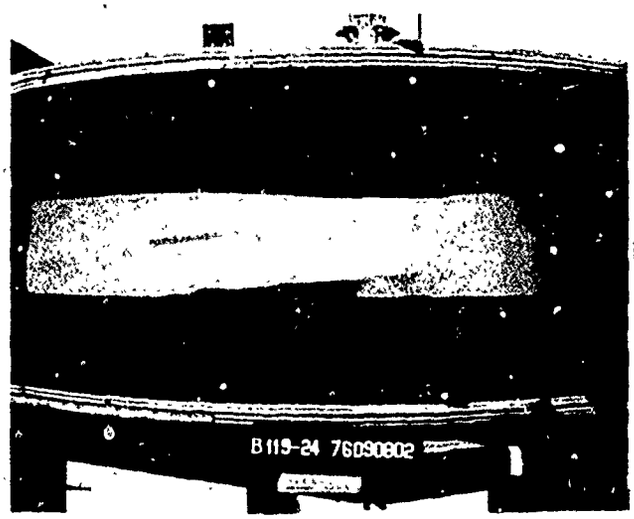

Figure 101

3/4 Inch Aluminum Honeycomb Test Panel, Outer Surface,
4 x 7 x 0.25 In. Fragment, 367 FPS Impact Velocity

6.5.6 Energy Absorption by Sheet Steel - The tests with homogenous sheet steel provided interesting results. The steel plate targets were bolted to a ridged picture frame which was well supported and clamped to the structure of the gun barrel. The test setup is shown on Figure 102. The data obtained from these tests were intended to verify the equation for energy absorption used in previous work.

$$E_A = \frac{LTt^2}{12\ COS^2\theta}$$

This equation accounts for the fragment surface perimeter which shears the target material and it also accounts for the angle of fragment impingement. This equation is defined as follows:

$$E_A = \frac{LTt^2}{12\ COS^2\theta} \quad \text{ft-lbs}$$

E_A = Energy Absorbed (ft-lbs)

L = Fragment frontal Peripheral Distance

W + t + W + t = 2(W + t) inches

T = Dynamic Shear Modulus for Steel (188,500 lb/in^2)

t = Sheet Thickness (inches) W = Width (inches)

θ = Is the angle between the fragment trajectory and the normal to the surface at the point of impingement.

Table 35 provides the data obtained for the 3 x 5 x 0.25 inch titanium fragment fired into various thickness sheet stainless steel. The 40 foot long 5-inch bore gun was used and all the target material used was 321 stainless in the soft or annealed condition. Different impact velocities were used depending on the target thickness. The target was oriented at 30° to the fragment trajectory (60° to the target normal line). This was done so reasonably large absorption levels could be expected and the effect of impact angle explored. The initial velocities were selected to be sure a penetration occurred. Figure 103 shows a plot of energy absorbed vs target

thickness while Figure 104 shows a plot of energy absorbed vs target thickness, squared. Thickness squared was used for convenience since the calculated absorption from the previously discussed equation plots as a straight line. Test damage photos are shown in Figures 105 through 112.

The test points for velocities below 800 FPS correlate well with the calculated curve on Figure 103 except for test point B-121-13. This test showed a higher than predicted level of energy absorption which was attributed to deflection of the target material due to inadequate support, see Figures 104 and 105. Verification of this judgement was obtained by rerunning the test as run B-121-14 with the target material bolted to back-up structure along both top and bottom edges, see photos Figures 107 and 108. All subsequent tests in this series were conducted with this type of backup support. The three points at velocities above 800 ft/sec showed energy absorption levels considerably lower than the plotted line.

To explore the difference between the low and high velocity shots, the two shots into the .087-.088 inch thick material were reviewed. The shot which agreed with the analytical curve was shot at 591 ft/sec and developed an impact energy level of 3081 ft-lbs. The picture of the target damage, Figures 114 and 115, (B-121-17) shows that the fragment was at the ballistic limit of the material and did not penetrate. Also the fragment was deflected from its trajectory during impact, and by hitting the target in a more flat-wise direction a considerable amount of material was destroyed and torn.

The other shot into this thickness of material had an impact velocity of 1006 ft/sec and developed an impact energy level of 8973 ft-lbs or almost three times the energy of the previous shot. Figure 111, (B-121-16) shows a relatively clean punched hole. The hole is not vertical which indicates the fragment turned after leaving the sabot stripper and entered the target, corner first. Also the target material was deeply deformed and dented by the impact prior to the hole being punched. It is believed that the relationship of the target surface angle and the fragment at the instant of pene-

tration was changed to a more normal angle. As shown on Figure 104 the curve of the absorption equation with the data points plotted, for data point B-121-16 the fragment trajectory and target surface angle would have only had to change 7.5 degrees toward normal to reduce the energy absorbed to the level shown. The corner first entry was also indicated by Figure 113 which shows that the fragment was deflected upward and hit high on the backstop clipping the upper support of the second fence. The corner entry into the target was probably the more significant cause for the reduced level of energy absorption.

Test photos, Figures 116 through 119 for test SB-121-21 and S/B-212-22 show the same fragment tilting on corner entry as previously discussed and also showed lower energy absorption characteristics.

The tendency for the fragment to turn in its trajectory path for these higher velocity shots is probably related to the test setup in that the sabot stopper/stripper at high sabot impact velocities caused the fragment to turn and achieve a corner first entry into the target material.

The four points which did correlate with the curve show that the curve was valid for design purposes. Also it appears that the energy absorption equation may be slightly conservative for actual blade fragment encounters. This belief is based on the fact that all the tests conducted were done with titanium fragments which were ground to size which meant that the fragments had extremely sharp knife-like edges on corners. Blade fragments recovered from actual incidents in most cases have dull edges and broken-off corners from being batted around the engine containment ring and probably have a lower penetration capability than the perfectly square edges and corners on the test fragments used. Figure 120 shows some typical fragments from an actual incident. It is interesting to note that during all of the testing there was little edge dulling and no corner damage on the test fragments used. The only damage noted was a small amount of bending of the fragment plate when it hit the backstop after penetrating the target.

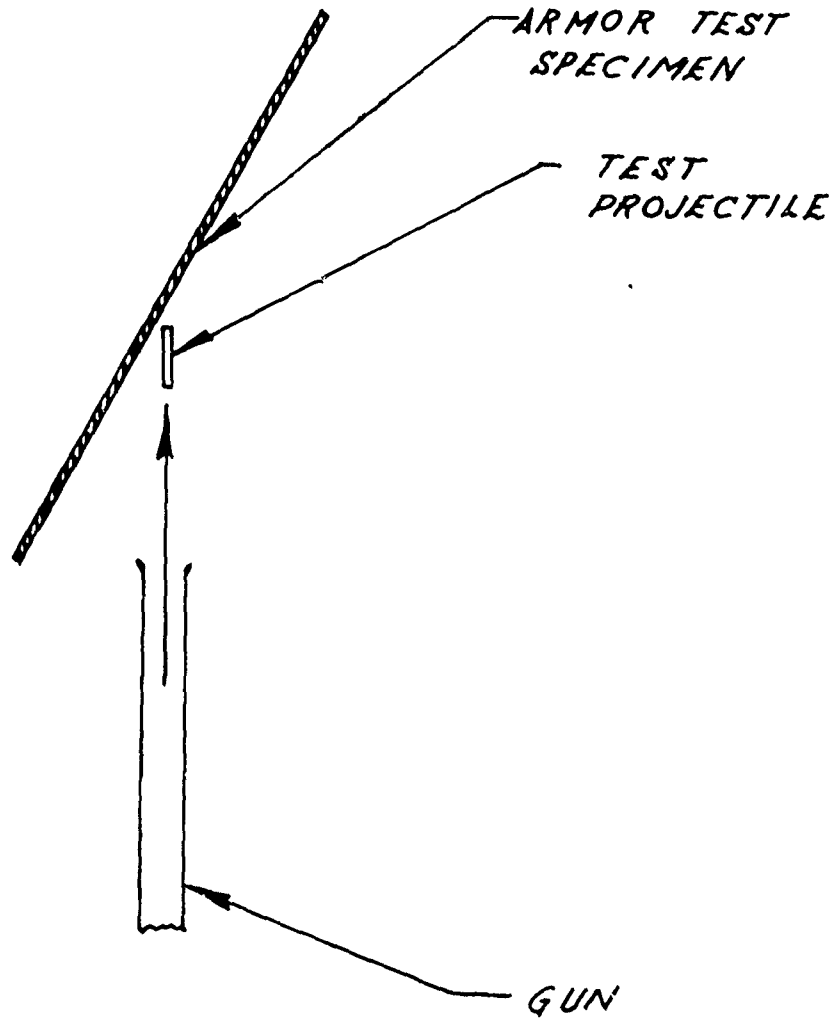

FIGURE 102
FLAT PANEL
TEST SETUP

TABLE 35 TEST RESULTS
TARGET - VARIOUS THICKNESSES OF SHEET STAINLESS STEEL SUPPORTED IN A STEEL FRAME
FRAGMENT 3 x 5 x 0.25 INCH TITANIUM FLAT PLATE
FRAGMENT IMPINGEMENT 60° FROM NORMAL

DATE 1976	RUN NO.	TEST SPONSOR		FRAGMENT WEIGHT		VELOCITY FT/SEC		ENERGY FT-LBS		ENERGY ABSORBED FT-LB	PERCENT ENERGY ABSORBED	TARGET THICKNESS INCHES	REMARKS
		FAA	DOUGLAS	GRAMS	POUNDS	INITIAL	FINAL	INITIAL	FINAL				
10-8	B-121-13	X		253.5	.5589	443	274	1703	651	1052	62	0.033	Target Frame Not Solidly Supported
10-11	B-121-14	X		250.7	.5576	471	335	1904	963	941	49	0.038	Penetrated
10-12	B-121-15	X		253.5	.5589	780	651	5280	3678	1602	30.3	0.062	Penetrated
10-14	B-121-16	X		259.4	.5718	1006	876	8973	6805	2168	24.1	0.088	Penetrated
10-20	B-121-17	X		257.7	.568	591	0	3081	0	3081	100	0.087	Contained
11-11	B-121-21	X		250.8	.5529	990	818	8415	5745	2670	31.7	0.127	Penetrated
11-12	B-121-22	X		248.7	.5482	826	520	5808	2301	3507	60.4	0.127	Penetrated

Target Material: Noted thickness 321 stainless steel in the annealed condition

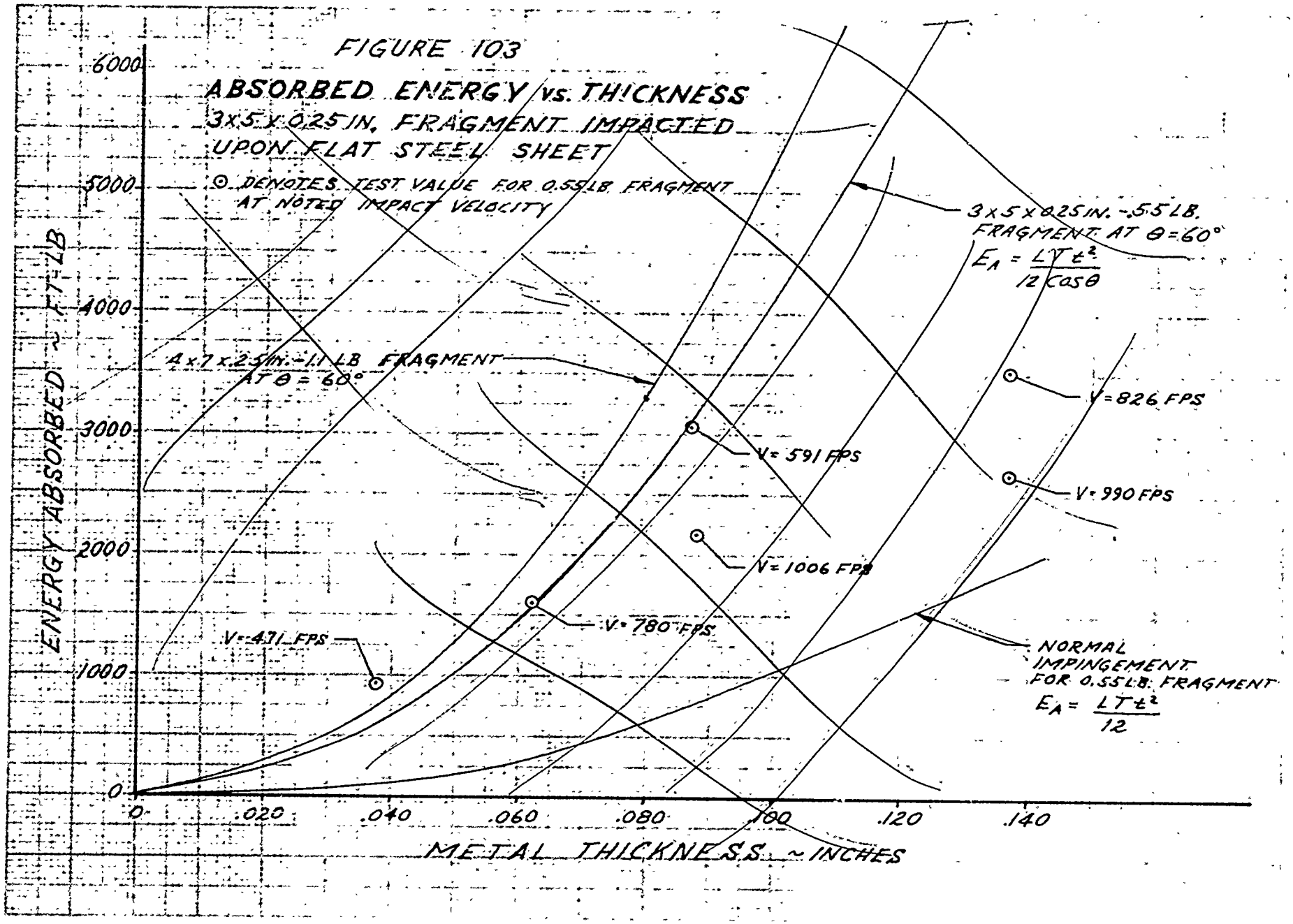
FIGURE 103
ABSORBED ENERGY vs. THICKNESS
3 x 5 x 0.25 IN. FRAGMENT IMPACTED UPON FLAT STEEL SHEET
⊙ DENOTES TEST VALUE FOR 0.55 LB FRAGMENT AT NOTED IMPACT VELOCITY
3 x 5 x 0.25 IN. - .55 LB. FRAGMENT AT θ = 60°
$E_A = \frac{LTt^2}{12 \cos\theta}$
4 x 7 x 2.5 IN. - 1.1 LB FRAGMENT AT θ = 60°
V = 826 FPS
V = 591 FPS
V = 990 FPS
V = 1006 FPS
V = 780 FPS
V = 471 FPS
NORMAL IMPINGEMENT FOR 0.55 LB. FRAGMENT
$E_A = \frac{LTt^2}{12}$
ENERGY ABSORBED - FT-LB
6000
5000
4000
3000
2000
1000
0
.020
.040
.060
.080
.100
.120
.140
METAL THICKNESS - INCHES

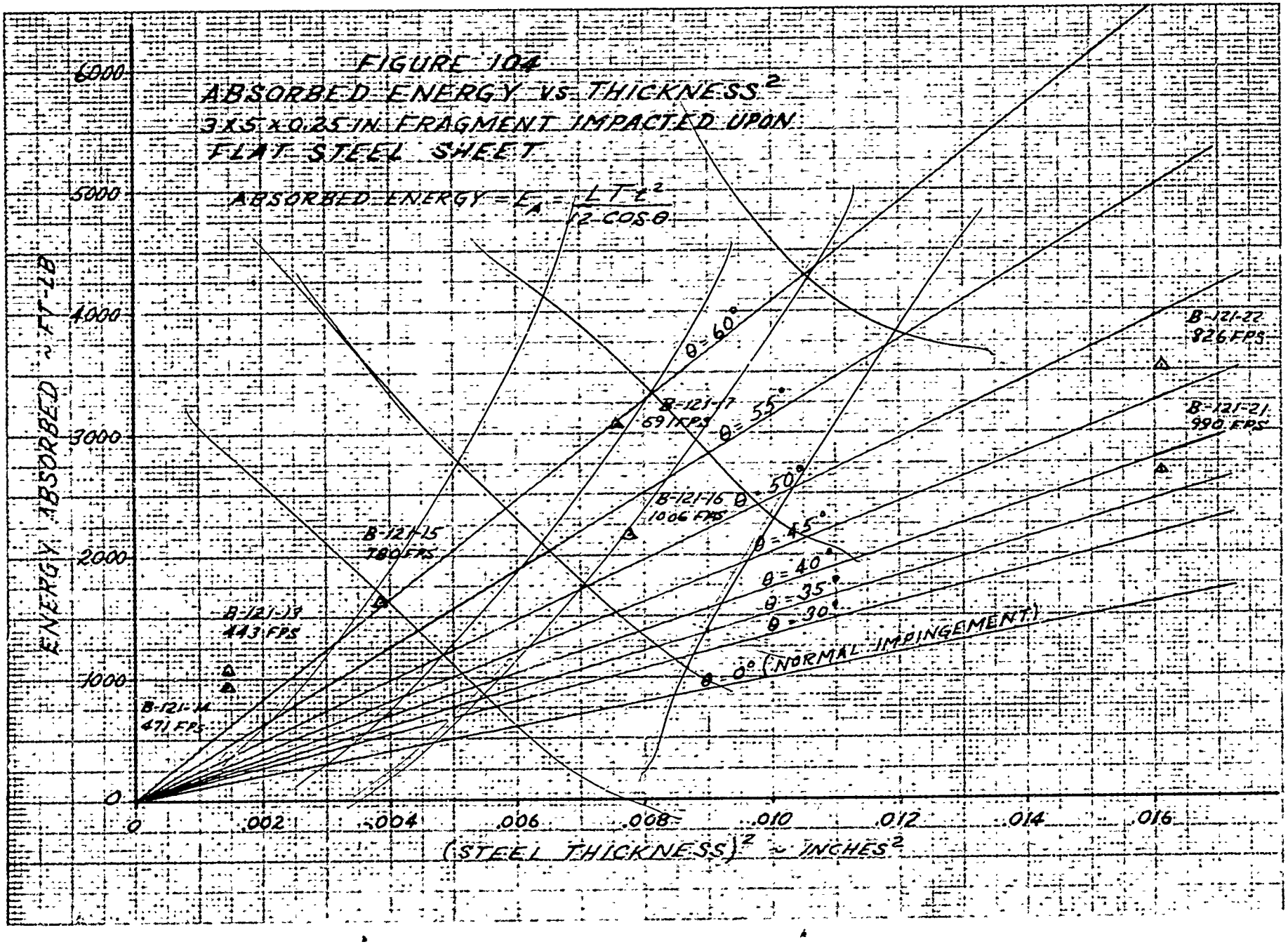
FIGURE 104
ABSORBED ENERGY VS THICKNESS²
3 X 5 X 0.25 IN. FRAGMENT IMPACTED UPON
FLAT STEEL SHEET
ABSORBED ENERGY = E_A = L T t² / 2 COS θ
ENERGY ABSORBED - FT-LB
6000
5000
4000
3000
2000
1000
0
0
.002
.004
.006
.008
.010
.012
.014
.016
(STEEL THICKNESS)² - INCHES²
θ = 60°
θ = 55°
θ = 50°
θ = 45°
θ = 40°
θ = 35°
θ = 30°
θ = 0° (NORMAL IMPINGEMENT)
B-121-22
926 FPS
B-121-21
990 FPS
B-121-7
691 FPS
B-121-16
1006 FPS
B-121-15
780 FPS
B-121-13
443 FPS
B-121-14
471 FPS

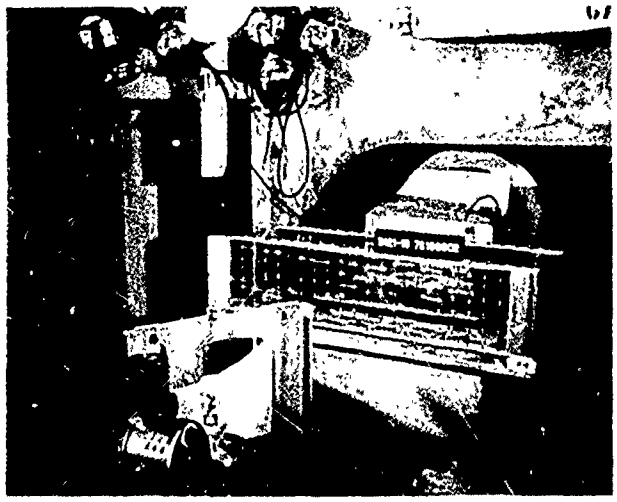

Figure 105

.033 In. Stainless Steel Sheet Test Setup, 3 x 5 x 0.25 In. Fragment at 443 FPS Impact Velocity

Figure 106

.033 In. Stainless Steel Sheet Test Panel, Back Surface, 3 x 5 x 0.25 In. Fragment, 443 FPS Impact Velocity

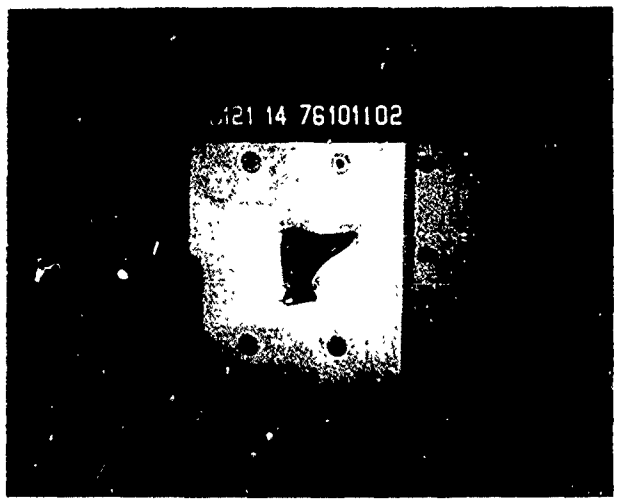

Figure 107

.038 In. Stainless Steel Test Panel, Front Surface,
3 x 5 x 0.25 In. Fragment, 471 FPS Impact Velocity

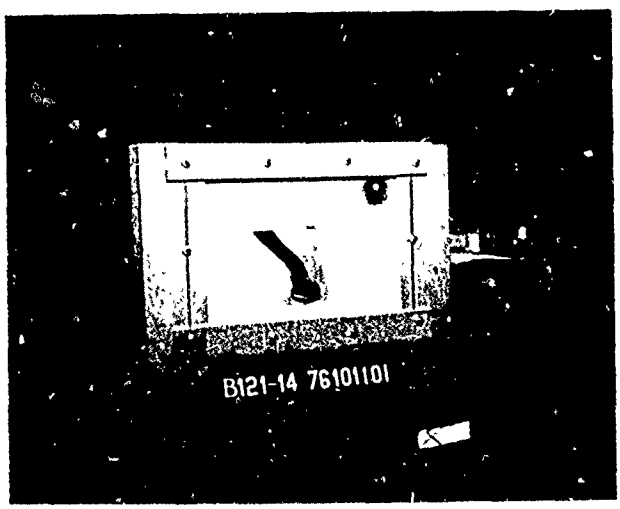

Figure 108

.038 In. Stainless Steel Test Panel, Back Surface,
3 x 5 x 0.25 In. Fragment,471 FPS Impact Velocity

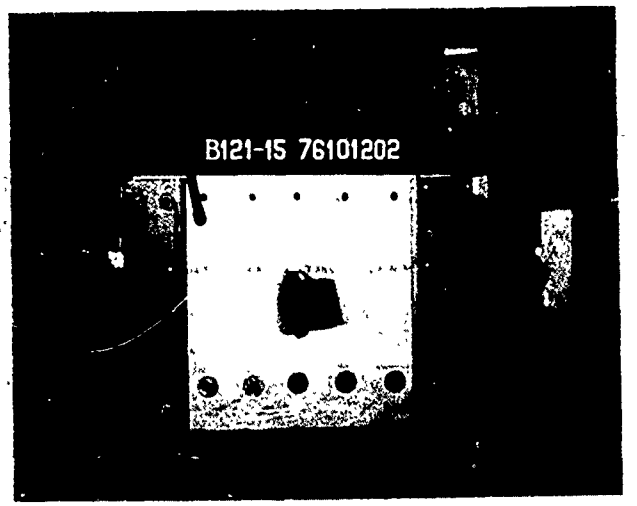

Figure 109

.062 In. Stainless Steel Test Panel, Front Surface,
3 x 5 x 0.25 In. Fragment, 780 FPS Impact Velocity

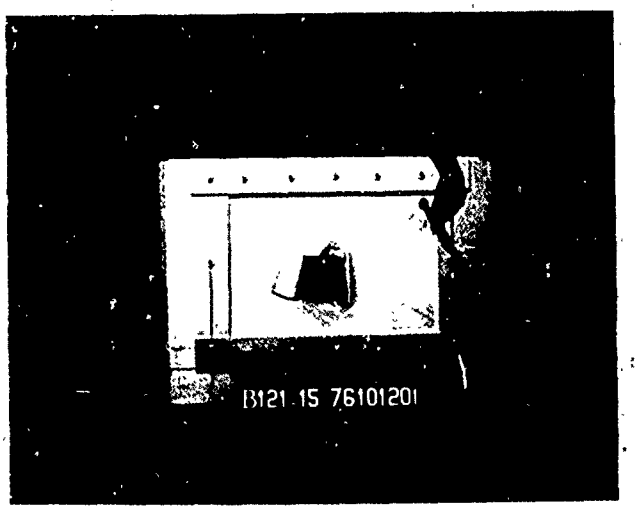

Figure 110

.062 In. Stainless Steel Test Panel, Back Surface,
3 x 5 x 0.25 In. Fragment, 780 FPS Impact Velocity

Figure 111

.088 In. Stainless Steel Test Panel, Front Surface,
3 x 5 x 0.25 In. Fragment, 1006 FPS Impact Velocity

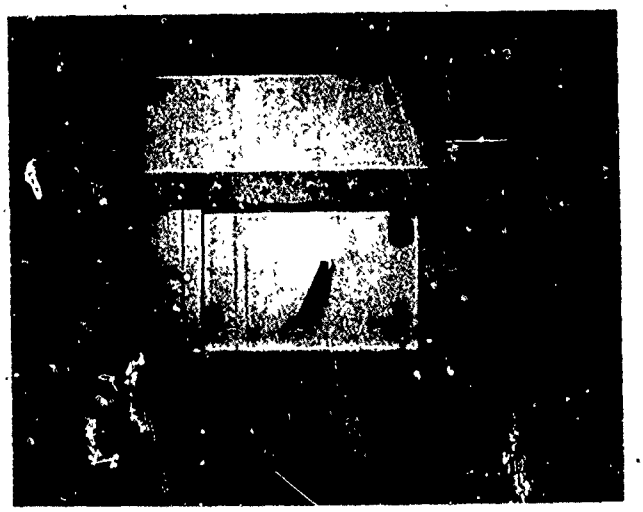

Figure 112

.088 In. Stainless Steel Test Panel, Back Surface,
3 x 5 x 0.25 In. Fragment, 1006 FPS Impact Velocity

Figure 113

Back Stop Fence After B-121-16 Test Shot

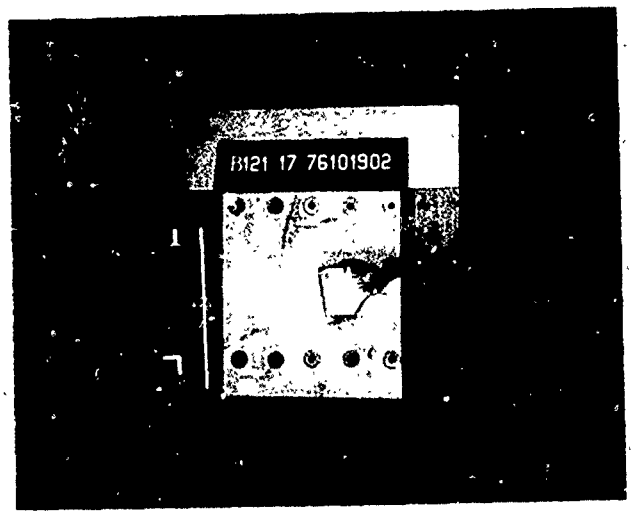

Figure 114

.081 In. Shainless Steel Test Panel, Front Surface,
3 x 5 x 0.25 In. Fragment, 591 FPS Impact Velocity

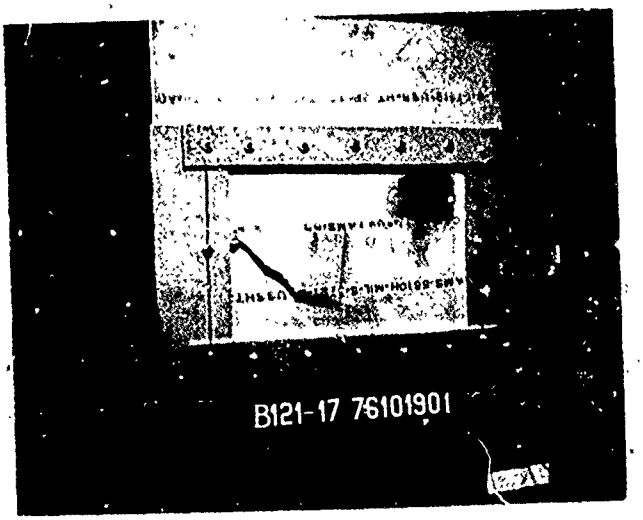

Figure 115

.081 In. Stainless Steel Test Panel, Back Surface,
3 x 5 x 0.25 In. Fragment, 591 FPS Impact Velocity

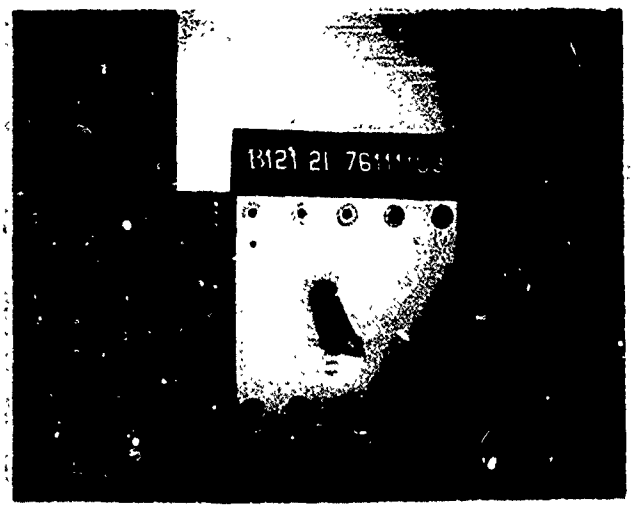

Figure 116

0.127 In. Stainless Steel Test Panel, Front Surface,
3 x 5 x 0.25 In. Fragment, 990 FPS Impact Velocity

Figure 117

0.127 In. Stainless Steel Test Panel, Back Surface,
3 x 5 x 0.25 In. Fragment, 990 FPS Impact Velocity

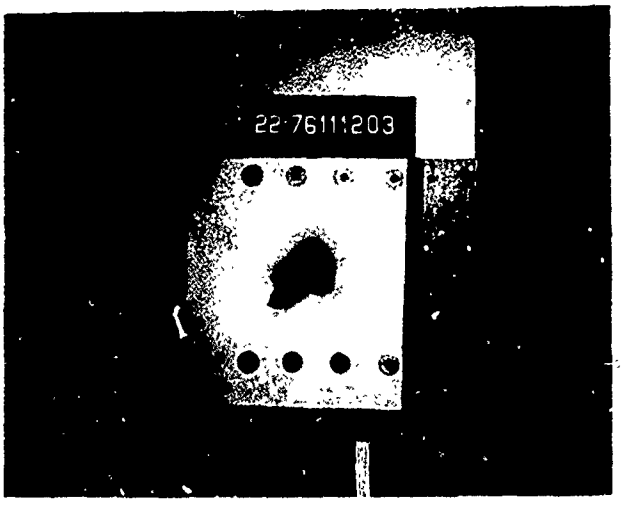

Figure 118

0.127 In. Stainless Steel Test Panel, Front Surface,
3 x 5 x 0.25 In. Fragment, 826 FPS Impact Velocity

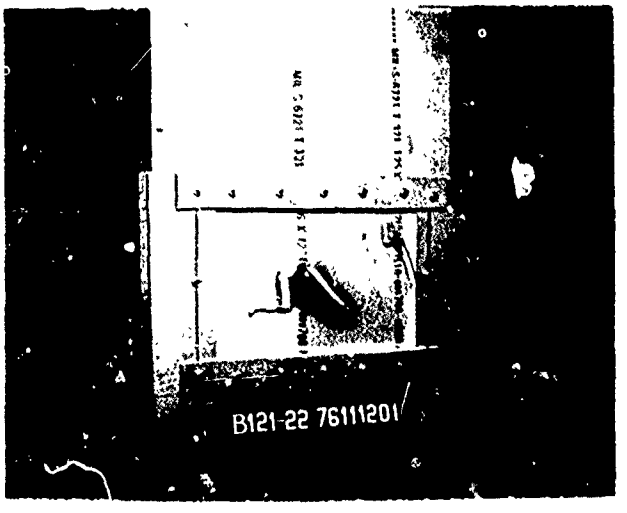

Figure 119

0.127 In. Stainless Steel Test Panel, Back Surface,
3 x 5 x 0.25 In. Fragment, 826 FPS Impact Velocity

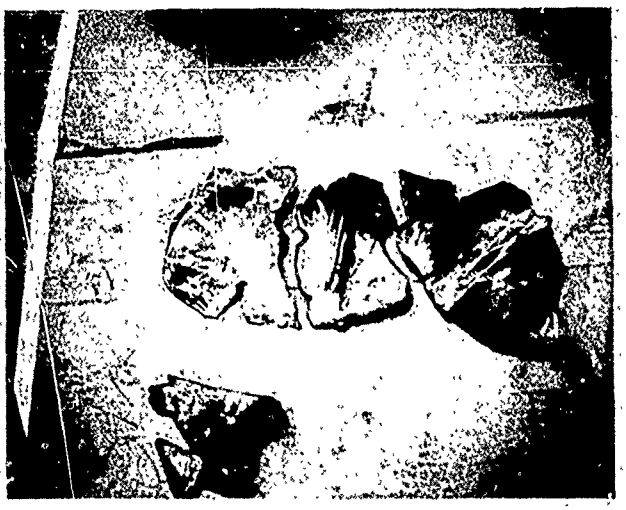

Figure 120

Typical Fan Blade Fragments from In-Service Fan Blade Failure

6.5.7 Effects of Fragment Size on Solid Sheet Stainless Steel Energy Absorption - These tests were conducted to establish the effect of fragment peripheral dimensions at the impact surface on energy absorption. A 4 x 7 x 0.25 inch titanium fragment was impacted against a 0.127 inch thick annealed sheet of 321 stainless steel. This fragment had a peripheral impact dimension of 8.5 inches as compared to the small fragment which had a peripheral impact dimension of 6.5 inches. This results in a 31% increase in periphery. The fragment mass was doubled to generate equivalent energy levels.

The same frame support and 60° from normal target impingement angle were used as discussed previously for the 3 x 5 x 0.25 inch fragment.

The tests results are shown on Table 36. Figures 121 through 126 show the impact damage. Because the fragment force was distributed over a larger periphery or area, the target material had sufficient strength to prevent penetration. The highest level of energy absorbed was 9505 ft-lbs exceeding the level which would be predicted by the energy absorption equation which predicted an energy level for penetration of 8614 ft-lbs or about 900 ft-lb error. For this type of experiment, having an error of less than 10% is considered very good and confirms the validity of the energy absorption equation. For all of the shots in this series the fragments hit the target fairly squared and did not have any tendency to deflect from the trajectory after hitting the sabot stopper/splitter. This may again be because of the lower impact velocity of the sabot stopper/splitter used for these tests.

TABLE 36 -TEST RESULTS
TARGET - 0.127 THICK SHEET STAINLESS STEEL SUPPORTED IN A STEEL FRAME
FRAGMENT - 4 x 7 x 0.25 INCH TITANIUM FLAT PLATE
FRAGMENT IMPINGEMENT 60° FROM NORMAL

DATE 1976	RUN NO.	TEST SPONSOR		FRAGMENT WEIGHT		VELOCITY FT/SEC		ENERGY FT-LBS		ENERGY ABSORBED FT-LBS	PERCENT ENERGY ABSORBED	TARGET THICKNESS INCHES	REMARKS
		FAA	DOUGLAS	GRAMS	POUNDS	INITIAL	FINAL	INITIAL	FINAL				
11-15	B-211-23	X		497.0	1.0957	525	0	4689	0	4689	100%	0.127	Contained
11-16	B-121-24	X		498.0	1.0979	614	0	6427	0	6423	100%	0.127	Contained
11-17	B-121-25	X		499.0	1.100	746	0	9505	0	9505	100%	0.127	Contained

Target Material - 0.127 inch thick 321 stainless steel in the annealed condition.

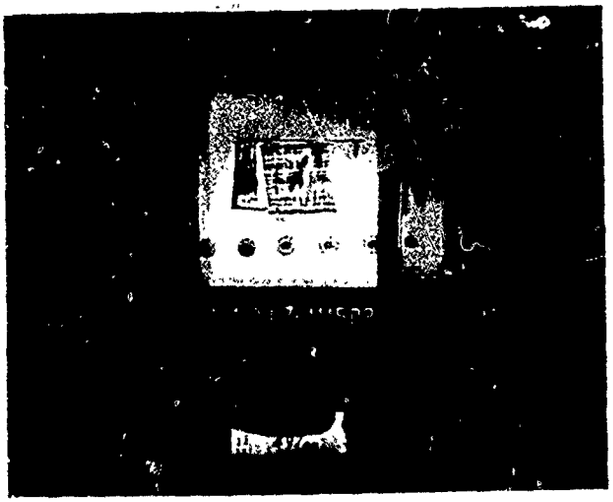

Figure 121

0.127 In. Stainless Steel Test Panel, Front Surface,
4 x 7 x 0.25 In. Fragment, 525 FPS Impact Velocity

Figure 122

0.127 In. Stainless Steel Test Panel, Rack Surface,
4 x 7 x 0.25 In. Fragment, 525 FPS Impact Velocity

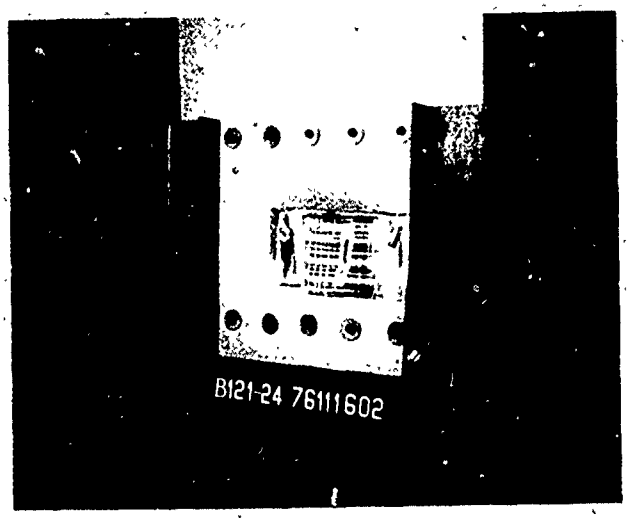

Figure 123
0.127 In. Stainless Steel Test Panel, Front Surface,
4 x 7 x 0.25 In. Fragment, 614 FPS Impact Velocity

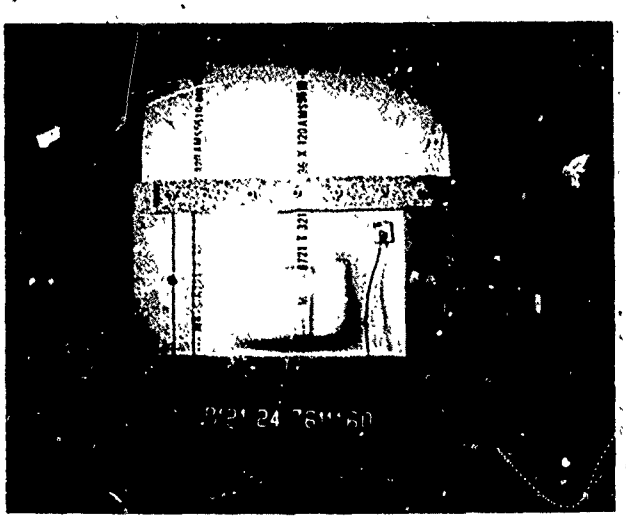

Figure 124
0.127 In. Stainless Steel Test Panel, Rack Surface,
4 x 7 x 0.25 In. Fragment, 614 FPS Impact Velocity

Figure 125
0.127 In. Stainless Steel Test Panel, Front Surface,
4 x 7 x 0.25 In. Fragment, 746 FPS Impact Velocity

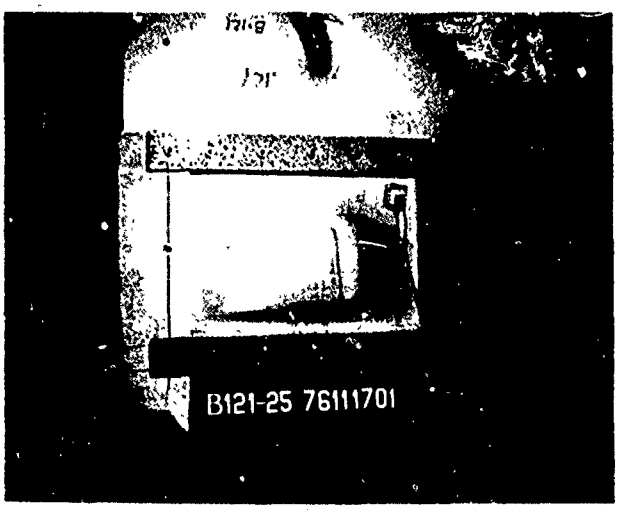

Figure 126
0.127 In. Stainless Steel Test Panel, Back Surface,
4 x 7 x 0.25 In. Fragment, 746 FPS Impact Velocity

6.5.8 Effect of Multiple Layers - This test was conducted to determine if two steel sheets stacked together absorbed the same amount of energy as an equivalent thickness single steel sheet. The test data presented in Table 37 was obtained by firing a 3 x 5 x 0.25 inch thick titanium fragment into two sheets of annealed 321 stainless steel material. A .048 and a .040 sheet bolted into the same frame used for previous sheet metal testing and the frame was set so that the impingement angle was 60° from the target surface normal line. The fragment impinged on the 0.48 inch thick sheet first. The large gun was used for this test.

The results showed that 1218 ft-lbs of energy was absorbed, which would be equivalent to $(t)^2 = .003$ or an equivalent thickness of .055 inch. This indicates that the .048 sheet absorbed most of the energy and the .040 backup sheet assisted very little.

Examination of the photographs, Figure 127 and 128 shows that the back sheet peeled away and probably offered little resistance to the fragment penetration. The equation used for equivalent thickness is

$$t_e = \sqrt{t_1^2 + t_2^2}$$

and for this case is $t_e = \sqrt{(048)^2 + (.040)^2} = \sqrt{.023 + .0016}$

$t_e = \sqrt{.0039} = .063$ compared to the correlation curve value of a t_e of .055. This appears to be reasonable agreement for this type of experiment.

TABLE 37 TEST RESULTS

TARGET - TWO LAYERS OF SHEET STAINLESS STEEL 0.048 INCH THICK ON IMPACT SIDE AND BACKED UP WITH AN 0.040 SHEET. BOTH SHEETS SUPPORTED BY A STEEL FRAME

FRAGMENT - 3 x 5 x 0.25 INCH TITANIUM FLAT PLATE

FRAGMENT IMPINGEMENT 60° FROM NORMAL

DATE 1976	RUN NO.	TEST SPONSOR		FRAGMENT WEIGHT		VELOCITY FT/SEC		ENERGY FT-LBS		ENERGY ABSORBED FT-LBS	PERCENT ENERGY ABSORBED	TARGET THICKNESS INCHES	REMARKS
		FAA	DOUGLAS	GRAMS	POUNDS	INITIAL	FINAL	INITIAL	FINAL				
11-10	B-121-20	X		259.4	.5718	749	651	4981	3763	1218	24.5	.048/ .040	Equivalent to About 0.050

Target Material: Double Layer 0.048 inch and 0.040 inch thick 321 stainless steel in the annealed condition.

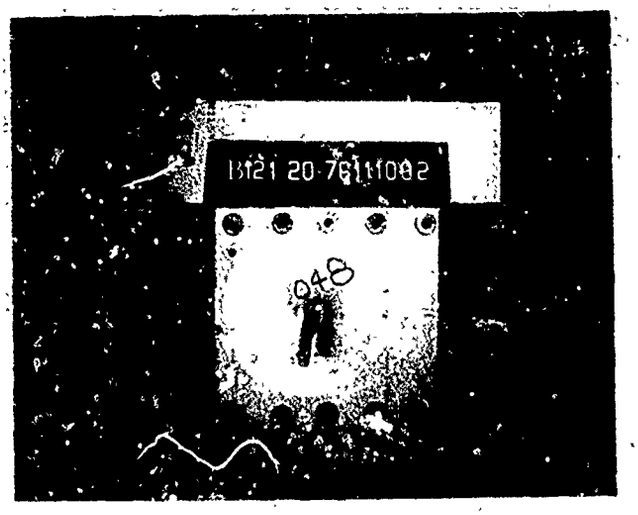

Figure 127
Laminated Stainless Steel Test Panel, .048 In. Face Sheet with .040 Backup Sheet, Front Surface, 3 x 5 x .025 In. Fragment, 749 FPS Impact Velocity

Figure 128
Laminated Stainless Steel Test Panel, .048 In. Face Sheet with Backup Sheet, Back Surface, 3 x 5 x 0.25 In. Fragment, 749 FPS Impact Velocity

6.5.9 Effects of Fragment Rotation - In actual blade failures fragment rotation exists with rotation about its center of gravity. This was simulated during impact by mounting the fragment 30° to its trajectory and striking the target tangentially. The sliding reaction of the fragment on the target creates a force on the fragment leading edge forward of its center of gravity. This reacts around the center of gravity causing the fragment to rotate or tumble. The test setup to simulate this type of condition is shown on Figure 129. Figures 131 through 134 show the fragment mounted in that sabot and the resulting target damage. The test results are given in Table 38.

The test results for test B-121-18, Table 38 show that considerable energy was absorbed by the 0.050 inch thick steel sheet target. This is borne out by the damage shown in the pictures. Approximately 2800 ft-lbs of energy or 58% of the initial energy was absorbed because of the rotation or tumbling action of the fragment. On a similar shot into a 0.63 thick steel plate which was positioned 30° to an unskewed fragment trajectory only 30% of the total energy was absorbed.

Test B-121-19, Table 38 was intended to provide an additional data point for .063 inch thick steel target material. During the sabot stripping action, the fragment was turned about its trajectory axis so it hit the target in an attitude of about 90° from the intended position. This resulted in a corner sliding into the target. Some tumbling did result but only 21 to 22% of the initial energy was absorbed, Figures 133 and 134 show the damage.

Test B-121-18 provides adequate evidence of the effect of fragment rotation or tumbling so no effort was made to repeat test B-121-19.

The fact that in many of the actual blade failure encounters fragments have rotation is probably beneficial. The tumbling action results in more nacelle structural damage but more energy is absorbed and in the end results in a much lower fragment exit velocity. Usually in armor design the fragment rotation is not considered which makes the design applicable to the most severe cases.

TABLE 38 TEST RESULTS

TARGET - TWO SHOTS ONE AT .050 INCH THICK CURVED SHEET STAINLESS STEEL; THE OTHER AT .063 INCH THICK CURVED SHEET STAINLESS STEEL

FRAGMENT - 3 x 5 x .25 INCH TITANIUM FLAT PLATE

FRAGMENT IMPINGEMENT TANGENTIAL TO TARGET WITH FRAGMENT SKEWED 30°

DATE 1976	RUN NO.	TEST SPONSOR		FRAGMENT WEIGHT		VELOCITY FT/SEC		ENERGY FT-LBS		ENERGY ABSORBED FT-LBS	PERCENT ENERGY ABSORBED	TARGET THICKNESS INCHES	REMARKS
		FAA	DOUGLAS	GRAMS	POUNDS	INITIAL	FINAL	INITIAL	FINAL				
11-2	B-121-18	X		255.7	.5637	755	491	4989	2110	2879	57.7	0.050	Absorbed 28% More Energy Than Equivalent Tangential Shot
11-9	B-121-19	X		250.7	.5527	760	672	4957	3876	1081	21.8	0.063	Fragment Turned and Entered Target Corner First

Target Material: Noted thickness 321 stainless steel in the annealed condition.

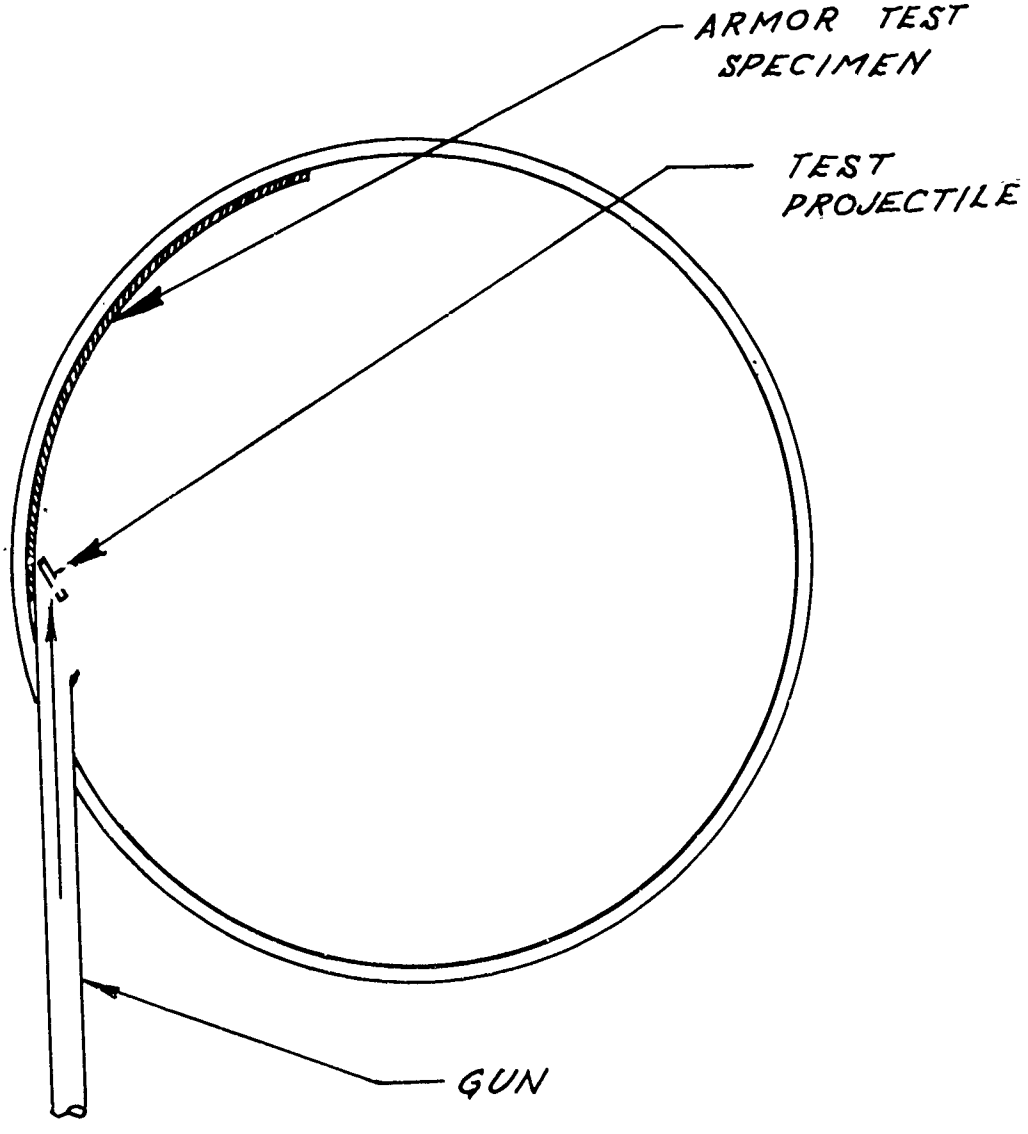

FIGURE 129
SKEWED SHOT
TEST SETUP

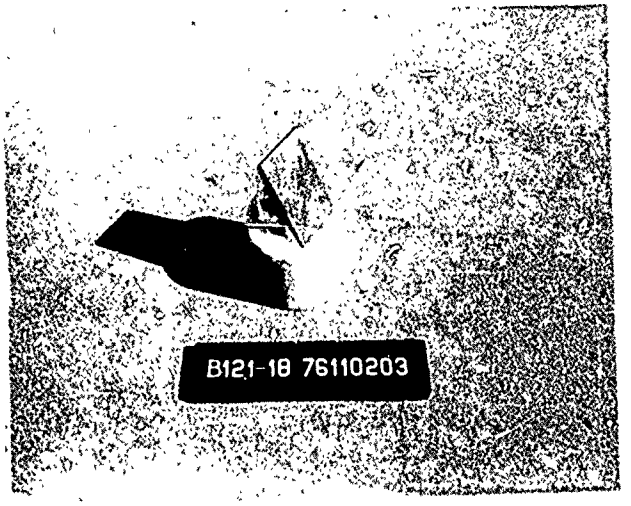

Figure 130

Fragment for Skewed Shot Mounted Onto Sabot

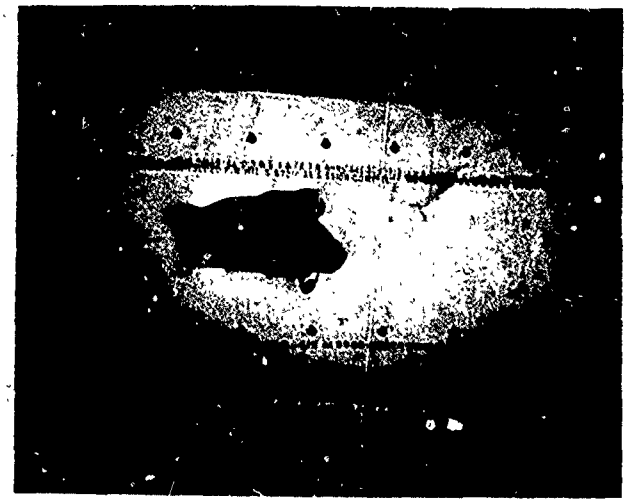

Figure 131

.050 In. Stainless Steel Test Panel, Inner Surface,
3 x 5 x 0.25 In. Fragment, 755 FPS Impact Velocity

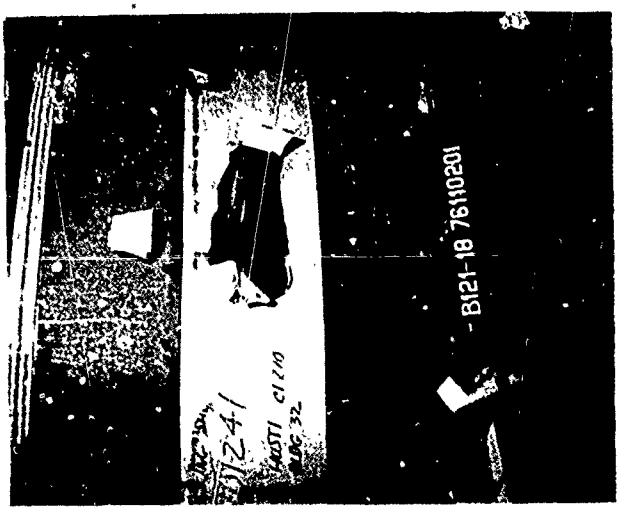

Figure 132

.050 In. Stainless Steel Test Panel, Outer Surface,
3 x 5 x 0.25 In. Fragment, 755 FPS Impact Velocity

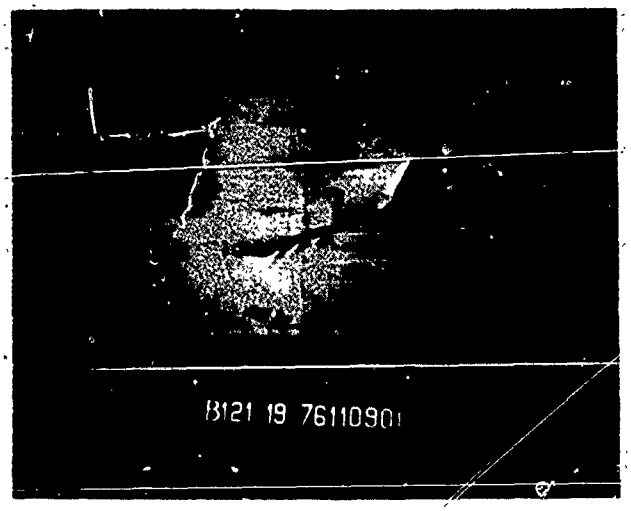

Figure 133.

.063 In. Stainless Steel Test Panel, Inner Surface,
3 x 5 x 0.25 In. Fragment, 760 FPS Impact Velocity

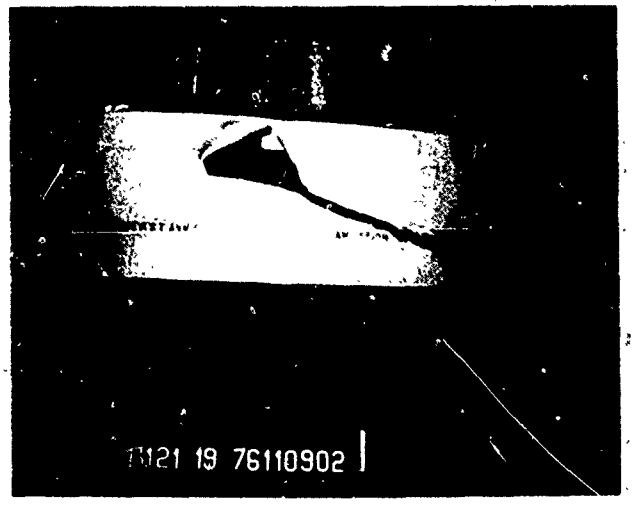

Figure 134.

.063 In. Stainless Steel Test Panel, Outer Surface,
3 x 5 x 0.25 In. Fragment, 760 FPS Impact Velocity

6.5.10 Kevlar Armor System

One of the difficulties with any armor installation is the mounting and restraint of the armor. The mounting must have sufficient integrity to withstand large impact loads with adequate load distribution into fixed structure. Where there are no direct paths to distribute armor impact loads or the basic structure is comparatively light, the added weight required to provide the necessary armor retention strength may be substantial.

Kevlar is a tough resilient aramid fiber material with a high tensile strength that can be used for lightweight containment systems for specific applications. Along with providing a lightweight installation for containment on inlet ducts, a wide Kevlar strap around the entire duct provides a means of arresting fragment energy while distributing the load over a large area around the inlet inner barrel without the use of a multitude of fasteners or the addition of heavy structure. Several layers of the cloth can be formed into pads to resist fragment cutting and tend to envelope and turn the fragment so that the loads are distributed into the arresting strap over a relatively wide area. The system depends on the fragment being turned from its trajectory and the strap stretching in the process of bringing the fragment to a stop. In order to establish the weight for such a system, development tests were conducted.

Based on discussions with the material supplier, Dupont, and others experienced in its use including the Aerospace Corporation, the application of this system has been determined to be basically restricted to an installation where the Kevlar can be installed so it has sufficient room to stretch. This means it must be wrapped around a structure as opposed to being put into a structure where there is a rigid back up. If the material were backed up by a honeycomb structure, for example, there would be little stretch developed and the fragment would cut through the cloth plies and penetrate. On the other hand, if it were installed on the outside of the honeycomb, the Kevlar would stretch and perform an arresting function. It could also be installed a sufficient distance from the item to be protected so the required stretch would take place short of the object.

Kevlar cloth must be treated with some type of sealant to prevent it from absorbing fluid moisture. Also a coating of the proper material will help prevent the tough fibrous Kevlar threads from chaffing the surface of the airplane structure on which it is mounted. In the Douglas tests, the Kevlar material was coated and cured with a type of silicone rubber. The method of cure, the cure temperature, and the type of coating is important as early attempts in the coating development at Douglas showed a marked reduction in the material tensile properties after curing. The selection of the proper thread size and weave also affects the containment capability.

The test data presented in Table 39 are the final Douglas funded results after development of a superior Kevlar system had been completed through evaluation of many Kevlar material configurations. The results show that the 4x7x0.25 inch fragment at a weight of 1.1 lbs. was well contained at an impact velocity of about 900 ft/sec. The data shows containment for a fragment oriented so the impact surface (the 4-inch dimension) was parallel to the target surface and one which was 90° to the surface. The target material for these two tests was a curved panel of 3/4 inch thick steel stresskin honeycomb. The test target specimen and Kevlar pads and belt were installed as shown in Figure 135. Photos of damage to these test specimens are shown in Figures 136 through 145.

The test data presented in Table 40 are the result of four shots with the 4x7x0.25 inch fragment into a curved 2-inch thick bonded aluminum honeycomb target. The first shot shows good containment with the fragment oriented 90° to the target surface. The second shots with the fragment oriented parallel to the target surface show that the system failed to contain. The indications are that with the slightly lower absorption capability of the aluminum honeycomb when compared to the previous stresskin shot, the initial velocity into the Kevlar was sufficient to cut through the cloth before the fragment could be turned.

By reviewing the previous successful shots with the stresskin it was found that considerable honeycomb core material had formed around the cutting edges of the fragment and effectively reduced the cutting capability. By reducing the cutting, the fragment was turned from its trajectory path and presented a large flat area to the Kevlar strap which adequately arrested

the fragment and dissipated the energy through tensile stretching. The aluminum honeycomb did not tend to wrap around the sharp cutting edges of the fragment and penetration resulted.

It was concluded that for aluminum honeycomb some sort of fragment blunting/deflecting and an additional amount of energy absorption would be required prior to the fragment entering the Kevlar system. If this was done then the same number of Kevlar layers of the previous test could be used.

A .050 inch thick sheet of stainless steel was installed between the first two layers of the Kevlar pad. The remaining pads and belt were kept the same as on the previous shot which had failed.

With the steel sheet combined with the Kevlar pads and belt, containment was accomplished. The punched out steel material from the .050 inch thick sheet wrapped around the fragment cutting edge (see Run B-119-22) and only eight layers of material were penetrated. The fragment was turned effectively and the strap provided the arresting function. The first layer of Kevlar provided very little energy absorption since it was between the steel plate and the honeycomb test specimens. It did however prevent the steel plate from chaffing the aluminum and helped keep the steel plate in place.

An additional test was accomplished to determine the effect of using a 17-7 steel sheet heat treated to 180,000 psi and installed between the first two layers of Kevlar in the same manner as the previous test. The test results showed the same containment capability, however, as may be seen on the photo for test B-119-23 the steel sheet cracked and had a smaller plug sheared out. The indications were that while the heat treated plate had ample energy absorbing capabilities to turn the fragment the punched out plug would not blunt the fragment as well as the soft sheet steel. In both cases a thinner steel sheet probably could have been used and the soft material would be favored. Photos of damage to these four test specimens are shown in Figures 146 through 165.

The conclusions reached from these and other Douglas tests were that: Kevlar does provide a good arresting system; some sort of fragment blunting

probably is required to prevent cutting through the pad and strap layers; coating the material is required to prevent fluid wicking; coating material and proper cure procedures are important to maintain tensile strength; coating the material is also needed to prevent chaffing of the structure the material is installed on; the material is only suitable for use where the ambient temperature is below 350°F.

TABLE 39- TEST RESULTS.

TARGET - 3/4 INCH THICK STEEL STRESSKIN CURVED PANEL BACKED WITH 6 2-PLY KEVLAR PADS (BONDED IN SILICONE RUBBER) AND A 6 PLY KEVLAR STRAP (EACH PLY COATED WITH SILICONE RUBBER)

FRAGMENT - 4 x 7 x 0.25 IN TITANIUM FLAT PLATE

TANGENTIAL IMPINGEMENT

	DATE 1976	RUN NO.	TEST SPONSOR		FRAGMENT WEIGHT		VELOCITY FT/SEC		ENERGY FT-LBS		ENERGY ABSORBED FT-LBS	PERCENT ENERGY ABSORBED	REMARKS
			FAA	DOUGLAS	GRAINS	POUNDS	INITIAL	FINAL	INITIAL	FINAL			
(1)	7-23	B-119-12		X	520.15	1.147	903	0	14523	0	14523	100%	Fragment Penetrated Stresskin and 2 Pad Layers. No Penetration of 16 Layers of Pad and Strap
(2)	8-19	B-119-18		X	519.0	1.144	903	0	14485	0	14485	100%	Fragment Penetrated Stresskin and All 18 Layers With a Corner but was Contained

(1) Fragment vertical target vertical

(2) Fragment horizontal target vertical

Target Material - Impingement Side - 0.016 inch thick 316L stainless steel perforated with 0.094 inch diameter holes 13% open area 60% hole pattern

Exit Side - 0.012 inch thick 316L stainless steel solid sheet

Core - 0.0035 inch thick ribbon 0.720 inch height 316L stainless steel 3/8 inch diamond pattern

Overall Panel Thickness - 0.748 inch

Panel Density - 180 lb/ft^2

TABLE 40 TEST RESULTS

TARGET - 2 INCH THICK ALUMINUM HONEYCOMB CURVED PANEL BACKED WITH 6 2-PLY KEVLAR PADS (BONDED IN SILICONE RUBBER) AND A 6 PLY KEVLAR STRAP EACH PLY COATED WITH SILICONE RUBBER

FRAGMENT - 4 x 7 x .025 INCH TITANIUM FLAT PLATE

TANGENTIAL IMPINGEMENT

	DATE 1976	RUN NO.	TEST SPONSOR		FRAGMENT WEIGHT		VELOCITY FT/SEC		ENERGY FT-LBS		ENERGY ABSORBED FT-LBS	PERCENT ENERGY ABSORBED	REMARKS
			FAA	DOUGLAS	GRAMS	POUNDS	INITIAL	FINAL	INITIAL	FINAL			
(1)	8-13	B-119-17		X	519.41	1.1450	898	0	14337	0	14337	100%	Fragment Corner Penetrated 16 Layers but was Contained
(2)	8-19	B-119-19		X	518.9	1.1439	895	591	14228	6204	8024	56.4%	Fragment Penetrated all Layers and was Liberated
(3)	8-25	B-119-22		X	517.5	1.1409	905	0	14510	0	14510	100%	Fragment Penetrated .050 Steel Sheet and 8 Kevlar Layers
(4)	8-31	B-119-23		X	517.5	1.1409	903	0	14446	0	14446	100%	Fragments Penetrated .050 Steel Sheet and 8 Kevlar Layers

(1) Fragment horizontal target vertical

(2) Fragment vertical target vertical

(3) Fragment vertical target vertical. .050 thick 321 stainless steel annealed sheet inserted.

(4) Same as (3) except steel sheet was 17-7 stainless steel heat treated to 180,000 PSI

Target Material: Same as Table 28

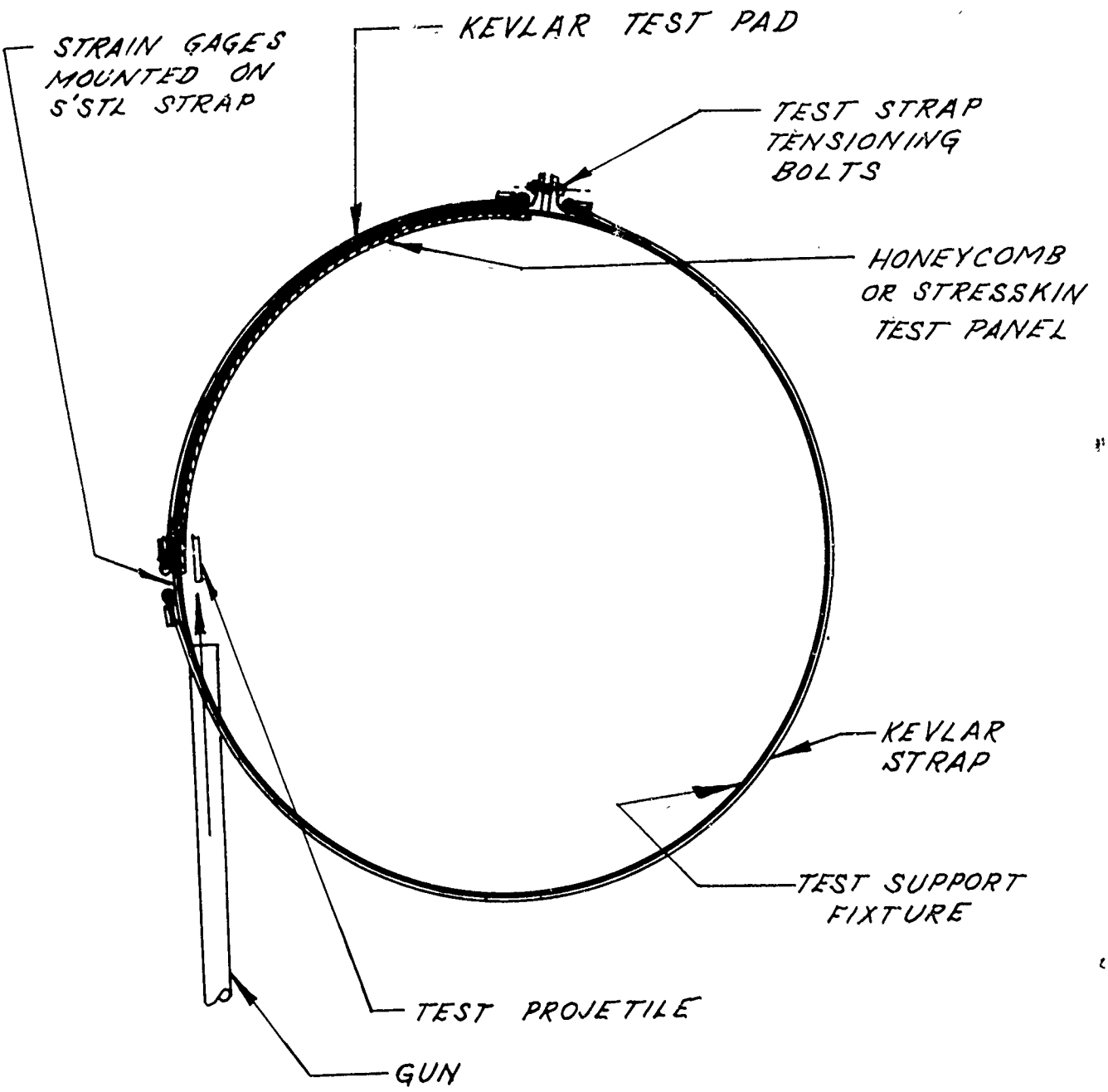

FIGURE 135
KEVLAR SHROUD
TEST SETUP

Figure 135
Containment with Kevlar Armor Strap Assy. Reinforcing 3/4 In. Steel Stresskin. 4 x 7 x 0.25 In. Fragment with 4 In. Width Parallel to Target Surface. Looking Upstream to Trajectory.

Figure 137
Containment with Kevlar Armor Strap Assy. Reinforcing 3/4 In. Steel Stresskin. 4 x 7 x 0.25 In. Fragment with 4 In. Width Parallel to Target Surface. Looking Downstream to Trajectory.

Figure 138

Edge View of Kevlar Armor Strap Assy. with Contained Fragment 4 x 7 x 0.25 In. Fragment with 4 In. Width Parallel to Target Surface, 903 FPS Impact Velocity

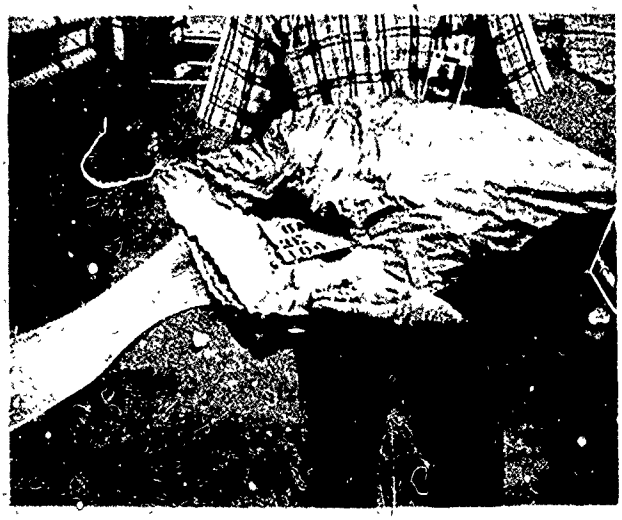

Figure 139

Kevlar Armor Strap Assy. with Layers Folded Back to Expose Contained Fragment. 4 x 7 x 0.25 In. Fragment with 4 In. Width Parallel to Target Surface, 903 FPS Impact Velocity

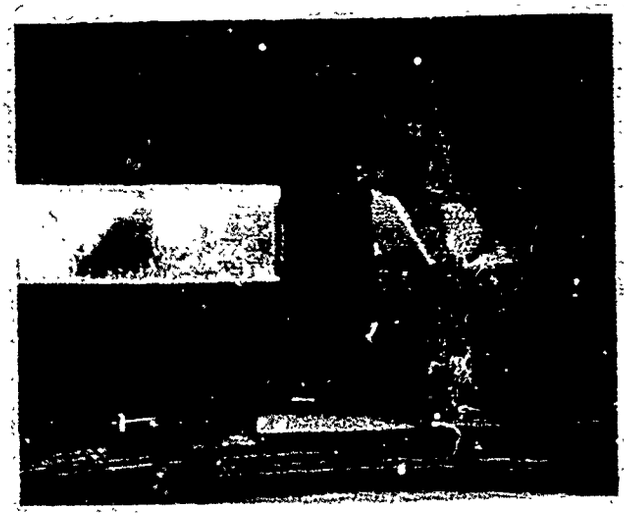

Figure 140

3/4 Inch Steel Stresskin Reinforced with Kevlar Armor Strap Assy., Inner Surface, 4 x 7 x 0.25 In. Fragment with 4 In. Width Parallel to Target Surface, 903 FPS Impact Velocity

Figure 141

Containment with Kevlar Armor Strap Reinforcing 3/4 In. Steel Stresskin. 4 x 7 x 0.25 In. Fragment with 0.25 In. Edge Parallel to Target Surface. Looking Downstream to Trajectory.

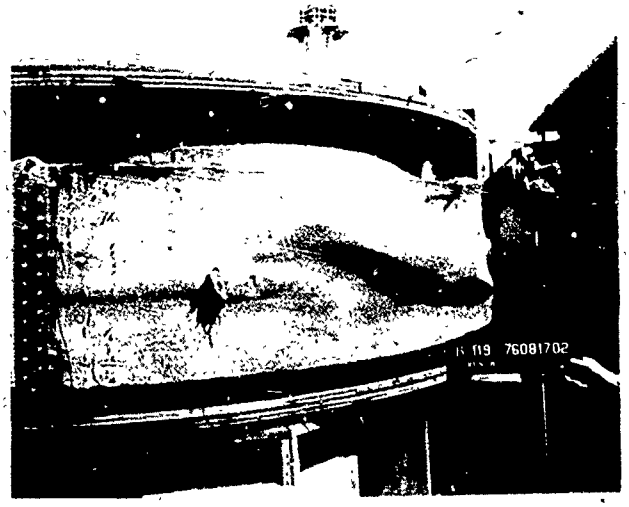

Figure 142

Containment with Kevlar Armor Strap Assy. Reinforcing 3/4 In. Steel Stresskin. 4 x 7 x 0.25 In. Fragment with 0.25 In. Edge Parallel to Target Surface. Looking Upstream to Trajectory

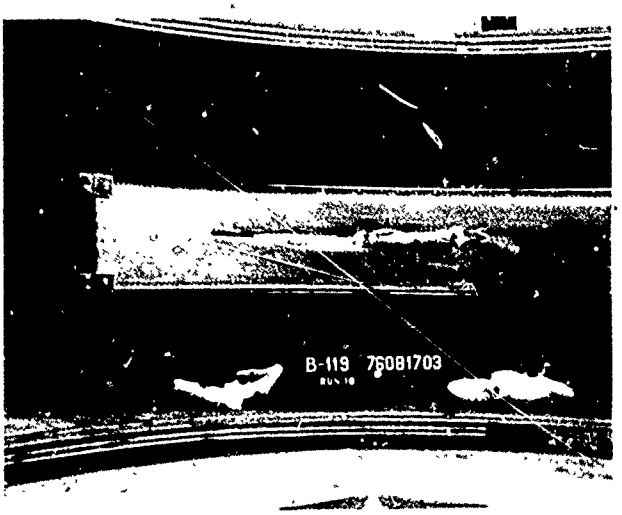

Figure 143

Inner Surface of 3/4 In. Steel Stresskin Reinforced by Kevlar Armor Strap Assy. 4 x 7 x 0.25 In. Fragment with 0.25 In. Edge Parallel to Target Surface, 903 FPS Impact Velocity

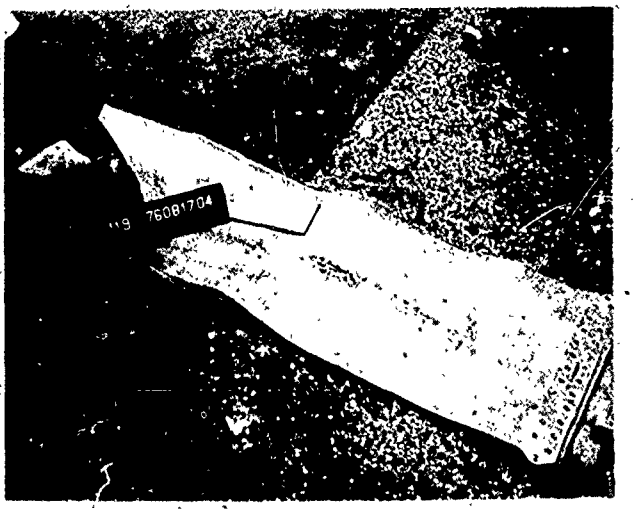

Figure 144

Inner Surface of Kevlar Armor Strap Assy. After Containment of 4 x 7 x 0.25 In. Fragment with 0.25 In. Edge Parallel to Target Surface

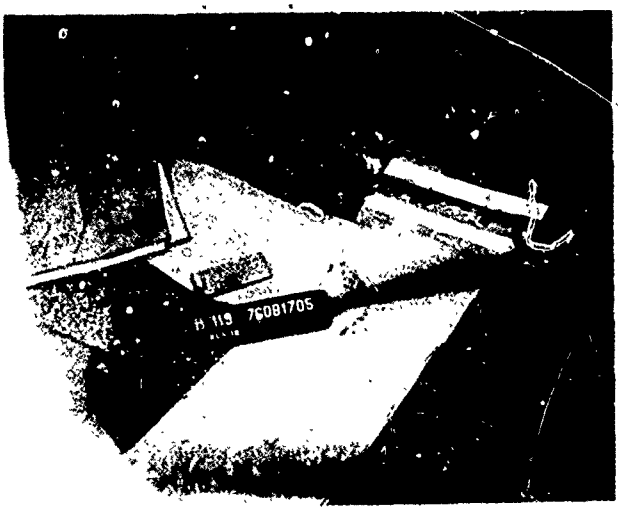

Figure 145

Kevlar Armor Strap Assy. with Layers Folded Back to Expose Contained Fragment. 4 x 7 x 0.25 In. Fragment with 0.25 In. Edge Parallel to Target Surface

Figure 146

Containment with Kevlar Armor Strap Assy. Reinforcing 2 In. Aluminum Honeycomb. 4 x 7 x 0.25 In. Fragment with 0.25 In. Edge Parallel to Target Surface. Looking Downstream to Trajectory.

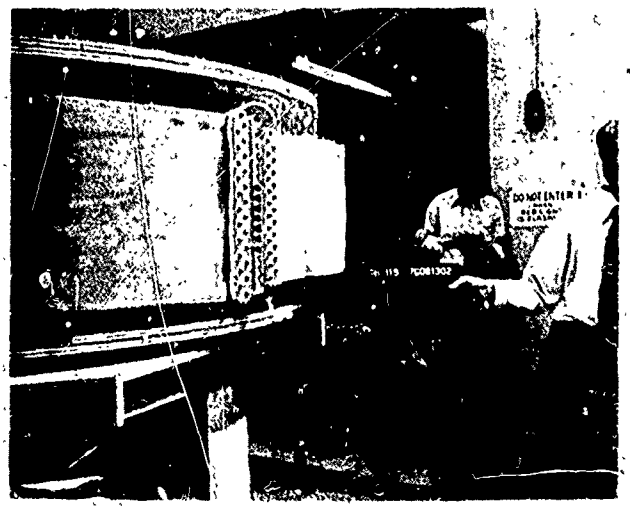

Figure 147

Containment with Kevlar Armor Strap Assy. Reinforcing 2 In. Aluminum Honeycomb. 4 x 7 x 0.25 In. Fragment with 0.25 In. Width Parallel to Target Surface. Looking Upstream to Trajectory.

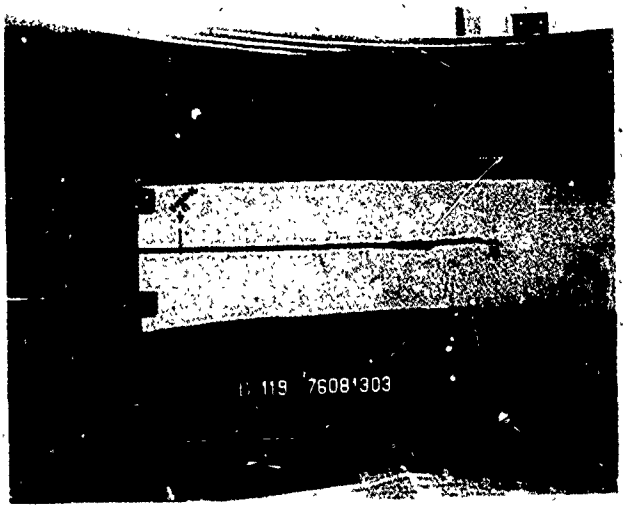

Figure 148
Inner Surface of 2 In. Aluminum Honeycomb Peinforced by Kevlar Armor Strap Assv. 4 x 7 x 0.25 In. Fraament with 0.25 In. Edge Parallel to Target Surface. 898 FPS Impact Velocity

Figure 149
Inner Surface of Kevlar Armor Stran Assy. with 4 x 7 x 0.25 In. Fraament Shot with 0.25 In. Edge Parallel to Target Surface

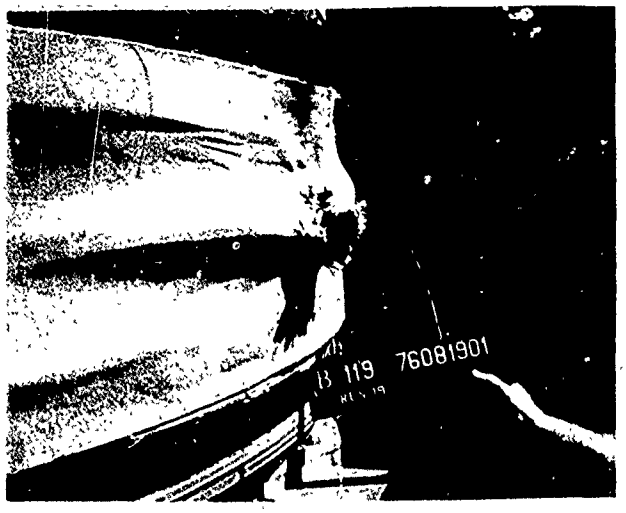

Figure 150

Non-Containment of 4 x 7 x 0.25 In. Fragment Shot with 4 In. Width Parallel to Target Surface. 2 In. Aluminum Honeycomb Target Reinforced by Kevlar Armor Strap Assy. 895 FPS Impact Velocity.

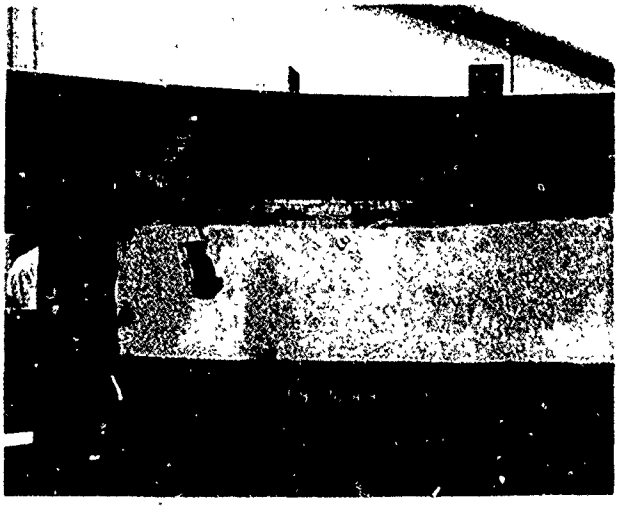

Figure 151

Inner Surface, 2 In. Aluminum Honeycomb Reinforced by Kevlar Armor Strap Assy. 4 x 7 x 0.25 In. Fragment Shot with 4 In. Width Parallel to Target Surface. Failed to Contain.

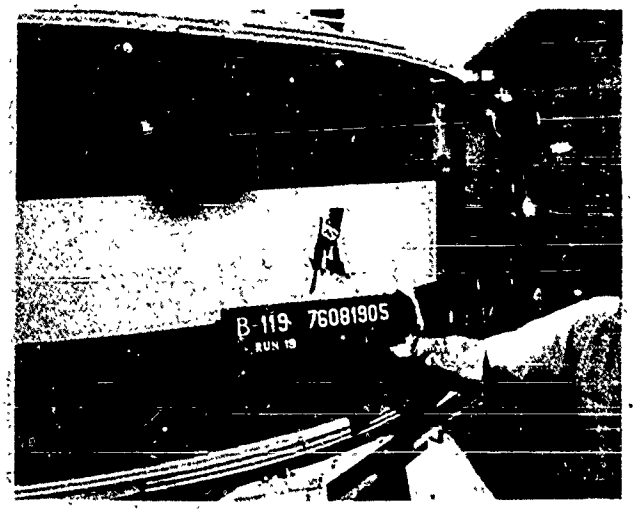

Figure 152

Outer Surface of 2 In. Aluminum Honeycomb After Removal of Reinforcing Kevlar Armor Strap Assy. 4 x 7 x 0.25 In. Fragment Shot with 4 In. Width Parallel to Target Surface. Containment Unsuccessful.

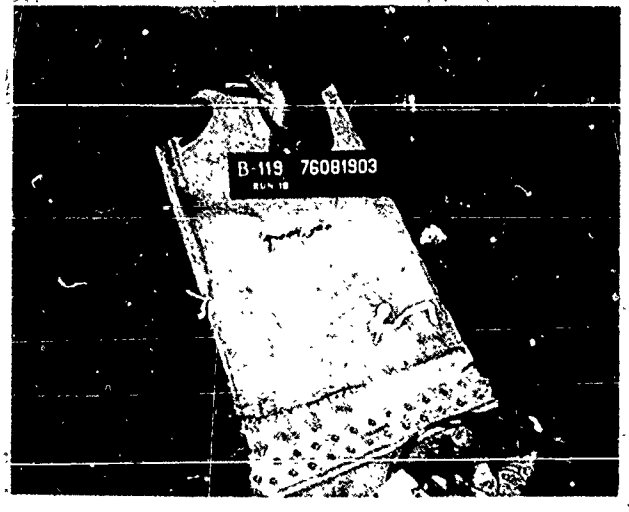

Figure 153

Inner Surface of Kevlar Armor Strap Assy. After Unsuccessful Containment of 4 x 7 x 0.25 In. Fragment Shot with 4 In. Width Parallel to Target Surface Made of 2 In. Aluminum Honeycomb.

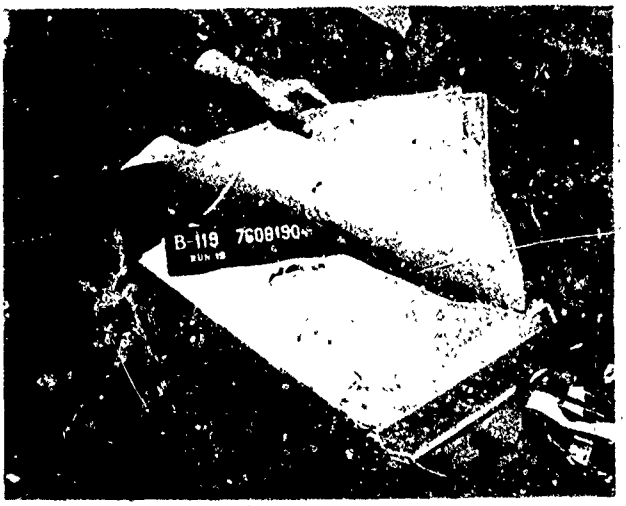

Figure 154

Internal Layers of Kevlar Armor Strap Assy. After Unsuccessful Containment of 4 x 7 x 0.25 In. Fragment Shot with 4 In. Width Parallel to Target Surface Made of 2 In. Aluminum Honeycomb.

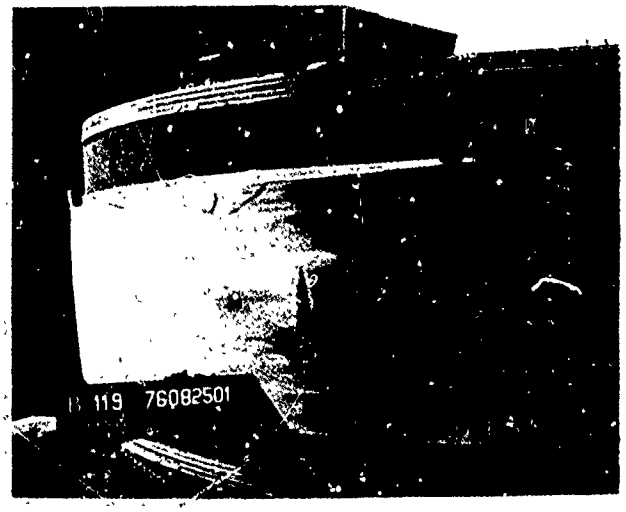

Figure 155

Containment with Kevlar Armor Strap Assy. and .050 In. Annealed Stainless Steel Peinforcinq Sheet Backinq Up 2 In. Aluminum Honeycomb. Lookinq at Outer Surface of Strap Assy. Downstream to Trajectory.

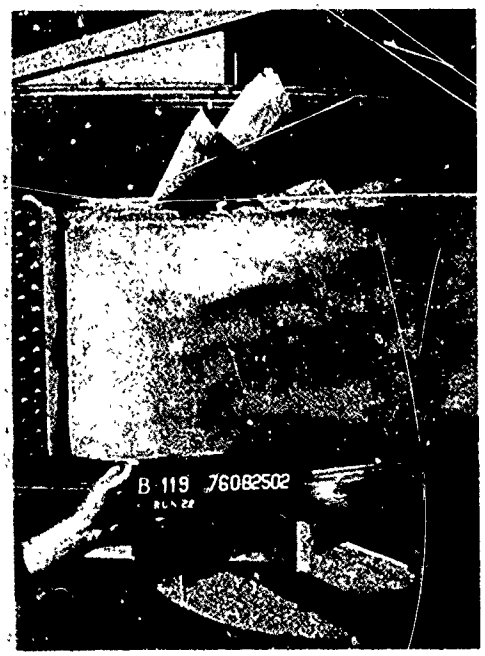

Figure 156

Containment with Kevlar Armor Strap Assy. and .050 In. Annealed Stainless Steel Peinforcinq Sheet Backinq Up 2 In. Aluminum Honeycomb. Lookinq Normal to Outer Surface of Strap Assy. at Point of Fraqment Arrestment.

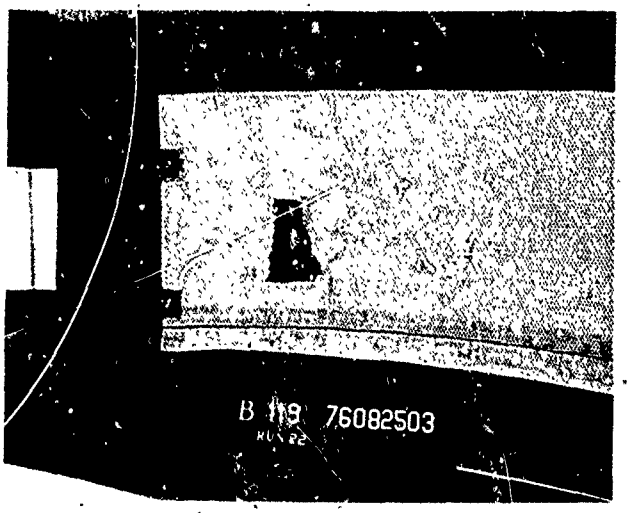

Figure 157

Inner Surface of 2 In. Aluminum Honeycomb Panel Reinforced by .050 In. Annealed Stainless Steel Sheet and Kevlar Armor Strap Assy. Successful Containment.

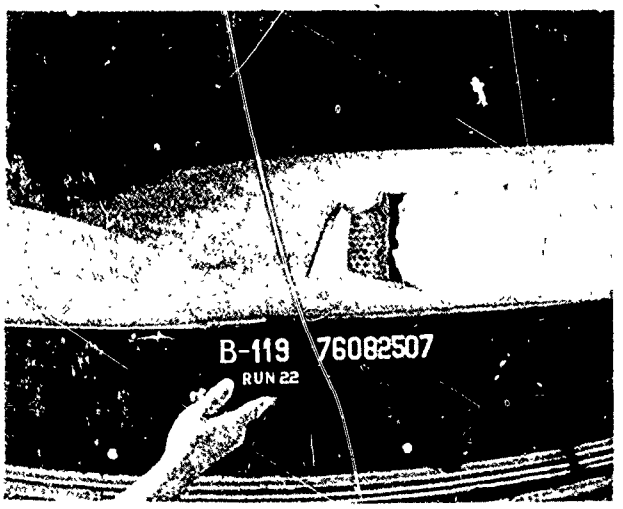

Figure 158

Outer Surface of 2 In. Aluminum Honeycomb Panel with Reinforcing .050 Steel Sheet and Kevlar Armor Strap Assy. Successful Containment.

Figure 159

Kevlar Armor Strap Assy. and .050 In. Annealed Stainless Steel Reinforcing Sheet After Disassembly.

Figure 160

Kevlar Armor Strap Assy. with Layers Folded Back to Expose Contained Fragment. Note, Steel Material Punched from .050 In. Steel Reinforcing Sheet Wrapped Around Edge of Fragment.

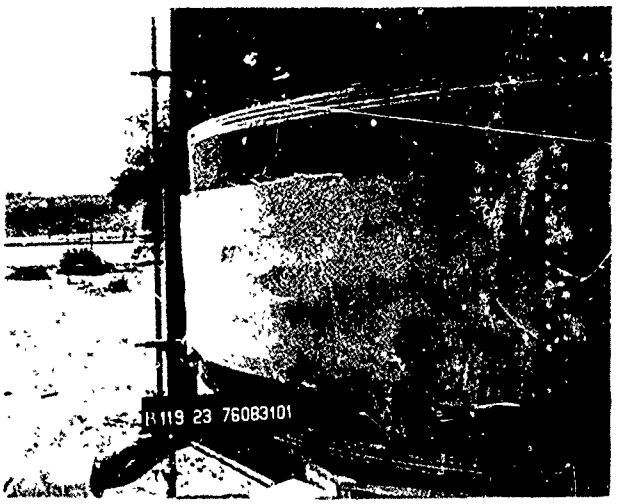

Figure 161

Containment with Kevlar Armor Strap Assy. and .050 In. Heat Treated Stainless Steel Reinforcing Sheet Backing Up 2 In. Aluminum Honeycomb. Looking at Outer Surface of Strap Assy. Downstream of Trajectory.

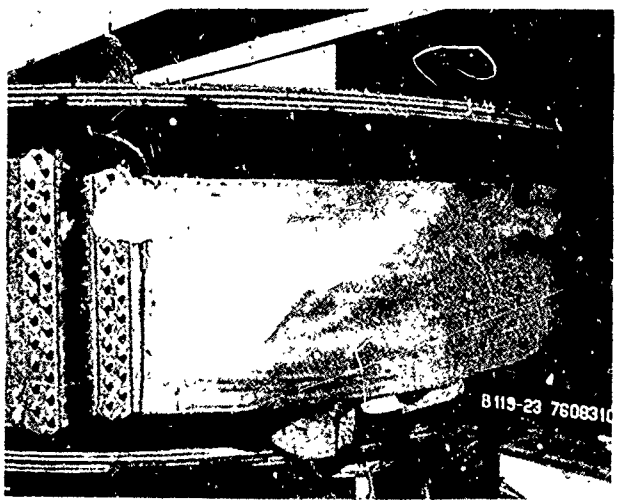

Figure 162

Containment with Kevlar Armor Strap Assy. and .050 In. Heat Treated Stainless Steel Reinforcing Sheet Backing Up 2 In. Aluminum Honeycomb. Looking at Outer Surface of Strap Assy. at Point of Fragment Arrestment.

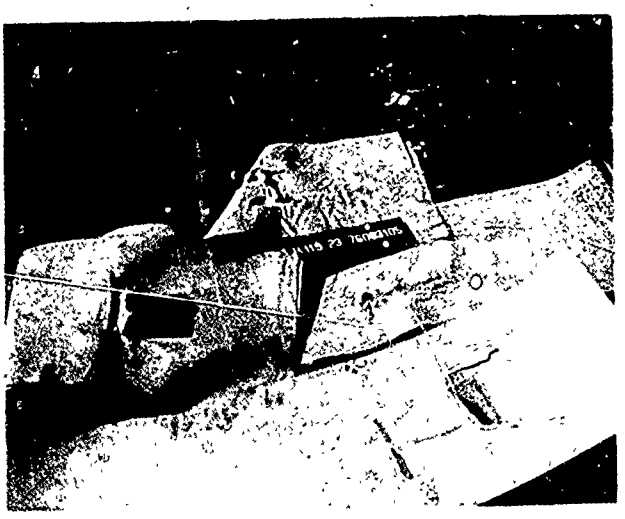

Figure 163

Kevlar Armor Strap Assy. and .050 In. Heat Treated Stainless Steel Reinforcing Sheet After Disassembly.

Figure 164

Inner Surface of 2 In. Aluminum Honeycomb Panel Reinforced by .050 In. Heat Treated Stainless Steel Sheet and Kevlar Armor Strap Assy.

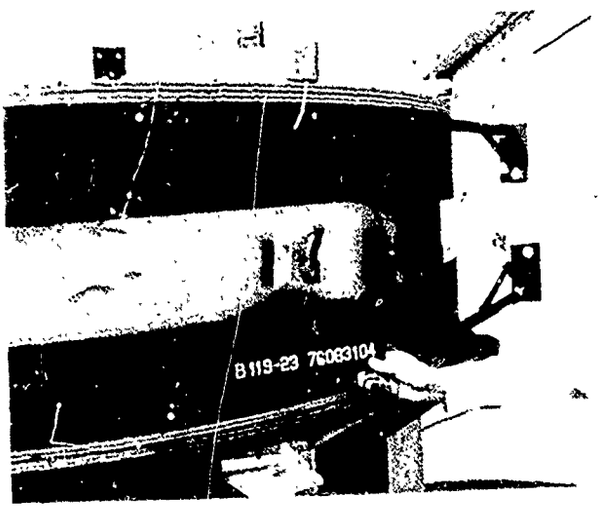

Figure 165
Outer Surface of 2 In. Aluminum Honeycomb Panel with Reinforcing .050 In. Heat Treated Stainless Steel Sheet and Kevlar Armor Strap Assy. Removed.

7.0 EFFECT OF INSTALLED ARMOR WEIGHT ON AIRPLANE PERFORMANCE

To assess the penalty involved for increasing the airplane weight by adding armor, the most weight effective conditions were selected, that is armor installed close to the engine and both the non-interchangeable and interchangeable installations were evaluated. The total weight required for the JT9D powered airplane and the CF6 powered airplane were very similar, so the evaluation was only accomplished for the JT9D powered three and four engine airplanes.

If Tables 7 and 8 are reviewed it will be noted that when armor is installed in the outer portion of the nacelle the installation weight is almost double of that when installed up close to the engine. The increased weight is caused by the greater armor area necessary to subtend a given fragment trajectory arc when installed further from the engine. Also Tables 7 and 8 show that to make the armor installations interchangeable so that engines or nacelles can be installed on either wing the installation weight was increased almost three times to gain interchangeability for the three engine airplane and about doubled for the four engine airplane.

Tables 41 and 42 show the total weight involved for non-interchangeable and interchangeable armor installations. The weight provides for armor to contain the one, two, and four blade fragments as well as inlet protection to contain the 3 x 5 x 0.25 inch fan blade fragment.

Table 41. Total Armor Weight for JT9D Powered Airplanes. Protected for 1, 2 and 4 Blade Failure. Armor Installed Close to Engine. Armored Nacelle and Engine Installation Not Interchangeable.

Fragment Size	3 Engine Airplane			4 Engine Airplane		
	Inner Armor Non-Interchangeable Pounds	Inlet Protection Pounds(1)	Total Weight Pounds	Inner Armor Non-Interchangeable Pounds (1)	Inlet Protection Pounds(2)	Total Weight Pounds
1 Blade	192	78	270	300	91	391
2 Blade	349	78	427	618	91	709
4 Blade	781	78	859	1380	91	1471

(1) Inlet only protected from 3 x 5 x 0.25 inch fan blade fragment

Table 42. Total Armor Weights for JT9D Powered Airpalnes. Protected for 1, 2 and 4 Blade Failure. Armor Installed Close to Engine. Armored Nacelle and Engine Installation Interchangeable.

Fragment Size	3 Engine Airplane			4 Engine Airplane		
	Inner Armor Inter-changeable Pounds	Inlet Pro-tection Pounds(1)	Total Weight Pounds	Inner Armor Inter-changeable. Pounds	Inlet Pro-tection Pounds(1)	Total Weight Pounds
1 Blade	585	118	702	600	182	782
2 Blade	1040	118	1157	1240	182	1422
4 Blade	2340	118	2457	2750	182	2932

(1) Inlet Only Protected from 3 x 5 x 0.25 Inch Fan Fragments

Projections made considering the growth of air traffic in the near future indicate that during the year of 1980 at least 10 million engine flight hours/year will be accumulated by wide body airplanes. Table 43 shows the additional amount of fuel which would be burned by the wide body fleet if the engines and inlets were armored. Also shown, is the cost incurred over the year span to purchase the additional fuel. No attempt was made to determine the cost of armor installation or the effect of the payload reduction. But this would be a sizeable additional expense.

Table 44 shows the additional amount of fuel burned and the cost if only inlet armor were installed.

Table 43.
1980 Fuel Cost for Additional Protection (Including Inlet Armor)
Projected 1980 Fleet Size of 971 Wide Body Transports and Fuel at 50¢/Gallon

		WEIGHT	FUEL PENALTY	FUEL COST ($)
Non-Interchangeable Armor	Trijet	859 lbs.	39 Million lbs/yr	3.0 (Million/yr)
	Quadjet	1471 lbs.	59 Million lbs/yr	4.5 Million/yr
Interchangeable Armor	Trijet	2457 lbs.	112 Million lbs/yr	8.6 Million/yr
	Quadjet	2932 lbs.	118 Million lbs/yr	9.0 Million/yr

Table 44.
1980 - Fuel Cost For Providing Inlet Protection Only
(Projected 1980 Fleet Size of 971 Wide Body Transports and Fuel at 50¢/Gallon)

		Weight/ Airplane	Fuel Penalty	Fuel Cost
Non-Interchangeable Armor	Trijet	78 lbs	3,600,000 lbs/yr	$274,000/year
	Quadjet	91 lbs	3,700,000 lbs/yr	$282,000/year
Interchangeable Armor	Trijet	118 lbs	5,400,000 lbs/yr	$412,000/year
	Quadjet	182 lbs	7,300,000 lbs/year	$564,000/year